Structural Analysis of Network Models in Tetrapod Skulls

Evolutionary Trends and Structural Constraints in Morphological Complexity, Integration, and Modularity

Memòria presentada per optar al grau de Doctor

Doctorat de Biodiversitat

Universitat de València

BORJA ESTEVE ALTAVA

Dirigit per en

Dr. Diego Rasskin Gutman

Agraïments

Esta iba a ser una tesis sobre robots; así conseguí engañar a Diego para empezar a trabajar con él. Por suerte, o por desgracia (nunca lo sabremos), abandoné mi fantasía *asimoviana* y empecé a estudiar cráneos y redes. Gracias a la confianza y el apoyo económico que Diego me ha ofrecido siempre estoy ahora agradeciendo el apoyo de otras personas e instituciones.

La meva família ha estat sempre el meu suport en tot moment, tant durant l'elaboració de la tesi com del camí que m'ha portat a concloure-la. És en va agrair en detall tot el que han fet, perquè és tant com haver-me fet a mi. Als meus pares, Pepe i Xelo, als meus avis, Salvador i Cosuelo, i als meus oncles, ties i cosins. Gràcies.

Molts amics han estat també al meu costat des de sempre: Xavi, Pau i Toni; d'altres han anat creixent amb els anys: Diego, Isabel, Noe, Bailón, Teresa, Laura, Carles, Víctor, Maria, Vitor, Ana, Miguel, Llopis, Neus, Helena, César, Gorri i Kasia. No entraré en detalls o hauria d'escriure un altre llibre igual de gros que aquest agraint-vos anys de frikisme, voley platja, partits del Barça al Samaruc, paelles, Magdalenes i converses (transcendentals i no tant). No obstant això, alguns mereixen menció extraordinària per la seva aportació concreta a la tesi: Xavi, per haver suportat tantes preguntes sobre MatLab, LaTeX i mil històries més, i sobre tot per ser el meu *"amigo informáaatico..."*; Maria, per ajudar-me en moltes correccions i dubtes encara que tinguem visions tan diferents de la ciència; Pau, pel disseny de la coberta i logística editorial. Kasiu, dzięki za bycie blisko tych ostatnie kilka miesiący.

I met many people in Vienna while I was writing this thesis. They made my time both fun and productive. Thanks to all. Ein besonderer Dank an Maria, Natasa, Rina, Lura und Manuel, die mich nicht nur in ihren Wohnungen aufgenommen haben sondern mich auch sofort in ihren Freundeskreis integrierten. Mención especial también para Laura, Joseba, Elisa y Dani, estos comen aparte, en un sentido literal y figurado... y que bien hemos comido ¿eh? Gracias chicos por hacer de la estancia un placer y ayudarme con

todo. Grazie anche a Laura Risatti, che in questi mesi è diventata la mia amica e colleghi di feste.

A Jesús Marugán, Hector Botella y Markus Bastir por estar cerca estos años, ofrecer consejo cuando fue necesario y colaborar en tirar esto adelante. También a Miquel De Renzi y Ángela Buscalioni, porque, si bien su influencia ha sido menos directa, partes de sus ideas también han permeado, casi por ósmosis, en mi trabajo.

Thanks to the people from the Konrad Lorenz Institute in Altenberg, Austria, Gerd Müller, Werner Callebaut, and Isabella Sarto-Jackson, for their help, advice, comments, and books (many books). I would also like to thank Eva Karner for her kindly help and friendship during this time.

Finally, I had the opportunity during this time to interact with expert colleagues who have enriched this thesis through personal discussions about my work or non-anonymous reviews of my articles: Ricard Solè, Chris Klingenberg, Michel Laurin, Daisuke Koyabu, Philipp Mitteroecker, Guillaume Dera, Nelly Gidaszewski, and Neus Martínez Abadías. Thanks to all.

Aquesta tesi no ha rebut suport econòmic a títol personal de ninguna beca d'investigació. Per això, no té res que agrair a cap administració, Conselleria, Ministerio o Secretaría de Estado de Ciencia e Innovación (segons l'any i partit polític). En aquest temps sí he rebut suport econòmic a través de diverses beques de col·laboració i contractes de tècnic de laboratori adscrites a projectes de recerca dirigits per en Dr. Diego Rasskin-Gutman (GV/2007/256 i BFU2008-00643) amb les quals he pogut subsistir (que no emancipar-me).

Estic molt agraït al **Institut Cavanilles de Biodiversitat i Biologia Evolutiva** de la Universitat de València per oferir-me un espai propi on desenvolupar la meva investigació. Els últims sis mesos d'aquesta tesi han estat generosament finançats amb una *Writing-up Fellowship* per part del **Konrad Lorenz Institute for Evolution and Cognition Research**.

Resum

D'ençà l'origen de l'anatomia comparada, les connexions entre les parts del cos han estat emprades com una eina metodològica per estudiar la forma dels animals. Així, notables naturalistes, com per exemple Pierre Belon o Johann Wolfang Goethe, empraren les connexions per reconèixer similituds entre òrgans en animals diferents, tot seguint una tradició que podríem remuntar a Aristòtil. Al segle XIX, Étienne Geoffroy St. Hilaire proposà el *principi de les connexions* com un criteri operatiu per identificar la similitud morfològica entre organismes, mitjançant les relacions estructurals (o topològiques) en lloc de la seva funció o forma (en anglès, *shape*). El principi de les connexions de Geoffroy formalitzà la noció intuïtiva de semblança orgànica pròpia del seu temps i donà peu a un nou programa de recerca en morfologia pura a un nivell estructural.

Diversos marcs conceptuals s'han proposat amb posterioritat amb l'objectiu d'emprar les relacions de connectivitat en sistemes anatòmics: la *correspondència estructural* de Woodger, el *principi bio-topològic* de Rashevsky i el *morfotipus diagramàtic* de Riedl. Malauradament, aquestes propostes oferien una metodologia massa obscura o abstracta, la qual cosa va dificultar la seva aplicació sistemàtica a problemes morfològics de caire quantitatiu. Recentment, Rasskin-Gutman proposà la Teoria de Grafs com un nou marc metodològic mitjançant el qual estudiar les relacions de connectivitat en sistemes anatòmics, en oferir per primer cop una anàlisi de xarxes morfològiques.

L'anàlisi de xarxes actual apareix a final dels anys 90 com una branca aplicada de la Teoria de Grafs que permetia treballar amb sistemes complexos. Aquesta nova Teoria de Xarxes esdevingué un marc conceptual i metodològic adient per analitzar les propietats emergents dels sistemes complexos, que són degudes a l'organització dels patrons de connectivitat entre les seves parts, per exemple, la robustesa, la auto-organització o la modularitat. Ben aviat, l'anàlisi de xarxes es va aplicar per estudiar un ampli ventall de sistemes biològics complexos, com les xarxes de regulació gènica, els sistemes neuronals o els ecosistemes. No obstant, aquesta nova metodologia no fou aplicada a l'estudi de sistemes anatòmics. L'esquelet dels vertebrats és un sistema anatòmic idoni per dur a

terme una anàlisi d'aquest tipus, per presentar una elevada complexitat estructural, ontogenètica i evolutiva. A més a més, la perdurabilitat del ossos permet també l'anàlisi comparativa de materials fòssils, la qual cosa facilita resoldre qüestions macro-evolutives.

En aquesta tesi he aplicat l'anàlisi de xarxes a l'estudi de l'organització de les sutures entre els ossos del crani dels tetràpodes; és a dir, els patrons de connectivitat que defineixen l'organització de l'estructura del crani. La importància d'aquestes connexions per entendre la morfologia del crani es deu a la seva funció com a zones de creixement i canvi de forma dels ossos i, per extensió, del conjunt del crani. Com a part d'aquest estudi també he desenvolupat un marc d'interpretació morfològica per als paràmetres analitzats amb què discutir els resultats obtinguts en un context evolutiu i ontogenètic. Tot plegat m'ha permès tractar les qüestions més punteres de la morfologia actual, com són la complexitat, la integració i la modularitat, des d'una perspectiva estructural totalment innovadora.

Objectius

L'objectiu d'aquesta tesi és dur a terme una anàlisi comparativa dels patrons de connectivitat en el crani dels tetràpodes. Dintre d'aquesta anàlisi s'avaluen qüestions relatives a l'evolució i l'ontogènia de la complexitat, integració i modularitat de la morfologia cranial. La hipòtesi general és que aquest tipus d'anàlisi pot (1) evidenciar propietats morfològiques que no són accessibles mitjançant l'estudi de la forma i la mida (*shape and size*), així com (2) enriquir la nostra comprensió de com l'organització de les sutures cranials influeix en altres propietats del crani i dels ossos que el composen. Els resultats, empírics i teòrics, d'aquesta anàlisi comparativa de xarxes cranials s'han emprat per establir la influència dels patrons de connectivitat en la formació i evolució de la morfologia del crani.

Per complir aquest objectiu he dut a terme les següents tasques:

- Construcció del model de xarxa.
- Interpretació morfològica dels paràmetres emprats.
- Anàlisi de les xarxes cranials i identificació de mòduls de connectivitat.
- Anàlisi filogenètica de tendències evolutives en la complexitat morfològica del crani, incloent-hi la programació i simulació de models computacionals que reprodueixen l'evolució del crani mitjançant la pèrdua i fusió d'ossos.

- Estudi comparatiu de la modularitat al crani dels tetràpodes per determinar els patrons de formació dels mòduls de connectivitat, incloent-hi la realització d'experiments teòrics de manipulació artificial dels models de xarxa.
- Construcció i anàlisi del morfoespai teòric del crani emprant models nuls com a regles generatives per capturar distintes hipòtesis ontogenètiques.
- Estudi detallat de la integració morfològica i la modularitat del crani humà, per a la qual cosa s'han inclòs també models de xarxes de cranis de nounats amb fusions prematures d'ossos (craniosinostosi).

Metodologia

La metodologia emprada en aquesta tesi està fonamentada en la Teoria de Xarxes i l'Anatomia Comparada dintre del marc conceptual de la Biologia Teòrica. Gran part de la metodologia utilitzada ha estat desenvolupada per primer cop en aquesta tesi.

Els cranis estudiats s'han formalitzat matemàticament mitjançant models de xarxes, en els quals els vèrtex i les arestes de la xarxa representen els ossos i les sutures del crani, respectivament. D'aquesta manera, he construït models de xarxes per al crani d'espècies actuals i extintes, així com per a nounats amb diverses craniosinostosis. Un total de 51 cranis han estat modelitzats d'aquesta manera (27 actuals, 17 fòssils i 7 nounats); aquests foren triats per a representar un ampli ventall de formes morfològiques, tot incloent-hi les patològiques.

Els models del crani han estat analitzats mitjançant tècniques i models nuls propis de la Teoria de Xarxes, amb l'objectiu de descobrir les propietats del crani derivades de la seva organització: complexitat, integració i modularitat. Aquesta anàlisi s'ha dut a terme utilitzant la plataforma de programació Matlab. Els models de xarxes i els scripts programats s'han inclòs en un apèndix que es farà accessible on-line de forma gratuïta.

Per a l'estudi de tendències evolutives s'ha dut a terme un Contrast Filogenètic Independent sobre una filogènia calibrada per a les espècies modelitzades, utilitzant el programa d'anàlisi filogenètic Mesquite. Així mateix, s'ha programat un model computacional que reprodueix l'evolució d'un crani ancestral teòric a través de la pèrdua i fusió d'ossos, amb l'objectiu d'avaluar la importància d'ambdós processos ontogenètics en la formació de patrons evolutius direccionals.

La construcció del morfoespai teòric s'ha dut a terme també en Matlab. Quatre models nuls s'han emprat com a regles generatives que simulaven diverses hipòtesis ontogenètiques,

que emfatitzen diferents factors implicats en l'establiment dels patrons de connectivitat: (1) a l'atzar (model de Erdös i Rényi), (2) amb preferència associada al nombre de connexions (model de Barabási i Albert), (3) per proximitat geomètrica (model de Gabriel), i (4) per proximitat geomètrica i simetria bilateral (model de Gabriel simètric). El darrer model ha estat creat específicament en aquesta tesi per a reproduir regles més reals biològicament.

Conclusions

Aquestes són les principals conclusions obtingudes en aquesta tesi:

Tendències Evolutives en la Complexitat Morfològica

1. La disminució del nombre d'ossos durant l'evolució del crani dels tetràpodes (Llei de Williston), deguda a la pèrdua i fusió d'ossos, s'acompanya d'un increment de la complexitat morfològica, en lloc d'una simplificació del crani com es pensava anteriorment.

2. Les pèrdues i fusions d'ossos afecten la complexitat del crani de forma diferent segons involucren ossos escollits a l'atzar o selectivament d'acord al seu nombre de connexions. Açò implica que el nombre de connexions estableix una restricció estructural a la pèrdua i fusió d'ossos. En estar les connexions entre ossos relacionades amb co-dependències funcionals i de creixement, un major nombre de connexions imposa restriccions més severes.

3. Un escenari evolutiu mixt pot explicar aquest increment de la complexitat morfològica: la pèrdua aleatòria dels ossos menys connectats i la fusió selectiva dels ossos més connectats.

4. En completar aquest escenari evolutiu, diverses restriccions estructurals han estat també identificades: (1) la necessitat d'un espai físic no restringit per cap eix corporal a l'hora de desenvolupar el crani ancestral, (2) un petit nombre d'ossos imparells inicials, i (3) una major freqüència de pèrdues que de fusions.

Integració Morfològica i Modularitat

5. El crani dels tetràpodes posseeix una organització de connexions a mig camí entre l'aleatorietat i la regularitat (*"small-world"*), que afavoreix la formació de mòduls de connectivitat.

6. Hi ha tres tipus de mòduls de connectivitat al crani: (1) bilateral, que agrupa ossos dels costats esquerre i dret alhora; (2) especular, que agrupa ossos d'un sol costat del crani; i (3) especular asimètric, que agrupa ossos d'un sol costat, però incloent-hi també un o més ossos imparells.

7. En general, la formació d'un mòdul bilateral depèn de la presencia d'ossos imparells en una determinada regió del crani, els quals actuen com a integradors d'ambdós costats del crani en un únic mòdul; quan aquesta integració no es dóna, es formen dos mòduls especulars asimètrics; i quan no hi ha ossos imparells, es formen dos mòduls especulars.

8. La formació dels mòduls de connectivitat tendeix a seguir un ordre jeràrquic a l'hora d'agrupar els ossos; aquests s'agrupen junts tot seguint la seva posició relativa dintre dels tres eixos corporals: dorsoventral, esquerra-dreta, i anteroposterior. Aquest ordre d'agrupació es troba molt influenciat per la presència d'ossos imparells.

Morfologia Teòrica

9. L'anàlisi del morfoespais teòric del crani ens indica que la regla de creixement que millor copsa la disparitat d'estructures cranials és la basada en la proximitat geomètrica (regla de Gabriel), quan els ossos es col·loquen amb simetria bilateral i hi ha ossos imparells (morfoespai Proximal Simètric).

10. L'extensió d'aquest morfoespai generatiu és asimètrica respecte al nombre de connexions: és més amplia (major disparitat en nombre de connexions) per a xarxes més grans, i més estreta per a xarxes més petites.

11. Els cranis dels primers tetràpodes ocupen la regió amplia del morfoespai durant els Períodes Devonià i Carbonífer. A mesura que la regió amplia comença a buidar-se durant el Mesozoic, els cranis més derivats ocupen regions més estretes del morfoespai, fins aplegar al Cenozoic.

12. Aquesta ocupació direccional del morfoespai està vinculada amb la Llei de Williston, la qual cosa suggereix que el crani dels tetràpodes ha evolucionat cap a organitzacions morfològiques més restringides, alhora que incrementava la seva complexitat com a conseqüència de la disminució del nombre d'ossos.

El Crani Humà

13. L'anàlisi detallat de la integració morfològica i la modularitat en el crani humà identificà dos mòduls de connectivitat ben definits: un facial organitzat entorn de l'os ethmoidal, i un cranià organitzat entorn de l'os esfenoïdal.

14. El mòdul facial té una agrupació jeràrquica d'ossos en blocs i el mòdul cranià té un patró regular de connectivitat. Aquesta distinta integració morfològica en cada mòdul defineix una organització semi-jeràrquica al crani humà, que reflecteix diferències fonamentals en els patrons ontogenètic de creixement i les restriccions estructurals específiques de cada regió.

15. Després de demostrar que els mòduls de connectivitat s'assemblen a unitats de creixement al·lomètric, es pot concloure que, a causa del seu paper ontogenètic com a llocs de creixement ossi, les relacions de connectivitat estableixen correlacions de forma i mida. Així doncs, les connexions són una font fonamental d'integració morfològica i modularitat.

16. Els cranis de nounats amb fusions prematures d'ossos (craniosinostosi) reprodueixen a una escala ontogenètica els patrons evolutius trobats a la Llei de Williston: un increment en la integració morfològica com a conseqüència de la disminució del nombre d'ossos. Açò podria suggerir una relació entre la craniosinostosi i els patrons macro-evolutius del crani.

17. Les craniosinostosis també afecten els patrons de connectivitat que determinen l'organització modular del crani humà. Les fusions medials, a les sutures metòpica i sagital, produeixen organitzacions modulars semblants a la del crani adult, mentre que les fusions en un sol costat, a les sutures hemicoronal i lambdoidal, produeixen mòduls asimètrics diferents als del crani adult.

Noves Vies de Recerca

18. Les futures anàlisis de xarxes han d'orientar-se cap a l'especialització en els grups d'estudi, amb l'objectiu de poder estudiar modificacions dels patrons de connexions a una escala més petita. Per exemple, les tortugues i els mamífers, per tenir un patró de connexions molt conservat, són més adients per a estudiar petites variacions com la formació del vomer imparell; mentre que els arcosaures, lepidosaures i amfibis, que ofereixen molta variació entre grups, poden ser emprats per estudiar transicions evolutives com el pas d'un entorn aquàtic a un terrestre o l'origen del crani de les aus.

19. Fer menester mètodes més sofisticats per a resoldre nous problemes morfològics, com l'anàlisi de seqüències ontogenètiques o la correlació entre la connectivitat dels ossos i la forma del crani.

20. Les eines desenvolupades en aquesta tesi per analitzar xarxes cranials són adients també per estudiar altres estructures esquelètiques, no-esquelètiques, o fins i tot estructures vegetals.

Contents

List of Figures

List of Tables

Prologue

Formerly there was talk on analogy, without anyone knowing what in particular was analogous. For want of anything better, there was endless talk about the consideration of forms, but no one appeared to see that the form is fugitive from one animal to another. Thus I will have provided the consideration of analogy with a basis it had previously lacked, when I proposed to bring research uniquely to bear on the mutual, necessary, and consequently invariable, dependence of the parts.

Étienne Geoffroy Saint-Hilaire, Anatomical Philosophy (1822)

Ever since classic anatomists like Étienne Geoffroy St. Hilaire, George Cuvier, or Richard Owen laid down the fundamental principles of comparative anatomy in the 19^{th} century, connections among anatomical parts have been essential for the recognition of biological homologies. Before Geoffroy's proposal of the *principe des connexions* as a methodological aid to study animal forms, other notable naturalists, such as Pierre Belon and Johann Wolfgang Goethe, also made use of this principle as a way to recognize similarities, a tradition that goes back to Aristotle. However, Geoffroy was the first author to establish connections among anatomical parts as an operational criterion to identify morphological similarity between organisms by means of structural (or topological) relations, rather than by their shape and function. Geoffroy's principle of connections formalized the intuitive notion of similarity already present in those days and set a new research program in pure morphology at the structural level.

Several conceptual frameworks afterwards have been proposed for the use of connectivity relations in anatomical systems, such as Woodger's *structural correspondence*, Rashevsky's *bio-topological principle*, and Riedl's *diagrammatic morphotype*. Unfortunately, these frameworks were either too methodologically obscure or too abstract to be applied systematically to the practical study of morphological variation and its quantification. More recently, Rasskin-Gutman proposed Graph Theory as a novel framework to address

connectivity relations in anatomical systems, introducing for the first time a pioneer network analysis of morphological structures.

Modern network analysis arose as an applied branch of Graph Theory for handling complex systems in the late '90s from the works by Watts, Strogatz, Barabási, Albert, and other physicists; thus, Network Theory became a novel conceptual and methodological framework to deal with the relational properties that emerge due to connections between parts in any organized complex system (e.g., robustness, self-organization, and modularity). Network analysis was readily applied to a wide range of complex biological systems, such as gene regulatory pathways, brain neuronal systems, or ecological communities. However, a seemingly natural arena to use this mathematical tool such as comparative anatomy has never been systematically studied using current network analysis tools. Among the anatomical systems that we can study using networks, the tetrapod skull is the most interesting one due to its high structural, developmental, and evolutionary complexity. Moreover, the skull perdurability allows also a large-scale comparative analysis using fossils, which, in turn, permits to use network analysis to assess macro-evolutionary questions about how the tetrapod skull has evolved.

In this thesis, I have applied modern network analysis to the study of the tetrapod skull. Current hot topics in skull morphology, such as complexity, integration, and modularity, have been assessed using skull network models, in which nodes and links represent bones and suture contacts, respectively. To this end, I have also developed a complete framework of anatomical interpretations for the most common parameters used in networks analysis, discussing the results in an evolutionary and developmental context.

Aims

The aim of this thesis is to carry out a comparative analysis of connectivity patterns in tetrapod skulls to assess problems on the evolution and ontogeny of morphological complexity, integration, and modularity. The general hypothesis is that this kind of analysis can reveal key morphological properties of the skull that most common studies, based solely on shape and size, would keep unravel. By following this general hypothesis, it is expected to generate new ways to assess the role of craniofacial suture organization in skull evolution and development.

In order to fulfill this aim I have carried out the following tasks:

- Construction of network models of tetrapod skulls

- Morphological interpretation of network parameters
- Network analysis of skulls and identification of connectivity modules
- Phylogenetic analysis of evolutionary trends in skull morphological complexity, which included the programming and simulation of a computational model of skull evolution by loss and fusion of bones
- Comparative analysis of the skull modularity in tetrapods to unveil patterns in the formation of connectivity modules; for this task, I have also performed experiments of artificial manipulation of connectivity patterns in network models
- Construction and analysis of theoretical morphospaces of the tetrapod skull, using null network models as generative rules that capture different developmental hypothesis of skull growth
- Detailed study of morphological integration and modularity in the human skull, which included the analysis of network models of newborn skulls with premature fusion of bones (i.e., craniosynostosis)

Division of Chapters

Introduction

Chapter 1 (Skull Development & Evolution) reviews the development and evolution of the tetrapod skull. The first section focuses on bone and suture formation. The second section focuses on the skull evolution in tetrapods, with emphasis on the evolutionary trend in bone number reduction known as Williston's Law.
Chapter 2 (The Analysis of Organismal Form) introduces the conceptual framework of form analysis followed in this thesis. The first section focuses on the different levels of morphological information: proportions, connections, orientations, and articulations. The second section reviews the historical background of connectivity information used in morphology.
Chapter 3 (Morphological Organization in Connectivity Patterns) reviews the problems related to morphological organization at a connectivity level.

Materials & Methods

Chapter 4 (Tools for Networks Analysis) describes the mathematical algorithms used in the analysis of skull networks and identification of connectivity modules.
Chapter 5 (The Skull Network Model) explains the abstraction process followed to build skull network models and the morphological interpretation given to each network parameter.
Chapter 6 (Null Models & Simulations) describes the null network models used in this thesis for comparative analysis, construction of generative morphospaces, and the computational model of skull evolution.
Chapter 7 (Sample & Phylogeny) introduces the sample of tetrapod skulls and the calibrated phylogeny used as evolutionary context for comparative analysis.

Results & Discussion

Chapter 8 (Network Analysis Results) shows the raw results of the network analysis for each tetrapod skull.
Chapter 9 (Evolutionary Trends in the Tetrapod Skull) discusses the analysis of evolutionary trends in morphological complexity related to the reduction in the number of skull bones by loss and fusion (Williston's Law), including the results of the computational model analysis.
Chapter 10 (Network Modularity in the Tetrapod Skull) discusses the formation of connectivity modules in skull networks. The first section offers a comparative overview of all groups. The second section explores the role of unpaired bones and body axes in the formation of modules using artificial modification of connectivity patterns in network models.
Chapter 11 (Theoretical Morphology and Morphospaces) examines the differential temporal occupation of the morphospace and the fit of the skull sample to different null network model-derived generative morphospaces.
Chapter 12 (The Human Skull Network) shows a detailed network and modularity analysis of the human skull. The first section focuses on the adult skull and includes a geometric morphometrics test of the correspondence of connectivity modules as units of allometric growth. The second and third sections focus on the skull of human newborns with different craniosynostosis conditions.

Part I

Introduction

1

Skull Development & Evolution

The tetrapod skull is a mosaic system made of bones with very different developmental and evolutionary origins, as well as multiple biological functions, including brain protection, feeding, and hosting of sensory organs. The coupling of all these functions is a consequence of the skull phenotypic integration at different scales: genetic, developmental, and morphological. In addition, together with soft tissues, the skull largely determines the shape of the head and the relative movement of its parts.

1.1 Developmental Biology of the Skull

Three germ layers form all the organs and tissues of vertebrates during embryogenesis: the endoderm forms internal organs, such as the gastrointestinal track, the respiratory system, and the endocrine glands; the mesoderm forms the musculoskeletal system, the gonads, and the connective tissues; the ectoderm forms the nervous system, the epidermis, and the boundaries with the exterior environment. In addition, the ectoderm forms also the neural tube, the precursor of the central nervous system, from which some cells (so-called neural crest cells) will migrate toward the cephalic region (Gilbert, 2006) (Fig. 1.1).

The tetrapod skull comprises cells from the mesoderm and the neural crest (Hall, 2005). Bones formed by each type of cells are indistinguishable in the adult, with some bones having a dual origin in the adult skull. During the development of the head, neural crest cells migrate from the neural tube to cephalic regions to form part of the skull (Kardong, 2005). Epigenetic information before, during, and after migration, is critical to understand the mechanisms acting on skull development (Franz-Odendaal, 2011). The extracellular matrix through which these cells move determines the direction and speed of the migration, and their final location in the future skull. Cell-cell contacts, secreted chemical signals, and matrix-mediated factors of the basal lamina induce bone formation.

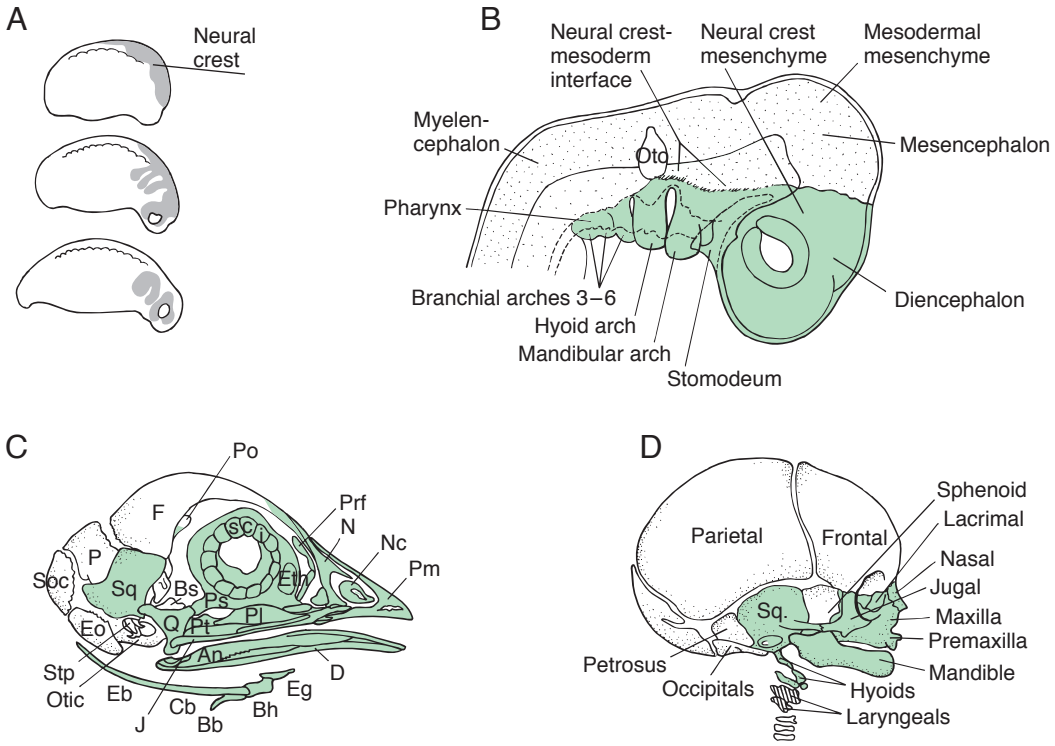

Figure 1.1: Neural crest cells (green) contribution to the formation of skull bones. A) Embryo of *Salamandra salamandra* showing the origin and migration of neural crest cells. B) and C) Mesodermal and neural crest cells contribution to the development of the head in *Gallus gallus*. D) Contribution in the human skull. From Kardong (2005).

After induction, cells begin a process of condensation that comprises a definite sequence of steps: initiation, boundaries setting, cell proliferation, cell adhesion, cell growth, and termination (reviewed in Franz-Odendaal, 2011). Prior to condensation, these cells have surface molecules (e.g., peanut agglutinin and alkaline phosphatase) that distinguish them from non-condensed neighbor cells (Hall and Miyake, 2000). The boundaries between induced and non-induced cells will determine the final size and shape of the condensation centers, and hence, also of many bones (Rice and Rice, 2008). The condensation of cells continues until the aggregate reaches the adequate size for its differentiation, then, condensation stops and differentiation begins. However, if the condensation center is too small, differentiation does not begin and the bone does not form at all; if too big, the condensation will form a larger bone (Willmore et al., 2007); still, development can buffer these defects with more cell migration and mechanisms that regulate cell population size.

During differentiation, cells within a center of ossification change their identity as matrix deposition proceeds (osteoblasts become osteocytes and chondroblasts become chondrocytes) and the future bone grows in size. The process of differentiation is an essential step in the development of skull bones that occurs due to up-regulation of tissue-specific genes[1] (Hall and Miyake, 2000).

1.1.1 Formation of Skull Bones

Mesenchyme condensations differentiate into skull bones either by intramembranous or endochondral ossification. In general, condensations from neural crest cells differentiate via intramembranous ossification, while condensations from mesodermal cells differentiate via endochondral ossification (Hall, 2005). However, bones formed by both mechanisms are indistinguishable in the adult; moreover, some individual bones comprise both kinds of bony tissue without trace of their origination mechanism or cellular type Kardong (2005); Gilbert (2006). Furthermore, condensations can also split, produce a boundary of apoptotic cells between them, and form more than one bone (e.g., the paired frontals in some species).

In intramembranous ossification, mesenchyme condensation centers differentiate directly to osteoblasts (Hall, 2005). After induction, osteoblasts secrete an extracellular matrix (of collagen-proteoglycans) that is able to bind calcium; osteoblasts embedded in the calcified matrix become osteocytes. First, the calcium deposition is amorphous, but after the calcification of the initial condensation, this process continues forming spicules that radiate out from the region where ossification began. Afterwards, mesenchyme cells surrounding the ossified region form the periosteum (the membranous coating of the bone). Cells on the inner surface of the periosteum also become osteoblasts that will produce bone within the membrane. Once formed the periosteum, bones can grow in thickness, but they do mainly in width by new bone deposition at their edges–changing in shape. Other tissues and cavities encapsulated by bones (e.g., dura mater and oral cavity) also stimulate bone growth, by means of transcription factors from the epidermis and activate bone-specific proteins in the extracellular matrix (Gilbert, 2006). Bones grow in size until they meet others and form a suture (Fig. 1.2).

[1] Up-regulation is the process by which a cell increases the quantity of a cellular component, such as RNA or protein, in response to an external variable; Down-regulation is the decreasing of cellular components.

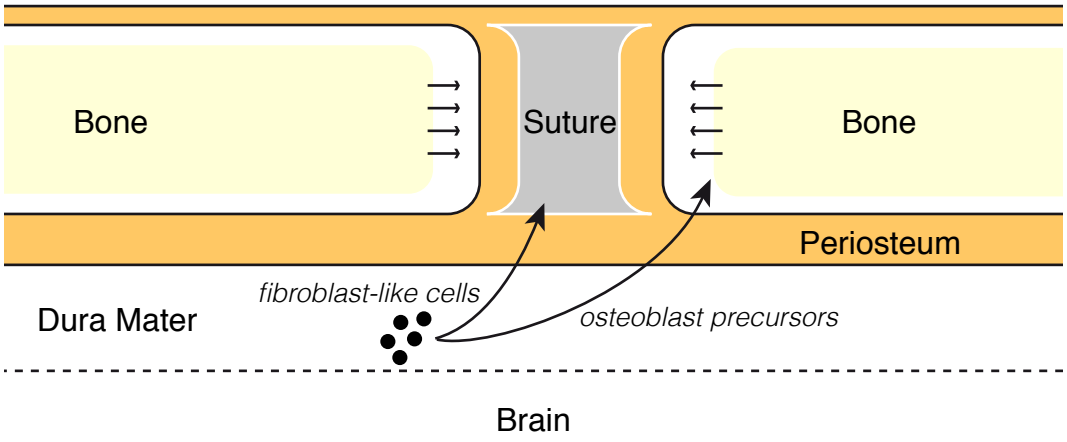

Figure 1.2: Schema of the sagittal suture anatomy. Sutures form in the meeting line between two bones late in development, when bones are already formed. The space between bones is occupied by fibroblast-like cells, which maintain suture patency. The balance between populations of different cell types (by proliferation and apoptosis) regulates suture patency and new bone formation; in this regulation, intercellular signaling and transduction of tensional forces are equally important. Sutures between the bones that protect the brain have an underlying dura mater, which supplies cell precursors to the growing bones and the fibrous tissue between them; interaction with the dura mater also regulates suture patency. However, most sutures lack of an underlying dura mater; in these, the periosteum, or other tissues, would function in the same manner that the dura mater supplying stem cells (see Rice, 2008, for a review of the factors affecting suture maintenance and fusion, as well as associated malformations because of premature fusions in humans).

In endochondral ossification, bones form from cartilage templates (Hall, 2005). Condensed cells first differentiate into cartilage and then are replaced by bone. Endochondral ossification has five steps: (1) determination of mesenchyme as future cartilage, (2) differentiation into chondrocytes, (3) proliferation and formation of the cartilage template of the bone, (4) matrix hypertrophy to enable mineralization, and (5) blood vessel invasion that brings new osteoblasts and chondroclasts to replace death chondrocytes. In each step, specific transcription factors, membrane adhesion proteins, and secreted enzymes participate in the induction-response signals between cells and prepare the template for ossification (Gilbert, 2006). Endochondral bone growth occurs both inside and at the boundaries of the cartilage template: inside, osteoblasts begin to form bone matrix and differentiate into

bone cells (osteocytes and osteoclasts); in the boundaries, new bone is formed in the perichondrium (equivalent to the periosteum) by replacement of chondrocytes as described before. Additionally, secondary ossification centers appear at the end-margins of bones. Cartilage growth plates appear between the primary and the secondary ossification centers (epiphyseal) forming new bone as in primary ossification centers. Thereby, bones can grow while keeping functional articulations. Furthermore, cartilage growth plates form also between bones (synchondrosis) forming new bone by replacing cartilage in a similar way (e.g., between the sphenoid and the occipital in humans).

Both type of bones change in shape after their formation by remodeling their boundaries, in response to cellular signals, external forces coming from other bones and tissues, and, exceptionally, also from the environment (e.g., sleep positions can cause deformities in newborns). There are three remodeling processes depending on the coordination of bone deposition and replacement at the suture sites: drift, displacement, and rotation (reviewed in Lieberman, 2011). In drift remodeling, new bone forms in one side by osteoblasts (apposition), while osteoclasts remove bone in other sides (resorption); this occurs usually in opposed sides of the bone. If the rates of bone apposition and resorption are well coordinated, then the bone drifts–as a tectonic plate–without a change in thickness. This type of remodeling is common in bony walls (where bones form the boundaries of skull cavities), for example, between the nasal floor and the palatal roof. (Enlow and Bang, 1956). Differences in the rates of apposition and resorption cause changes in thickness and shape. An example of this is the displacement remodeling, in which bones grow at one side but they are not removed in other sites; as a consequence, bones increase in size and change in shape. Finally, the combination of drift and displacement can also cause the rotation of bones; here, the regions of apposition and of resorption are not opposed but adjacent, creating an axis of rotation.

In summary, intramembranous ossification forms most bones of the skull in a cartilage-independent process, while some skull bones (e.g., those of the cranial base) are formed by replacement of cartilage templates. Therefore, the initial shape of intramembranous bones depends on the direction and speed of growth, whereas the initial shape of endochondral bones depends on the cartilage template. In addition, changes in shape occur also after formation by remodeling at the boundaries of bones (cranial base synchondrosis and craniofacial sutures).

1.1.2 Development of Craniofacial Sutures

Craniofacial sutures are fibrous joints that connect most bones of the tetrapod skull (Fig. 1.3). Sutures are formed when and where two bones meet; this is determined by factors that regulate bone growth, as well as the position and number of ossification centers. Once formed, sutures act as primary sites of bone growth (proliferation of osteoblasts, differentiation, and bony matrix deposition) and as mechanical stress absorbers (Rice, 2008).

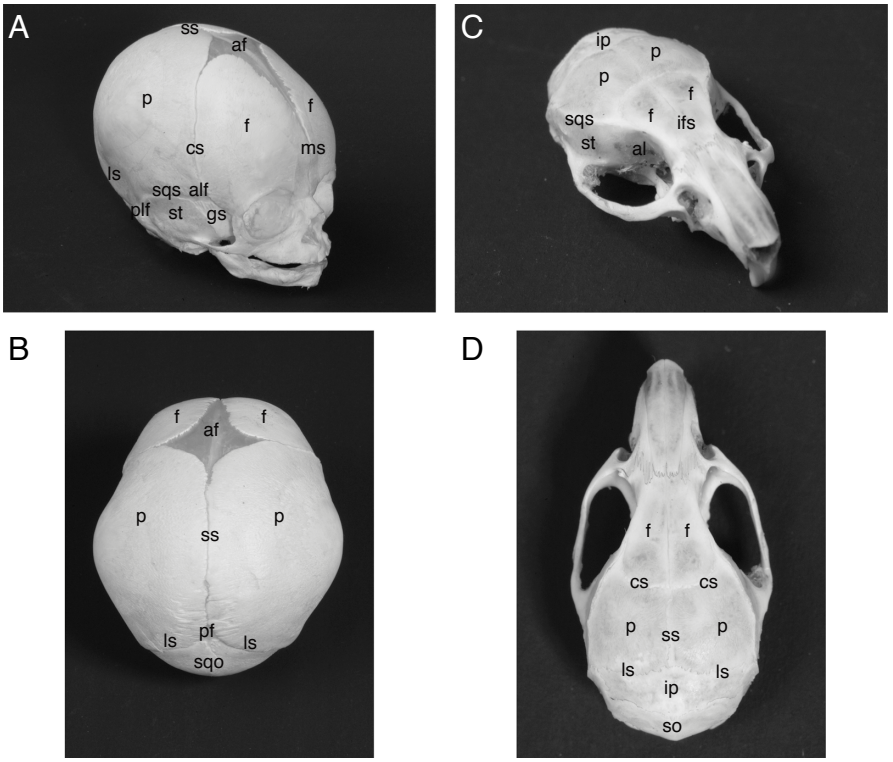

Figure 1.3: Calvarial bones, sutures, and fontanelles in human and mouse. A and B) Neonate human. C and D) Mature mouse. *Labels: af, anterior fontanelle; alf, anterior lateral fontanelle (sphenoidal); al, alisphenoid bone; cs, coronal suture; f, frontal bone; gs , greater wing of sphenoid bone; ifs, interfrontal suture; ip, interparietal bone; ls, lambdoidal suture; ms, metopic suture (interfrontal); p, parietal bone; pf, posterior fontanelle; plf, posterolateral fontanelle (mastoid); so, supraoccipital bone; sqo, squamous part of occipital bone; sqs, squamosal suture; ss, sagittal suture; st, squamous part of temporal bone.* From Rice (2008).

The proper functioning of sutures depends on their maintenance and their occlusion (obliteration) at the right time. Sutures of the calvaria are more likely to fuse during adulthood, whereas facial sutures keep their patency throughout life (the reason may lie in their role as stress absorbers of forces generated during mastication). The fusion of two bones prevents further growth at that location; the growth of bones in other locations of their boundaries (compensatory growth) generates characteristic changes in the shape of the skull (Fig. 1.4).

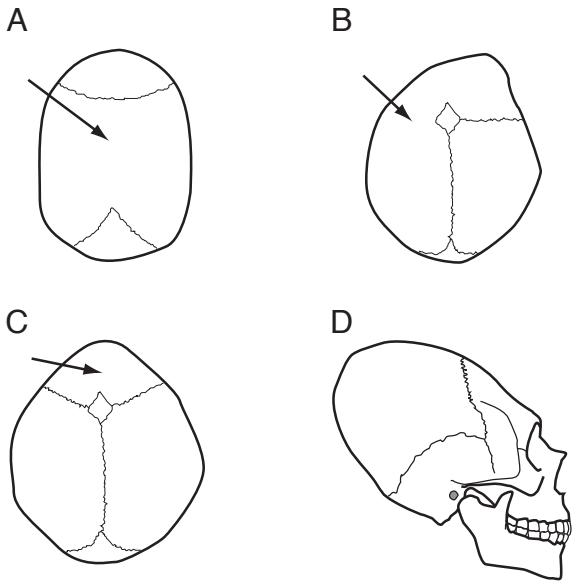

Figure 1.4: Skull malformations due to premature fusion of bones in humans. A) Scaphocephaly by premature fusion of the sagittal suture. B) Plagiocephaly by premature fusion of the hemicoronal suture. C) Trigonocephaly by premature fusion of the metopic suture. D) Turricephaly by premature fusion of the coronal and the lambdoid sutures. From Lieberman (2011).

1.1.3 The Functional Matrix Hypothesis

Bones are the hardest and most perdurable components of the head, and yet they are malleable enough to change in size and shape during development and evolution, varying in morphology and coopting new functions. The coordinate variation of the components of the head emphasizes its integration at genetic, developmental, and morphological lev-

els. In this context, it is useful to briefly introduce one hypothesis that seeks to explain the causes of morphological variation during head development, skull bone growth, and suture patency: the functional matrix hypothesis (Moss and Young, 1960; Moss, 1962). Its relevance for the study of the tetrapod skull morphology resides in two points: first, it represents an epigenetic, externalist explanation against the previous idea stating that genetic factors determine completely bones development and growth; second, its success in explaining many craniofacial disorders by biomechanical induction, for example, malformations of the brain, such as bigger size (hydrocephaly), smaller size (microcephaly), and absence of brain (anencephaly), are related to the formation of skulls that fit these modified brain cavities (Lieberman, 2011). This also explains the great acceptance of the functional matrix hypothesis in the medical community.

The functional matrix hypothesis claims that functional units, which are groups of different tissues and cavities interacting to perform a function, are the proximate causes of the development and growth of skull bones, as well as the formation, maintenance, and obliteration of sutures. Examples of functional matrices are the brain, the eyeballs, the nasal cavity, the oral cavity, and the tooth roots. Here, the role of bones is just to accommodate these matrices (i.e., other tissues and organs) with a proper shape and size that permit to carry on the function at hand. By secondary compensatory growth, the skull accommodates the demands of its neighboring non-skeletal tissues and functional cavities. Thus, bones develop passively in response to requirements of the surrounding tissues and organs; bones play no active part in their own development and evolutionary change. In summary, form follows function. In its first proposal, the hypothesis stated the exclusivity of epigenetic factors in morphogenesis of bones, but this strong claim has been moderated after evidences of genetic regulatory mechanisms acting in skull ontogeny, which were introduced to the central corpus of the hypothesis more recently (reviewed in Martínez-Abadías, 2007).

On the other hand, the discovery of intrinsic genetic regulatory factors affecting location and differentiation of bones and sutures challenged the claim that functional matrices are the only actors in skull morphology (Lieberman, 2011). Moreover, analysis of shape correlations pointed out strong interactions between bones that cross (participate in) multiple functional matrices; thus, challenging again the idea of discrete functional matrices as cranial units of change, because they share many of their components that overlap. In addition, some skull morphologies remain invariant even when functional matrices are modified, for example, in the orbits of mammalian skulls, where the angle between the

long axis and the midline of the face is always 90°, independently of changes in the size of brain, eyes, and oral cavity (Lieberman, 2011).

Taken in perspective, the FMH points out the relevance of epigenetics in skull development, the role of mechanical and chemical inductions between tissues, and the developmental integration of the skull because of epigenetic and genetic factors. Indeed, all these aspects are essential to explain the evolvability and the evolution of the skull.

1.2 The Evolution of the Skull

The skull of tetrapods is a mosaic structure in many senses. Its bones have different ossification mechanisms and different cellular origins, mixed in many individual bones (see 1.1); in addition, different regions of the skull have also different evolutionary origins and phylogenetic histories. This section introduces the general evolution of the tetrapod skull according to the principal reference textbooks (Hildebrand, 1988; Benton, 2005; Kardong, 2005).

Three regions are usually identified in the vertebrate skull: the chondrocranium, the dermatocranium, and the splanchnocranium (see Kardong, 2005, Chapter 7). In modern forms of terrestrial vertebrates, parts of chondrocranium and dermatocranium are integrated in various structures and in some individual bones. The splanchnocranium, the first structure in evolutionary origin, is a skeletal structure associated with gills and jaw elements in gnathostomes. The chondrocranium, second in origin, is a cartilaginous structure that supports and protects the brain. Finally, the dermatocranium is a bony head shield in early gnathostomes that derived into dermal bones in terrestrial vertebrates. The position of the posterior elements of the chondrocranium, in direct contact with the cervical vertebra, as well as their ossification mechanism and shape, suggested to the early anatomists a vertebral origin of these elements and, by extension, of all the skull. Johann Wolfgang von Goethe, Lorenz Oken, or Richard Owen among others, proposed that skull bones are just modified vertebrae, a continuum in the serial homology of the vertebrate body plan; this was rejected also by equally distinguished naturalists, such as Louis Agassiz, George Cuvier, or Thomas Henry Huxley. However, some recent studies suggested that at least for some parts of occipital bones a vertebral origin is possible (reviewed in Kuratani, 2005).

The first vertebrates that developed a skull-like structure were the ostracoderms, a group of jawless fishes (Agnatha) that lived during the Ordovician-Devonic Period (488-420 Ma ago). This structure consisted in a shield of dermal bones overlying the head,

with a primitive lateral line system, or a similar sensory organ, furrowing these dermal bones. Some of the first gnathostomes (Placodermi and Acanthodii) also had head shields composed of dermal bone plates and well ossified braincases, with the jaw attached to it; while others (Chondrichthyes), had no bones at all and lacked a dermatocranium. Instead, chondrichthyans have a highly developed chondrocranium that provides the scaffold for ethmoidal and orbital structures. On the other hand, the skull of bony fishes (Osteichthyes) posses a complete dermatocranium composed of small and medium size bones. In successive radiations, bony fishes evolved toward more freedom in bone articulation, which allowed their movement and functional diversification. For instance, teleost fishes (Actinopterygii) perform suction feeding by multiple kineses between jawbones, maxilla, and premaxilla. Most homologous bones in the skull of tetrapods appeared for the first time in bony fishes. Thus, the skull of sarcopterygian fishes (Sarcopterygii) resembles in topology and articulation to those found in actinopterygians. In addition, the ancestors of tetrapods, lobe-finned fishes (Rhipidistia), possessed some novelties in the skull configuration; for example, the separation of two discrete units in the braincase, the ethmoidal and the otioccipital, joined together by a flexible articulation.

Early tetrapods evolved from rhipidistian fishes during the Middle Devonian (400 Ma ago). They inherit many skull features from their ancestors; however, early tetrapods have also novel features in the skull, more suitable for a terrestrial environment, such as one pair of nasal bones, stapes bones (related to hearing, but still too massive to do it), and lack of opercular bones covering the lost gills. In addition, freedom of bone articulation (gained in the evolution of bony fishes) decreases in early tetrapods; this reduction occurs because of the tight association between the bones of the chondrocranium and dermatocranium. Thus, the skull became more robust and compact, restricting movements between bones. Nevertheless, early tetrapods still keep some skull features that reveal their aquatic past, for example, the lateral line system in juveniles with aquatic development. Other features not related to the skull are also linked with this aquatic ancestry, for example, reproduction by laying eggs in water.

In modern amphibians (Lissamphibia), the skull has fewer and thinner bones than in primitive tetrapods. For instance, in albanerpetontids (Albanerpetontidae), frontal bones are fused and the prefrontal bones are lost; in salamanders (Caudata), the bones of the braincase are fused with parietals; in frogs (Salientia), bones are thin, only partially ossified, or they do not ossify at all; however, in caecilians (Gymnophiona), fusions and losses of bones produced skulls highly ossified and compact.

In primitive amniotes, the skull comprises an extensive cover of dermal bones and a relatively small interior braincase. Temporal openings are the most relevant feature of the skull in amniotes; each major group of amniotes has a different number of openings: none in anapsids, two in diapsids, and one in synapsids (Fig. 1.5). Temporal openings serve as attachment for muscles and reduce stress forces from jaw and neck movements; in taxonomy, temporal openings define taxa within amniotes.

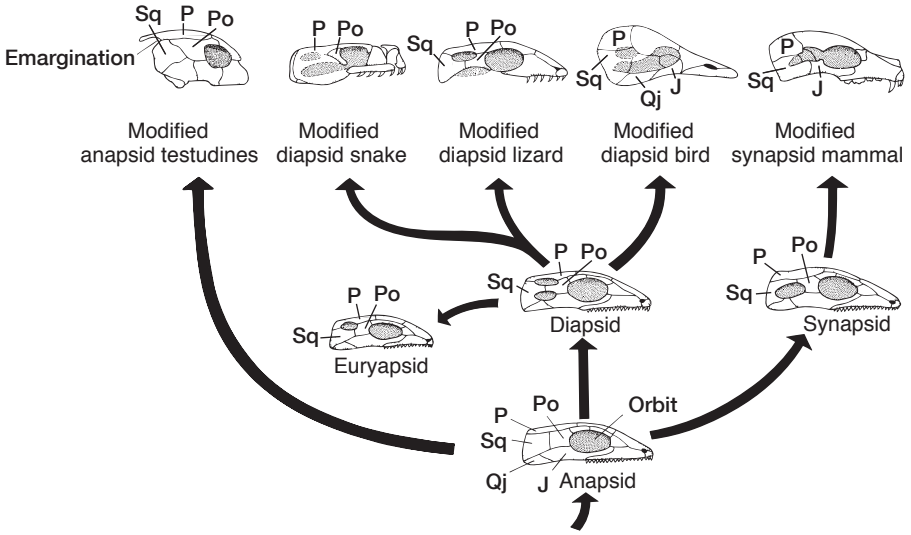

Figure 1.5: Types of temporal openings in tetrapods. Modified from Kardong (2005).

The anapsid skull, like that of turtles (Testudines and extinct relatives), lacks of temporal openings. Instead, modern terrestrial turtles (Polycryptodira) possess temporal emarginations that function as temporal openings. Mainly because of the lack of temporal openings, the phylogenetic position of turtles has been traditionally controversial. The place of turtles within the amniotes varies depending on the nature of data used for classification (molecular, developmental, or morphological) and the inclusion, or not, of extinct species (reviewed in Laurin and Gauthier, 2012). Thus, morphological and fossil studies usually place turtles as a basal group in Amniota; here, the temporal openings are a plesiomorphy, the ancestral state found in basal tetrapods. Another popular hypothesis based on morphological data places turtles as a sister group of Diapsida; developmental data support this hypothesis (Rieppel, 1995; Werneburg and Sánchez-Villagra, 2009). On the other hand, molecular data tend to place turtles within Diapsids, either as a sis-

ter group of living Lepidosaurs or living Archosaurs; here, the temporal openings are an apomorphy, a character reversal of the diapsid condition found in their common ancestor.

The diapsid skull, characteristic of Diapsida (lepidosaurs, crocodiles, birds, and extinct relatives), has two temporal openings: a lower one, formed by the jugal, the postorbital, and the squamosal; and an upper one, formed by the parietal, the postorbital, and the squamosal. Some modern forms lack the lower and/or upper temporal bars, which generates new configurations of the temporal opening that deviate from the original diapsid pattern. In snakes, the loss of contact between the postorbital and the jugal merges the lower temporal opening with the orbit; this modification permits the mobility of bones anterior to the orbits (prokinesis). In lizards, the lower temporal bar is lost, so there is only the upper opening; this modification permits the mobility between the neurocranium and the outer dermatocranium (mesokinesis). In birds, the skull diverges greatly from the basic plan because of the high amount of fusions and losses of bones and the encephalization of the cranial vault; in addition, as much as in the post-cranial skeleton, these bones are lighter and thinner than in their extinct relatives (which is advantageous for flight). The three modified diapsid skulls have an extra cranial kinesis (streptostyly) by which the quadrate can rotate in relation to the dorsal braincase (see Kardong, 2005, pg. 260-270 for an extensive description of skull kinesis and biomechanical mechanisms). A fourth type of configuration appeared, independently, in different groups of marine reptiles (Ichthyosaurs, Placodonts, and Plesiosaurs), the euryapsid skull, in which the lower temporal opening is absent, due to the great development of the squamosal-jugal suture sealing it.

The synapsid skull, characteristic of Synapsida (mammals and extinct relatives), has only the lower temporal opening, formed by the jugal, the postorbital, the squamosal, and the quadratojugal. In modern mammals, the postorbital bone is lost, so the temporal opening merges with the orbit; the bar formed by the connection between the squamosal and the jugal forms the zygomatic arch. In addition to the evolutionary change of the temporal opening, synapsids develop a secondary palate. This structure is formed by the growth of premaxillas, maxillas, and palatines toward the midline, forming a mouth roof that separates the respiratory and the oral track. A secondary palate appears also in some turtles and in crocodiles, in which also participates the pterygoid bones, this is a homoplasic character. Like the postorbital, many other bones are lost in modern mammals (e.g., prefrontal, supratemporal, and quadratojugal) as part of a much larger tendency in bone number reduction in vertebrates, an evolutionary trend commonly known as the Williston's Law.

1.2.1 The Williston's Law

The tetrapod skull has suffered many and different morphological changes during its evolution in diverse lineages, for example, enlargement and shortening of the rostrum in porpoises and humans (Lieberman, 1998; Galatius et al., 2010), miniaturization in lizards and anurans (Rieppel, 1984; Trueb and Alberch, 1985), and expansion of the cranial vault in birds (Marugán-Lobón and Buscalioni, 2003; Bhullar et al., 2012). However, the reduction in number of skull bones has occurred in all lineages since the origin of the skull in vertebrates. For instance, early tetrapods have fewer skull bones than fish ancestors, while amniotes have fewer than early tetrapods (Benton, 1990). This trend was first described by Samuel W. Williston (1914) as *"a law in evolution* [by which] *the parts in an organism tend toward reduction in number, with the fewer parts greatly specialized in function,"* during his studies on the skull of Permian reptiles. William K. Gregory further reported this trend from basal fishes to modern tetrapods, proposing losses and fusions of bones as its driving mechanisms (Gregory, 1927, 1929, 1933, 1934, 1935). To further explain this trend, Gregory proposed the principle of anisomerism: the tendency of systems composed of many similar parts (polysomerism) to reduce the number of parts by specialization of the remaining ones. A similar idea, *the instability of the homogeneous*, was proposed by Herbert Spencer (1889) as a law in evolution and of change in general: a system composed of homogeneous parts transforming into a system with heterogeneous parts by integration and differentiation. Furthermore, both Williston and Gregory rejected the possibility of new bone formation, or in any case, they thought this to be a very rare event that does not affect the general trend.

The Williston's Law has been supported as a large-scale evolutionary pattern within and between major groups (Table 1.1); from primitive to modern species, the number of skull bones decreases affecting often the same bones, such as the postfrontal, prefrontal, and supratemporal (Goodrich, 1958; Estes, 1961; Gaffney, 1979; Carroll, 1988; Benton, 1990; Rieppel, 1993; Laurin, 1996; Sereno, 1997; Sidor, 2001; Kardong, 2005). These parallels suggest that Williston's Law is both an anagenetic and a cladogenetic evolutionary trend. In an anagenetic (or phylogenetic) trend, evolutionary change occurs along a non-branching lineage, in the successive transition of species. Stephen J. Gould criticized the existence of anagenetic trends from the perspective of the Hypothesis of Punctuated Equilibrium (Gould and Eldredge, 1977). Since lineages would not change in its lifetime, morphological change only occurs during speciation events; thus, anagenetic trends are nothing but illusions of accumulated cladogenetic processes (Alberch, 1980; Gould, 1990).

In a cladogenetic trend, evolutionary changes occur in the branching (speciation) of lineages, which change in the same direction on average (McKinney, 1990). In addition, evolutionary trends are classified as passive or driven according to their pattern of change (McShea, 1994). In passive trends, the initial state of the character (e.g., number of bones) originates close to a lower or higher boundary; thus, an increase of variance alone can cause a directional evolutionary pattern, emerging without a driving force (Gould, 1988). For skull bone number, the evolutionary pattern would be characterized by a decrease in the mean and the minimum number of bones at each time, but without extinctions of lineages with a number of bones close to the maximum in origin. On the other hand, in driven trends some mechanisms actively push the character change in one direction, such as directional changes of the environment shaping the topography of the adaptive landscape in one direction (e.g., in Bergmann's and Cope's rules) and developmental canalization (Rasskin-Gutman and Esteve-Altava, 2008; Esteve-Altava and Rasskin-Gutman, 2009). This would generate an evolutionary pattern in which mean, maximum, and minimum number of bones decreases at each time, as well as within lineages.

Traditionally, Williston's Law has been interpreted as an evolutionary trend toward simplification of the skull (Hildebrand, 1988; Sidor, 2001), a counter-evidence of the progressive increase in complexity during the history of life (Williams, 1966, pg. 43). However, measuring morphological complexity is tricky (see 3.1); too often, the number of different elements, or a derived metric, is the direct measure of complexity (Bonner, 1988; Valentine et al., 1994; Sidor, 2001), a practice that has been used even though this approach has been explicitly discouraged (McShea, 1991, 1993).

The evolutionary mechanisms that account for the reduction in number of bones in the skull are the loss and the fusion of bones (Sidor, 2001). These two mechanisms occur at different rates, target different bones, and involve different developmental processes. Some authors agree that the broadly occurrence of this trend in the phylogeny of tetrapods reflects a process of canalization (Benton, 1990). Thus, miniaturization of the skull would provoke a reduction in the number of bones until a minimal functional number is reached (Rieppel, 1984); throughout this process, Riepple argues, the skull loses first non-essential bones to keep its structure.

Other internal causes can be argued as well to explain bone number reduction, such as developmental shifts and constraints (see, e.g., Alberch and Gale, 1985). For instance, heterochrony in craniofacial sutures maintenance or obliteration (Depew et al., 2008), and retardation (until loss) of ossification centers (Benton, 1990). On the other hand, it has been argued that the reduction in bone number would have a selective advantage

by promoting more rigid skulls, because the concomitant loss of sutures would reduce bone mobility (kinesis), buffering mastication stress forces (Sidor, 2001). All in all, the net reduction in bone number is a developmentally biased process that assumes that the emergence of new bones is highly improbable (if not impossible), because disruptions in the development of ossification centers is easier than the formation of new ones (Sidor, 2001). However, studies of comparative anatomy and development of the skull have neither found the causes and mechanisms of this bias, nor what are the commonalities among all these bones that are lost or fused (this questions have been addressed in Chapter 9).

Table 1.1: Skull bones commonly absent in tetrapods according to different authors: [1]Gaffney (1979); [2]Hildebrand (1988); [3]Benton (1990); [4]Sidor (2001); [5]Benton (2005); and [6]Kardong (2005). From Esteve-Altava et al. (2013b).

Transitions	**Lost Bones***	**Fused Bones**
Rhipidistians to Early Tetrapods	Extrascapular, Extranasals, and Opercular (6, p 258)	
Early Tetrapods to Modern Amphibians	Squamosal (3); Ectopterygoid, Jugal, Postfrontal, Postparietal, Prefrontal, Quadratojugal, Stapes, and Tabular (3; 6, p 258); Intertemporal, Lacrimal, Nasal, and Postorbital (6, p 258)	Frontals, Parietals, and Parietal-Braincase bones (5, p 102)
Primitive Amniotes to Derived Turtles	Epipterygoid, Nasal, and Quadratojugal (1)	Basisphenoid-Parasphenpid, Epipterygoid-Parietal, Frontal-Nasal, Frontals, and Premaxillas (1); Vomers (1; 5, p 231); Basioccipital-basisphenoid (5, p 114)
Primitive Amniotes to Archosaurs, including Birds	Vomer (5, p 267); Postfrontal, Postorbital, Postparietal, Prefrontal, Stapes, and Tabular (6, p 269)	Jugal-Postorbital (5, p 270), Nasals (5, p 216); Parietal-Frontal (5, p 211), Premaxillas (5, p 266, 270)
Primitive Amniotes to Derived Squamates	Epipterygoid (3); Jugal (3; 6, p 266); Lacrimal (3; 5, p 243; 6, p 266); Quadratojugal and Squamosal (3; 5, p 233, 243; 6, p 266); Postfrontal and Tabular (6, p 266)	Parietals (3; 5, p 233); Premaxillas (5, p 233)
Primitive Amniotes to Derived Mammals	Parasphenoid (2, p 149), Quadratojugal (2, p 149; 6, p 272); Ectopterygoid, Orbitosphenoid, Septomaxilla, and Supratemporal (4); Jugal (5, p 329); Postfrontal, Postorbital, and Prefrontal (2, p 149; 4; 6, p 272); Tabular (4; 6, p 272); Postparietal and Stapes (6, p 272)	Ectopterygoid-Pterygoid (2, p 149); Alisphenoid-Epipterygoid, Basioccipital-Exoccipital-Supraoccipital, Basioccipital-Basisphenoid-Parasphenoid, Exoccipital-Interparietal, Frontals, Interparietals, Jugal-Maxilla, Jugal-Squamosal, Nasals, Opisthotic-Supratemporal, Premaxilla-Maxilla, Premaxilla-Septomaxilla, Premaxillas, Pterygoids, Quadrate-Quadratojugal, and Vomers (4); Ophisthotic-Prootic-Squamosal (4, 6, p 274); Parietals (4; 5, p 290)

**Discriminating between genuinely lost bones and fused ones is a very hard task, especially in fossil skulls. Thus, fused bones column includes only those bones explicitly indicated as such in the literature used, while lost bones column includes all bones with an uncertain evolutionary fate.*

2

The Analysis of Organismal Form

Organismal form is the result of many processes acting at different levels of organization during morphogenesis, from the genes that codify and regulate the expression of different proteins involved in cell migration, division, and differentiation, to the geometric and developmental constraints involved in the epigenetics that carry the embryo toward a stable form often identified as the adult (Müller and Newman, 2003; Hallgrimsson and Hall, 2011). Constructional approaches have also been used to study the causal elements of organismal form (see Seilacher, 1991; De Renzi, 1997, 2009a,b). Form is a rich concept that includes not only the shape of anatomical parts, but also their size, arrangement, and relative orientation of these parts. In sum, these morphological features can be seen as different levels of morphological information that, together, account for the actual form of organisms. Thus, a separate analysis permits the identification of specific processes of each level, which otherwise would be hidden to observation because of multiple layers of simultaneous information (Rasskin-Gutman and Buscalioni, 2001).

2.1 Levels of Morphological Information

The levels of morphological information[1] are four: *proportions*, *articulations*, *orientations*, and *connections* (Rasskin-Gutman, 1995); each level has associated its own morphological descriptors, formalization, and type of morphospace (Table 2.1). Since levels of morphological information rely on different descriptors, each one needs a different formalism. Moreover, each level gives insights about level-specific constraints and mechanisms that generate form and affect its evolution (Rasskin-Gutman and Buscalioni, 2001). Thus, they provide also different sources of morphological information for comparative analysis.

[1]These levels were originally termed as *levels of morphological organization* (Rasskin-Gutman, 1995; Rasskin-Gutman and Buscalioni, 2001; Rasskin-Gutman, 2003). Instead, I have preferred to call them levels of information, using the term organization only in a system context as in Chapter 3.

However, current morphological studies focus mostly in the level of proportions (i.e., size and shape), in part, because morphometrics provides a robust methodological framework of analysis for proportions, such as in Geometric Morphometrics. In contrast, the lack of specific quantitative tools has neglected the study of the other levels of morphological information.

Table 2.1: Levels of morphological information according to Rasskin-Gutman (1995).

Level	**Descriptor**	**Formalization**	**Morphospace**
Proportions	Element	Character Matrix	Hyperspace
Connections	Compound	Boundary Patterns	Connectospace
Orientations	Compound	Angles, Positions	Dispospace
Articulations	Mechanism	Angles, Distances	Conformationspace

2.1.1 The Level of Proportions

The level of proportions deals with the analysis of shape and size. Usually, the analysis of shape focuses on a particular region that falls within a more complex anatomical system, such as the nasal cavity (Bastir et al., 2007) or the cranial base of the skull (Bastir et al., 2008). In others, the analysis focus on isolated bones (Lockwood et al., 2002; Harvati, 2003) or entire anatomical systems (Lieberman et al., 2007). In contrast, the analysis of size focuses on entire organisms to look for allometric relationships (West et al., 1997), ecogeographic correlations (Esteve-Altava and Rasskin-Gutman, 2009), and evolutionary trends (Alroy, 1998). For methodological reasons, body mass often replaces body size in these analyses.

In modern Geometric Morphometrics (Fig. 2.1), morphological descriptors of proportions are coordinates of landmark points located within the shape of an anatomical part and distances between them, which are formalized in matrices of characters. This information is also useful to construct morphospaces (Pierce et al., 2008), to guide phylogenetic analysis (Rohlf, 2002), and to study genotype-phenotype relations (Martínez-Abadías et al., 2012), as well as to establish patterns of morphological integration and modularity (Klingenberg, 2009). Since landmark points represent the 'same' points in related structures, the analysis of proportions is only possible between close related forms. Thus, beyond certain degree of dissimilarity, as in very distant species, landmark based methods cannot be used.

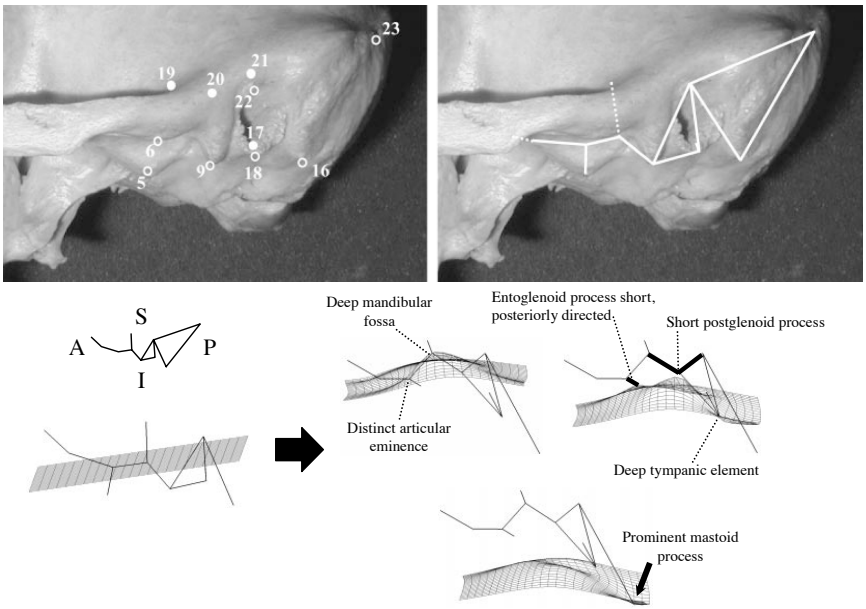

Figure 2.1: Analysis of form at the level of proportions. In this example, information of proportions in the human temporal bone was gathered using a landmark-based approach, in which shape and size were captured by the particular position of each landmark point, and then formalized as a matrix of coordinates (i.e., characters). Modified from Lockwood et al. (2002).

2.1.2 The Level of Connections

The level of connections captures the topological relations between anatomical parts, that is, their arrangement in a morphological system. Anatomical elements are the components of morphological systems of higher order; their contacts define their boundaries, which usually have developmental and functional roles (Rasskin-Gutman and Buscalioni, 2001; Rasskin-Gutman, 2003, 2005). In addition, topological arrangements between anatomical parts are structural relations essential to recognize homologies and novelties. These connectivity relations configure a framework of analysis of morphology at a structural level, in which we can define the connectivity pattern of parts as the number and the distribution of its connections to other parts. In this context, topological arrangements (connections) are not only formal boundaries, but also capture biological interactions and dependences between parts (Riedl, 1975).

The descriptors of form at the connectivity level are the discrete anatomical units that compose the system and the relations between them (Fig. 2.2). Morphological connections

are formalized in adjacency matrices, in which rows and columns represent elements and the presence or absence of a common boundary between two elements is noted as 1 or 0 respectively. Formal models for this information, for example, Cellular Automata and Graph Theory, have been classified as *Parameter Free-Models* because of their lack of generative parameters and geometric constraints (Dera et al., 2008). This feature makes the connectivity level suitable for comparative studies at higher taxonomic levels, in contrast with the level of proportions, which depends on the structural similarities to compare landmark coordinates (see 2.1.1). Thus, morphological connectivity has been used to analyze the evolution of structural patters and morphospaces occupation in skeletal systems across very different taxa, such as pelvic girdles, limbs, and skulls (Rasskin-Gutman and Buscalioni, 2001; Rasskin-Gutman, 2003), as well as echinoderm shells (Laffont et al., 2011), because identifying discrete anatomical units and relations is a straightforward task.

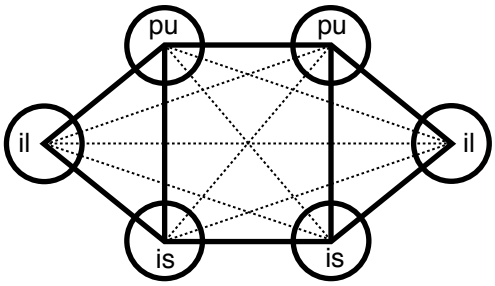

	il	pu	is	il	pu	is	
il	0	1	1	0	0	0	
pu	1	0	1	0	1	0	left
is	1	1	0	0	0	1	
il	0	0	0	0	1	1	
pu	0	1	0	1	0	1	right
is	0	0	1	1	1	0	

Figure 2.2: Analysis of form at the level of connections. The bones of the pelvic girdle and their physical connections (left) are formalized in an adjacency matrix (right); bold lines represent possible connections and dashed lines impossible (i.e., not observed). The adjacency matrix codifies and captures the structural information between anatomical discrete units. Modified from Rasskin-Gutman and Buscalioni (2001).

2.1.3 The Level of Orientations

Besides being connected, two elements can also show different orientations in space. The model descriptors in this level are discrete anatomical elements, which are formalized as angles between parts (Rasskin-Gutman and Buscalioni, 2001). Orientations have been extensively studied for the cranial base flexion in primates (Fig. 2.3).

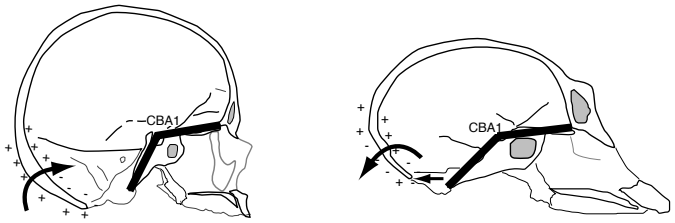

Figure 2.3: Analysis of form at the level of orientation. In this example, the elements of the study are different skull parts, for which relative orientations are formalized by their angles. From Lieberman (2011).

2.1.4 The Level of Articulations

In contrast with the level of connections and orientations, which capture static relationships between anatomical elements, the level of articulations captures dynamical relations between parts that show mobility functions (Fig. 2.4). Although the descriptors are dynamical mechanisms of articulation that define the range of possible positions, the formalization is similar to that of orientation, that is, angles and distances (Rasskin-Gutman and Buscalioni, 2001). The level of articulations capture biomechanic and kinematic systems in functional morphology; for example, those concerned with locomotion, masticatory system, and cranial kinesis (Weishampel, 1995).

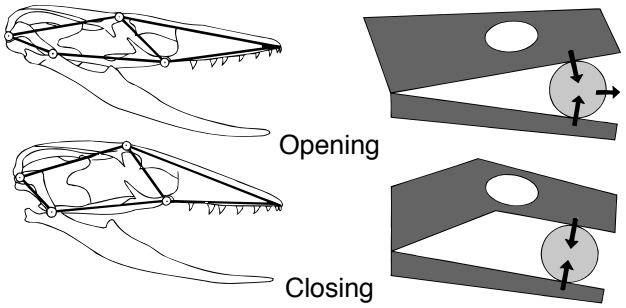

Figure 2.4: Analysis of organismal form at the level of articulation. In this example of the kinesis of a lizard skull, some joints between bones show mobility, endowing lizards with a particular feeding mechanism that allows them to close both tooth rows on the prey. Modified from Kardong (2005), after T. H. Frazzetta.

2.1.5 Causal Relationships between Levels of Information

Levels of morphological information interact during development at each scale of organization (from cells to tissues, parts, and organs to the organism) determining the final form of an organism (Fig. 2.5). For instance, in the formation of the tetrapod limbs (Rasskin-Gutman, 2003):

> *"The initial state of a developing limb bud is a proliferation of mesenchymal cells. The shape and size of the individual cells determine relations of connectivity among them, which are prominent at this stage. The resulting mass of cells, packed together, forms a bud. Thus, the connectivity properties of the individual cells generate a higher level of organization, the limb bud, which exhibits, on its own, properties of proportion (size and shape) far removed from the proportions exhibited by the individual cells. In turn, the proportions of the limb bud determine the number and position of cell condensations that appear in the mesenchyme of pre-cartilage areas, forming the primordia of future bones of the limb, which start to assume identities of their own. Later, each condensed pre-cartilage center shows a preferential orientation as well as connectivity relations at a new organizational level; where the future bones are the new elements, and the individual cells are no longer suitable to describe the system."*

Causal relationships are more explicit between connections of anatomical parts and their proportions. Since parts tend to evolve and develop in coordination with other connected parts, shape variations are not independent between them. More specifically, landmark positions, whose covariation is used to analyze shape changes, are not independent as is commonly assumed; instead, landmark covariation is constrained by the connections of the parts on which they are located (Chernoff and Magwene, 1999; Magwene, 2001, 2008; Klingenberg, 2009). However, a more general causal relationship between each level of morphological information has never been tested empirically. In this context, the use of networks and connectivity considerations in shape analysis is just a starting point to study the relationships between all levels. In fact, as the quoted example points out, causal relationships appear at each level of morphological organization. Thus, developmental constraints between connections, proportions, orientations, or articulations have a direct effect on the morphology in the next higher scale of organization.

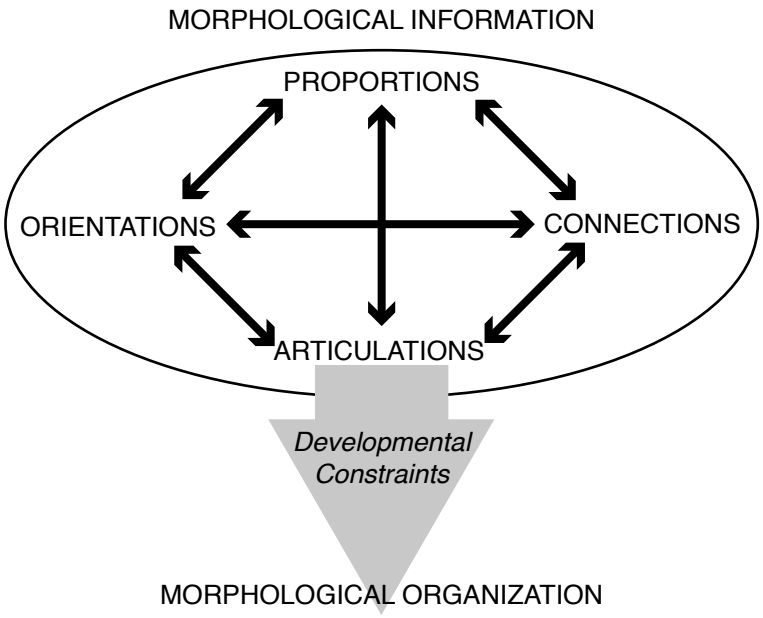

Figure 2.5: Morphological organization and information. At each scale of organization, the levels of morphological information interact with each other by means of developmental constraints (two-way arrows). The nested succession of developmental constraints between levels originates the morphological organization of the next scale, in which the levels of information begin a new set of developmental relations. Modified from Rasskin-Gutman (2003).

2.2 From the *Principe des Connexions* to Networks

Ever since classic anatomists like Johann Wolfgang von Goethe, George Cuvier, Étienne Geoffroy Saint-Hilaire, or Richard Owen laid down the fundamental principles of comparative anatomy and morphology in the 19^{th} century, connections among anatomical elements have been essential for the recognition of biological homologies between anatomical parts in different species. After that, some key authors in theoretical biology and mathematical biology have attempted to formalize the intuitive notion of similarity and morphological organization by means of axiomatic and mathematical models. However, from a historical point of view, it is interesting that the main 20^{th} century authors reviewed here did not acknowledge the work of their predecessors at all, making their contributions to seem disconnected from each other.

2.2.1 Étienne Geoffroy Saint-Hilaire's Principle of Connections

In the early 19$^{\text{th}}$ century, Étienne Geoffroy Saint-Hilaire proposed the use of the 'principle of connections' as a methodological rule to study animal form. A body part in an animal is recognized as the same part in other animals neither by its function nor by its shape, but by its situation and contact with others (Geoffroy Saint-Hilaire, 1818). Thus, the principle of connections formalized the intuitive notion of similarity of those days and set a new research program in pure morphology at the structural level (Nuño de la Rosa, 2012). Other notable naturalists before Geoffroy, such as Pierre Belon, and Johann Wolfgang Goethe, also made use of this principle as a way to recognize similarities, a tradition that goes back to Aristotle. For instance, Goethe used this principle implicitly to point out the presence of an intermaxillary bone in the human mandible (reviewed in Nuño de la Rosa, 2012). However, Geoffroy was the first to establish connections as an operational criterion to identify morphological similarity among different parts and organisms; by means of their structural relations to other parts (Fig. 2.6), rather than by their shape and function. Thus, placing the criterion of structure before function and shape in the recognition of homologies.

With this tool in their hands, Geoffroy and his followers attempted to discover homologies even when the form and function of body parts were different or intermediary forms were unknown, that is, even between body plans and the four *embranchements* proposed by Georges Cuvier (Appel, 1987). For instance, Geoffroy found homologies between the bones of the ear in mammals, reptiles, and birds and those of the operculum in fishes. In Geoffroy's own words *"an organ is sooner altered, atrophied, or annihilated than transposed"* (Appel, 1987). Laurencet and Meyranx used the principle of connections in an essay on the organization of mollusks, suggesting a unification between the vertebrate and cephalopod embranchments; their presentation in the *Académie des sciences* was the trigger that started the famous debate between Cuvier and Geoffroy (Appel, 1987; Le Guyader, 2003). Since the debate, and notwithstanding interpretations of its results (Rosen, 1916; Gould, 2002; Le Guyader, 2003), the principle of connections became a tool to identify homology for prominent zoologists, such as Richard Owen, Milne Edwards, and, more recently, Adolf Remane (Appel, 1987; Ochoa and Barahona, 2009). However, the aim to build a formal framework was abandoned in the following decades, and connections remained just as an heuristic, implicit tool until the mid 20$^{\text{th}}$ century.

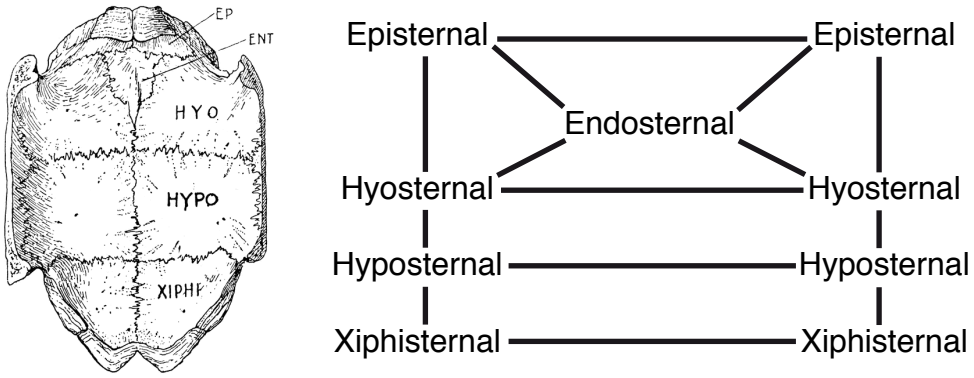

Figure 2.6: Connections between plastron bones. According to Geoffroy, the same invariable arrangement is found in the sternum of birds but fussed in the adult form. Lines indicate connections. Modified from Russell (1916).

2.2.2 Joseph Henry Woodger's Structural Correspondence

In 1945 Joseph H. Woodger proposed a formal framework to deal with phenotypic transformations during development based on correspondences between the parts of an organism (Woodger, 1945). Woodger's aims were to identify similarities between parts of an organism and study phenotypic transformations during development and evolution; to do so, he used Group Theory to codify topological information. Thus, anatomical parts were classified by three grouping rules: (1) *being distal to*, (2) *being postaxial to*, and (3) *being articulated to* other parts. Thus, two parts are the 'same' in different organisms or developmental stages if they establish the same set of relations, that is, if they have 'structural correspondence' (Fig. 2.7).

Just like the principle of connections, structural correspondence captures homology in different organisms identifying 'types' or '*Bauplanë*' (Rieppel, 2006). In this context, Woodger introduced the concept of *Bauplan* to define the *"homologous structural plan underlying evolutionary transformations within a taxonomic group"* (Raff, 1996). Bauplan (plural: Baupläne) is the German word for building plan or blueprint in English, but it is often used as a synonym of body plan or unity of type in a morphological context. Although the concepts of Bauplan and type, as well as the very work of Woodger, received much criticism from advocates of 'population-thinking' in the context of the Modern Synthesis (Simpson, 1961; Mayr, 1982; Hull, 1988), current evolutionary theory can accommodate completely his ideas (Rieppel, 2006; Nicholson and Gawne, 2013). Whatever position we adopt about the ideas proposed by Woodger, his structural formalization of

correspondence was an important step in the search of rational criteria to capture the intuitive observation of similarities (i.e., homology identification) between organisms.

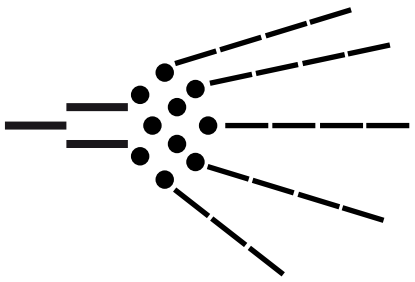

	1*p*	2*p*	3*p*	4*p*	5*p*
level 0	x				
level 1	x	x			
level 2	x	x	x		
level 3	x	x			
level 4	x	x	x	x	x
level 5	x	x	x	x	x
level 6	x	x	x	x	x
level 7	x	x	x	x	

Figure 2.7: Structural correspondences in the tetrapod limb. Lines and dots represent the bones of the limb, which establish different morphological relations with others. The relation of *being distal to* divides the set of bones into nine exclusive sub-sets: from level 0 for those elements that are not distal to any other, to level 8 for those elements that are distal to all others. Then, the second relation, being *postaxial to*, divides each level into four p groups. Thus, each bone in the limb has an unambiguous characterization according to the intersection of rows and columns in the matrix of relations. For instance, the fourth metacarpal is the 4p of level 5 and the ulna is the 1p of level 1. Woodger needed a third relation, *articulating with*, to capture different arrangements when comparing two limbs. Modified from Woodger (1945, Fig. 2).

2.2.3 Nicolas Rashevsky's Relational Biology

Nicolas Rashevsky is known as one of the founders of mathematical biology. His works on relational biology revolved around the integration of organismal functions into a systemic framework based on relations, which he formalized as networks (Rashevsky, 1954). To analyze the changes in functional organization, Rashevsky used the transformations of the networks; a notion inspired by, or at lest related to, the topological transformation introduced by D'Arcy Thompson (Thompson, 1992). Thus, *"the topological spaces or complexes by which different organisms are represented are all obtained from one or at most from a few primordial spaces or complexes by the same transformation, which contains one or more parameters, to different values of which correspond different organisms"* (Rashevsky, 1954); he called this the 'principle of bio-topological mapping' (Fig. 2.8).

Rashevsky was a pioneer in representing the complexity of biological organization by means of Graph Theory, a step beyond the use of Group Theory that we find in Woodger. However, the application of this framework of analysis to morphological systems was only discussed briefly (Rashevsky, 1960). In such a framework, nodes would represent anatomical structures and links functional relations. Although this proposal was very interesting for morphology, it was not further developed neither by Rashevsky, nor by his prominent disciple, Robert Rosen (Rosen, 1991, 2000), or any theoretical morphologists afterwards.

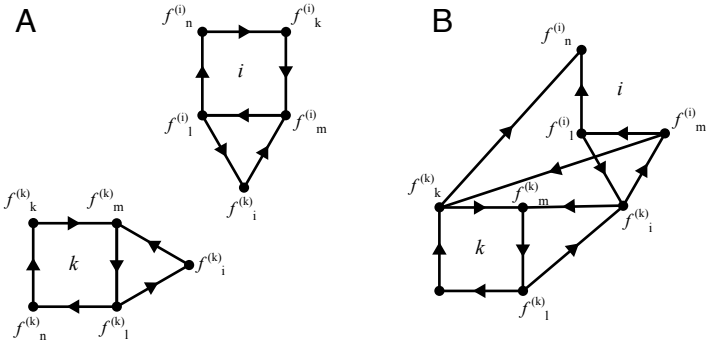

Figure 2.8: Bio-topological mapping between cells. A) Two populations of cells with the same functional organization (i and k). Nodes represent biological functions of the cells and links physiological relations between biological functions. During the development of an organism, tissues differentiate in structure and function, thus *"a biological function which originally is possessed by all cells, is lost by some of them and retained by others"*. B) This is represented by the lost of f_i in k cells and the lost of f_k in i cells. Now functionalities of both populations are coupled. More complicated transformations can be added sequentially. Rashevsky interest was how to *"derive the graph of this organism from the graph of the original homogeneous colony"*, that is, elucidate the logic of these transformations. Modified from Rashevsky (1954).

2.2.4 Rupert Riedl's Diagrammatic Morphotype

It was Riedl (1975) who firstly introduced graph diagrams as a representation of the mammalian skull anatomy, using positional relationships (i.e. connectivity) to identify homologies. To my knowledge, this is the first record of a skull represented as a network.

In *Order in Living Organisms*, Riedl offers a deep reasoning on the origin and maintenance of body plans and evolutionary trends by means of the concept of 'burden' in structures and events. This concept explains the integration of organismal form and its patterns of variation as a consequence of an increase in hierarchical nested developmental constraints on traits during evolution, linking evolution and development (Wagner and Laubichler, 2004; Schoch, 2010).

In his defense on the necessity of concepts like morphotype and ground plan, Riedl introduced the idea of a 'diagrammatic morphotype' (Fig. 2.9), in which only minimal descriptors of form are used *"as in a structural formula"* (Riedl, 1978, pg. 249). Thus, capturing the topological information that defines the morphotype of the tetrapod skull in terms of homology and developmental dependencies.

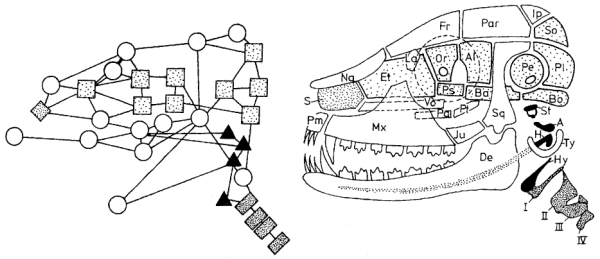

Figure 2.9: The diagrammatic morphotype of the mammalian skull (left). From Riedl (1978, pg. 250).

2.2.5 Modern Use of Networks in Morphology

In the last decade, Rasskin-Gutman renewed the interest in studying morphology at a connectivity level within the frame of evolutionary developmental biology (Rasskin-Gutman, 1995; Rasskin-Gutman and Buscalioni, 2001; Rasskin-Gutman, 2003). To formalize the topology or structural relation of parts in the pelvic girdle of archosaurs, Rasskin-Gutman introduced models based on Graph Theory, in which each vertex represented a pelvic bone, ilium, ischium, and pubis, and each edge represented their physical junctions (Rasskin-Gutman, 1995; Rasskin-Gutman and Buscalioni, 2001). The analysis of the theoretical morphospace of connections in the pelvic girdle revealed an evolutionary trend toward the loss of connections, and hence, compactedness in the graph model (i.e., a measure of morphological complexity described in 4.1.3 as Density of connections) during the early evolution of birds. The use of graphs was then extended to the analysis of

the skull (Rasskin-Gutman, 2003), in which vertices represented skull bones and edges sutures. For 2D skull graphs (Fig. 2.10), a network analysis was carried out to quantify the degree distribution (i.e., frequency of bones with a given number of connections) and to identify building blocks (i.e., small regular motifs such as triangular loops). This analysis, along with computational simulations, revealed the structural relation among the bones that participate in the formation of skull openings. Furthermore, it demonstrated that the analysis of connectivity patters is suitable to study macroevolutionary patterns of structural changes.

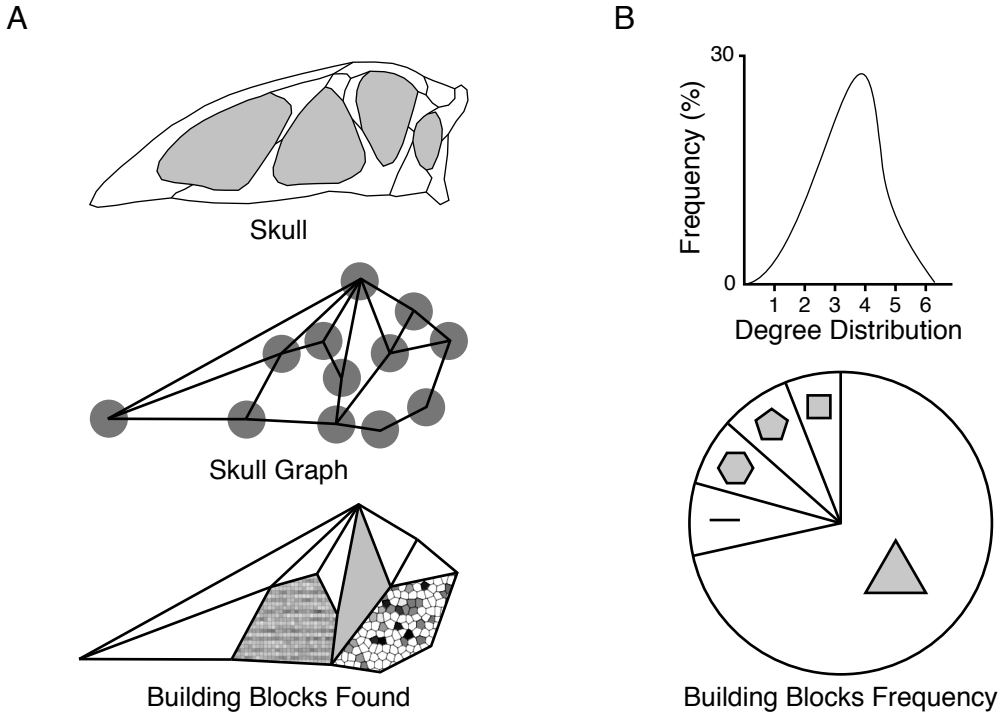

Figure 2.10: Analysis of skull networks by Rasskin-Gutman. (A) Diagram of the skull in 2D, graph representation, and blocks found. (B) Network analysis of degree distribution and frequency of blocks. Modified from Rasskin-Gutman (2003).

Rasskin-Gutman also introduced the use of computational models to explore changes in connectivity patterns in the skull of archosaurs and to explore the morphospace of connections (Rasskin-Gutman, 2003). This computational model, based on cellular automata, was programmed to generate skull-like networks according to empirical connectivity pat-

terns found in the skull of archosaurs; using different initial growth rules, bones were added or deleted until the maximum number of bones was reached. The results of this model were used to infer macroevolutionary dynamics in skull connectivity patterns, such as emergence of novelties, convergence, and stasis, as well as to offer a null hypothesis of skull evolution at a connectivity level.

More recently (and in the context of this thesis), network analysis has been proposed to tackle morphological complexity, integration, and modularity in the vertebrate skull (Esteve-Altava et al., 2011), to study evolutionary trends and structural constraints in the morphological complexity of the tetrapod skull (Esteve-Altava et al., 2013b,c), assess the modular organization of the human skull (Esteve-Altava et al., 2013a), and explore the theoretical morphospaces of the tetrapod skull (Esteve-Altava and Rasskin-Gutman, 2013).

3

Morphological Organization in Connectivity Patterns

The intuitive notion of biological organization evokes a group of units establishing interactions in order to perform a function. Beyond its functional component, organization entails the presence of a structure of relations between the parts of the system (Rashevsky, 1954, 1960). In this context, *parts* are entities that can be identified as isolated from others by means of their boundaries (Weiss, 1971); bones are the parts of the skull, isolated and identifiable of other bones and tissues by their boundaries (either sutures between bones or periosteum between bones and other tissues). In the same manner, a *system* is a group of parts interacting, which produces a particular behavior (e.g., shape variation) as a consequence of their coordination, not fully determined by the properties of each part in isolation (Weiss, 1971); the skull is a system composed of bone parts with a collective behavior in development, growth, function, and evolution. For instance, after a craniosynostosis, the entire skull buffers shape changes, by growth in other parts of the skull, instead of collapsing entirely (see 1.1.2). Henceforth, I use the above-mentioned definitions of parts and systems. They are simple enough, and, at the same time, they allow to identify individual skull bones as parts and the skull as the system of study in this thesis. Furthermore, they are both suitable for the kind of abstraction I have used to build network models (see 5.1).

At a connectivity level, morphological organization emerges from the relations among anatomical parts. These relations are not established at random; rather, they form distinguishable connectivity patterns, which give the system its characteristic structure. The order of this structure can range from randomness to regularity; connectivity patterns in morphological systems are organized between these two extremes (i.e., they are never totally random, nor totally regular). In the context of this thesis, connectivity patterns are captured in the set of sutures that connect skull bones, which emerge during development, by genetic and epigenetic factors, producing morphological order. The idea of

morphological organization is often linked to the complexity, hierarchy, integration, and modularity of morphological systems. In the next sections, I will discuss these features of morphological organization in the context of connectivity patterns of morphological systems in general, and of the skull in particular.

3.1 Morphological Complexity

Complexity is an attribute of any organized system; a stage of organization often said to occur *at the edge of chaos*, meaning that complexity emerges in those systems between order (regularity) and disorder (stochasticity). Sometimes it is defined as unpredictability within a structured disorder (Lewin, 1992; Waldrop, 1992; Solé and Goodwin, 2000), as the functional multi-tasking and structural stability of a system (Taylor, 2005), or as the amount of information for a minimal description of the system (Wicken, 1979; Hinegardner and Engelberg, 1983). There is agreement in that complexity is reached somewhere in between regular and stochastic states of order (Solé and Goodwin, 2000, Fig. 2.2), but this is not enough when trying to quantify how much complexity a morphological structure has. In addition, colloquial meanings of complexity have blurry operational definitions in biology in general, and morphology in particular, which too often lead to misunderstandings (reviewed in McShea and Brandon, 2010, pg. 48-50).

Morphological complexity is usually defined as the number of different parts; this (colloquial) meaning of morphological complexity appears, more or less explicitly, in evolutionary and anatomical studies (e.g., Gregory, 1927, 1929, 1933, 1935; Williams, 1966; Hildebrand, 1988; Sidor, 2001; McShea and Hordijk, 2013). However, morphological complexity arises not only with number of parts, but also with their relative arrangement (McShea, 1991; Valentine, 2003). Quantifying morphological complexity only as the number of bones ignores non-linear bone relations that define structural organization, as well as those that create developmental and functional dependences among them. To solve this, Daniel W. McShea and Robert N. Brandon (2010) propose to focus on a straightforward definition of organismal complexity based on variance (diversity): the number of different types of parts (see also Bonner, 1988). However, in the case of the skull, to identify a bone as being different from another bone it is necessary to know the connectivity patterns of both bones. This makes connectivity patterns fundamental, although only implicit, in this notion of morphological complexity.

On the other hand, morphological complexity can be quantified explicitly by analyzing the connectivity patterns between skull bones (Rasskin-Gutman, 2003; Esteve-Altava

et al., 2013c), using Network Theory as the operational framework to quantify these relations. This is precisely what I have done in this thesis. Thus, morphological complexity at a connectivity level is defined here as richness of interactions, both as a net amount of interactions and local patterns of connectivity.

The definition of morphological complexity proposed here resembles that of Herbert A. Simon (1962): *"a large number of parts that interact in a non-simple way"*. The simplicity, or complexity, of interactions is readily quantified by some network parameters, such as density of connections, clustering coefficient, and shortest path length (see 5.2.3). The origin of *"non-simple"* interactions is, according to Simon, in the near-decomposability of the system; in other words, in its hierarchical arrangement of parts and in its modularity.

3.2 Hierarchy

Morphological systems are hierarchical in two sense (Mayr, 1982): in a multi-scale sense (aggregative), in which each anatomical part is composed of tissues, cells, and so on downwards in the hierarchy, while parts make up organs, bodies, and so on upwards in the hierarchy (Rasskin-Gutman and Esteve-Altava, 2009); and also in the same morphological scale (constitutive), in which parts interact with each other as blocks within blocks due to a differential integration (Fig. 3.1). The hierarchical organization of the skull morphology, development, and evolution promotes the phenotypic integration of developmental units, as well as the formation of modules of shape that are correlated (Bastir, 2008). As a consequence, morphological systems change in form, growth, and function in a coordinate way (Weiss, 1971).

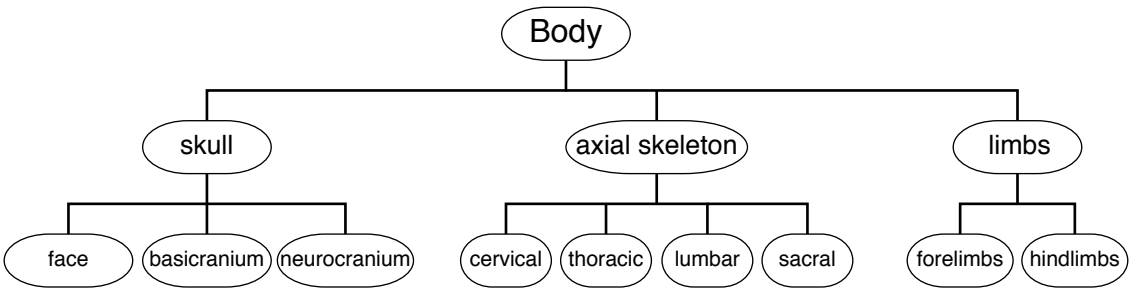

Figure 3.1: Hierarchical organization of the body represented as a hierarchical system made up of different modules within modules. From Bastir (2008), modified from Chernoff and Magwene (1999).

Hierarchy is a particular state of order easily recognized by analyzing patterns of connectivity (Fig. 3.2). In general, it is described as parts establishing nested relations at different scales (Ozekhan, 1971). In this thesis, I will use notions of hierarchy that spring directly from patterns of connectivity, which in turn are related to integration and modularity.

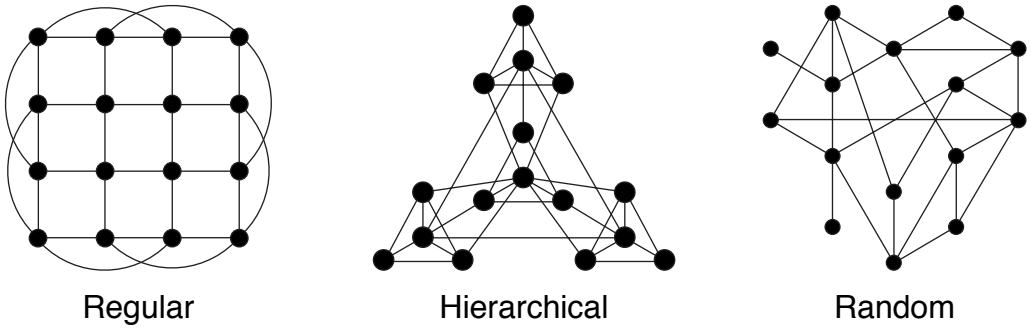

Figure 3.2: Types of organization in networks: regular, hierarchical, and random. Modified from Barabási and Oltvai (2002).

3.3 Morphological Integration

Morphological integration means association between morphological traits (Terentjev, 1931; Olson and Miller, 1958; Cheverud, 1982), which is generally defined as the covariation among morphological traits due to common developmental and/or functional causes. Depending on the definition of trait and unit of variation, the interpretation of integration varies in the context of genetics, development, morphology, and evolution (e.g., Piagliucci and Preston, 2004). For instance, in Geometric Morphometrics, traits are positions of landmarks and associations are correlations of phenotypic variance between morphological structures, that is, how much two traits change together (reviewed in Klingenberg, 2008, 2010). Since morphological integration is the observation of a pattern of covariation, the causal mechanisms need to be elucidated according to an *a priori* causal hypothesis (Chernoff and Magwene, 1999; Magwene, 2001). Thus, current research on morphological integration focuses on the conciliation of phenotypic covariance with predictive models based on genetic, developmental, functional, and evolutionary hypotheses (Marugán-Lobón and Buscalioni, 2003; Goswami, 2006; Hallgrímsson and

Lieberman, 2008; Lieberman et al., 2008; Finarelli and Goswami, 2009; Goswami et al., 2009; Mitteroecker, 2009; Goswami and Polly, 2010; Sanger et al., 2011; Mitteroecker et al., 2012).

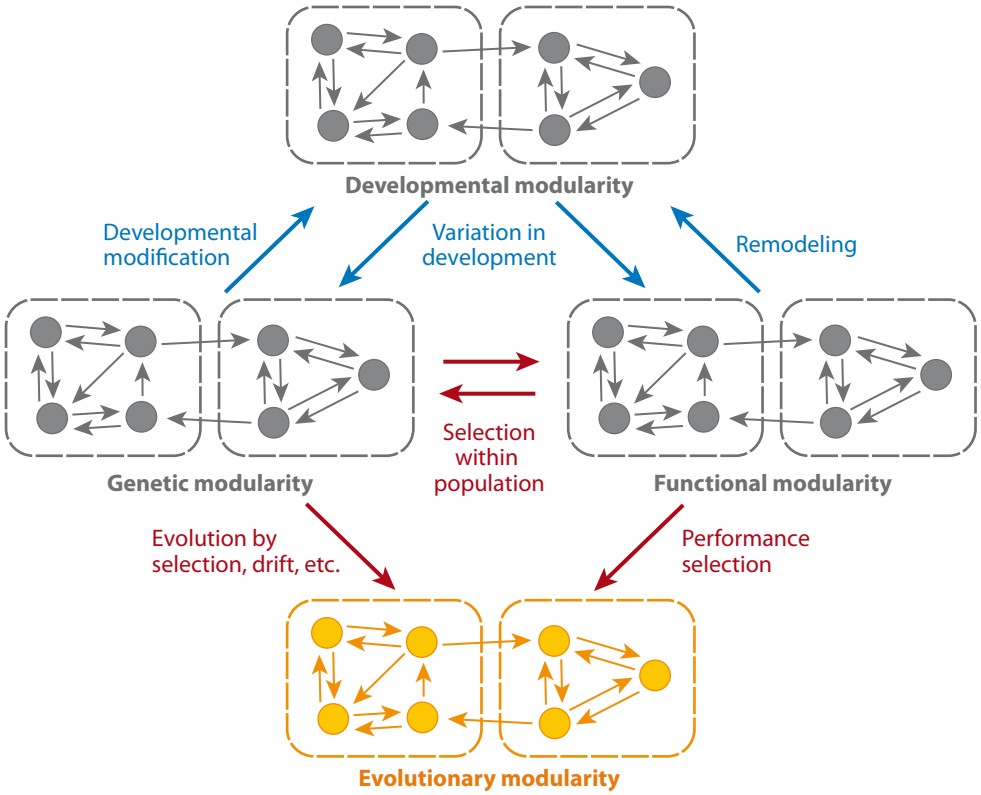

Figure 3.3: Sources of morphological integration and the formation of modules. Colors indicate processes between genetic, developmental, and functional scales in the origin of evolutionary modules. Modified from Klingenberg (2008)

In a broader framework, Christian P. Klingenberg (2008) defines morphological integration using also network terms, like *"interaction"* of processes and *"degrees of connectivity"* between parts, and sketches the different sources of morphological integration: genetics, development, function, and evolution also as networks (Fig. 3.3). Thus, Klingenberg uses network concepts to define processes and functions that cause morphological integration and its counterpart modularity; however, he does not address the structural integration of morphological systems itself. Although recognizing that the analysis of network interactions permits the identification of integration in some contexts (e.g., genetic regulatory

networks), Klingenberg is skeptical to study morphological integration using network connectivity patterns: *"studies of morphological data, however, do not have this information on the network of interactions between the measured traits, but need to infer interactions from the patterns of covariation among traits"* (Klingenberg, 2008). The skepticism of Klingenberg on the use of connectivity patterns to quantify morphological integration comes from identifying the nodes of the morphological network as morphometric traits (landmarks positions or distances between them). This was precisely the point of Paul M. Magwene in his studies on the use of proximity graphs to establish correlation between morphometric traits and to analyze morphological integration and modularity (Magwene, 2001, 2008).

In this thesis, I use morphological networks in an entirely different way. Here, the nodes of the network represent solely the anatomical parts of the skull, that is, its bones. In the same manner, links represent solely the physical connection of these bones, that is, sutures. Skull bones are morphological parts able to vary at all morphological levels of information (size, shape, orientation, and connection); most of this variation occurs at the boundaries of bones where connections are established. Thus, it is expected that two connected bones would be more related, or morphologically integrated (i.e., likely to covary in size, shape, orientation, and connection), than two disconnected bones; just because a connection sets a developmental and functional dependency between them (see 5.2.2). Thus, if connections between bones act as sites of morphological integration, it is reasonable to quantify the integration among skull bones using their connectivity patterns. An advantage of studying morphological integration at the connectivity level is that network models offer *a priori* hypotheses about morphological integration–directly from the patterns of organization of structures. Some of these hypotheses concern how different parts (groups of bones) of the skull are integrated between them, in other words, the modular organization of the skull.

3.4 Modularity

Morphological systems acquire a modular organization due to differences in the degree of integration between groups of parts, that is, a heterogeneous integration of the system. More precisely, a morphological module is (1) a delineated group of parts more integrated internally than externally, (2) that persist in time according to its scale, and (3) that is reusable, constructed as a block co-optable (in theory) under different needs (Bolker, 2000; Callebaut, 2005).

We can identify morphological modules in the skull according to different definitions of integration (first condition). Functional modules group bones that interact to perform a specific function, such as protection of the brain, hosting sensory organs, and feeding (Cheverud, 1982). Developmental modules group bones with the same genetic and epigenetic regulatory factors; for example, skull bones have been classified as chordal or pre-chordal according to mesodermal or neural crest origin (Santagati and Rijli, 2003); also, different regions that develop within the same morphogenetic field (Weiss, 1939; Waddington, 1956; Wolpert, 1977). Finally, evolutionary modules group bones that co-evolve together in coordination; for example, at the level of proportions, these modules are usually identified by measuring coordinated changes in shape and size (Cheverud et al., 1983; Magwene, 2001; Bookstein et al., 2006; Adams et al., 2004; Bastir and Rosas, 2005; Bastir et al., 2005; Goswami, 2006; Willmore et al., 2006; Mitteroecker and Bookstein, 2007; Klingenberg, 2008, 2010; Mitteroecker et al., 2012).

At a pure structural, a connectivity module is defined as a group of parts with more connections between them than to other parts outside the group. This definition of module is also valid for any other biological system because of its generality (Callebaut and Rasskin-Gutman, 2005; Schlosser and Wagner, 2004). In order to identify modules, we need a level-specific operative definition of module and adequate tools to quantify the integration of parts. Here, connectivity modules in the skull have been identified according to the organization of connections between bones to form highly connected groups, by means of a network analysis of their global connectivity patterns (see 4.2).

Part II

Material & Methods

4

Tools for Networks Analysis

The analysis of network models requires a specific set of tools: concepts, descriptions, and algorithms; Network Theory is the branch of mathematics that supplies them. Here, I describe the tools used in the present thesis to analyze skull networks. Other reviews and books offer more complete lists of parameters and methods (Albert and Barabási, 2002; Dorogovtsev and Mendes, 2003; Newman, 2003; Newman and Girvan, 2004; Newman et al., 2006; Mason and Verwoerd, 2007).

Network parameters have been scripted in a MATLAB environment (MATLAB, 2010) using the Brain Connectivity Toolbox (Rubinov and Sporns, 2010) and Ezyfit 2.41 Toolbox (Moisy, 2010). See Appendix A for code descriptions.

4.1 Network Model

A network *G(N,K)* is the combination of two sets: a set of nodes (N) and a set of links (K), in which each link has two endpoints that represent a connection between two nodes. The most common representation of a network is a drawing of dots joined by lines; the way used to represent a network is trivial as long as the same relations between nodes are kept.

4.1.1 Model Descriptors

The number of nodes and links are the raw descriptors of network models: nodes represent the elements of the system, bones; while links represent their relations, suture contacts. Thus, a link connecting two nodes indicates the presence of a mutual relation. Non-reciprocal relations are indicated by directed links; variation in the interaction strength is indicated by weighted links. In this thesis, skulls have been modeled as undirected, unweighted networks (see 5.1).

The Adjacency Matrix

The adjacency matrix $A_{i,j}$ is the mathematical structure that codifies the information on nodes' connection. For undirected, unweighted networks this is a symmetric binary matrix of size N x N, where 1 indicates presence and 0 indicates absence of connection. The adjacency matrix defines the connectivity pattern of the network: the number and the particular distribution of connections between nodes. It also defines the neighborhood, connectivity context, of each node as all the nodes to which it connects.

$$A_{i,j} = \begin{bmatrix} a_{1,1} & a_{1,2} & a_{1,3} & a_{1,j} \\ a_{2,1} & a_{2,2} & a_{2,3} & a_{2,j} \\ a_{3,1} & a_{3,2} & a_{3,3} & a_{3,j} \\ a_{i,1} & a_{i,2} & a_{i,1} & a_{i,j} \end{bmatrix}$$

4.1.2 Element Descriptors

The element descriptors are the connectivity parameters measured for individual nodes, that is, the connectivity context that defines the role of each node in the network.

Node Connectivity

The node connectivity (Eq. 4.1) is the sum of connections a specific node has to other nodes in the network:

$$k_i = \sum_{i=1}^{j=n} A_{i,j} \tag{4.1}$$

Clustering Coefficient

The node clustering coefficient (Eq. 4.2) measures the presence of connections between the neighbors of a node: the amount of neighbors that are also connected between them. Formally, the clustering coefficient is the ratio between the total number of links connecting its nearest neighbors and the total number of all possible edges between all these nearest neighbors, which is $k_i(k_i - 1)/2$:

$$C_i = \frac{\sum(\tau_i)}{\sum k_i(k_i - 1)} \tag{4.2}$$

where τ_i is the number of connections between the neighbors of node i.

Shortest Path Length

The shortest path length between two nodes (Eq. 4.3) is a pair-wise measure of their shortest distance:

$$\ell_{i,j} = d(n_i, n_j) \tag{4.3}$$

where $d(n_i, n_j)$ is the minimum distance in number of links to connect nodes i and j. By default, links have length one; thus, the shortest path between two connected nodes is 1. Non-connected nodes have higher shortest path length depending on how well connected they are to others. Of course, many paths exist between any two nodes, being or not the shortest ones. Imagine, for example, a group of islands connected by bridges. The only way to travel from one to another is crossing these bridges; if there is no direct bridge, we travel through different islands, across different bridges, to our destination. The same occurs when we 'walk' within a network. Here, the path length refers to the number of links we must 'cross' to go from one node to another; as if we were crossing bridges between islands[1].

Within-module Connectivity Coefficient

The within-module connectivity coefficient of a node (Eq. 4.4) is the normalized number of connections this node has to other nodes in the same module:

$$Z_i = \frac{k_i - \hat{k}_{si}}{var(K_s)} \tag{4.4}$$

where k_{si} is the number of connections of node i within its module and K_s are the connections of all nodes within the module.

Participation Index

The node participation index (Eq. 4.5) is a measure of how uniform is the distribution of connections to nodes that do not belong to the same module:

$$P_i = 1 - \sum_{s=1}^{N_M} \left(\frac{k_{si}}{k_i} \right)^2 \tag{4.5}$$

If a node has all its connections within its module P_i is equal to 0; rather, if the distribution of all node connections is uniform to all modules then P_i is equal to 1.

[1] This is not just a metaphor, a similar problem known as the *Seven Bridges of Königsberg* was solved by Euler in 1741, in which it is the first work on Graph Theory.

The Definition of Single Node Roles

The most straightforward way to define the role (functional importance) of a node in the network is by the number of connections; a *hub* is a node with the highest connectivity in the network, for example, one or two standard deviations more than the mean connectivity. This definition of node roles, based solely on the number of connections, is not useful when comparing different networks that have disparity of connectivities. A more precise definition of hub uses the node within-module connectivity (Z_i), instead of the raw connectivity (Guimerà et al., 2007). This definition not always agrees with the definition of hubs as nodes with a higher number of connections. Although defined as a single node parameter, this makes sense only within a modular context (see 4.2).

Thus, in a modular context, a node can also act either as a *connector*, if it spreads its connections among different modules (connecting modules) or as a *local* node if it keeps most connections within its module. The role of each node within a given modular structure is characterized by two complementary parameters: Z_i and P_i. The ZP space divides nodes in four categories: (1) *local hubs*, when Z_i is high and P_i is low; (2) *connector hubs*, when Z_i and P_i are high; (3) *connector non-hubs*, when Z_i is low and P_i is high; and (4) *local non-hubs*, when Z_i and P_i are low (Fig. 4.1).

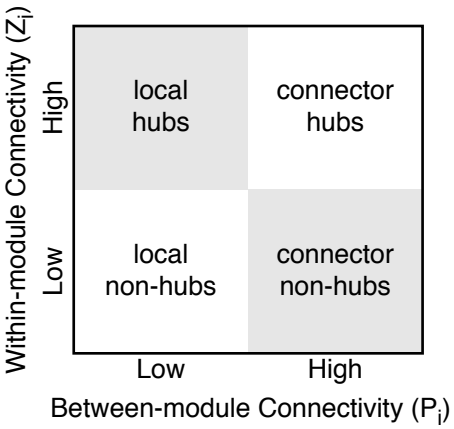

Figure 4.1: ZP space definition. A taxonomy of node roles according to two dichotomies, local/connector and non-hub/hub, results in four roles: connector hubs, local hubs, connector non-hubs, and local non-hubs (Guimerà and Nunes-Amaral, 2005).

In a biological network, disparity of roles among nodes reveals heterogeneity in the network organization. This tells us that not all nodes have the same number of connections

and that not all nodes participate equally in the inter-connectedness of the system. Also, the distinction between connectors and local nodes tells us which are the nodes that maintain the integration between modules.

4.1.3 System Descriptors

System descriptors are parameters that capture properties of the entire network and are derived from the combination of node parameters. These descriptors are useful to compare organization between different systems: (1) biological and non-biological systems, (2) biological systems at different scales, and (3) different systems of the same kind.

Density of Connections

The density (Eq. 4.6) is the number of existing connections with respect to the maximum possible, which is $N(N-1)/2$:

$$Density = \frac{2K}{N(N-1)} \tag{4.6}$$

Density measures completeness: how many connections are realized of the total possible; a complete network has a density equal to 1.

Heterogeneity and Connectivity Distribution

The heterogeneity (Eq. 4.7) is the variance of connectivity of the nodes in the network:

$$H = \frac{\sqrt{var(K)}}{mean(K)} \tag{4.7}$$

A finer analysis of the network's heterogeneity is possible by looking at the specific frequency of nodes with a given number of connections in the network. The connectivity distribution (Eq. 4.8) is the frequency of occurrence of nodes with k connections:

$$P(k) = \frac{N_k}{N} \tag{4.8}$$

$P(k)$ is the probability to find a node with a given number of connections in the network. In the same manner, the cumulative connectivity distribution (Eq. 4.9) captures the frequency of nodes with connectivity equal or greater than k; it is a common methodological choice to avoid the statistical fluctuations of the $P(k)$ in networks with a small number of nodes (Dorogovtsev and Mendes, 2003, Appendix A):

$$P_{cum}(k) = \frac{N_{k' \geq k}}{N} \tag{4.9}$$

Theoretical Connectivity Distributions

The functional form of the $P(k)$ characterizes the heterogeneity of the network. Moreover, the $P(k)$ function informs about the possible nature of the mechanisms that formed the network, for example, power-law distributions by preferential attachment, or binomial distribution by random processes (Albert and Barabási, 2002). Regardless of the lack of a one-to-one mapping between $P(k)$ functions and mechanisms, the fit of the $P(k)$ to a specific theoretical distribution aids in finding out specific mechanisms of network formation (see 5.2.3). Usually, it is convenient to analyze how the $P(k)$ fits four theoretical distributions: binomial, linear, exponential, and power-law (see 4.1). All these functions share a heterogeneous distribution of connections among nodes; the only theoretical distribution for homogeneity is a point indicating that all nodes are equally connected.

Table 4.1: Theoretical models of connectivity distribution

Theoretical Model	**Function**
Binomial	$P(k) = a + b \cdot k + c \cdot k^2$
Linear	$P(k) = a + b \cdot k$
Exponential	$P(k) = a \cdot e^{b \cdot k}$
Power-Law	$P(k) = a \cdot k^{-\gamma}$

Mean Clustering Coefficient and Clustering Distribution

The mean clustering coefficient ($\overline{C}$) is the arithmetic mean of the clustering coefficient of all nodes in the network (Eq. 4.2). The $C(k)$ is the distribution of the clustering coefficient mean of all nodes with k connections; similarly to the $P(k)$, this distribution describes the structure of the network. For instance, a right-skewed distribution indicates the presence of highly clustered groups of nodes or *blocks* (Mason and Verwoerd, 2007).

Mean Shortest Path Length and Diameter

The mean shortest path length ($\overline{L}$) is the arithmetic mean of the shortest path length between all pairs of nodes in the network (Eq. 4.3). Conversely, the diameter of a network is the longest one of all these shortest path lengths. Together with the $\overline{C}$, the $\overline{L}$ identifies the presence of the small-world effect when compared with randomly generated networks.

4.1.4 Organization Descriptors

Organizational descriptors capture the connectivity patterns that promote hierarchical and modular structures. Often, their analysis requires the use of null models (see 6.1) and grouping techniques (see 4.2.2).

The Small-World Effect

The small-world effect is an organization feature of networks characterized by highly clustered nodes, like in a regular network, and a small mean shortest path length, like in a random network (Watts and Strogatz, 1998). This is a pervasive feature of many real networks; to identify the presence of the small-world effect in the network, the values of $\overline{C}$ and $\overline{L}$ are compared with those of a random network with the same number of nodes and connections (Watts and Strogatz, 1998). Small-world networks have higher values of $\overline{C}$ than regular and random networks, and similar or lower values of $\overline{L}$. However, a common problem in the analysis of the small-world effect in networks with few nodes (i.e., $n < 100$) is that the value of $\overline{C}$ cannot be sufficiently higher than for random networks; hence, the detection of the small-world is unreliable. To circumvent this problem, the analysis can be corrected so that for any number of nodes, a network is small-world if $[(\overline{C}/\overline{C}_{rand})/(\overline{L}/\overline{L}_{rand})] \geq 0.012n^{1.11}$ (Humphries and Gurney, 2008). The heterogeneity of the connectivity pattern in small-world networks is related with the emergence of modular organizations.

Community Structure

Networks have community structure if nodes are grouped into densely connected sets. In this context, the definition of module is simple: a group of nodes with more connections among them than to other nodes outside the module; however, detecting modules is very tricky. Indeed, this is an NP-complete problem (non-deterministic polynomial time problem), which means that evaluationing all possible partitions to find the best solution takes too much computational time. This is because the number of partitions on which we look for an optimal one is extremely huge. The number of possible partitions of a set of n elements is called the nth Bell number; for instance, the Bell number for a small network of 21 nodes, like the human skull, is aprox. $4.75{\cdot}10^{14}$. The use of heuristic tools overcome this problem, for example, traditional clustering techniques based on similarity/dissimilarity matrices, oriented algorithms based on prior information, and spin-glass models (see Porter

et al., 2009, for an extensive review). The method used here to detect modules in skull networks is explained in section 4.2.

Hierarchy

A hierarchical organization occurs if network modules are, simultaneously, composed of smaller modules (blocks or motifs). The number of nested layers of modules varies from one network to another, which can be different even within modules in the same network. Two system descriptors indicate presence of hierarchical organization in networks: connectivity distribution, $P(k)$, and clustering distribution, $C(k)$. Right-skewed $P(k)$ and $C(k)$ indicate that the neighborhoods of less connected nodes are highly clustered while those of highly connected nodes (i.e., hubs) are sparsely connected, which would suggest that hub nodes are acting as inter-connectors between blocks. Indirectly, modularity detection methods that grouped together nodes hierarchically could reveal also the presence of a hierarchy. Both approaches were used to identify the presence of hierarchy and building blocks in skull networks.

4.2 Analysis of Modularity in Networks

A heuristic approach was used to identify connectivity modules in skull networks: an agglomerative hierarchical clustering analysis on a similarity matrix, which was derived from the connectivity pattern of all nodes in the network. The outcome is a dendrogram of nested groups of nodes. The best of all partitions was then identified using an index of quality. The following sections describe the steps taken in this thesis to carry out a modularity analysis: (1) quantification of nodes similarities, (2) agglomerative grouping of nodes, and (3) identification of the best partition.

4.2.1 Topological Overlap

The topological overlap (Eq. 4.10) is a normalized measure of similarity that estimates the extent to which two nodes connect to the same other nodes:

$$TO(n_i, n_j) = TO(n_j, n_i) = \frac{J(n_i, n_j)}{min(k_i, k_j)} \tag{4.10}$$

where $J(n_i, n_j)$ is the total amount of neighbors in common between two nodes and $min(k_i, k_j)$ the lowest connectivity of both nodes. Two nodes that share all their connections (with the same other nodes) have a TO of 1, whereas two nodes without any neighbor in common have a TO of 0.

The TO was the similarity matrix used in the agglomerative cluster analysis; This has been extensively used to analyze modularity in different types of networks (Ravasz et al., 2002; Solé et al., 2007), because it is expected that nodes in the same module connect to the same nodes (nodes with the same neighbors belong to the same module). This measure of similarity has been extensively used in social networks, where it is called *structural equivalence* (Breiger et al., 1975).

4.2.2 Hierarchical Clustering Analysis

The hierarchical clustering analysis[2] brings together nodes with a higher TO in single branches until all nodes form one single group. After each match, the TO matrix is recalculated; grouped nodes act as a new element in the grouping process. The final outcome is a dendrogram that shows hierarchically nested partitions. We can use the inconsistency coefficient to know which partitions are consistent enough (Jain and Dubes, 1988). However, inconsistency cannot identify the best cut-off point of the dendrogram; to do this, I use a quality index based on connectivity, which is similar to an optimization factor, described in the next section.

4.2.3 Newman-Girvan Q Value

The modularity Q-value (Eq. 4.11) compares the within-module connectivity with a random distribution of connections, as an index of quality:

$$Q = \sum_{m=1}^{M} \left[\frac{k_s(m)}{K} - \left(\frac{k_m}{2K} \right)^2 \right] \tag{4.11}$$

where M is the number of modules, $k_s(m)$ is the sum of connections from nodes to the same module m, and k_m is the sum of all connections of nodes in module m (Newman and Girvan, 2004). The Q-value is calculated for each bifurcation in the dendrogram; the highest value indicates the best partition of the network (Fig. 4.2).

[2]This method should not be confused with the model descriptors: C_i, $\overline{C}$, and $C(k)$ described in 4.1. In these parameters the term clustering refers to the presence of triangular motifs of connection, whereas hierarchical clustering analysis refers to a method of aggrupation.

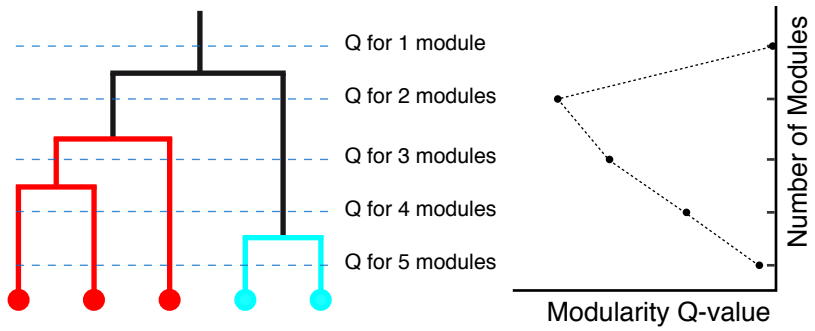

Figure 4.2: Schema of the identification process of the best partition. The five possible partitions are indicated with dashed lines; the modularity Q-value is measured in each bifurcation. The highest value indicates the best partition according to connections within and between modules.

5

The Skull Network Model

The use of network models in biology has also introduced many new concepts from more specialized literature on Network Theory in order to describe and explain biological systems, such as small-world, scale-free, and hubs (reviewed in Proulx et al., 2005; Knight and Pinney, 2009). However, since network analysis has not been applied extensively to anatomical systems, most concepts in Network Theory lack any morphological interpretation (but see Rasskin-Gutman, 2003; Esteve-Altava et al., 2011, 2013c,a). On the other hand, we also lack a reference framework for network models construction in morphological systems, which is important to interpret the outcomes of the network analysis. Here, I explain the abstraction process followed to build skull network models and how network parameters can be interpreted in the context of the development and evolution of the skull morphology.

5.1 Building Skull Network Models

A network is a set of elements interacting; thus, the first step to build a network model is to identify the type of element and interaction. Elements and interactions must have unique definitions so that they can be unequivocally identified in all regions of the system and, in a comparative framework, also in other related systems. Figure 5.1 summarizes the abstraction process from morphological systems to network representations. Here, skull network models have been built using descriptions of skull contacts from the specialized literature, which have been supported by the observation of drawings and digitized images available on-line (Rowe, 2002; MCPA2, 2005). Information about bones and presence/absence of sutures was codified in an adjacency matrix.

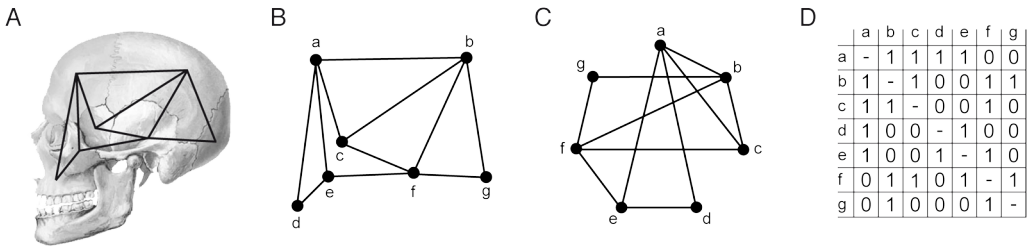

	a	b	c	d	e	f	g
a	-	1	1	1	1	0	0
b	1	-	1	0	0	1	1
c	1	1	-	0	0	1	0
d	1	0	0	-	1	0	0
e	1	0	0	1	-	1	0
f	0	1	1	0	1	-	1
g	0	1	0	0	0	1	-

Figure 5.1: Abstraction process to build morphological networks. The process begins with A) the identification of elements and interactions, then B) abstracting any other type of information but the structure, C) including physical position in the space, and finished with D) the codification of structural information in an adjacency matrix of presence (1) and absence (0) of contacts. From Esteve-Altava et al. (2011).

For simplicity, elements of the network have been defined as skull bones as they are found in adult organisms, that is, a rigid body of ossified tissue. The structural relationship modeled as a connection is the presence of a suture surface between them. These definitions have been chosen in order to perform a broad comparative analysis between distantly related species of tetrapods, including extant and extinct species. A definition of element and connection with more information (e.g., weighted links according to the length of the suture) would describe better the real structure of extant skulls, but hamper the comparative analysis with extinct forms. In practice, bones may be only partially ossified, and yet they are solid enough to be considered bones, for example, some cartilaginous bones. When that happens, the decision whether to consider these bones as elements of the network, and hence part of the network model, or not is somehow subjective. In these cases, the decision has been taken according to expert descriptions in the literature and personal judgment. Doubts about suture joints because of different degrees of obliteration and cartilaginous bounds have been solved in the same manner.

As it occurs in the construction of any model, or use of any representation system, the construction of skull networks is susceptible to some errors and simplifications that, if they are not identified (and fixed or assumed), can lead to some misunderstanding. These building errors/simplifications can be classified in three groups (excluding typing errors):

- Identification of elements and relations
- Typological simplifications
- Illusions of symmetry

5.1.1 Identification of Elements and Relations

The first, and most important, step in network analysis is the construction of a proper network model for the system of interest and the questions asked. To do this, the units of description and the relations modeled must be selected carefully: model descriptors must have precise definitions to enable their identification in all the objects of the study. However, this is not always a straightforward task neither in theory nor in practice (Butts, 2009). Think, for example, in an ecological study that aims to capture trophic interactions between species. Although identifying a predator-prey relation is pretty easy, a broader definition of the trophic relation that includes symbiosis, parasitism, or scavenging may introduce some doubts. In addition, the definition of taxonomic species is not always in total accordance with ecological species, and species definition is subject to change. For the same real ecosystem, different network models, created attending to different criteria, can give different outcomes.

In skull networks the units of description are bones and physical junctions. However, the bone unit may change widely, for example, during development. For instance, the frontal bone in the human skull is a single unpaired bone in the adult, but two paired bones at birth. A different approach could use the ossification centers as elements of the skull network, but that would exclude fossil skulls from the analysis. The same applies to the definition of physical junction as the structural relation between bones. To use suture joints is an easy way to identify most of the contacts occurring in the skull, but excludes from the network those bones that join the skull in a different way, such as the mandible. Moreover, a dichotomous definition of relation between bones (i.e. presence or absence) may obscure differences in the strength of junctions because of their length. On the other hand, this binary definition can take into account all interactions even when the length of the contact is unknown, which is common in fossils.

5.1.2 Typological Simplifications

The skull is one of the most variable parts in size and shape of the anatomy of tetrapods (Goodrich, 1958; Hildebrand, 1988; Kardong, 2005), and yet its topological structure is conserved to a great extent within taxa. However, there is also variation at the species level, especially at the anatomical regions where several bones meet, or is likely that they meet (Berry and Berry, 1967). For instance, in the pterion region of the human skull where the temporal, parietal, sphenoid, and frontal bones meet (Fig. 5.2); moreover, left and right sides of the skull can have also different pterion configurations (Saheb et al.,

2011). Contrary to what may seem, this source of intraspecific variation is not only due to developmental or environmental contingencies, but also heritable (Wang et al., 2006).

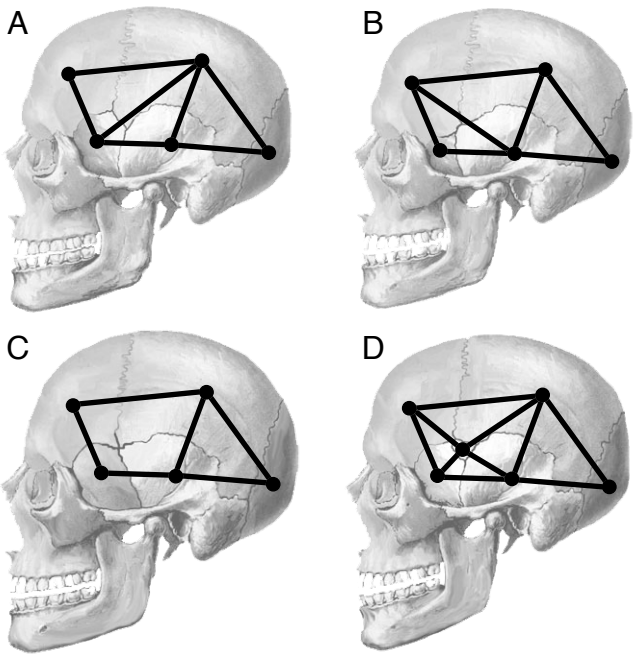

Figure 5.2: Variation in the connectivity pattern of the pterion region in the human skull. A) Sphenoparietal, sphenoid and parietal bones contact; B) frontotemporal, frontal and temporal bones contact; C) stellate, the four bones meet in a single point (i.e., counting as no contact); and D) epipteric, a wormian bone appears in the intersection of the four bones, contacting to all of them. From Esteve-Altava et al. (2011).

Given this amount of potential variation due to local connectivity configurations and the presence of wormian bones (i.e., extra bones), it is arguable that taking into account only the 'type' form would lead to some misrepresentation or, at least, oversimplification of the structural organization of the skull; different individual skulls could have some local variation in their connectivity pattern, and hence, could show a slight variation in their network properties. However, type forms, as those described in the literature, were preferred for the kind of questions addressed in this study: patterns of structural organization, evolutionary trends, and construction rules in the tetrapod skull. In this context, the skull network model represents a consensus ('average') form of the skull in a species, which is also the most commonly found in real skulls. To include the kind of

variation mentioned requires methodological shifts practically impossible in fossil forms: the use of 'averaged networks' for adults, a temporal layered approach of the network development, and in-depth empirical studies on variation of the suture patterns in each species.

5.1.3 Illusions of Symmetry

A particular example of the typological error in the construction of skull network models is the tendency to symmetrize suture patterns when the 'type' form is described from real skulls. Figure 5.3 shows an example of this error in a turtle skull roof, where this is quite common. Here, the pattern of connection between left and right side bones is asymmetric (Fig. 5.3A) because the left prefrontal and the right frontal have a suture contact whereas their contralateral pairs have not an equivalent contact. However, representations and descriptions tend to omit, or minimize, this kind of variation by symmetrizing the connectivity patterns (Fig. 5.3B).

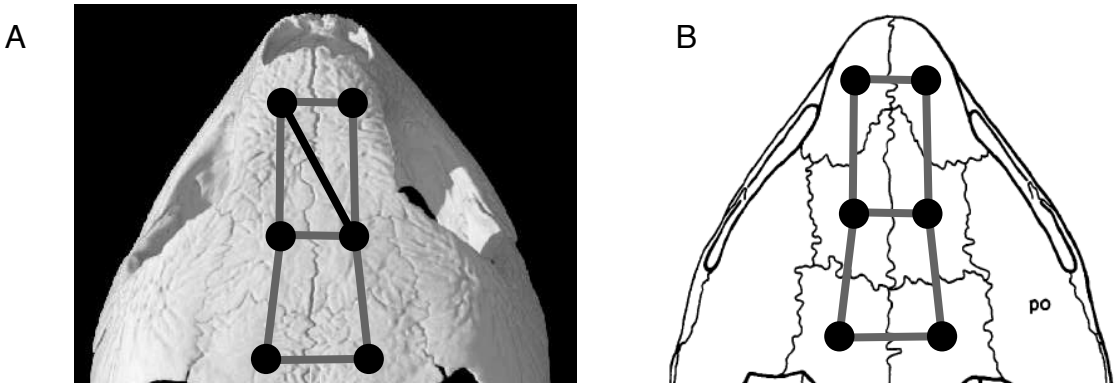

Figure 5.3: Example of the illusion of symmetry error in the skull roof of the turtle *Emys orbicularis*. A) CT scan of the skull in dorsal view from Digimorph (Jamniczky and Russell, 2007). B) Skull roof drawing (Gaffney, 1979).

This error is widespread, especially in fossil descriptions, in which connectivity patterns may be obscured by the conservation of specimens and taphonomic processes (see, e.g., De Renzi et al., 2002). For instance, differences in the description of *Seymouria baylorensis* mainly arose due to the dorsoventral compression of the skull and the incomplete conservation of some suture joints (White, 1939; Laurin, 1996). The origin of this error

lays in the well-established idea that the vertebrate body plan is symmetric bilaterally by default; a condition broken in some internal structures such as the heart (Rasskin-Gutman and Izpisua-Belmonte, 2004; Ibañes and Izpisúa-Belmonte, 2009). Thus, small disruptions of bilateral symmetry are thought to occur due to errors or fluctuations during development because of alterations of the developmental program or environmental stress (Valen, 1962; Hallgrímsson, 1998; Willmore et al., 2005). However, in the context of early development, it has been recognized that this kind of symmetric pattern, in which four elements meet in a point, is physically unstable (Fig. 5.4A), and that other accommodations (Fig. 5.4B-D) are more stable (Thompson, 1992).

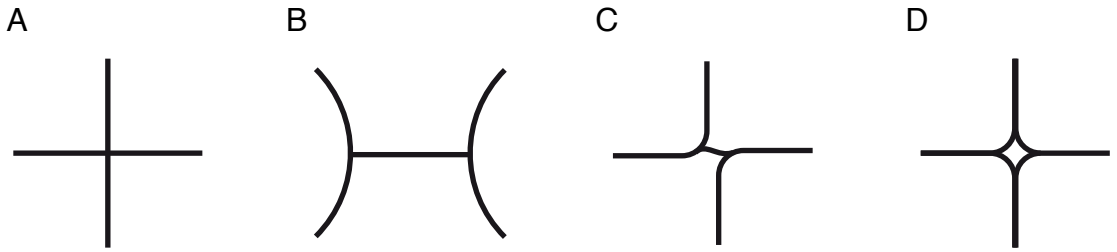

Figure 5.4: Example of patterns of intersection of four anatomical elements in one plane: A) a single point shaping a cross meeting point, B) a H-shape, C) a K-shape, and D) a rounded off shape with an empty space that stabilize the transitory single point stage. Notice that A and D would render the same connectivity pattern. Modified from Thompson (1992, pg. 490).

Regarding the identification of symmetric patterns in the four-cells developmental stage D'Arcy Thompson wrote, *"considering the physical stability of the other arrangement, the great preponderance of cases in which it is known to occur, the difficulty of recognizing the polar furrow in cases where it is very small and unless it be specially looked for, and the natural tendency of the draughtsman to make an all but symmetrical structure appear wholly so, I was wont to attribute to error or imperfect observation all those cases where the junction-lines of four cells are represented as a simple cross"*. This example comes from the observation of frog eggs during development at the four-cells stage, where the cross arrangement is transitory and tends to change to other, more stable arrangements, such as the H-shape and K-shape. This phenomenon is also observed in skulls, where H-shapes and K-shapes are common, for example, in the pterion sphenoparietal and

frontotemporal shapes, respectively. The single-point meeting of four bones (Fig. 5.4 A), as for four cells, is just an illusion. At a small scale of detail the instability of the cross is solved by an *"empty space or by a little drop of extraneous fluid"* (Fig. 5.4 D) that avoids a fourfold contact (Thompson, 1992). This would explain the stability of the symmetric pattern across the midline in skulls, but not exclude that the K-shape and the H-shape are also present in nature, and as such they are also a source of variation.

The skull network models constructed for this study assume that the connectivity patterns are symmetric across the midline; therefore, fourfold contact are impossible and were computed as no contact when observed.

5.2 Morphological Interpretation of Network Models

The interpretation of network parameters in a morphological context is a starting requirement to analyze skull network models. In this thesis, interpretations have been co-opted from earlier studies on morphological networks (Rasskin-Gutman and Buscalioni, 2001; Rasskin-Gutman, 2003; Magwene, 2008), as well as re-interpreted from studies of other types of biological networks (Guimerà et al., 2007; Dunne et al., 2008a; Horvath and Dong, 2008; Xu et al., 2011) and non-biological networks (Dorogovtsev and Mendes, 2003; Newman et al., 2006).

Although most of the concepts used to interpret network parameters have a deep background in other type of studies of the organismal form, for example, at the level of proportions, it is not the aim of this section to deal with the causal correlation between connections and proportions. The morphological interpretations that are offered here concern only the level of connections (Fig. 5.5).

5.2.1 Interpreting Model Descriptors

The model descriptors of the skull network, nodes and links, represent skull bones and suture joints, respectively. As such, they are discrete anatomical units with their own developmental features, structure, and functions. For instance, bones are hard parts with characteristic shapes that protect soft parts of the head and provide insertion surfaces for the muscles, whereas suture joints are fibrous attachments between bones that act as primary sites of bone growth and stress forces diffusors (see 1.1). The structural and functional roles of bones and sutures in the skull are useful to interpret the morphological meaning of properties derived from the skull suture pattern, that is, the connectivity

pattern captured in the adjacency matrix.

Abstraction Level	Network Theory	Morphology
Model Descriptors	Node	Bone
	Link	Suture
	Adjacency Matrix	Skull Suture Pattern
Element Descriptors	Connectivity	Burden Rank
	Clustering Coefficient	Co-relation
	Shortest Path Length	Proximity
	Z score	Compactedness
	Participation Index	Cohesiveness
System Descriptors	Density	Complexity
	Heterogeneity	Irregularity
	Connectivity Distribution	Burden Architecture
	Clustering Coefficient Distribution	Co-relation Architecture
	Mean Clustering Coefficient	Integration by Co-relation
	Mean Shortest Path Length	Integration by Proximity
Organization Descriptors	Small-World Effect	Order
	Hierarchy	Nestedness
	Community Structure	Modularity

Figure 5.5: Morphological Interpretation of Network Descriptors.

5.2.2 Interpreting Element Descriptors

The descriptors of network elements capture morphological properties of bones that appear as a consequence of the number and targets of their suture connections in the skull. Moreover, the interpretation of element descriptors is important because they are the basis for the computation of system descriptors.

Connectivity as Bone Burden-Rank

The boundaries of skull bones are of two types. One is the boundary of bones with other tissues, such as connective, muscular, or membranes that cover the brain, neural system, and sensory organs in general. The other type is the boundary with other skull bones

in the suture joints. Without neglecting the importance of the bone boundaries with other tissues (e.g., Moss's Functional Matrix, see 1.1.3), the role of craniofacial sutures as primary sites of bone growth determines the overall general morphology of the skull (Rice, 2008). Moreover, suture joints also participate in other functions, such as intracranial movements of bones (Jaslow, 1990) and strain sinks (Rafferty et al., 2003). Thus, it is expected that bones with more suture connections have central structural and functional roles affecting the morphology of the entire skull.

In this context, the more connections a bone has, the more dependences it establishes during development with other bones. This can also be interpreted as the presence of more developmental constraints or shape correlations among bones, because they are growing, acquiring shape, and functioning in coordination. Riedl's concept of burden (1978), captures this association between the number of connections (relations or dependences) between parts and the intensity of constraints, due to acquired developmental and evolutionary compromises (Schoch, 2010). Thus, bones with higher connectivity would have a higher burden rank than those with fewer connections, which would carry a relatively minor role in the skull structure maintenance (Esteve-Altava et al., 2013a). These roles, played during both development and evolution (Wagner and Laubichler, 2004), are important to understand the evolutionary patterns of skull morphology in vertebrates concerning bone losses and fusions (Esteve-Altava et al., 2013b,c).

Clustering Coefficient as Bone Correlation

The clustering coefficient of a bone (C_i) measures the presence of suture connections between its neighbors. Following the morphological interpretation of connectivity as developmental dependence between bones, C_i captures a kind of co-dependence of second order, or correlation (Dorogovtsev and Mendes, 2003). Groups of correlation can emerge as the interdependence between bones increases due to this second order relation. This clustering allows also for some flexibility to avoid developmental constraints thanks to the redundancy in the connectivity pattern. Thus, C_i is interpreted morphologically as an estimate of correlation of a bone with its neighbors; in other words, the level of integration of a bone in the skull.

Shortest Path Length as Bones Effective Proximity

The shortest path length between two bones ($\ell_{i,j}$) indicates the proximity of these bones in a network context. Since distances in networks are measured as the number of connections

that separate two elements, proximity has to be understood as the range of interdependence between two bones. Thus, two bones separated by two connections (i.e., with a suture contact to the same bone but not between them) have less co-dependence than two bones connected directly, and more than other two bones with a $\ell_{i,j} = 3$. As a consequence, correlation between bones would be higher if they are 'near' and lower if they are 'far' in the network; for example, in stress forces flow (Rafferty et al., 2003; Moazen et al., 2009) or in shape co-variations (Woo, 1931; Pearson and Woo, 1935). In this context, $\ell_{i,j}$ also captures integration between bones, but at a larger range than C_i.

Z Score as Bone Contribution to Module Compactedness

The within-module connectivity (Z_i) measures the contribution in number of connections of a bone to its module. As the contribution of the bone increases, all bones in the module are more packed. Consequently, there is an increasing in correlations and proximity between bones in the module. Thus, Z_i captures the contribution of a bone to its module compactedness. Rasskin-Gutman (2003) introduced the term compactedness as a synonym of density in morphological networks. Here, the term is used in a more restrictive way, as the contribution of one bone to its module density.

Participation Index as the Bone Contribution to Between-Modules Cohesiveness

The participation index of a bone in a modular organization (P_i) captures the number of suture connections to other bones outside the module; thus, generating cohesion between the different modules of the skull and creating the physical boundary between them. Bones with a higher P_i are responsible to maintain the cohesiveness and semi-independence between skull modules. Thus, the P_i is interpreted as the contribution of bones to skull cohesiveness. Horvath and Dong (2008) interpreted cohesiveness as interdependence due to the C_i of nodes. Here, the term cohesiveness is reserved for the role that some bones play in the integration of different modules, which illustrates better the meaning of the word.

5.2.3 Interpreting System Descriptors

System descriptors refer directly to some of the most important structural properties of the skull form.

Density of Connections as Morphological Complexity

The network density is the number of existing connections in the network of the total possible given the number of elements. In a network with density equal to 1 all elements are connected, that is, they are interacting. The relative number of connections is an index of the number of functional responses; thus, density has been interpreted as a measure of complexity in many other biological networks (Sporns, 2002; Newman and Forgacs, 2005; Proulx et al., 2005; Dunne et al., 2008a). It is expected that systems with more relationships would show more complex behaviors, and perform more functions. Thus, density is interpreted here as an estimate of morphological complexity of the skull network (Rasskin-Gutman, 2003; Esteve-Altava et al., 2013c).

Heterogeneity as Topological Irregularity

In a skull network, the primary difference between bones arises because of their number of connections. The skull has a regular or homogeneous arrangement of bones if all bones have the same connectivity. Conversely, if bones have a different number of connections, homogeneity turns into heterogeneity. The heterogeneity statistic is thus interpreted as the first descriptor of irregularity in skull networks.

It is an old claim in studies on evolutionary trends in skull morphology that a reduction in the number of bones (i.e., Williston's Law) is compensated by a differentiation of the remaining bones (see 1.2.1). This pattern-process is known as anisomerism, in contrast to polysomerism that accounts for patterns of less specialized, similar anatomical elements. In this context, heterogeneity has been also interpreted as anisomerism (Esteve-Altava et al., 2013c).

Connectivity and Clustering Distributions as the Skull 'Architectural Plan'

The literature on complex networks refers to the connectivity and clustering coefficient distributions of the network, *P(k)* and *C(k)*, as the system architecture; an analogy that illustrates the importance of these parameters to characterize structural patterns and generative processes (Barabasi and Bonabeau, 2003; Wutchy et al., 2006; Sales-Pardo et al., 2007; Horvath and Dong, 2008; Knight and Pinney, 2009). Notice that *P(k)* and *C(k)* capture the frequency of bones with a given connectivity and their clustering coefficient, respectively. With these two statistics one can build 'identical' skull networks, that is, the family of all isomorphic network; different in the labels of each element, but equal in structure (see 2.2.5). It is still a matter of discussion whether or not we can assume

that sharing an architectural plan means also sharing analogous generative processes and properties (Fox-Keller, 2005).

In morphology, the concept of architectural plan, body plan, or Bauplan has more connotations that in network science. However, the interpretation of the *P(k)* and the *C(k)* parameters as the morphological architectural plan makes sense at this structural, topological level. A step further in this interpretation is to consider similarities in skull network architectures as an evidence of the 'unity of type' or homology (see 2.2.4).

Clustering Coefficient and Path Length as Morphological Integration

The mean clustering coefficient ($\overline{C}$) and the mean shortest path length ($\overline{L}$) of the network are both parameters related to information flow and correlation in the system. Thus, $\overline{C}$ captures short-range information correlation due to redundancy among neighbor bones, while $\overline{L}$ determines the speed of information transmission to distant bones in the skull depending of their effective proximity.

In any morphological system there are three types of information flows, let's call them functional, developmental, and evolutionary. The functional information flow is related to the daily activity of the skulls in performing its functions, for example, the diffusion of stress forces acting on skull bones from injuries and feeding activity (Moazen et al., 2009), a flow that is determined by the presence and nature of suture junctions. The developmental information flow occurs between different skull bones during their coordinated development and growth in the form of allometric growth patterns (Huxley, 1932; Sardi et al., 2007; González et al., 2010). For instance, the premature closure of sutures leads to different types of deformities due to the compensatory and coordinate growth in other skull bones than are not directly involved in the suture closure (Hukki et al., 2008). Finally, evolutionary information flow is that observed as correlated variation between traits (or *"structured associations between the evolutionary divergence"*) because of the functional, developmental, and genetic integration, which allows to define morphological integration and modularity in morphological systems (Klingenberg, 2010). Therefore, $\overline{C}$ and $\overline{L}$ are interpreted as components of the morphological integration of the skull network, because of their central role in 'short' and 'long' correlation between bones determining the skull morphology.

5.2.4 Interpreting Organization Descriptors

The organization descriptors of the network are quantified by comparing the values of parameters of empirical networks with those of theoretical models (described in 6.1). These descriptors inform us on emergent patterns of organization in the skull, such as modularity and hierarchy. For instance, a network is said to be more or less regular in relation to a theoretical regular network, for which we know the expected values of some parameters. Thus, organization descriptors are interpreted as the organizational principles of skull networks.

The Small-World Effect as a State of Order

The identification of a network as a small-world network is made by comparing its $\overline{C}$ and $\overline{L}$ with those of a random equivalent network. Small-world networks are more clustered that random ones, sometimes more than regular networks too, and yet the proximity between elements is as small as it is in random networks or even slightly smaller (Watts and Strogatz, 1998). The presence of the small-world effect in a skull indicates that it exhibits a particular order in the suture pattern, between regularity and randomness. Riedl (1978) glimpsed this property of morphological order as *"a region of unspecified probability, a no-man's-land between accident and necessity"*. As a result of this mixed pattern of order some regions of the skull show an orderly arrangement of bones, while other regions are undistinguishable from randomness. The reason for this is the presence of some short-cut connections between bones that otherwise would be 'far away'. The bones that establish these special sutures are usually the skull hubs, or those bones identified as contributors to cohesiveness. As a consequence, modularity emerges in these skull networks.

Hierarchy as Nestedness of Building Blocks

A hierarchical structure in the skull network exists when groups of bones within modules tend to group also in smaller sub-modules or blocks. These blocks tend to be particularly highly clustered, so we can identify hierarchical organizations by looking at the architectural plan of the skull. The formation of small blocks occurs between less connected bones that tend to cluster, while more connected ones hierarchically integrate the blocks. Furthermore, hierarchical networks that represent any kind of systems are characterized by right-skewed *P(k)* and *C(k)*; ideally, both following power-law distribution functions (Wutchy et al., 2006).

Community Structure as Modularity

The presence of community structure in a network model of the skull is interpreted directly as the presence of a modular organization in the skull. In this context, a skull connectivity module is a set of bones more connected to bones within the module than to other bones outside the module. Modularity, like integration, is a multi-layered concept in morphology that arise at different levels of organization: developmental, genetic, functional, and evolutionary, and converge in morphological modules (Callebaut and Rasskin-Gutman, 2005; Klingenberg, 2008). Traditionally, morphological modules are inferred from data of covariation of morphological traits, usually sets of landmarks that tend to change together; thus, they are also called variational modules (Wagner et al., 2007).

Connectivity modules differ from variational modules in that they are inferred from the topological arrangement of anatomical units, and not the shapes of these units. The morphological information for variational and connectivity modules comes from completely different sources (Rasskin-Gutman, 2003). Since suture connections have precise roles in the skull development and function, connectivity modules have also a developmental and functional foundation, in addition to be originally structural or topological modules.

6

Null Models & Simulations

The comparative analyses carried out in this study require the use of null models to ascertain the presence of specific connectivity patterns. In addition, the study of evolutionary trends in skull networks has been complemented with computational model simulations. This chapter describes the special features of null models used here, as well as the computational model constructued to simulate skull evolution.

Null models and computational models have been scripted in a MATLAB environment (MATLAB, 2010) and they can also run in GNU Octave (Eaton, 2002) with few modifications. See Appendixs B and C for code descriptions.

6.1 Null Network Models

Null models are a special kind of models. They are not only idealized representations of strategies and scenarios for a given phenomenon, but they also provide a comparative baseline to analyze other models. For networks, it is most informative to analyze the growth rules and constraints that might cause connectivity patterns. The properties of empirical networks, when compared with those of the null models, reveal plausible mechanisms of network formation, which are interpreted here as plausible developmental and evolutionary processes. Even assuming that there is not a one-to-one mapping between the construction rules of networks and their properties (Fox-Keller, 2005), null models are useful heuristic tools.

Null models described in this section have been used for the following tasks:

- Providing null hypotheses of network organization in Chapter 4
- Setting initial premises of computational models of skull evolution in Chapter 9
- Constructing generative morphospaces in Chapter 11

- Providing hypotheses of developmental mechanisms in Chapter 12

6.1.1 The Regular Network

A network is regular if all its nodes have the same number of connections (Fig. 6.1). In addition, a network is strongly regular, $SRN(N, k_i, \lambda, \mu)$, if there are integers values for the common neighbors of every two adjacency nodes (λ) and every two non-adjacent nodes (μ) (Godsil and Royle, 2004).

Figure 6.1: Example of a regular network with $N = 10$ and $k_i = 4$ and a $SRN(10, 3, 0, 1)$. Single node properties are the same for all nodes because all of them are isomorphic.

Regular models represent highly ordered networks, in which all nodes are isomorphic in connectivity. Thus, network properties are precisely determined by the network descriptors: N, k_i, λ, and μ. For instance, the $P(k)$ function characteristic of regular networks is just a point because all nodes have the same connectivity. The fit of an empirical network to a regular model indicates that it has a homogeneous pattern of connections, which suggests possible causal biological mechanisms. For instance, the scutes in a turtle shell organized as a honeycomb. This regular pattern is formed by stationary accretion of keratin, a mechanism of homogeneous growth in all directions, which forms the characteristic growth rings of the scutes; in other words, a 'regular' mechanism related to a regular pattern.

6.1.2 The Erdös & Rényi Random Network

The Erdös & Rényi null model, *ER*, consist in a set of N nodes connected at random with a probability p (Erdös and Rényi, 1959); the choice whether or not to join two nodes are made independently for all pairs of nodes. The *ER* model captures a type of network where all connections are equally possible and there are no constraints. Some of

the properties of these networks are size-dependent and, for example, as the number of nodes increase the $P(k)$ tends to a Poisson distribution, the $\overline{L}$ increases as the logarithm of the number of nodes, and clusters tend to disappear (Dorogovtsev and Mendes, 2003). The value of p affects the completedness of the network. The higher the value of p, the higher the network density, mean clustering coefficient, and the lower the mean shortest path length. Thus, a network with $p = 0$ is totally disconnected and one with $p = 1$ is complete.

If the parameters of a network are significatively similar to those of a *ER* network, we cannot reject a mechanism of formation without preference of linkage (i.e., at random). In other words, the biological mechanisms that produce this organization are unbiased. On the contrary, a significant deviation from this null model would suggest that the biological mechanisms have linkage preferences, for example, constraints that prevent some links while facilitating others. For instance, the cranial cavity that hosts the human brain has a spherical shape that imposes a bias in the probability of connection between the occipital bone and the nasal bones, which is physically impossible given their range of shape. This is an example of a structural constraint on a connectivity pattern. Many processes can bias a pure random pattern of connection; as a consequence, real networks deviate from the *ER* null model. However, this null model is still valid as a comparative model to establish the presence of some network features, for example, the small-world effect.

6.1.3 The Random Equivalent Network

A random equivalent network, *REN*, is a random null model that has the $P(k)$ of another network as a restriction. This null model is constructed by rewiring at random the connections of another network while keeping its functional form (Luczak, 1990). Both, the *REN* and *ER* are null models of randomness; but the *REN* model stresses the relation between the $P(k)$ and the randomness in other network properties: the presence of hubs, the formation of clusters, and the reduction of path lengths. Again, a significant deviation indicates that the mechanism of formation is biased.

6.1.4 The Watts & Strogatz Model

The model of Watts & Strogatz (1998) is a mechanism to create networks with a small-world organization like those found in real systems, such as social networks, neural systems, and power grids. The process starts with a regular network that is sequentially rewired at random, with probability p (all nodes have an opportunity to change or keep

their connection). By increasing the parameter p from 0 to 1, a network switches from regular to random; the small-world organization is a transition state in this process (Fig. 6.2). Two network parameters, $\overline{C}$ and $\overline{L}$, show characteristic values for small-world networks, which are not found in regular and random networks; small-world networks have higher $\overline{C}$ than regular and random networks, and less or equal $\overline{L}$. In contrast, the $P(k)$ functions in these networks is similar to that of random networks (Albert and Barabási, 2002).

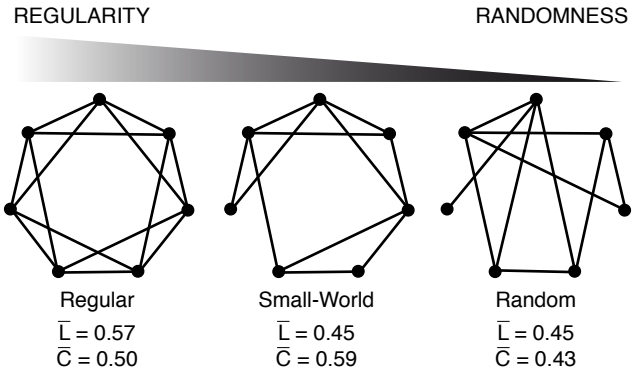

Figure 6.2: The Watts & Strogatz model creates small-world networks by introducing randomness in an initial regular network. Modified from Watts and Strogatz (1998).

6.1.5 The Barabási & Albert Model

The model of Barabási & Albert (1990) is a preferential attachment mechanism of network growth that generates power-law $P(k)$s. Barabási and Albert called these networks scale-free because of their topology, invariable at all scales. In this model, new nodes are connected sequentially to old nodes (already present in the network) with a probability that depends on the number of connections of the old nodes (Fig. 6.3); the nodes with more connections will get more new connections (*"the rich get richer"*). As a consequence of the topology generated by preferential attachment, scale-free networks show: a presence of hubs, a constant diameter, a $C(k)$ independent of k, and a tolerance to random losses of nodes (Barabási and Albert, 1990; Albert et al., 2000; Albert and Barabási, 2002).

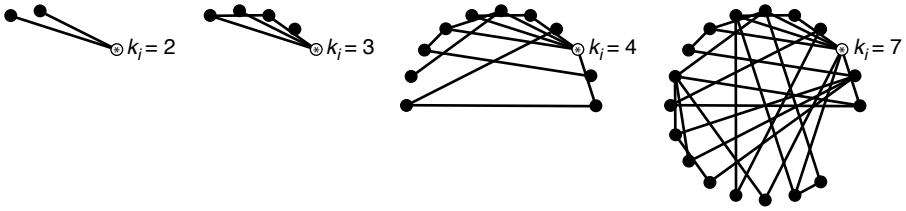

Figure 6.3: Example of a growth sequence by the Barabási & Albert model. The node marked with an asterisk has the highest probability to capture a new link as the network grows. Thus, the number of its connections increases progressively, until it becomes a network hub.

6.1.6 The Gabriel Network

A Gabriel network is kind of proximity network (Gabriel and Sokal, 1969). In contrast with all the previous networks, proximity networks are spatially constrained: two nodes only connect if they satisfy a geometric requirement. In a Gabriel network, *GN*, two nodes are connected if, and only if, the sphere whose diameter is the line between both nodes does not have any other node within its volume (Fig. 6.4).

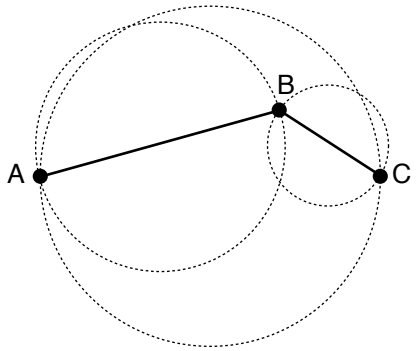

Figure 6.4: Geometric requirement in a 2D Gabriel network. Two nodes in a Gabriel network are connected if there are no other nodes in the space between them. Since other nodes are out of the circumference between A–B and B–C, connections between both pairs are possible (black lines); but, nodes A and C are disconnected because within its circumference there is a third node, B.

The *GN* null model states that the connectivity pattern of a node in the network is constrained by geometric distances, which prevent some connections and facilitate others. A deviation from a *GN* null model indicates that nodes can overcome those constraints that prevent their connection. When nodes have a regular distribution in space, the properties of *GN*s are equal than those found in regular networks (Gabriel and Sokal, 1980); however, here I use this model to work with random distributions of nodes in a 3D space. In this case, network properties largely depend on the number and exact position of nodes. A numerical analysis helps to identify the range of possible network properties in this scenario (Fig. 6.5).

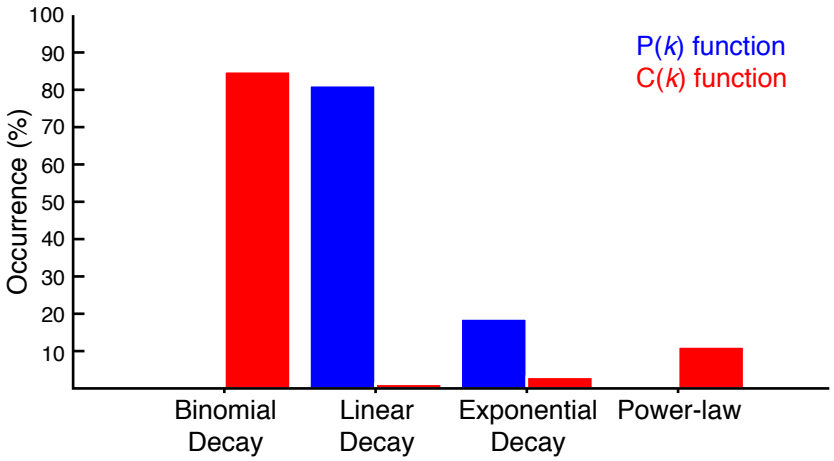

Figure 6.5: Numerical analysis of Gabriel networks. Histogram showing the occurrence of different $P(k)$ and $C(k)$ functions in 10,000 *GN*s of 21 nodes located at random. These *GN* networks are mainly characterized by a linear $P(k)$ and a binomial $C(k)$.

Proximity network models in general, and in particular the *GN* null models, capture an important developmental constraint in skulls: the impossibility of creating a suture contact between distant bones. Not because of the physical distance between ossification centers, but by the presence of insurmountable obstacles between them during development: cavities, openings, and other bones. Imagine each node in the network as an ossification center of the skull that starts to grow, constantly in all directions, taking the shape of a perfect sphere (in an idealized space). Two ossification centers would form a suture connection where they meet, which will inhibit the formation of new contacts there. Thus, a connection established previously will prevent new connections. For instance, this occurs in the pterion region of the human skull, where the parietal, the frontal, the temporal, and the

sphenoid bones meet. If the sphenoid and the parietal connect first, a frontal-temporal join is impossible; if the frontal and the temporal connect first, a sphenoid-parietal join is impossible (see Fig. 5.2). Virtually, this is the same problem observed in the scutes of turtle's shells, but now nodes are randomly distributed instead of regularly. Following the analogy of growth of ossification centers, a *GN* null model assumes two fundamental premises: (1) node positioning is random, and (2) node growth is homogeneous in speed and direction. The premise of homogeneous growth is the main null hypothesis of growth that this model offers to skull networks.

6.1.7 The Symmetric Gabriel Network

Symmetric Gabriel Networks, *SGN*, has been developed here as a null model for the analysis of skull networks, to account for fundamental properties of anatomical systems, i.e., bilateral symmetry. Thus, the properties of this model offer a better fit to real skull networks. SGN has been used here for the construction of computational models (see 9.2) and theoretical morphospaces in Chapter 11. Nodes in this model preserve bilateral symmetry. Additionally, some nodes can be located in the midline of the two bilaterally symmetric groups. The remaining spatial variables are random. *SGN* null models show slightly different properties than *GN* (Fig. 6.6).

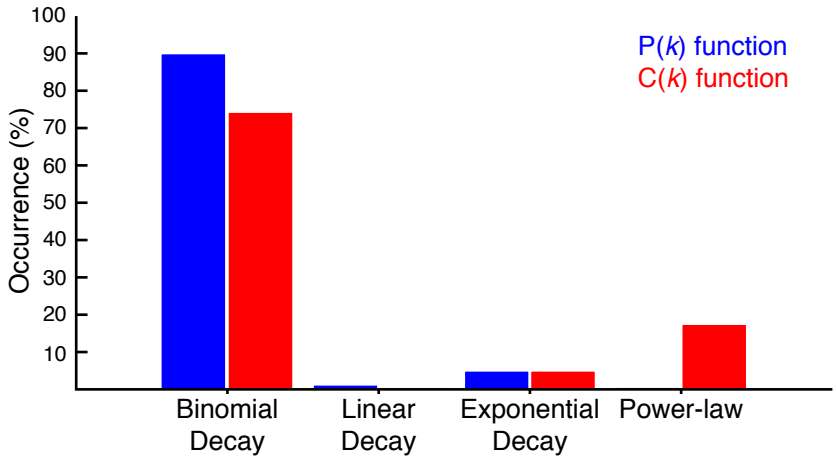

Figure 6.6: Numerical analysis of symmetric Gabriel networks. Histogram showing the occurrence of different $P(k)$ and $C(k)$ functions in 10,000 *SGN*s of 21 nodes: 14 located symmetrically and 5 in the midline (like in the human skull). For this type of network the $P(k)$ and $C(k)$ have a binomial distribution in most cases.

6.2 Computational Model of Skull Evolution

This section describes the computational model used in Chapter 9 to simulate the evolution of the skull by losses and fusions of bones (Fig. 6.7).

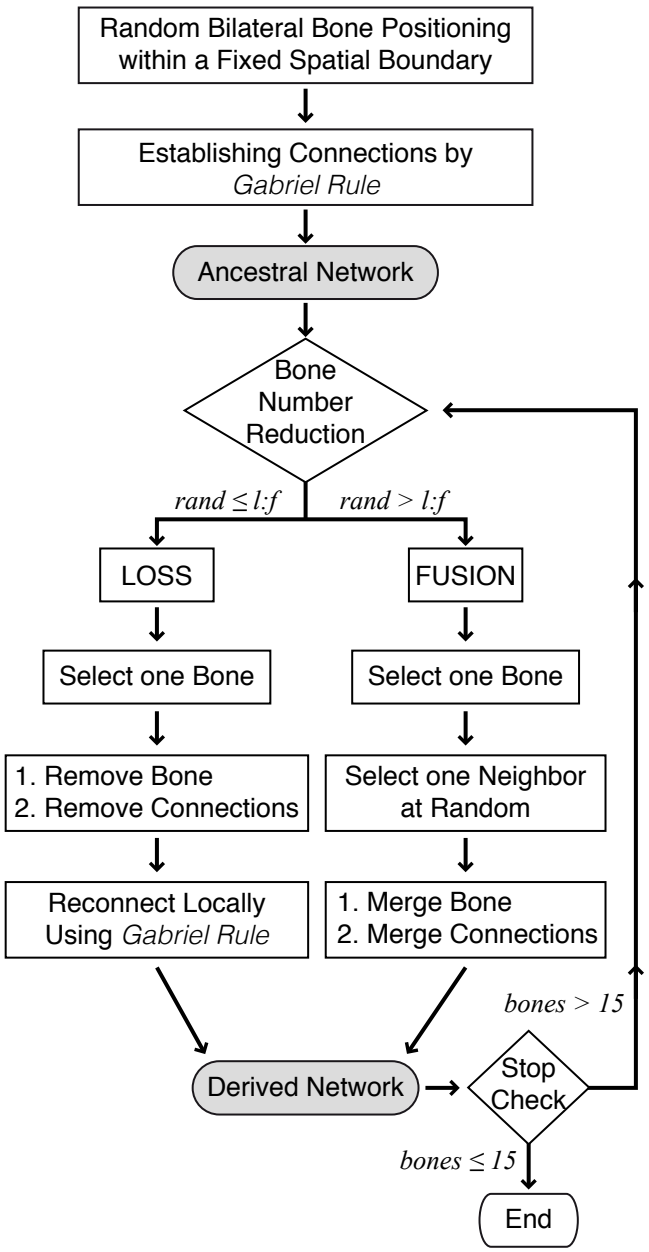

Figure 6.7: Computational model flowchart

The model starts each simulation with the generation of a random position vector that defines the coordinates of each initial bone in a fixed 3D Euclidean spatial boundary. We add an anatomically sound constraint: bones must preserve bilateral symmetry unless they are unpaired. Thus, paired bones are positioned with bilateral symmetry on both sides of the left-right axis at random locations; while unpaired bones are positioned along the midline in the left-right axis and randomly in the other axes. Once bones have been positioned (Fig. 6.8A) the Gabriel rule determines their junctions (Fig. 6.8B), forming a hypothetical ancestral skull network, in which each node represents a bone and each link represents a bone junction (Fig. 6.8C).

Then, the number of bones is reduced iteratively, by deciding between fusion and loss. The difference between these two mechanisms is that, for losses, the space left by the removed bone is locally re-wired again using the Gabriel rule; for fusions, connections are not lost, instead the 'new' bone inherits these connections. Reduction in the number of bones continues while the simulated skull network has more than 15 bones, otherwise the simulation stops. The reduction between the initial number of bones (60-67, see below) to 15 bones is a reasonable range that covers the empirical sample from the skulls with the highest number of bones, 56 (*Ichtyostega* and *Seymouria*) to the skull with the fewest, 18 (*Anser*). Figure 6.9 shows a 2D toy example of the bone number reduction process starting with only 12 bones and ending with 5.

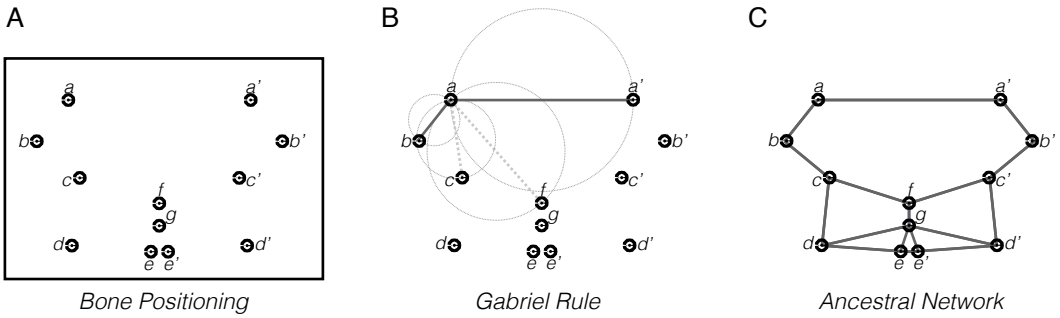

Figure 6.8: Simplified 12-bone positioning and Gabriel rule connection establishment. This network will be used as the hypothetical ancestral skull network in the example of bone number reduction shown in Figure 6.9. A) Positioning bones at random but preserving bilateral symmetry in a 2D boundary space. Note that bones f and g are medially positioned unpaired bones. B) Establishing connections among bones by applying the Gabriel rule: two bones connect if, and only if, the sphere whose diameter is the line between both bones does not have any other bone within its volume. In this 2D example, we show only the application of this rule to bone a. Circles have been drawn only for four bones (a', b, c, and f). Following the Gabriel rule, only a-a' and a-b will connect (solid line), whereas a-c and a-f will not (dashed line). C) After applying the Gabriel rule to all pairs of bones, a network among all bones is formed.

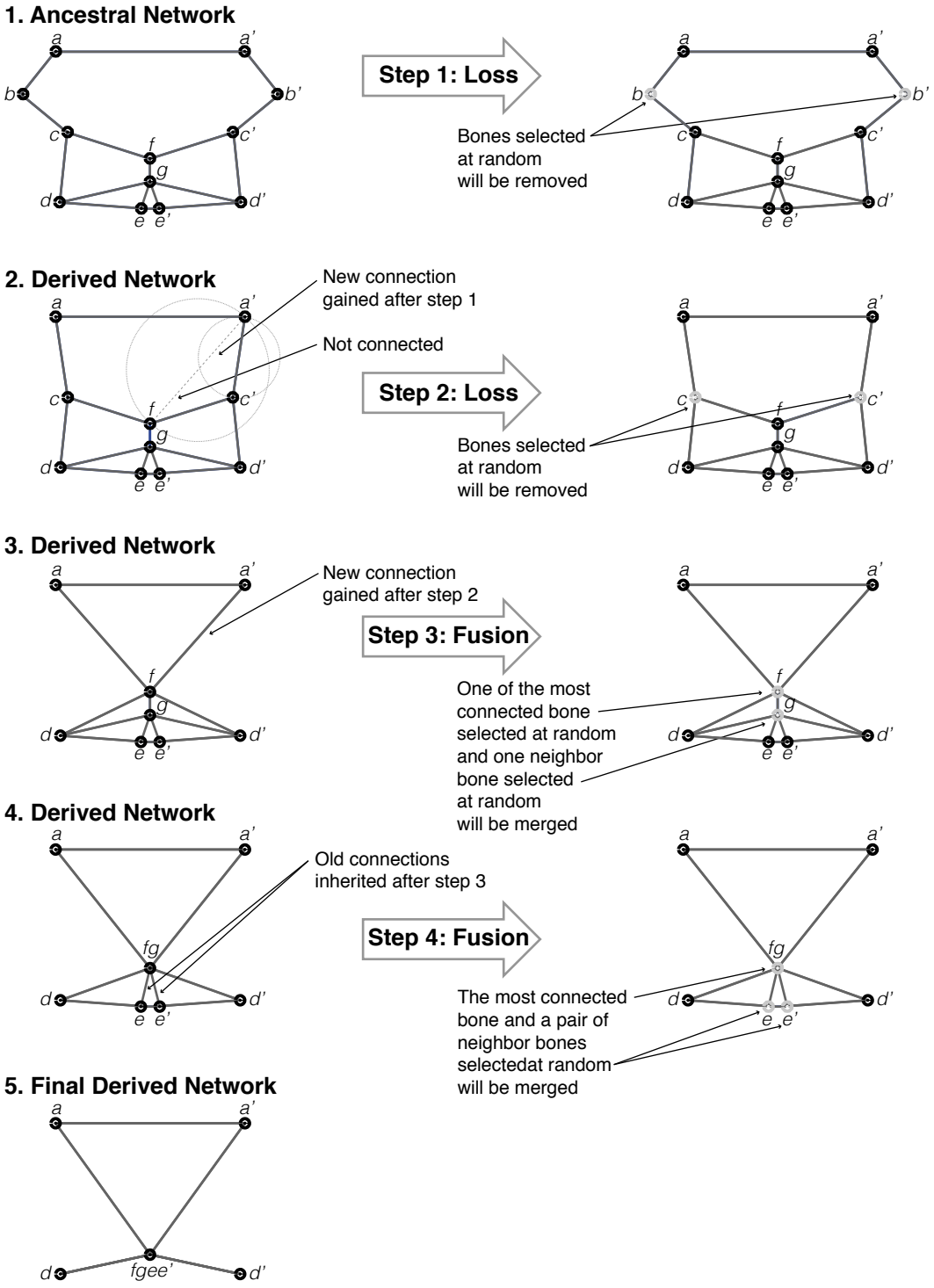

Figure 6.9: Simplified 2D example starting with the 12-bone ancestral network from Figure 6.8. The simulation reduced the number of bones by applying two loss and two fusion events (*l:f* was set to 0.5) to the initial network until a 5-bone derived network was reached. Note that bilateral symmetry is always preserved.

7

Sample & Phylogeny

For the present study I have built three-dimensional unweighted network models for 44 adult skulls of different tetrapod species. Taxa were selected to show the diversity of tetrapod skull morphologies, including extinct basal forms, depending on the available literature for a proper network modeling. In addition, seven network models were made for the human skull (*Homo sapiens*), one for each craniosynostosis condition analyzed in Chapter 12.

Figure 7.1 shows the general phylogenetic context of Tetrapoda used in this thesis.

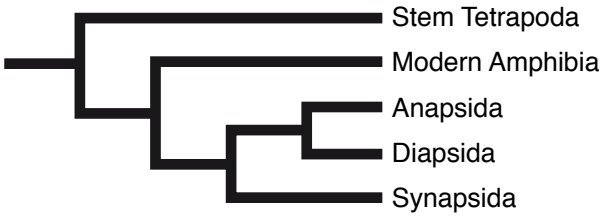

Figure 7.1: Basic phylogenetic context.

7.1 The Sample

- **Stem Tetrapoda**
  - †*Ichthyostega sp.* Säve-Söderbergh, 1932; from Kardong (2005)
  - †*Seymouria baylorensis* Broili, 1904; from Laurin (1996)
- **Modern Amphibia**
  - *Epicrionops petersi* Taylor, 1968; from Trueb (1993); Nussbaum (1977)
  - *Salamandra salamandra* Linnaeus, 1758; from Trueb (1993)
  - *Gastrotheca walkeri* Duellman, 1980; from Trueb (1993)
- **Anapsida**
  - †*Procolophon pricei* Lavina, 1983; from Carroll and Lindsay (1985)
  - †*Proganochelys quenstedti* Baur, 1887; from Gaffney (1990)
  - *Podocnemis unifilis* Troschel, 1848; from Gaffney (1979)
  - *Chelodina longicollis* Shaw, 1794; from Gaffney (1979)
  - †*Kayentachelys aprix* Gafney et al. 1987; from Sterli and Joyce (2007)
  - †*Chisternon undatum* Leidy, 1872; from Gaffney (1979)
  - *Chelydra serpentina* Linnaeus, 1758; from Gaffney (1979)
  - *Carettochelys insculpta* Ramsay, 1886; from Gaffney (1979)
  - *Gopherus polyphemus* Daudin, 1802; from Gaffney (1979)
  - *Testudo graeca* Linnaeus, 1758; from Gaffney (1979)
- **Diapsida**
  - †*Petrolacosaurus kansensis* Lane, 1945; from Reisz (1981)
  - †*Youngina capensis* Broom, 1914; from Carroll (1988); Gardner et al. (2010)
  - †*Rhamphorhynchus muensteri* Meyer, 1846; from Padian (1984)
  - *Crocodylus moreletii* Duméril & Duméril, 1851; from Goodrich (1958)
  - †*Stegosaurus armatus* Marsh, 1877; from Gilmore (1914); Weishampel et al. (1993)

  - †*Corythosaurus casuarius* Brown, 1914; from Ostrom (1961)
  - †*Plateosaurus engelhardti* Meyer, 1837; from Weishampel et al. (1993)
  - †*Dromaeosaurus albertensis* Matthew & Brown, 1922; from Carroll (1988)
  - *Anser anser* Linnaeus, 1758; from Kardong (2005)
  - *Sphenodon punctatus* Evans, 1980; from Goodrich (1958)
  - *Iguana iguana* Linnaeus, 1758; from Estes et al. (1988)
  - *Python regius* Shaw, 1802; from Estes et al. (1988); Kardong (2005)
  - *Hemitheconyx caudicinctus* Duméril, 1851; from Estes et al. (1988); Payne et al. (2011)
  - *Tupinambis teguixin* Linnaeus, 1758; from Estes et al. (1988)
  - *Diplometopon zarudnyi* Nikolskii, 1907; from Maisano et al. (2006)
  - *Stenocercus guentheri* Boulenger, 1885; from Torres-Carvajal (2003)
  - *Varanus salvator* Laurenti, 1768; from Estes et al. (1988); Rieppel (1993)

- **Synapsida**
  - †*Ennatosaurus tecton* Efemov, 1956; from Maddin et al. (2008)
  - †*Dimetrodon gigas* Cope, 1877; from Case (1904)
  - †*Jonkeria ingens* Hoepen, 1916; from Boonstra (1936)
  - †*Thrinaxodon liorhinus* Seeley, 1894; from Estes (1961)
  - *Ornithorhynchus anatinus* Shaw, 1799; from Kardong (2005)
  - *Phascolarctos cinereus* Goldfuss, 1817; from Louys et al. (2009)
  - *Didelphis virginiana* Kerr, 1792; from Kardong (2005)
  - *Homo sapiens* Linnaeus, 1758; from Gray (1918)
  - *Pteropus lylei* Andersen, 1908; from Giannini et al. (2006)
  - *Mus musculus* Linnaeus, 1758; from Goodrich (1958)
  - *Canis lupus* Linnaeus, 1758; from Mead and Fordyce (2009)
  - *Tursiops truncatus* Montagu, 1821; from Mead and Fordyce (2009)

7.2 Phylogenetic Context

Comparative anatomy is the study of the body structures across a range of species, which is accomplished by means of the comparative method within a phylogenetic context. Usually, these studies are made by comparing two or more phenotypic variables, such as body size or morphological measurements (Laurin, 2004; González-José et al., 2008; Laurin et al., 2009). The statistical techniques to perform these comparisons are regression and correlation for continuous variables, and contingency tables for discrete variables (Zar, 1999). However, the evolutionary relationship between the species under comparison violates the underlying assumption of independence between individuals that these methods assume (Felsenstein, 1985). In Chapter 9 this problem has been dealt with by using a phylogenetic independent contrast FIC4 (Laurin, 2004) to assess correlations between skull network parameters within a phylogenetic hypothesis.

7.2.1 Calibrated Phylogeny

The main prerequisite for a comparative analysis of morphological variables, like those quantified in the skull's network organization, is the use of a calibrated phylogeny, with which to perform valid statistical comparisons (Fig. 7.2).

The phylogenetic framework of analysis for this thesis is a supertree assembled according to consensus phylogenies for stem tetrapods (Laurin, 2004), amphibians (Cannatella, 2008), anapsids (Meylan, 2001; Hugall et al., 2007), diapsids (Okajima and Kumazawa, 2010; Hugall et al., 2007), and synapsids (Springer et al., 2003; Pace et al., 2008; Phillips et al., 2009). The assembly of major clades (Amphibia, Anapsida, Diapsida, and Synapsida) follows consensus phylogenies discussed in The Tree of Life Web Project (Laurin, 2011; Laurin and Reisz, 2011; Laurin and Gauthier, 2012). The lengths of the branches were calibrated by the minimal divergence time of the crown group, in million years of evolution (Ma). For this, time data were collected from the Paleobiological Database (available at http://paleodb.org), as well as phylogenies used to construct the supertree. When two branching events apparently occur at the same time, branch lengths were set to 3 as suggested in Laurin (2004). The supertree was constructed in Mesquite (Maddison and Maddison, 2011). Calibration was made assisted by the Stratigraphic Tool for Mesquite (Josse et al., 2011); recent geologic time scales were used (Gradstein et al., 1995; Roscher and Schneider, 2006; Gibbard et al., 2010).

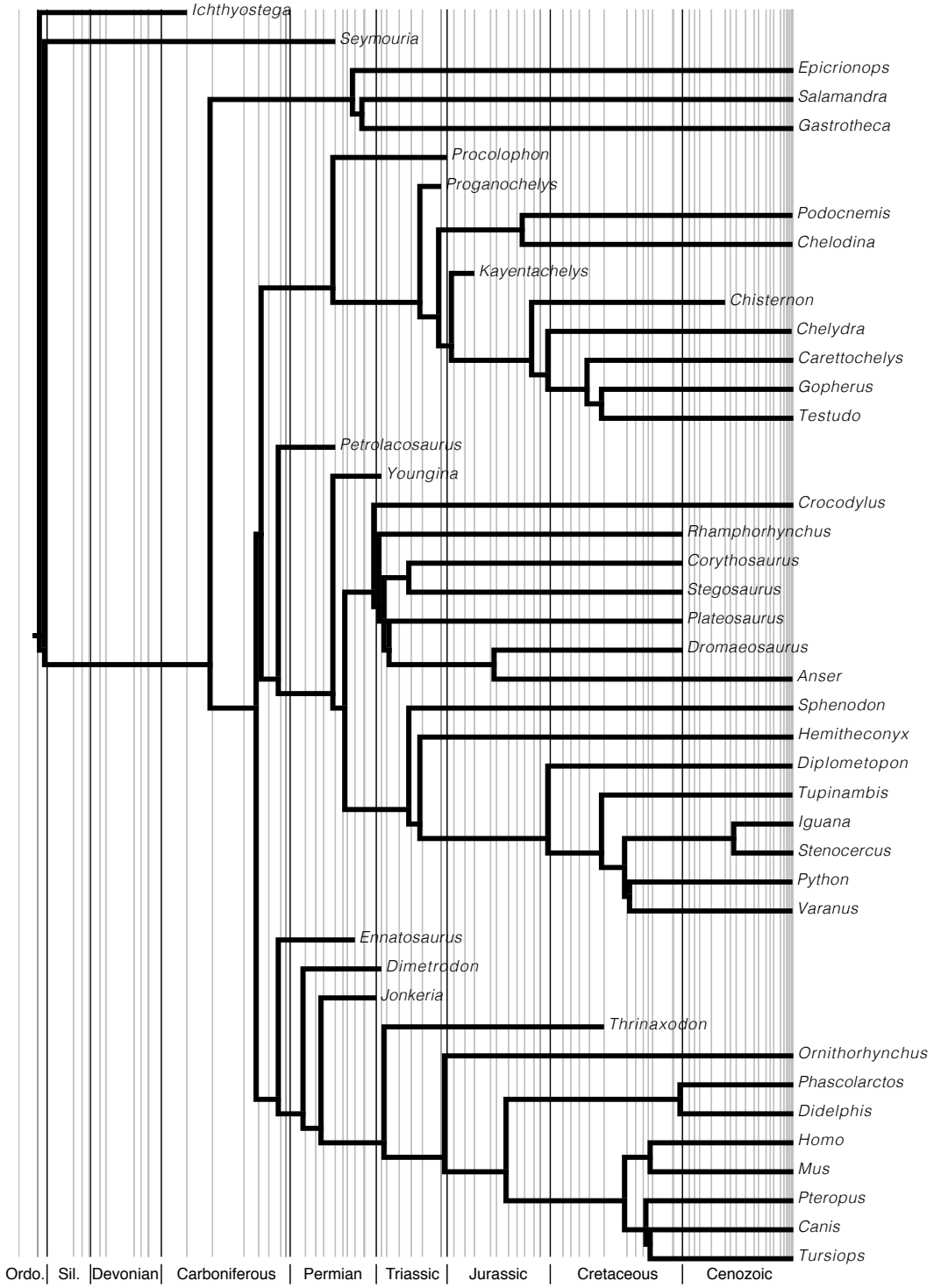

Figure 7.2: Calibrated phylogeny for the sample of study.

Part III

Results & Discussion

8

Network Analysis Results

This chapter summarizes the results of the network analysis of the 44 tetrapod skulls in two figures for each skull. The first set of figures show the values of network parameters, as well as the goodness of fit of $P(k)$ and $C(k)$. The second set of figures show the connectivity modules identified, the skull topological overlap matrix, the dendrogram generated in the hierarchical clustering analysis, a diagram of the skull in three different views (dorsal, ventral, and lateral), and the ZP space.

Ichthyostega sp. (Stem Tetrapoda)

Nodes	56
Links	148
Density	0.10
Clustering Coefficient	0.39
Shortest Path Length	2.94
Heterogeneity	0.38
Small-World	*Yes*
Modularity Q-value	0.50

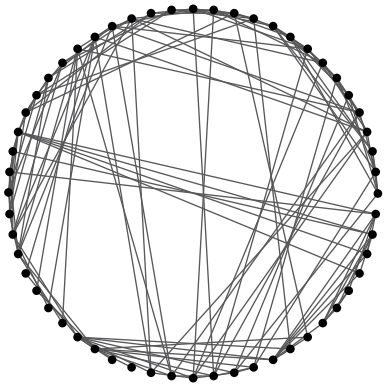

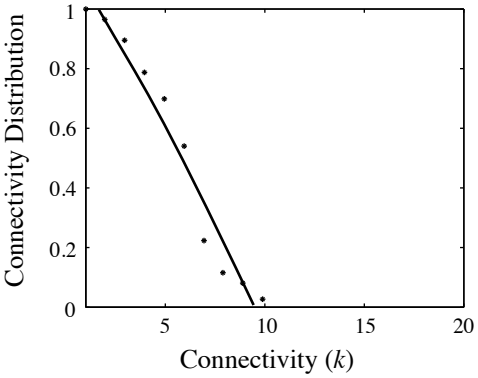

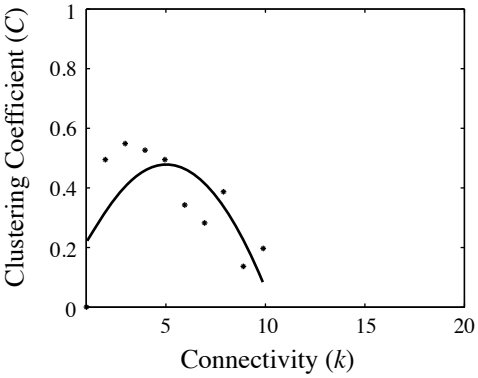

Best fit:

$P_{cum}(k) = 1.16 - 0.09\,k - 0.003\,k^2$

$\boldsymbol{r} = 0.98$ *(binomial)*

$\boldsymbol{r} = 0.98$ *(linear)*

$\boldsymbol{r} = 0.91$ *(exponential)*

$\boldsymbol{r} = 0.76$ *(power-law)*

Best fit:

$C(k) = 0.07 + 0.16\,k - 0.016\,k^2$

$\boldsymbol{r} = 0.71$ *(binomial)*

$\boldsymbol{r} = 0.24$ *(linear)*

$\boldsymbol{r} = 0.18$ *(exponential)*

$\boldsymbol{r} = 0.02$ *(power-law)*

Figure 8.1: Network analysis of the skull of *Ichthyostega sp.*

Ichthyostega sp. (Stem Tetrapoda)

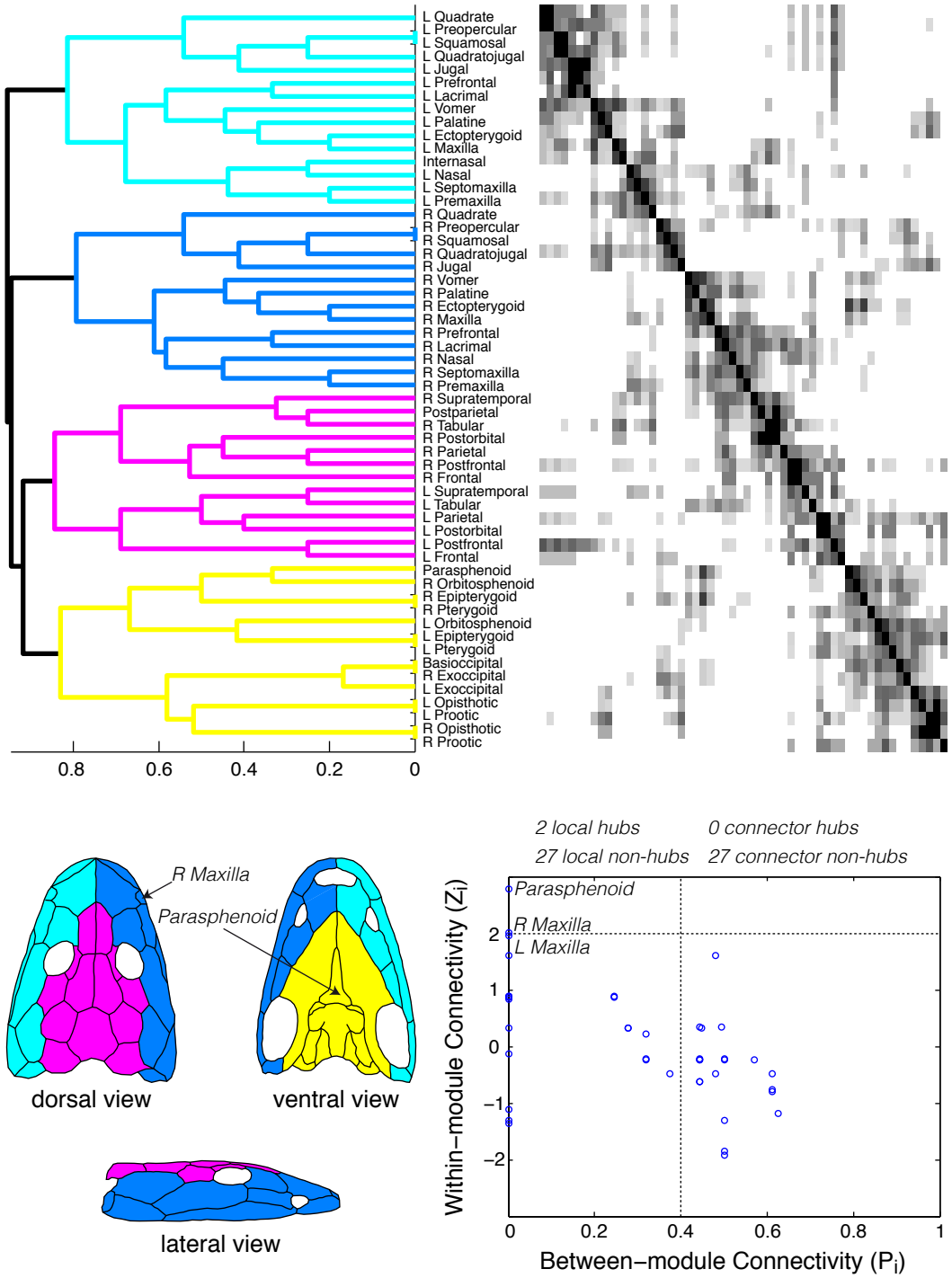

Figure 8.2: Connectivity modules in the skull of *Ichthyostega sp.*

Seymouria baylorensis (Stem Tetrapoda)

Nodes	56
Links	144
Density	0.09
Clustering Coefficient	0.38
Shortest Path Length	3.00
Heterogeneity	0.37
Small-World	*Yes*
Modularity Q-value	0.54

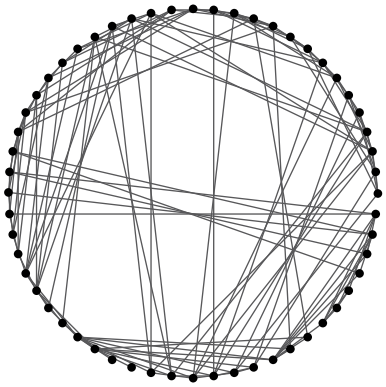

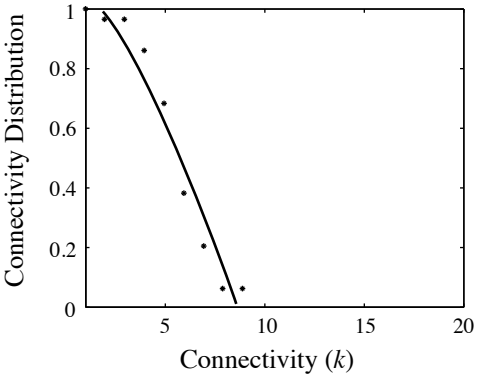

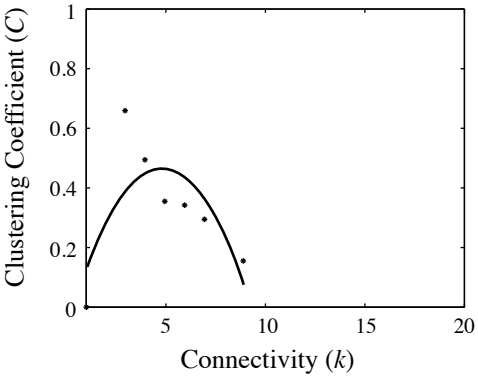

Best fit:

$P_{cum}(k) = 1.14 - 0.06\,k - 0.007\,k^2$

$\boldsymbol{r} = 0.97$ *(binomial)*

$\boldsymbol{r} = 0.97$ *(linear)*

$\boldsymbol{r} = 0.88$ *(exponential)*

$\boldsymbol{r} = 0.73$ *(power-law)*

Best fit:

$C(k) = -0.07 + 0.22\,k - 0.02\,k^2$

$\boldsymbol{r} = 0.74$ *(binomial)*

$\boldsymbol{r} = 0.14$ *(power-law)*

$\boldsymbol{r} = 0.07$ *(linear)*

$\boldsymbol{r} = 0.05$ *(exponential)*

Figure 8.3: Network analysis of the skull of *Seymouria baylorensis*.

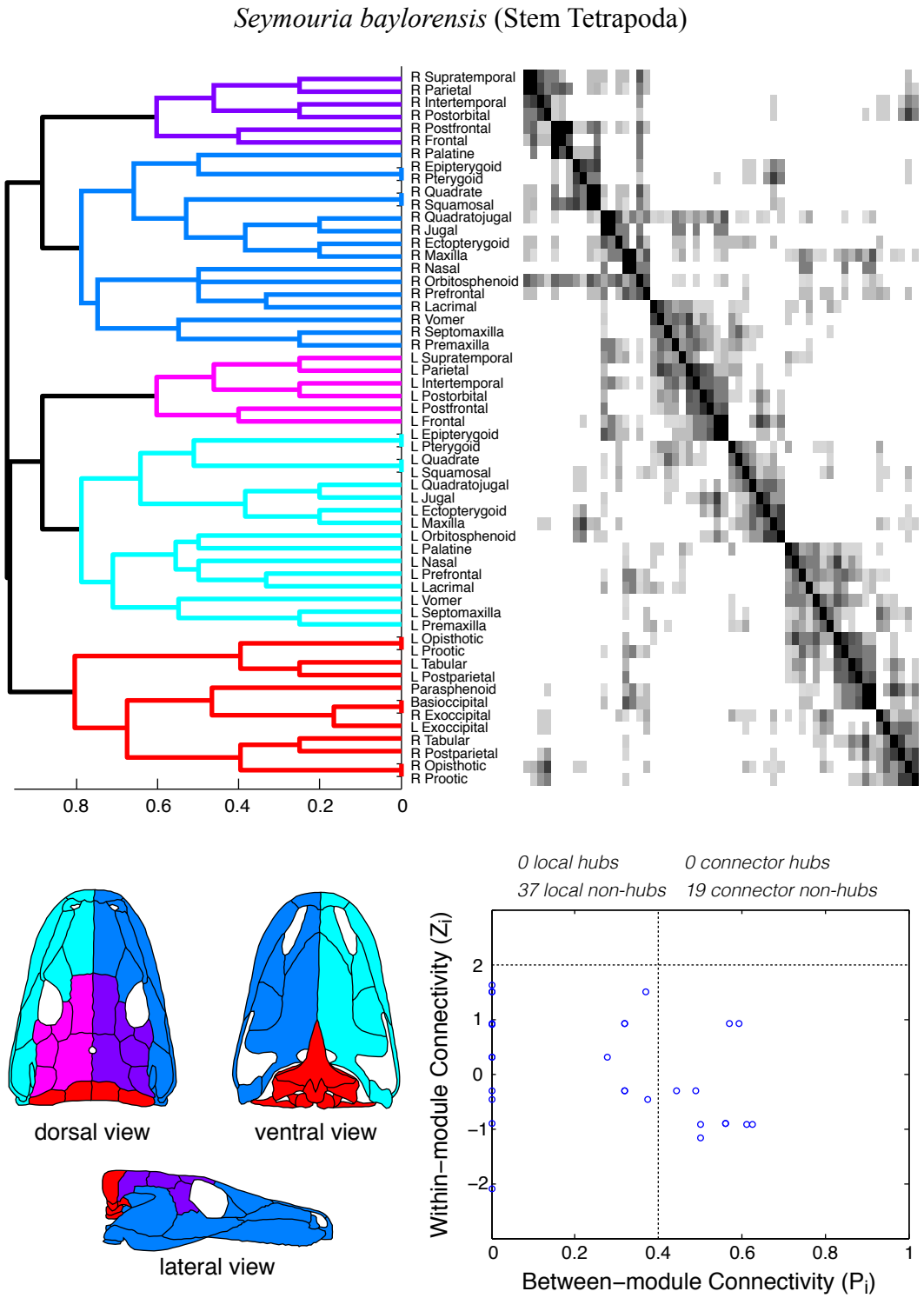

Figure 8.4: Connectivity modules in the skull of *Seymouria baylorensis*.

Epicrionops petersi (Amphibia: Gymnophina)

Nodes	23
Links	51
Density	0.20
Clustering Coefficient	0.59
Shortest Path Length	1.96
Heterogeneity	0.63
Small-World	*Yes*
Modularity Q-value	0.28

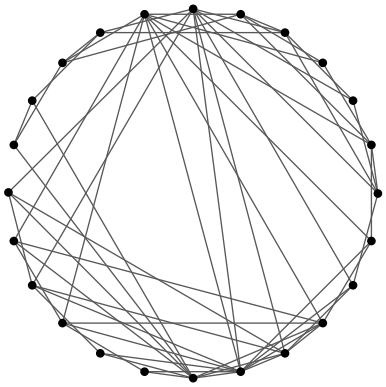

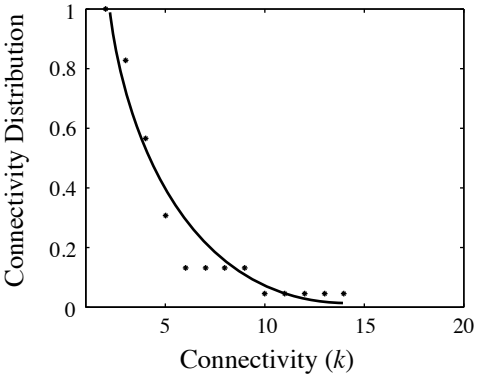

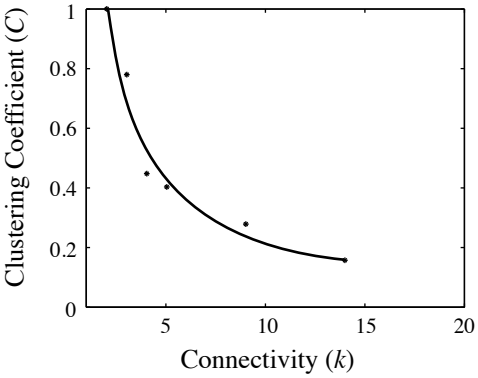

Best fit:

$P_{cum}(k) = 2.2\ e^{-0.37\,k}$

$\boldsymbol{r} = 0.98$ *(exponential)*

$\boldsymbol{r} = 0.97$ *(binomial)*

$\boldsymbol{r} = 0.95$ *(power-law)*

$\boldsymbol{r} = 0.84$ *(linear)*

Best fit:

$C(k) = 1.98\ k^{-0.96}$

$\boldsymbol{r} = 0.98$ *(power-law)*

$\boldsymbol{r} = 0.96$ *(exponential)*

$\boldsymbol{r} = 0.94$ *(binomial)*

$\boldsymbol{r} = 0.84$ *(linear)*

Figure 8.5: Network analysis of the skull of *Epicrionops petersi*.

Epicrionops petersi (Amphibia: Gymnophina)

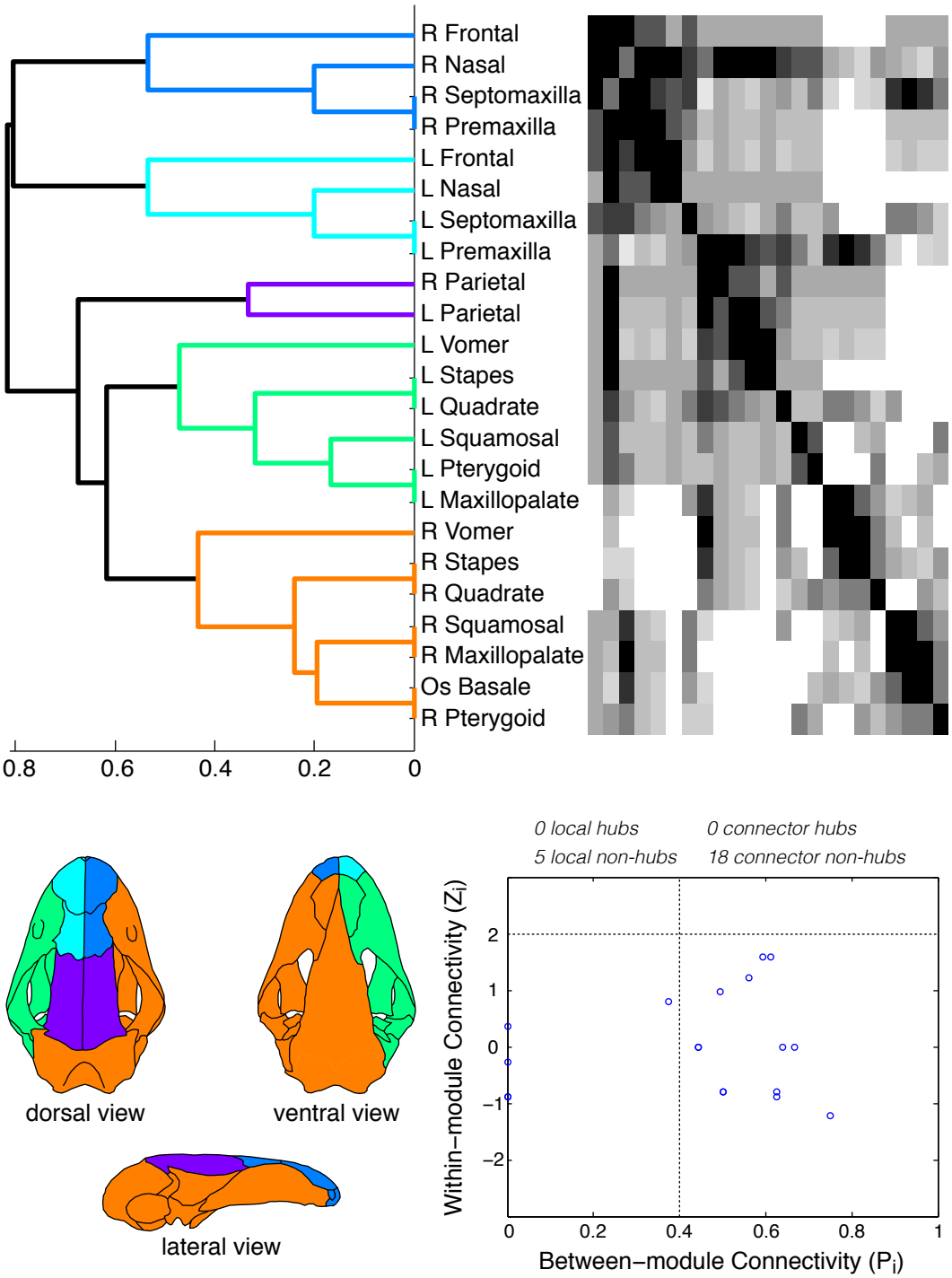

Figure 8.6: Connectivity modules in the skull of *Epicrionops petersi*.

Salamandra salamandra (Amphibia: Caudata)

Nodes	25
Links	52
Density	0.17
Clustering Coefficient	0.45
Shortest Path Length	2.61
Heterogeneity	0.27
Small-World	*Yes*
Modularity Q-value	0.49

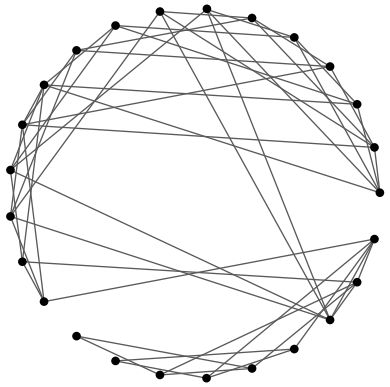

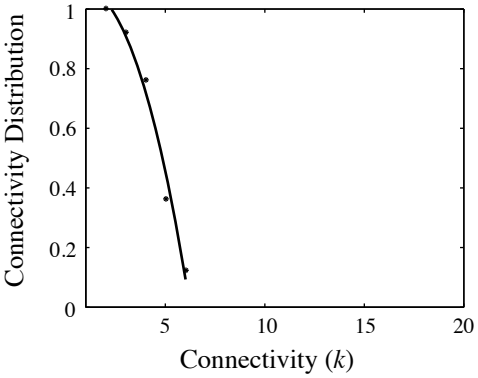

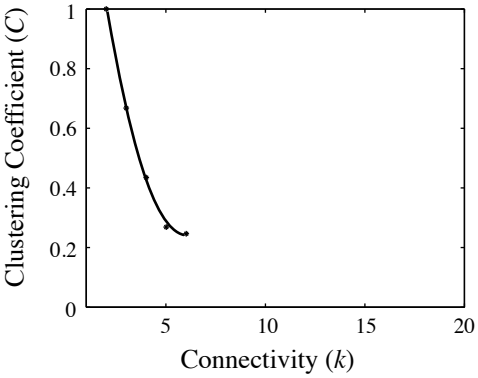

Best fit:

$P_{cum}(k) = 1 + 0.09\ k - 0.04\ k^2$

$\boldsymbol{r} = 0.99$ *(binomial)*

$\boldsymbol{r} = 0.97$ *(linear)*

$\boldsymbol{r} = 0.90$ *(exponential)*

$\boldsymbol{r} = 0.83$ *(power-law)*

Best fit:

$C(k) = 1.98 - 0.58\ k + 0.05\ k^2$

$\boldsymbol{r} = 0.99$ *(binomial)*

$\boldsymbol{r} = 0.99$ *(power-law)*

$\boldsymbol{r} = 0.99$ *(exponential)*

$\boldsymbol{r} = 0.96$ *(linear)*

Figure 8.7: Network analysis of the skull of *Salamandra salamandra*.

Salamandra salamandra (Amphibia: Caudata)

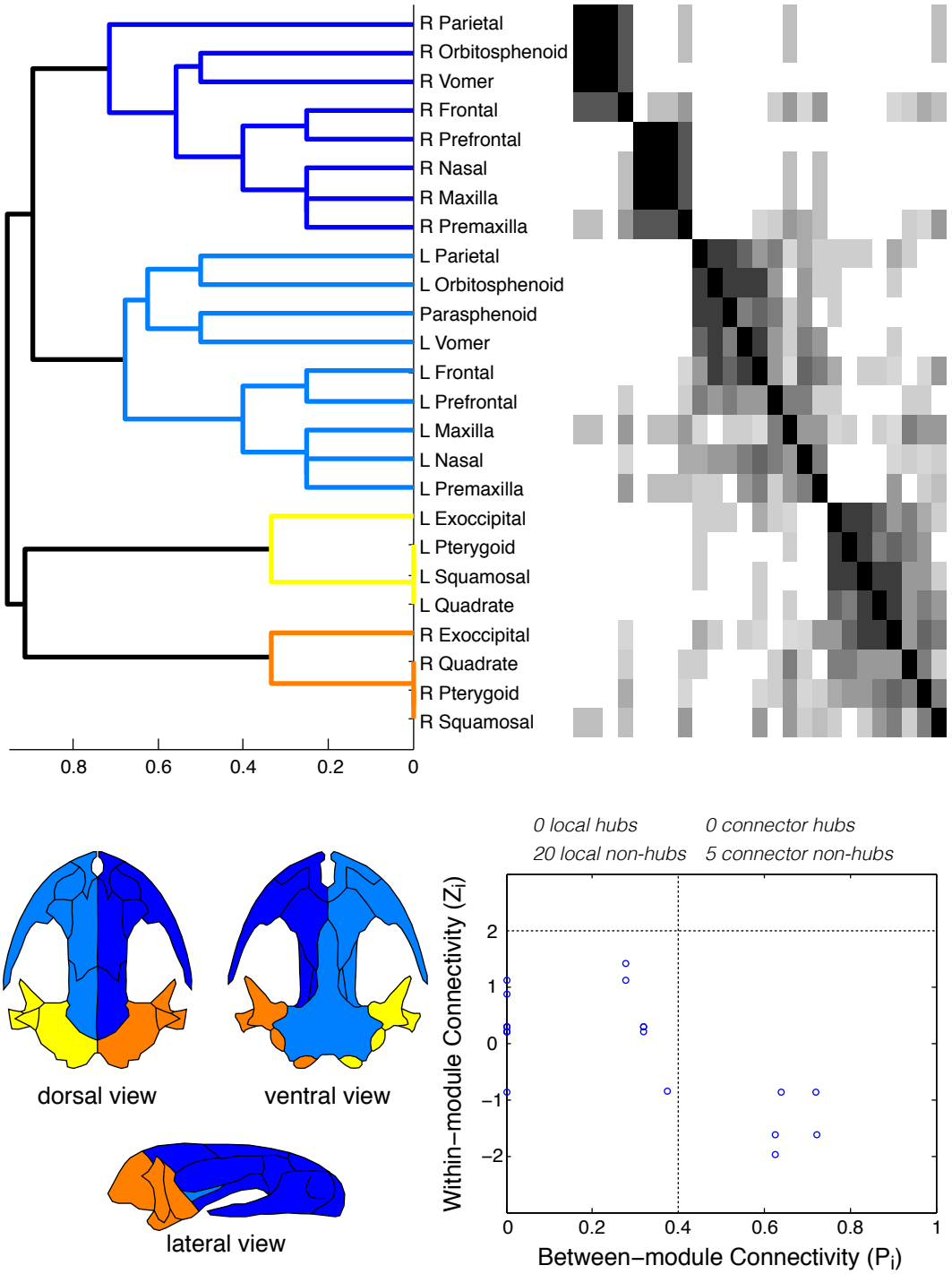

Figure 8.8: Connectivity modules in the skull of *Salamandra salamandra*.

Gastrotheca walkeri (Amphibia: Anura)

Nodes	22
Links	43
Density	0.19
Clustering Coefficient	0.44
Shortest Path Length	2.26
Heterogeneity	0.41
Small-World	*Yes*
Modularity Q-value	0.43

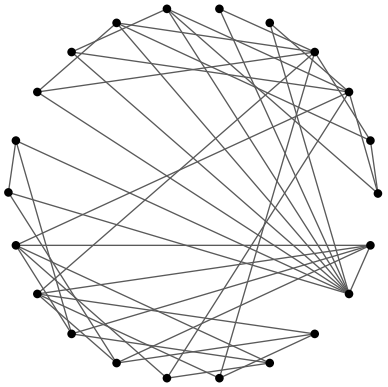

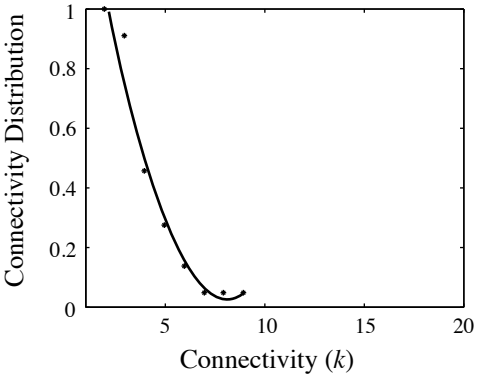

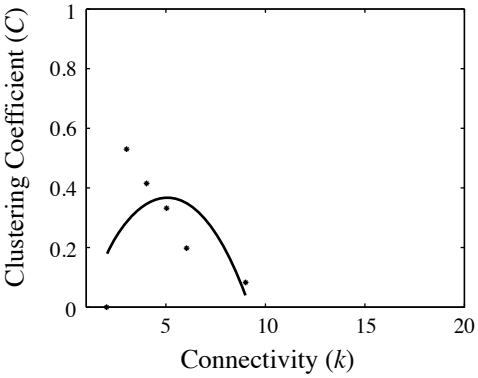

Best fit:

$P_{cum}(k) = 1.87 - 0.46\,k + 0.028\,k^2$

$\boldsymbol{r} = 0.98$ *(binomial)*

$\boldsymbol{r} = 0.97$ *(exponential)*

$\boldsymbol{r} = 0.92$ *(power-law)*

$\boldsymbol{r} = 0.92$ *(linear)*

Best fit:

$C(k) = -0.15 + 0.21\,k - 0.02\,k^2$

$\boldsymbol{r} = 0.63$ *(binomial)*

$\boldsymbol{r} = 0.06$ *(power-law)*

$\boldsymbol{r} = 0.19$ *(exponential)*

$\boldsymbol{r} = 0.27$ *(linear)*

Figure 8.9: Network analysis of the skull of *Gastrotheca walkeri*.

Gastrotheca walkeri (Amphibia: Anura)

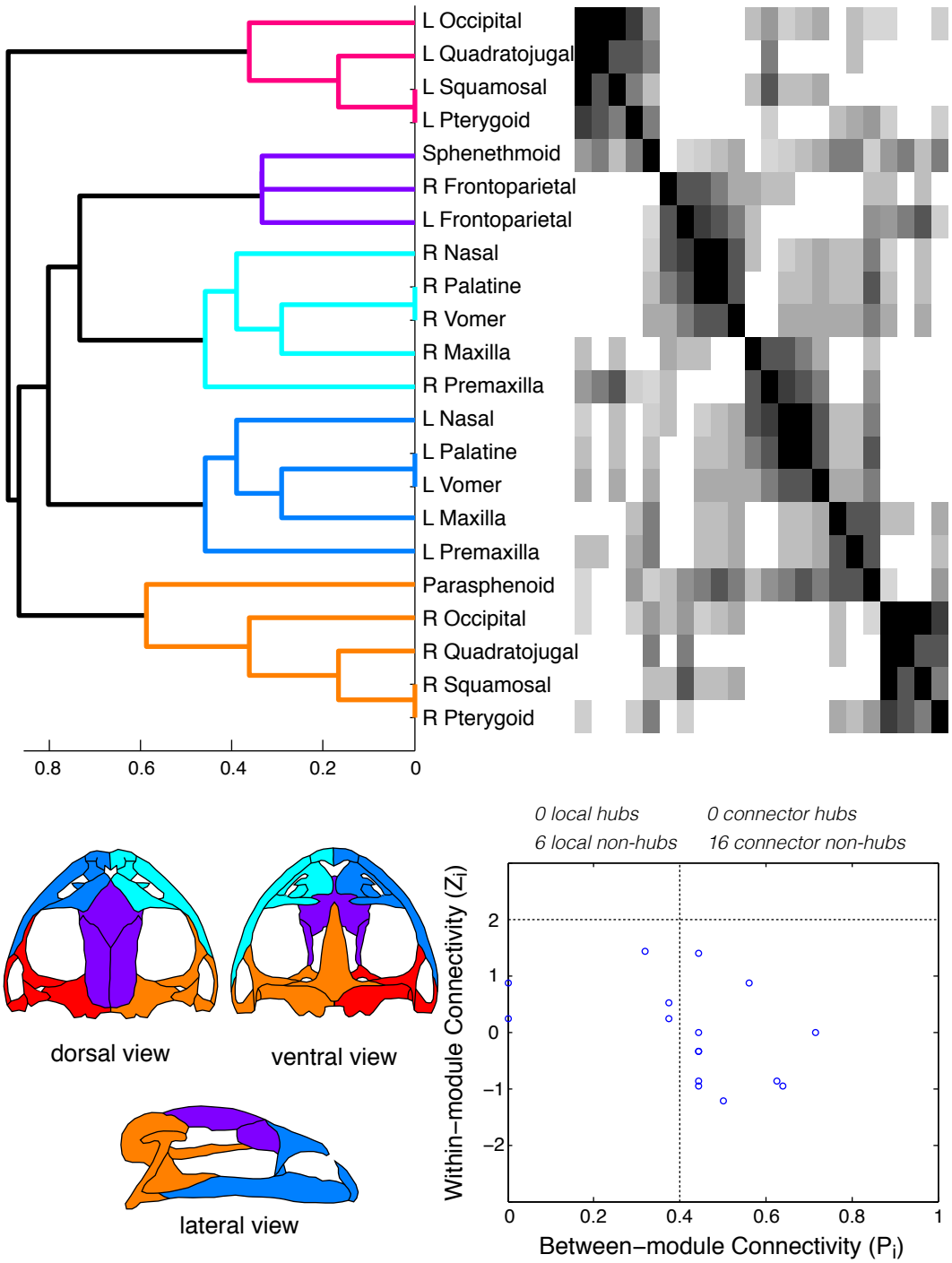

Figure 8.10: Connectivity modules in the skull of *Gastrotheca walkeri*.

Procolophon pricei (Reptilia: Procolophonomorpha)

Nodes	45
Links	120
Density	0.12
Clustering Coefficient	0.45
Shortest Path Length	2.69
Heterogeneity	0.38
Small-World	*Yes*
Modularity Q-value	0.54

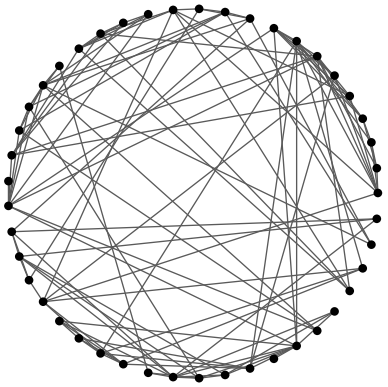

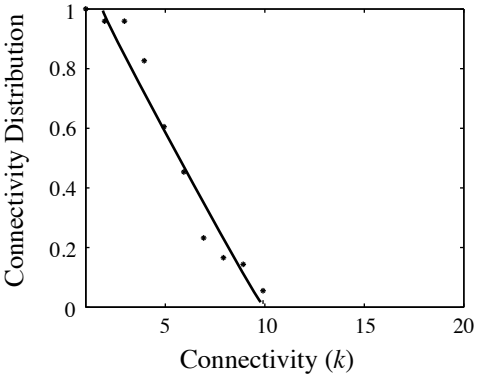

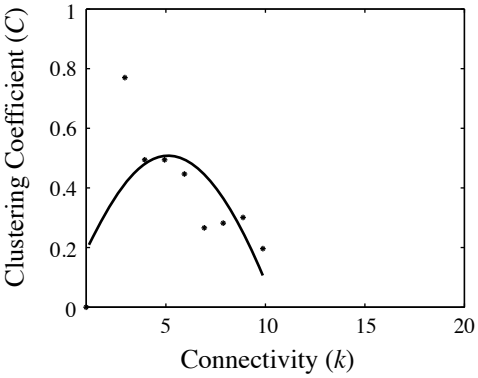

Best fit:

$P_{cum}(k) = 1.26 - 0.14\,k + 0.001\,k^2$

$\boldsymbol{r} = 0.98$ *(binomial)*

$\boldsymbol{r} = 0.98$ *(linear)*

$\boldsymbol{r} = 0.93$ *(exponential)*

$\boldsymbol{r} = 0.78$ *(power-law)*

Best fit:

$C(k) = 0.02 + 0.19\,k - 0.02\,k^2$

$\boldsymbol{r} = 0.67$ *(binomial)*

$\boldsymbol{r} = 0.17$ *(linear)*

$\boldsymbol{r} = 0.13$ *(exponential)*

$\boldsymbol{r} = 0.07$ *(power-law)*

Figure 8.11: Network analysis of the skull of *Procolophon pricei*.

Procolophon pricei (Reptilia: Procolophonomorpha)

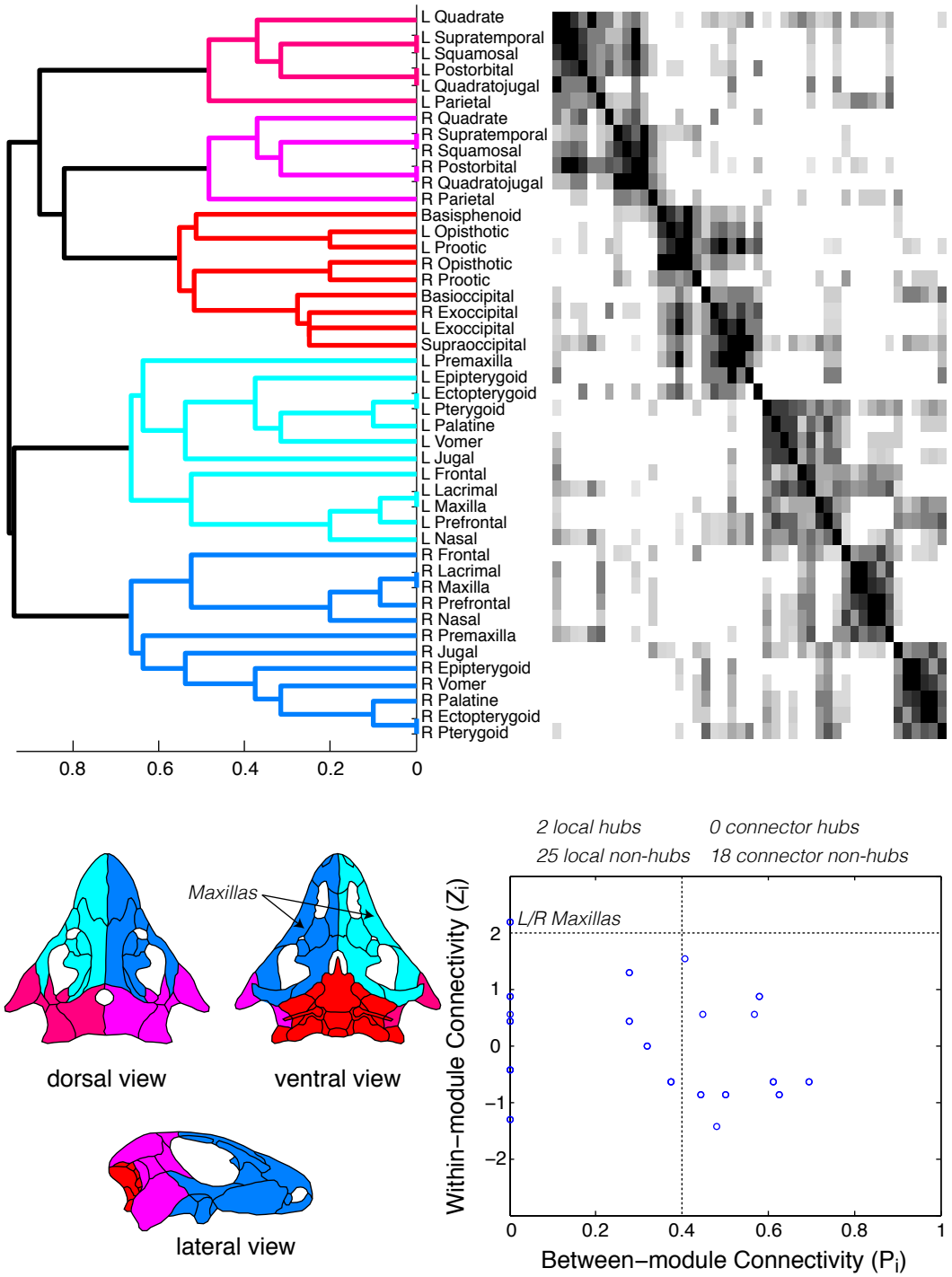

Figure 8.12: Connectivity modules in the skull of *Procolophon pricei*.

Proganochelys quenstedti (Reptilia: Testudines)

Nodes	43
Links	111
Density	0.12
Clustering Coefficient	0.43
Shortest Path Length	2.66
Heterogeneity	0.33
Small-World	*Yes*
Modularity Q-value	0.45

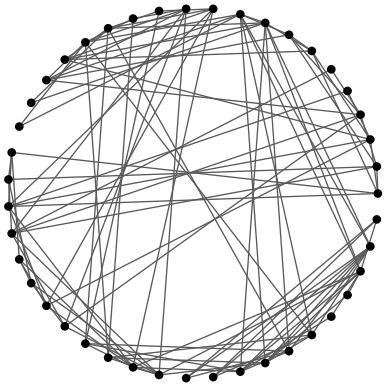

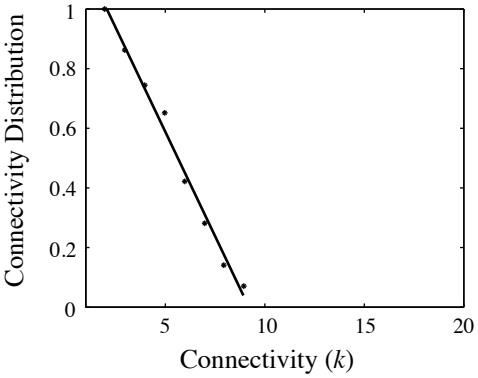

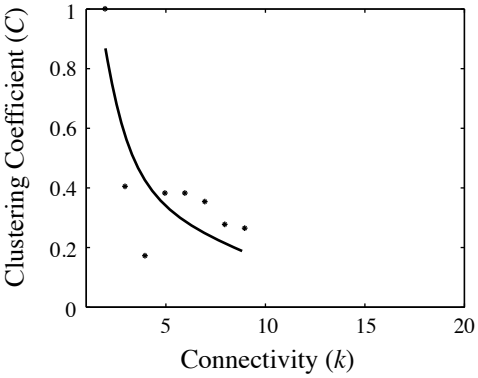

Best fit:

$P_{cum}(k) = 1.3 - 0.14\ k$

$\boldsymbol{r} = 0.99$ *(linear)*

$\boldsymbol{r} = 0.99$ *(binomial)*

$\boldsymbol{r} = 0.96$ *(exponential)*

$\boldsymbol{r} = 0.89$ *(power-law)*

Best fit:

$C(k) = 1.78\ k^{-1.03\ k}$

$\boldsymbol{r} = 0.85$ *(power-law)*

$\boldsymbol{r} = 0.75$ *(exponential)*

$\boldsymbol{r} = 0.60$ *(linear)*

$\boldsymbol{r} = 0.39$ *(binomial)*

Figure 8.13: Network analysis of the skull of *Proganochelys quenstedti*.

Proganochelys quenstedti (Reptilia: Testudines)

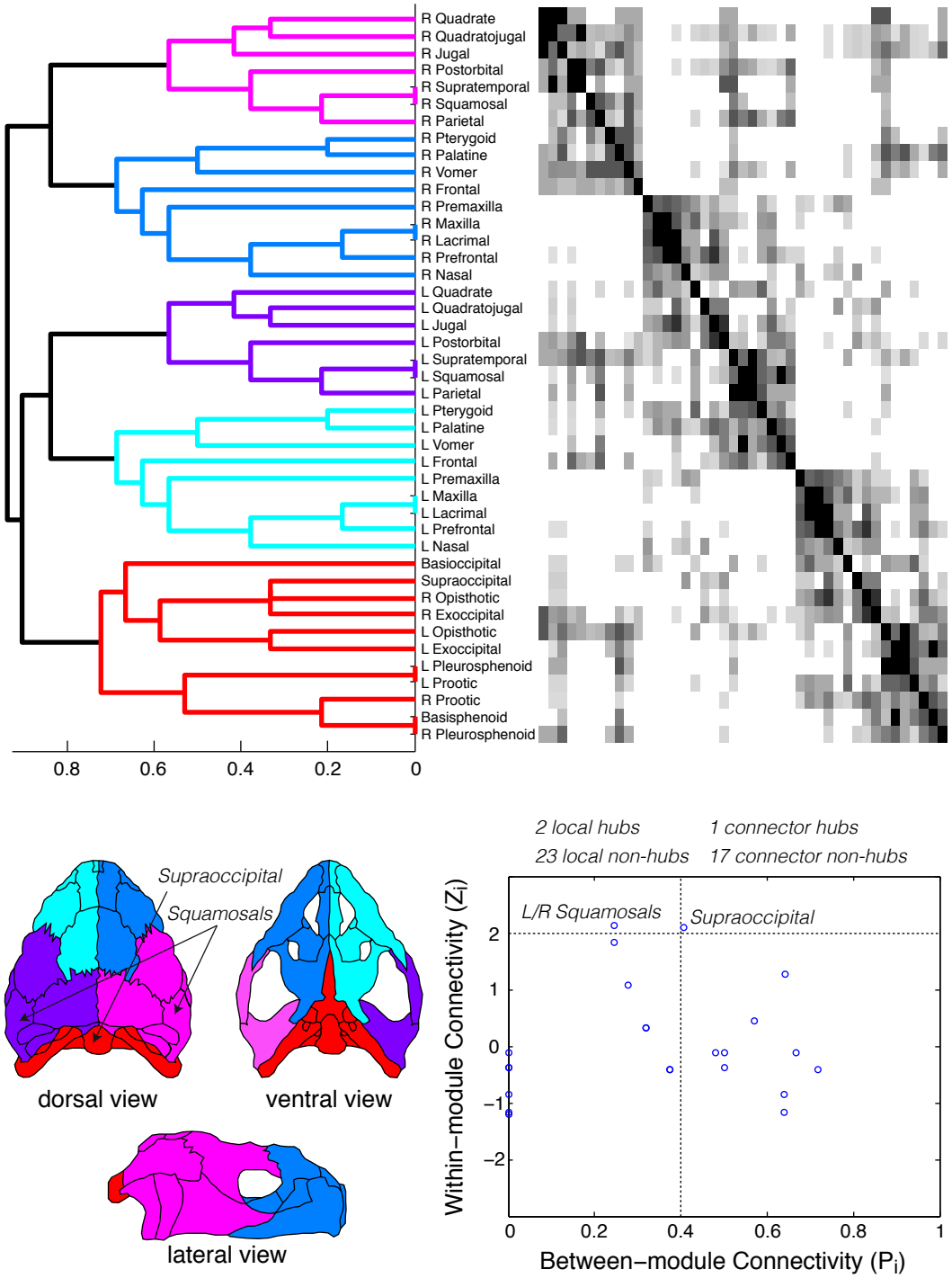

Figure 8.14: Connectivity modules in the skull of *Proganochelys quenstedti*.

Podocnemis unifilis (Reptilia: Testudines)

Nodes	34
Links	90
Density	0.16
Clustering Coefficient	0.34
Shortest Path Length	2.41
Heterogeneity	0.41
Small-World	*Yes*
Modularity Q-value	0.40

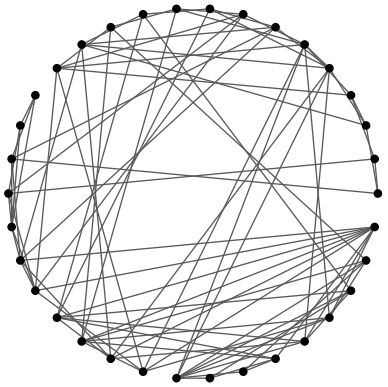

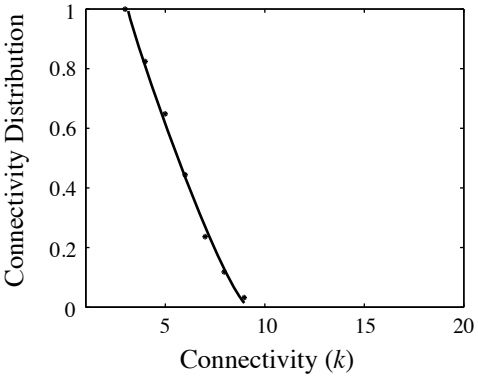

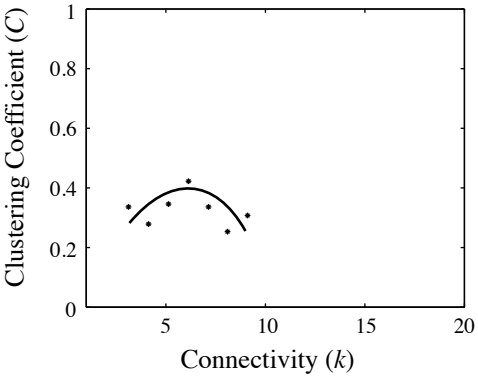

Best fit:

$P_{cum}(k) = 1.77 - 0.27\ k + 0.009\ k^2$

$\boldsymbol{r} = 0.99$ *(binomial)*

$\boldsymbol{r} = 0.99$ *(linear)*

$\boldsymbol{r} = 0.97$ *(exponential)*

$\boldsymbol{r} = 0.93$ *(power-law)*

Best fit:

$C(k) = 0.34 + 0.003\ k - 0.001\ k^2$

$\boldsymbol{r} = 0.32$ *(binomial)*

$\boldsymbol{r} = 0.21$ *(linear)*

$\boldsymbol{r} = 0.20$ *(exponential)*

$\boldsymbol{r} = 0.14$ *(power-law)*

Figure 8.15: Network analysis of the skull of *Podocnemis unifilis*.

Podocnemis unifilis (Reptilia: Testudines)

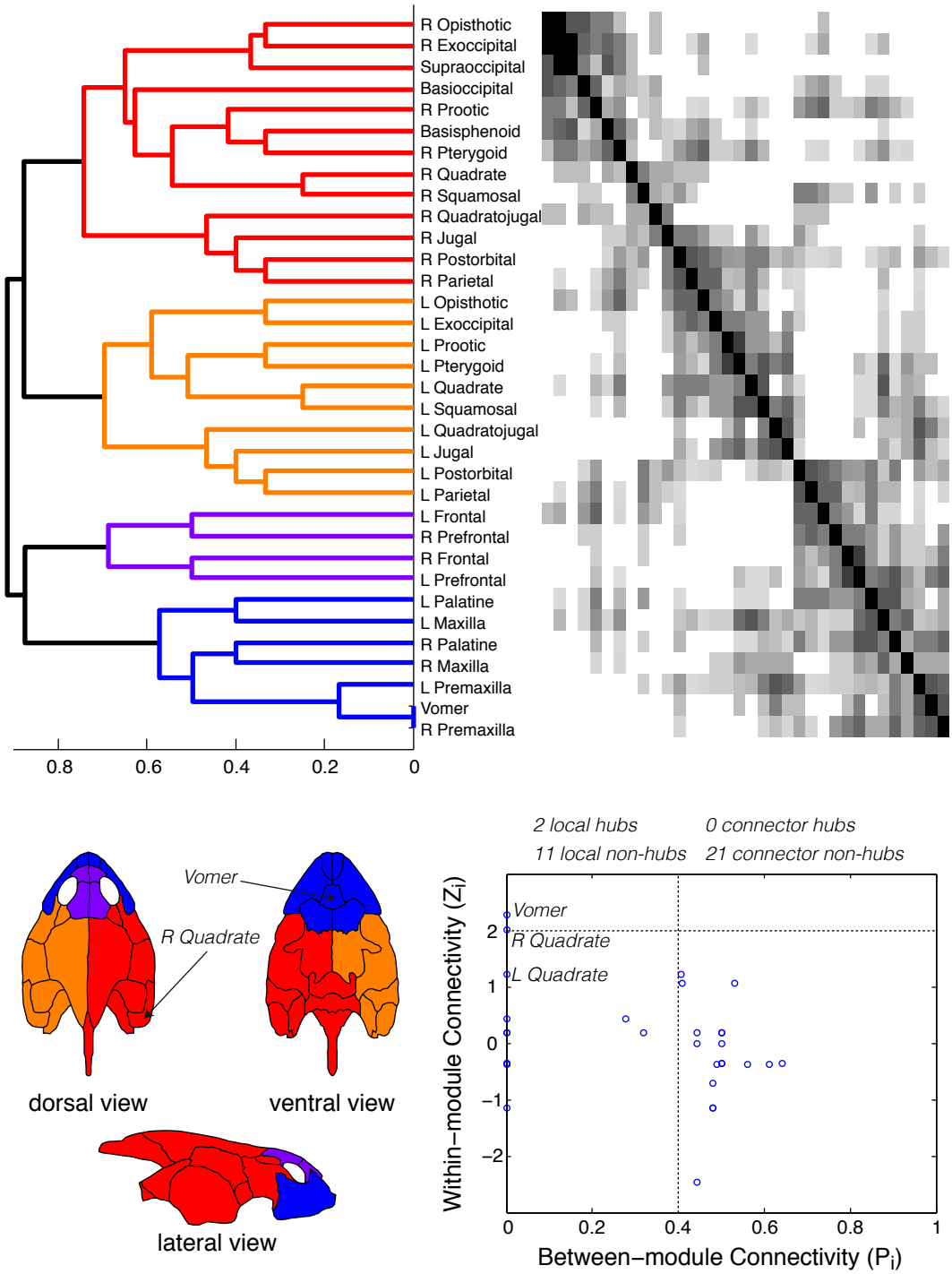

Figure 8.16: Connectivity modules in the skull of *Podocnemis unifilis*.

Chelodina longicollis (Reptilia: Testudines)

Nodes	33
Links	80
Density	0.15
Clustering Coefficient	0.43
Shortest Path Length	2.56
Heterogeneity	0.40
Small-World	*Yes*
Modularity Q-value	0.44

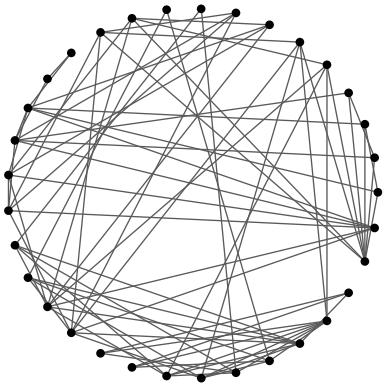

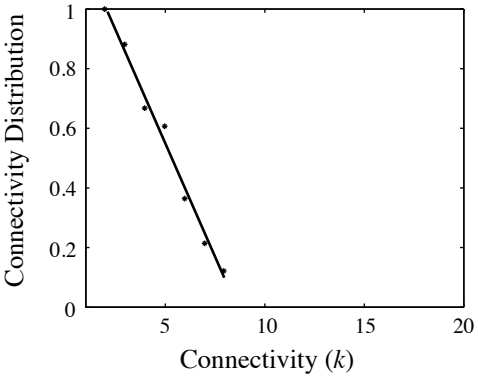

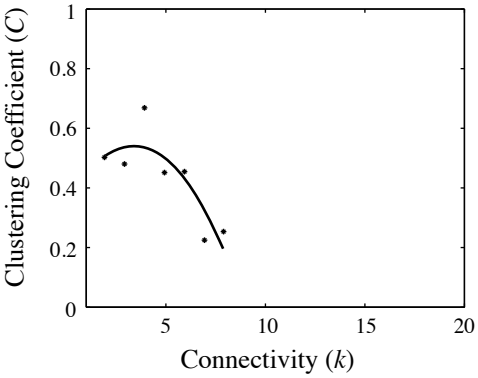

Best fit:

$P_{cum}(k) = 1.3 - 0.16\,k + 0.001\,k^2$

$\boldsymbol{r} = 0.99$ *(binomial)*

$\boldsymbol{r} = 0.99$ *(linear)*

$\boldsymbol{r} = 0.97$ *(exponential)*

$\boldsymbol{r} = 0.91$ *(power-law)*

Best fit:

$C(k) = 0.34 + 0.11\,k - 0.017\,k^2$

$\boldsymbol{r} = 0.85$ *(binomial)*

$\boldsymbol{r} = 0.74$ *(linear)*

$\boldsymbol{r} = 0.68$ *(exponential)*

$\boldsymbol{r} = 0.57$ *(power-law)*

Figure 8.17: Network analysis of the skull of *Chelodina longicollis*.

Chelodina longicollis (Reptilia: Testudines)

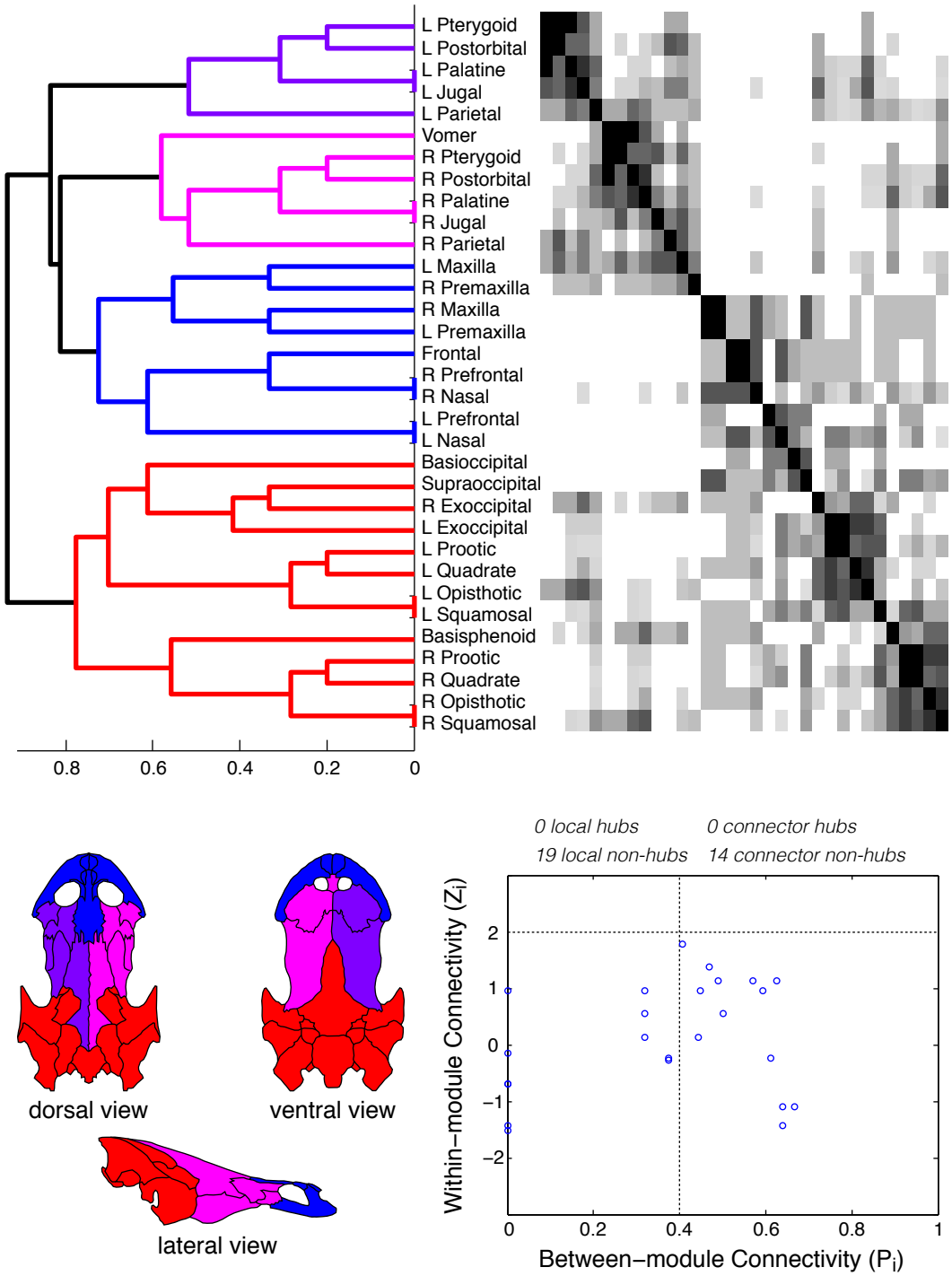

Figure 8.18: Connectivity modules in the skull of *Chelodina longicollis*.

Kayentachelys aprix (Reptilia: Testudines)

Nodes	38
Links	101
Density	0.14
Clustering Coefficient	0.41
Shortest Path Length	2.53
Heterogeneity	0.32
Small-World	*Yes*
Modularity Q-value	0.46

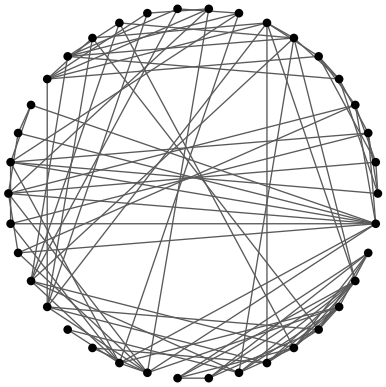

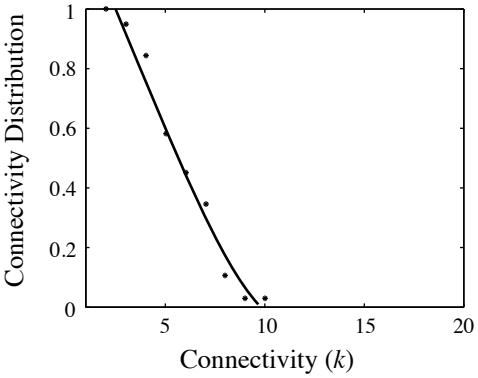

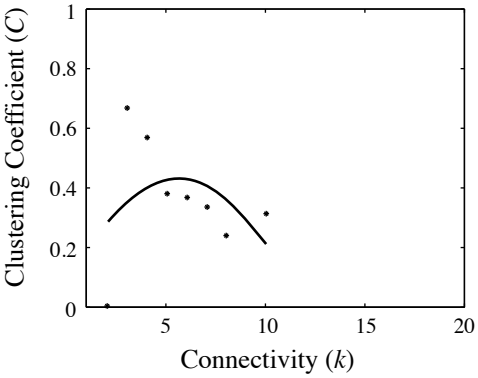

Best fit:

$P_{cum}(k) = 1.42 - 0.18\ k + 0.004\ k^2$

$\boldsymbol{r} = 0.99$ *(binomial)*

$\boldsymbol{r} = 0.98$ *(linear)*

$\boldsymbol{r} = 0.94$ *(exponential)*

$\boldsymbol{r} = 0.86$ *(power-law)*

Best fit:

$C(k) = 0.08 + 0.13\ k - 0.011\ k^2$

$\boldsymbol{r} = 0.38$ *(binomial)*

$\boldsymbol{r} = 0.10$ *(linear)*

$\boldsymbol{r} = 0.08$ *(exponential)*

$\boldsymbol{r} = 0.03$ *(power-law)*

Figure 8.19: Network analysis of the skull of *Kayentachelys aprix*.

Kayentachelys aprix (Reptilia: Testudines)

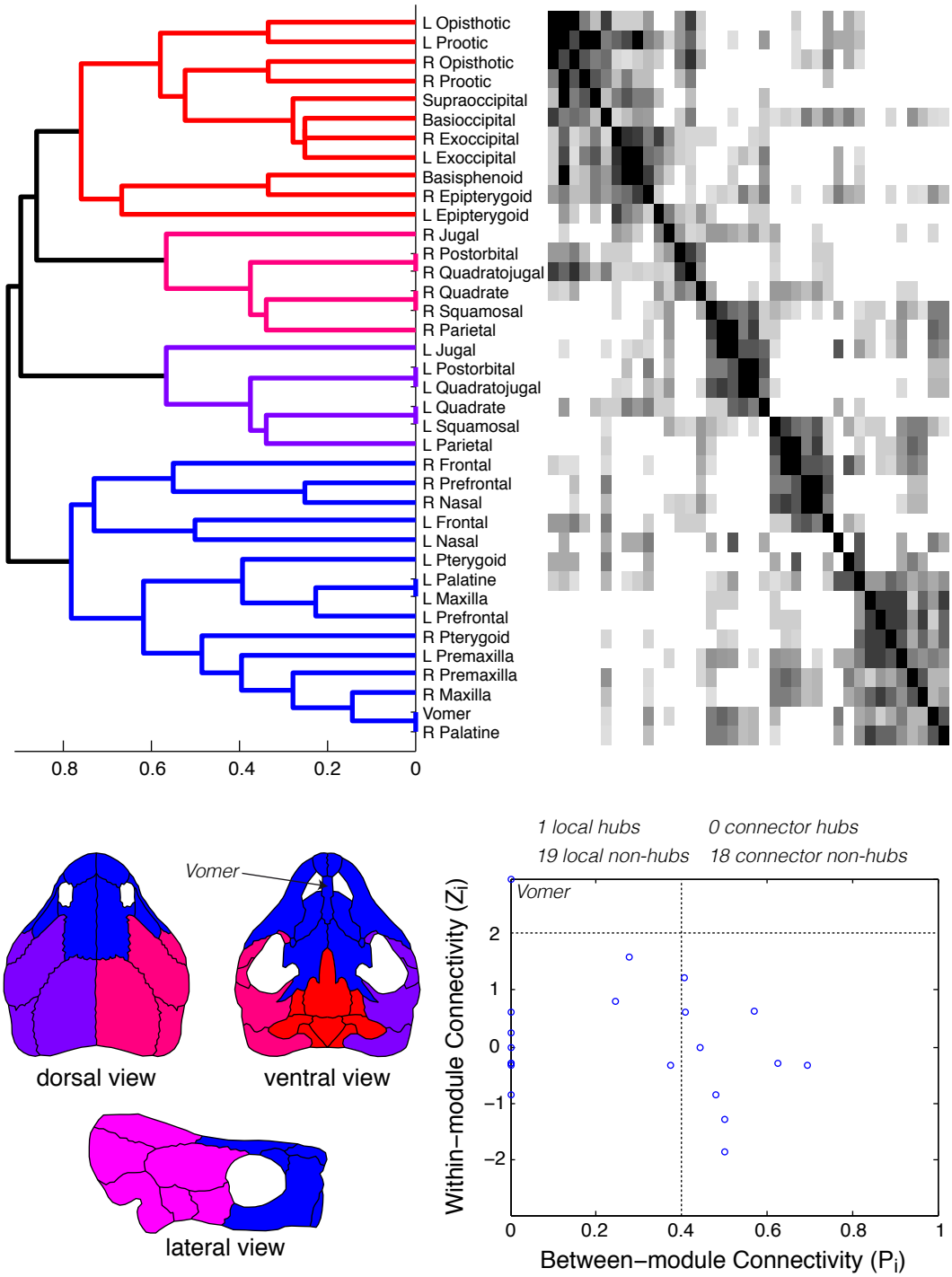

Figure 8.20: Connectivity modules in the skull of *Kayentachelys aprix*.

Chisternon undatum (Reptilia: Testudines)

Nodes	36
Links	98
Density	0.16
Clustering Coefficient	0.44
Shortest Path Length	2.43
Heterogeneity	0.39
Small-World	*Yes*
Modularity Q-value	0.38

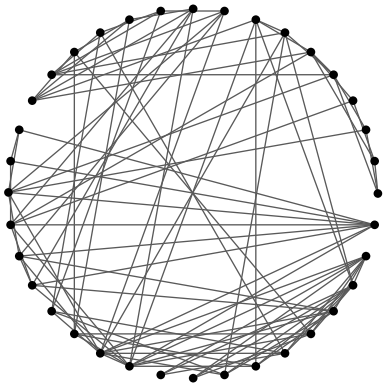

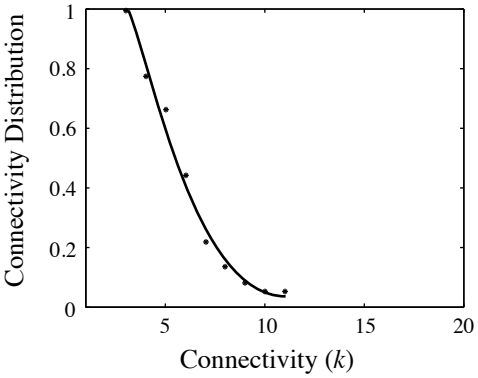

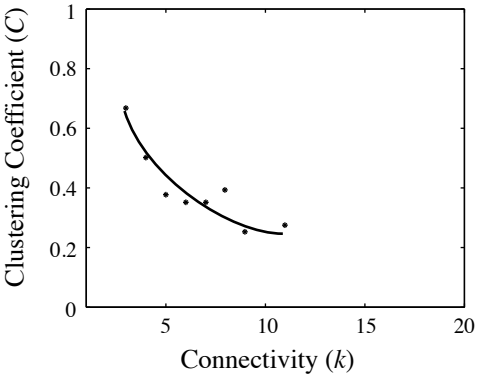

Best fit:

$P_{cum}(k) = 1.9 - 0.35\,k + 0.016\,k^{2}$

$\boldsymbol{r} = 0.99$ *(binomial)*

$\boldsymbol{r} = 0.98$ *(exponential)*

$\boldsymbol{r} = 0.95$ *(linear)*

$\boldsymbol{r} = 0.94$ *(power-law)*

Best fit:

$C(k) = 1.4\,k^{-0.72}$

$\boldsymbol{r} = 0.94$ *(power-law)*

$\boldsymbol{r} = 0.92$ *(binomial)*

$\boldsymbol{r} = 0.90$ *(exponential)*

$\boldsymbol{r} = 0.84$ *(linear)*

Figure 8.21: Network analysis of the skull of *Chisternon undatum*.

Chisternon undatum (Reptilia: Testudines)

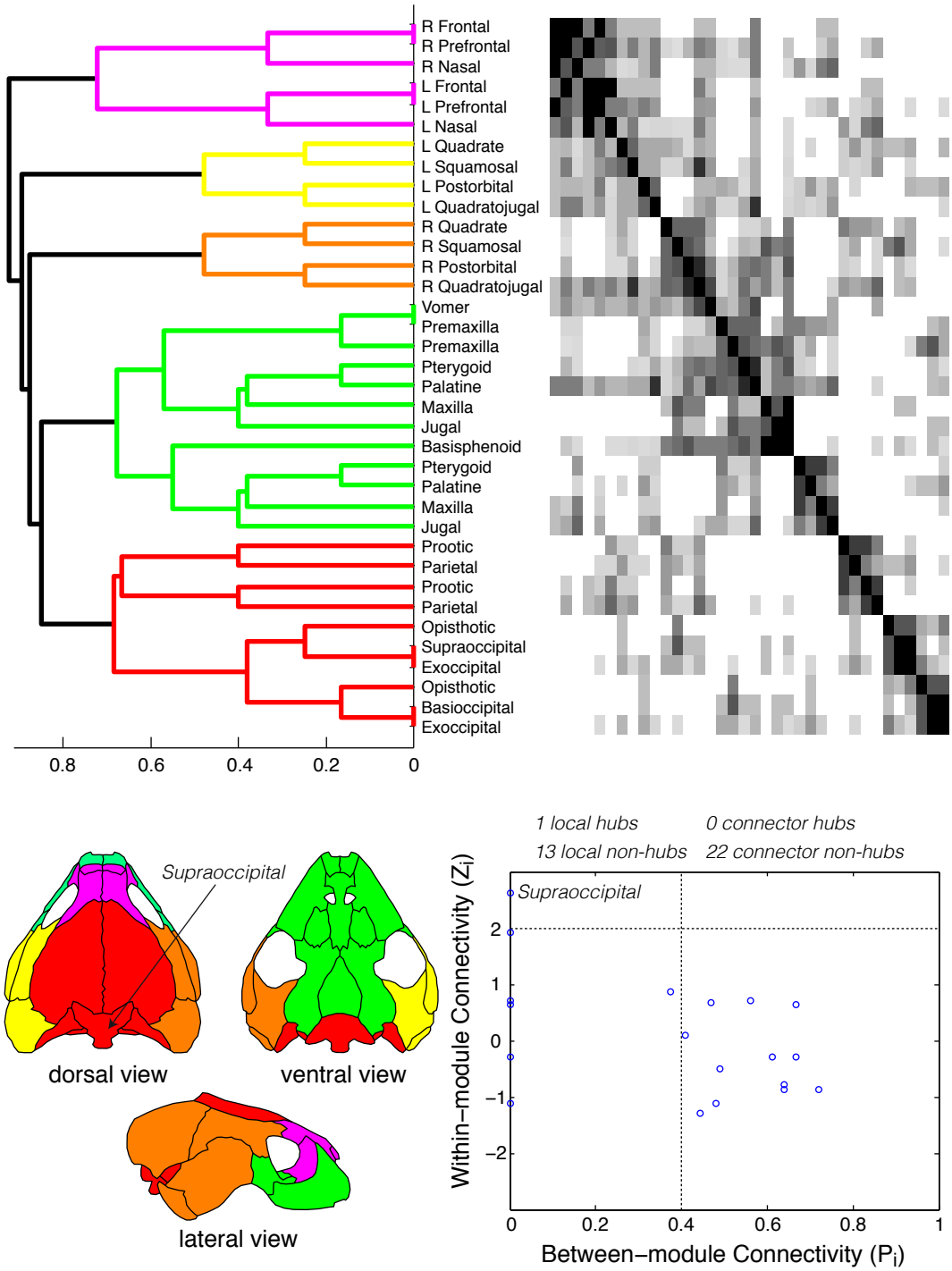

Figure 8.22: Connectivity modules in the skull of *Chisternon undatum*.

Chelydra serpentina (Reptilia: Testudines)

Nodes	36
Links	91
Density	0.14
Clustering Coefficient	0.44
Shortest Path Length	2.47
Heterogeneity	0.35
Small-World	*Yes*
Modularity Q-value	0.45

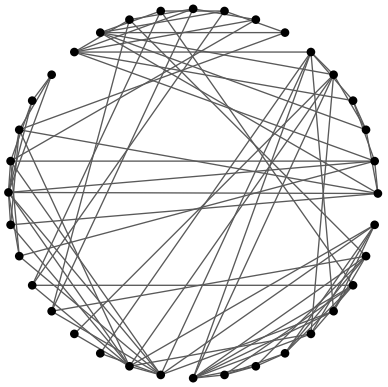

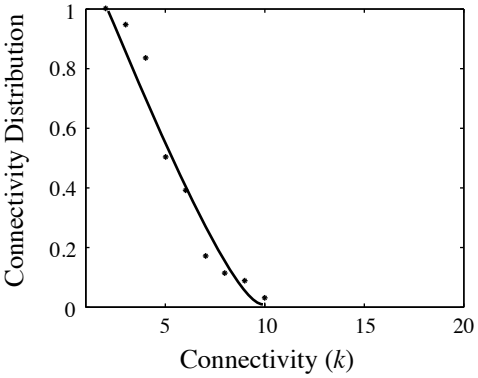

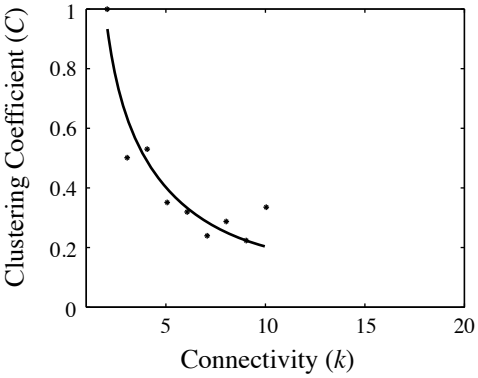

Best fit:

$P_{cum}(k) = 1.57 - 0.26\,k + 0.01\,k^2$

$\boldsymbol{r} = 0.98$ *(binomial)*

$\boldsymbol{r} = 0.97$ *(linear)*

$\boldsymbol{r} = 0.95$ *(exponential)*

$\boldsymbol{r} = 0.88$ *(power-law)*

Best fit:

$C(k) = 1.45 - 0.32\,k + 0.02\,k^2$

$\boldsymbol{r} = 0.95$ *(binomial)*

$\boldsymbol{r} = 0.92$ *(power-law)*

$\boldsymbol{r} = 0.86$ *(exponential)*

$\boldsymbol{r} = 0.80$ *(linear)*

Figure 8.23: Network analysis of the skull of *Chelydra serpentina*.

Chelydra serpentina (Reptilia: Testudines)

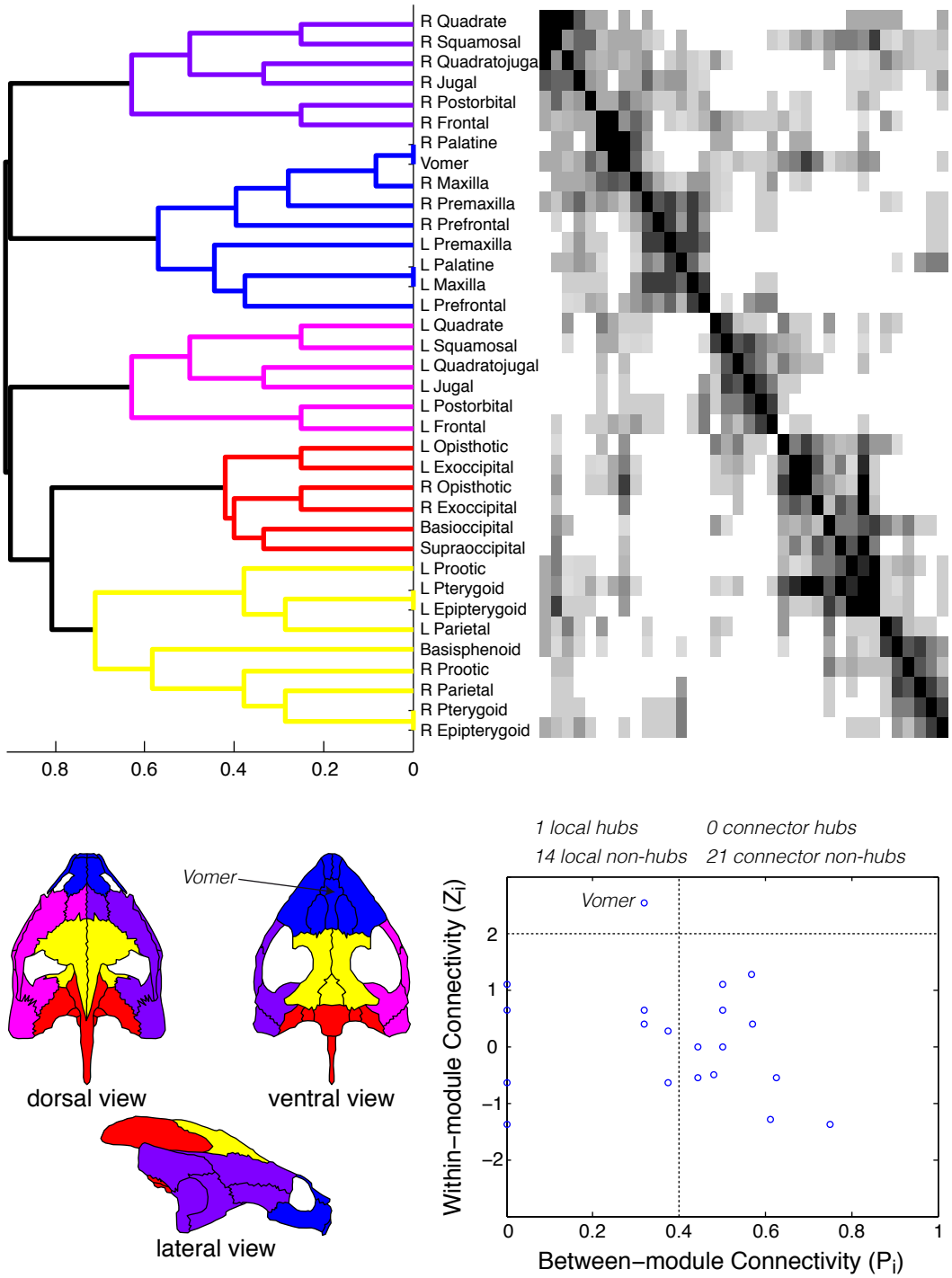

Figure 8.24: Connectivity modules in the skull of *Chelydra serpentina*.

Carettochelys insculpta (Reptilia: Testudines)

Nodes	36
Links	92
Density	0.12
Clustering Coefficient	0.39
Shortest Path Length	2.50
Heterogeneity	0.39
Small-World	*Yes*
Modularity Q-value	0.40

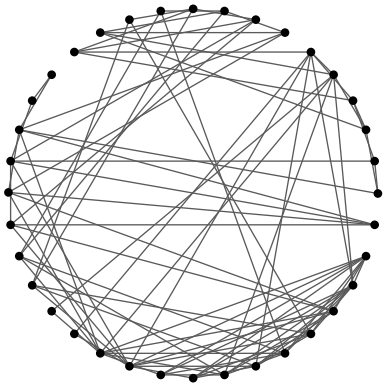

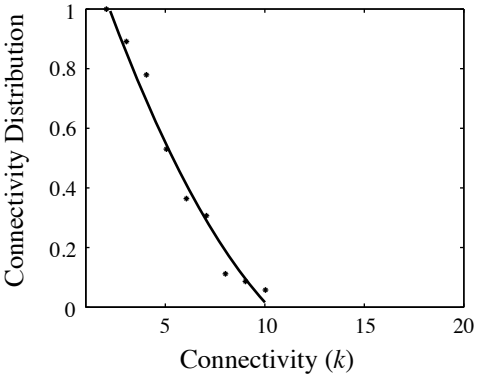

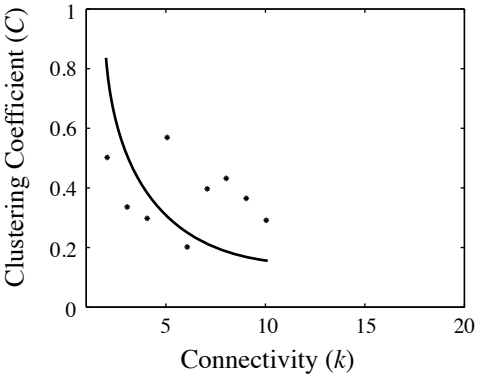

Best fit:

$P_{cum}(k) = 1.43 - 0.2\,k + 0.007\,k^{2}$

$\boldsymbol{r} = 0.99$ *(binomial)*

$\boldsymbol{r} = 0.98$ *(linear)*

$\boldsymbol{r} = 0.97$ *(exponential)*

$\boldsymbol{r} = 0.90$ *(power-law)*

Best fit:

$C(k) = 0.5\,k^{-0.17}$

$\boldsymbol{r} = 0.31$ *(power-law)*

$\boldsymbol{r} = 0.27$ *(exponential)*

$\boldsymbol{r} = 0.27$ *(binomial)*

$\boldsymbol{r} = 0.27$ *(linear)*

Figure 8.25: Network analysis of the skull of *Carettochelys insculpta*.

Carettochelys insculpta (Reptilia: Testudines)

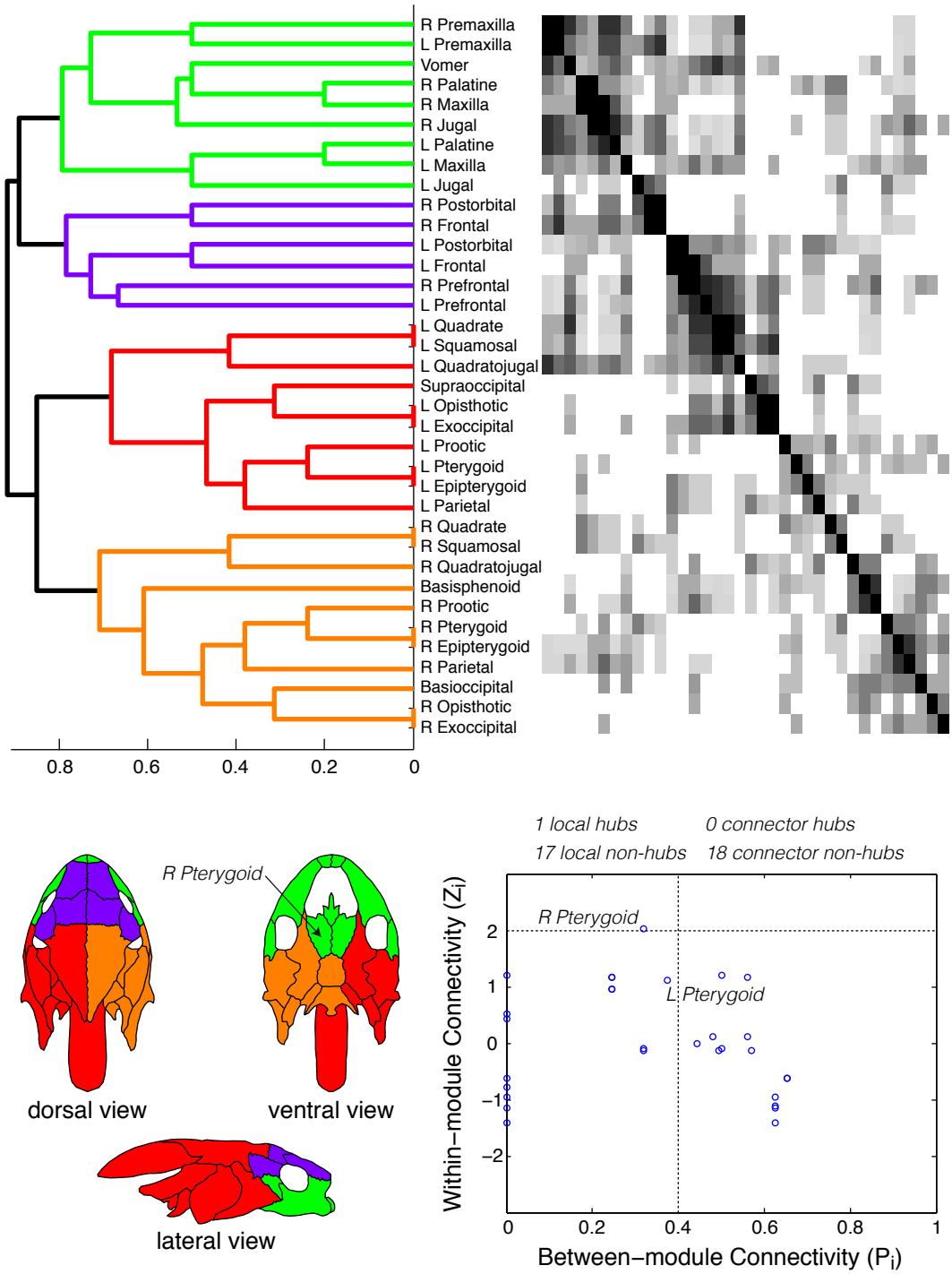

Figure 8.26: Connectivity modules in the skull of *Carettochelys insculpta*.

Gopherus polyphemus (Reptilia: Testudines)

Nodes	36
Links	90
Density	0.14
Clustering Coefficient	0.44
Shortest Path Length	2.46
Heterogeneity	0.38
Small-World	*Yes*
Modularity Q-value	0.43

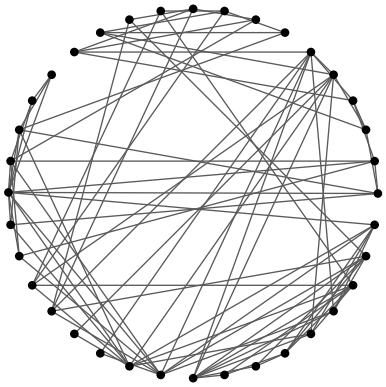

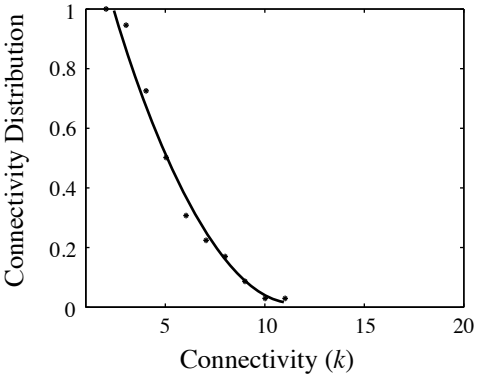

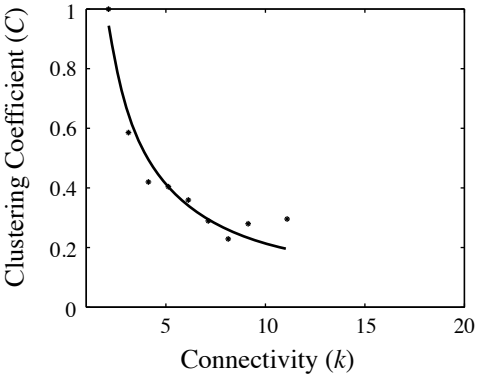

Best fit:

$P_{cum}(k) = 1.58 - 0.27\,k + 0.012\,k^{2}$

$\boldsymbol{r} = 0.99$ *(binomial)*

$\boldsymbol{r} = 0.98$ *(exponential)*

$\boldsymbol{r} = 0.96$ *(linear)*

$\boldsymbol{r} = 0.91$ *(power-law)*

Best fit:

$C(k) = 1.81\,k^{-0.94}$

$\boldsymbol{r} = 0.97$ *(power-law)*

$\boldsymbol{r} = 0.94$ *(binomial)*

$\boldsymbol{r} = 0.92$ *(exponential)*

$\boldsymbol{r} = 0.78$ *(linear)*

Figure 8.27: Network analysis of the skull of *Gopherus polyphemus*.

Gopherus polyphemus (Reptilia: Testudines)

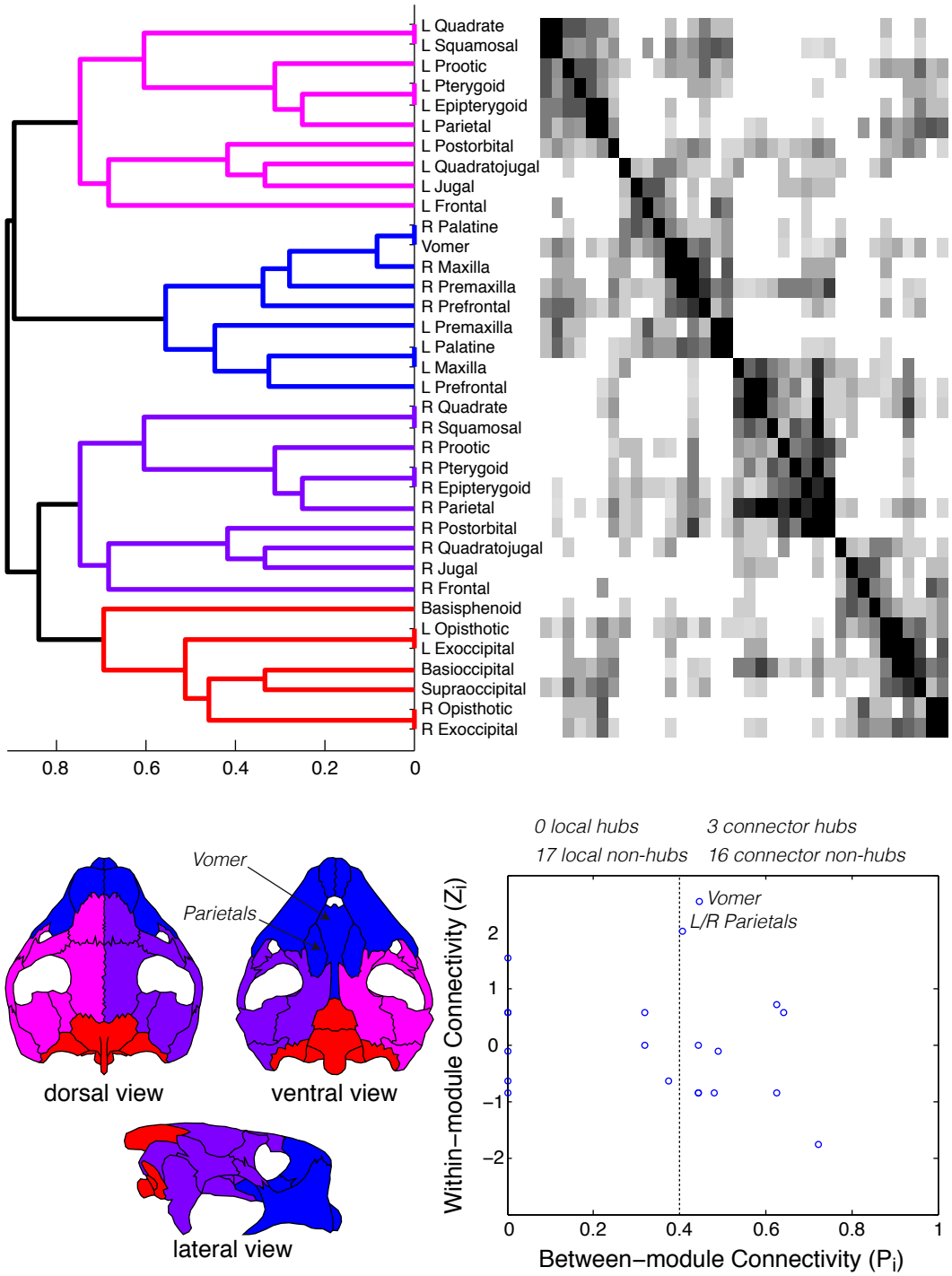

Figure 8.28: Connectivity modules in the skull of *Gopherus polyphemus*.

Testudo graeca (Reptilia: Testudines)

Nodes	34
Links	94
Density	0.17
Clustering Coefficient	0.45
Shortest Path Length	2.36
Heterogeneity	0.42
Small-World	*Yes*
Modularity Q-value	0.42

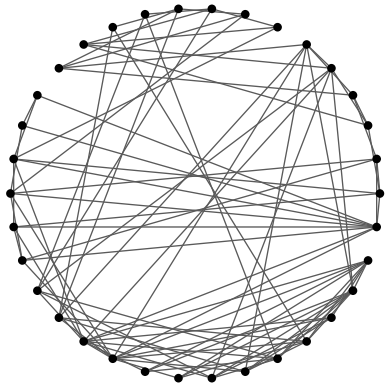

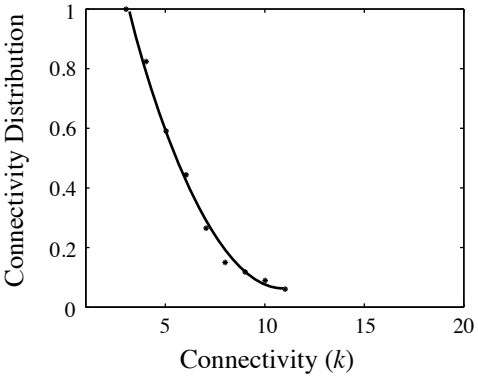

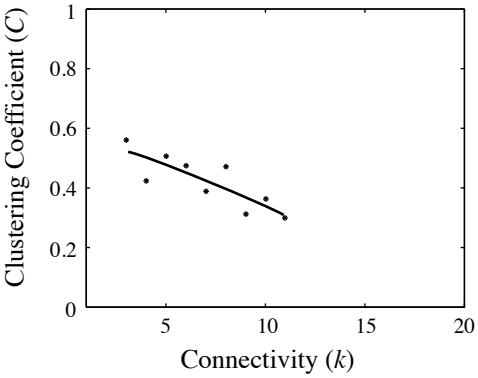

Best fit:

$P_{cum}(k) = 1.92 - 0.35\,k - 0.02\,k^2$

$\boldsymbol{r} = 0.99$ *(binomial)*

$\boldsymbol{r} = 0.99$ *(exponential)*

$\boldsymbol{r} = 0.96$ *(power-law)*

$\boldsymbol{r} = 0.95$ *(linear)*

Best fit:

$C(k) = 0.57 - 0.01\,k - 0.001\,k^2$

$\boldsymbol{r} = 0.83$ *(binomial)*

$\boldsymbol{r} = 0.83$ *(linear)*

$\boldsymbol{r} = 0.82$ *(exponential)*

$\boldsymbol{r} = 0.80$ *(power-law)*

Figure 8.29: Network analysis of the skull of *Testudo graeca*.

Testudo graeca (Reptilia: Testudines)

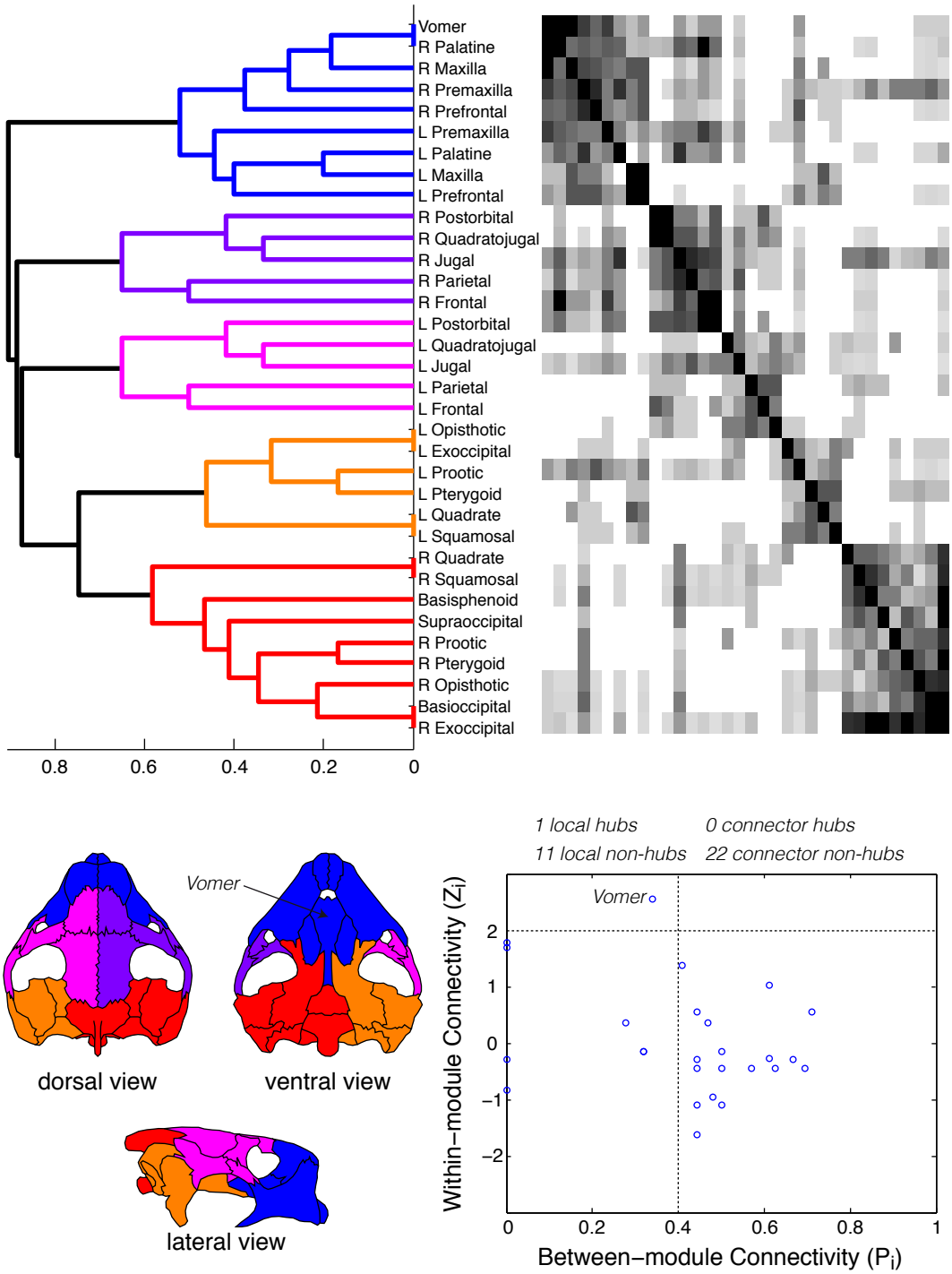

Figure 8.30: Connectivity modules in the skull of *Testudo graeca*.

Petrolacosaurus kansensis (Reptilia: Araeoscelida)

Nodes	55
Links	132
Density	0.09
Clustering Coefficient	0.47
Shortest Path Length	3.06
Heterogeneity	0.43
Small-World	*Yes*
Modularity Q-value	0.54

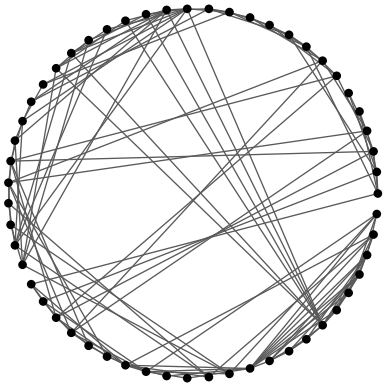

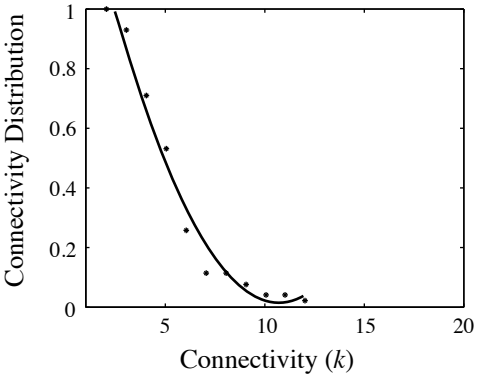

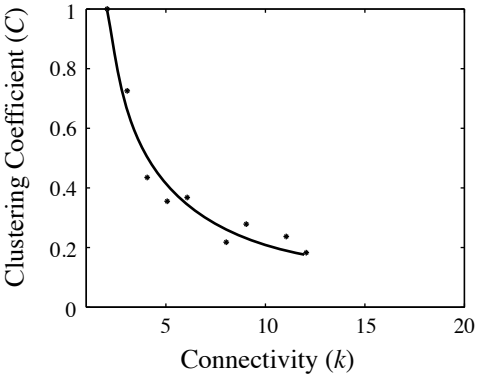

Best fit:

$P_{cum}(k) = 1.64 - 0.31\ k + 0.014\ k^2$

$\boldsymbol{r} = 0.99$ *(binomial)*

$\boldsymbol{r} = 0.97$ *(exponential)*

$\boldsymbol{r} = 0.92$ *(linear)*

$\boldsymbol{r} = 0.90$ *(power-law)*

Best fit:

$C(k) = 1.97\ k^{-0.98}$

$\boldsymbol{r} = 0.98$ *(power-law)*

$\boldsymbol{r} = 0.96$ *(binomial)*

$\boldsymbol{r} = 0.95$ *(exponential)*

$\boldsymbol{r} = 0.83$ *(linear)*

Figure 8.31: Network analysis of the skull of *Petrolacosaurus kansensis*.

Petrolacosaurus kansensis (Reptilia: Araeoscelida)

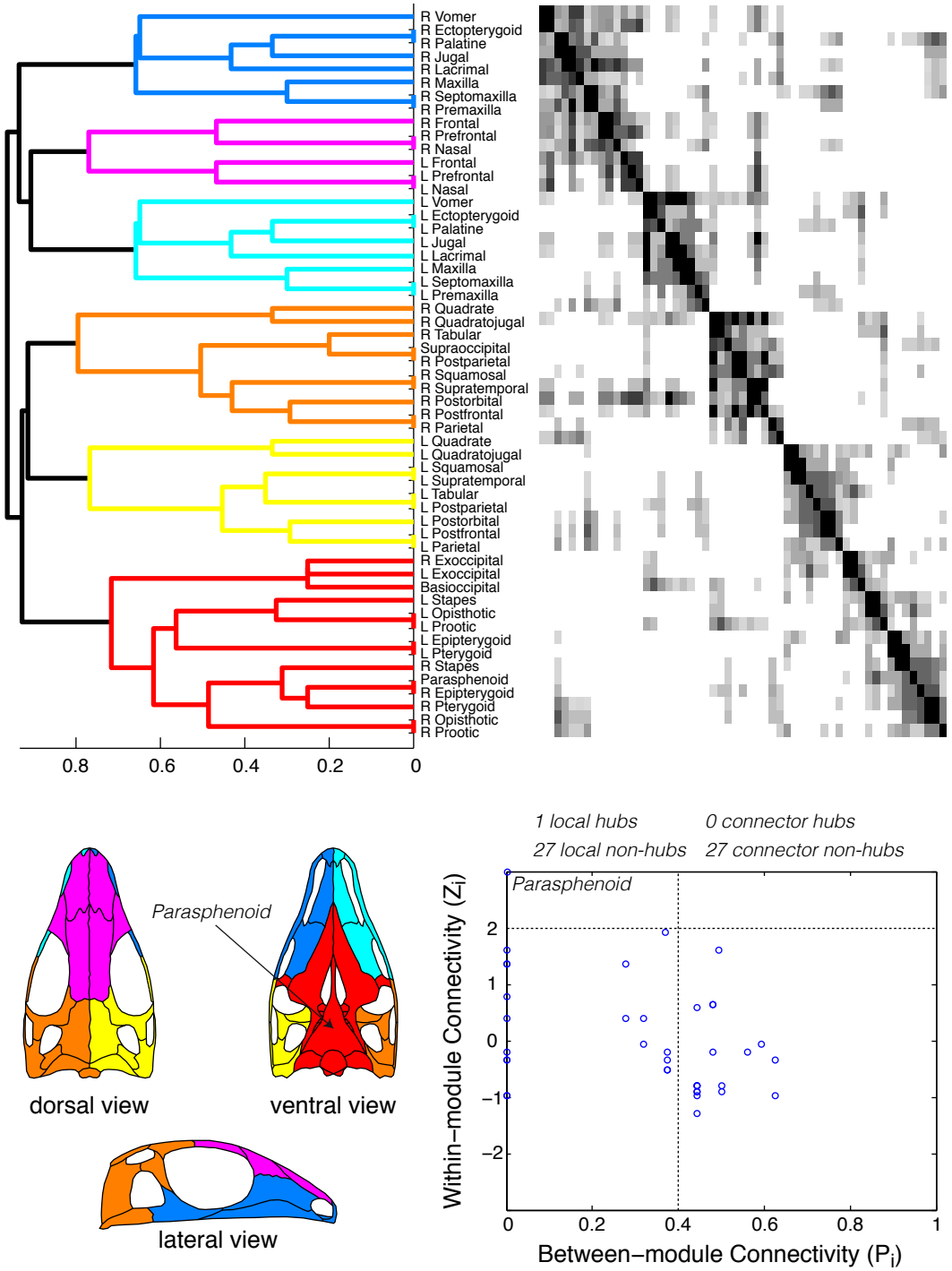

Figure 8.32: Connectivity modules in the skull of *Petrolacosaurus kansensis*.

Youngina capensis (Reptilia: Diapsida)

Nodes	53
Links	122
Density	0.09
Clustering Coefficient	0.38
Shortest Path Length	3.12
Heterogeneity	0.41
Small-World	*Yes*
Modularity Q-value	0.52

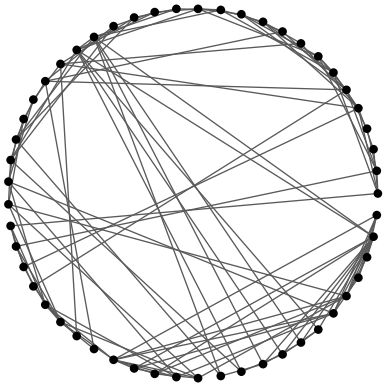

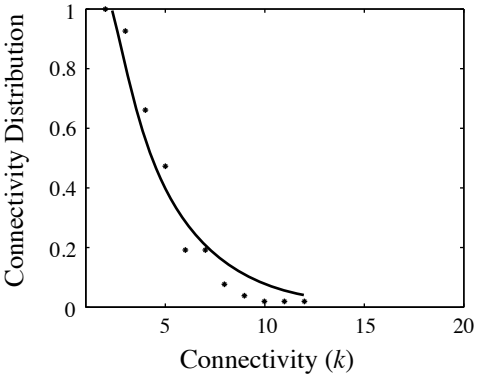

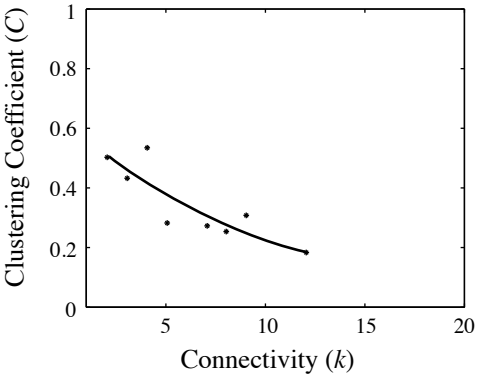

Best fit:

$P_{cum}(k) = 2.2\ e^{-0.34\,k}$

$\boldsymbol{r} = 0.97$ *(exponential)*

$\boldsymbol{r} = 0.96$ *(binomial)*

$\boldsymbol{r} = 0.92$ *(linear)*

$\boldsymbol{r} = 0.91$ *(power-law)*

Best fit:

$C(k) = 0.62\ e^{-0.1\,k}$

$\boldsymbol{r} = 0.86$ *(exponential)*

$\boldsymbol{r} = 0.86$ *(binomial)*

$\boldsymbol{r} = 0.85$ *(linear)*

$\boldsymbol{r} = 0.83$ *(power-law)*

Figure 8.33: Network analysis of the skull of *Youngina capensis*.

Youngina capensis (Reptilia: Diapsida)

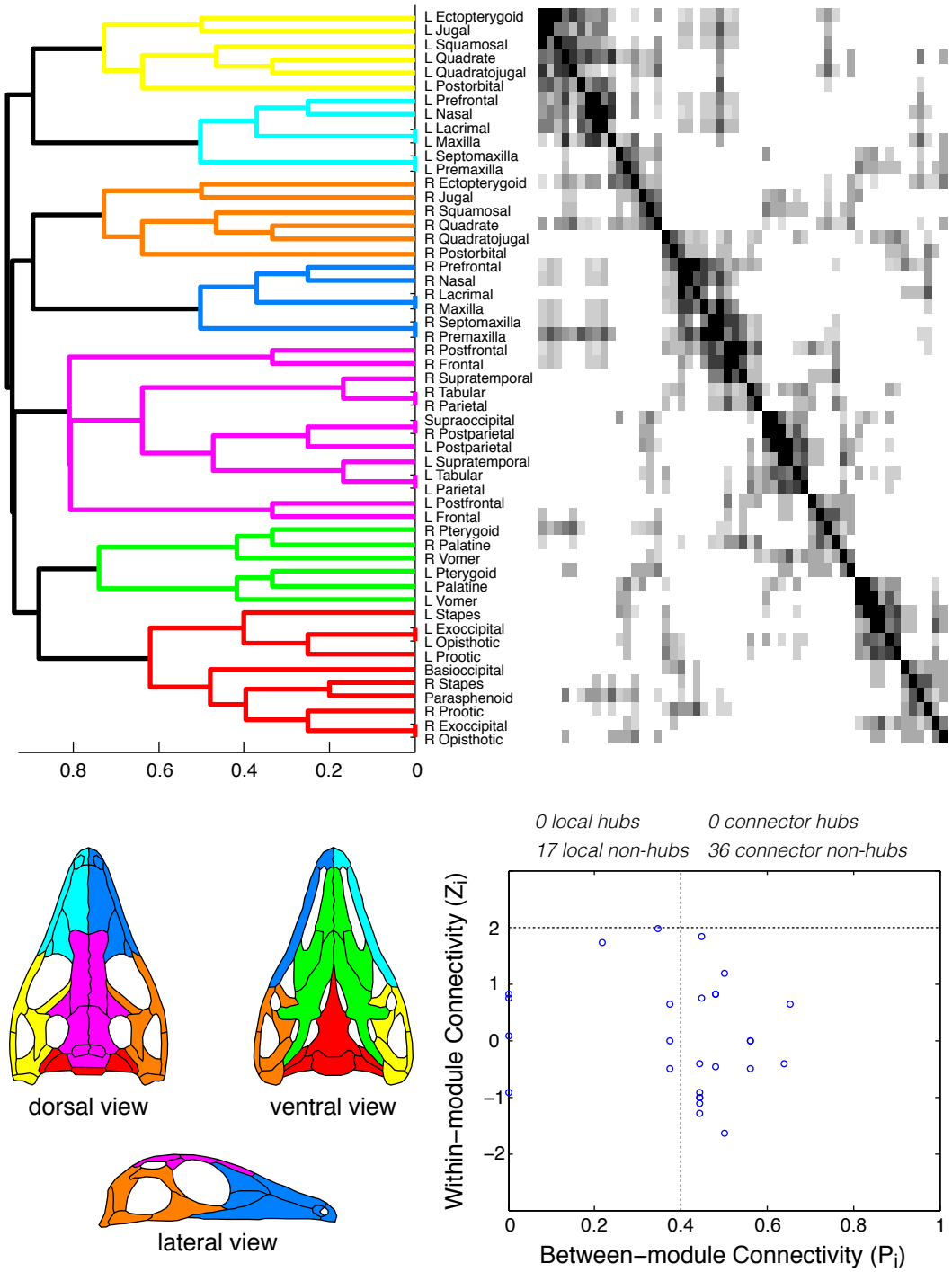

Figure 8.34: Connectivity modules in the skull of *Youngina capensis*.

Rhamphorhynchus muensteri (Reptilia: Pterosauria)

Nodes	41
Links	95
Density	0.12
Clustering Coefficient	0.31
Shortest Path Length	2.79
Heterogeneity	0.38
Small-World	*Yes*
Modularity Q-value	0.46

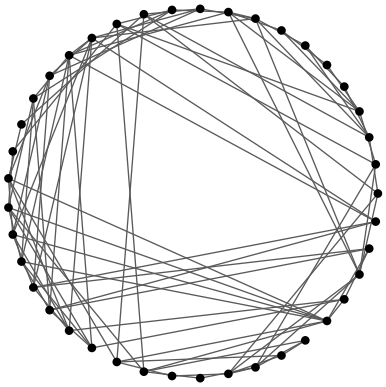

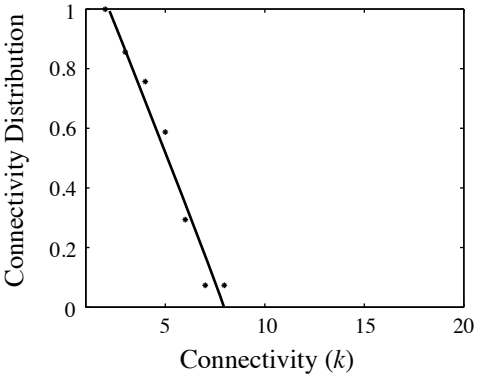

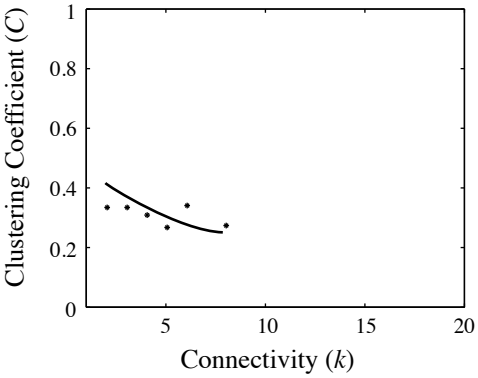

Best fit:

$P_{cum}(k) = 1.35 - 0.16\,k - 0.001\,k^2$

$\boldsymbol{r} = 0.98$ *(binomial)*

$\boldsymbol{r} = 0.98$ *(linear)*

$\boldsymbol{r} = 0.93$ *(exponential)*

$\boldsymbol{r} = 0.86$ *(power-law)*

Best fit:

$C(k) = 0.35\,e^{-0.03\,k}$

$\boldsymbol{r} = 0.56$ *(exponential)*

$\boldsymbol{r} = 0.56$ *(linear)*

$\boldsymbol{r} = 0.56$ *(binomial)*

$\boldsymbol{r} = 0.56$ *(power-law)*

Figure 8.35: Network analysis of the skull of *Rhamphorhynchus muensteri*.

Rhamphorhynchus muensteri (Reptilia: Pterosauria)

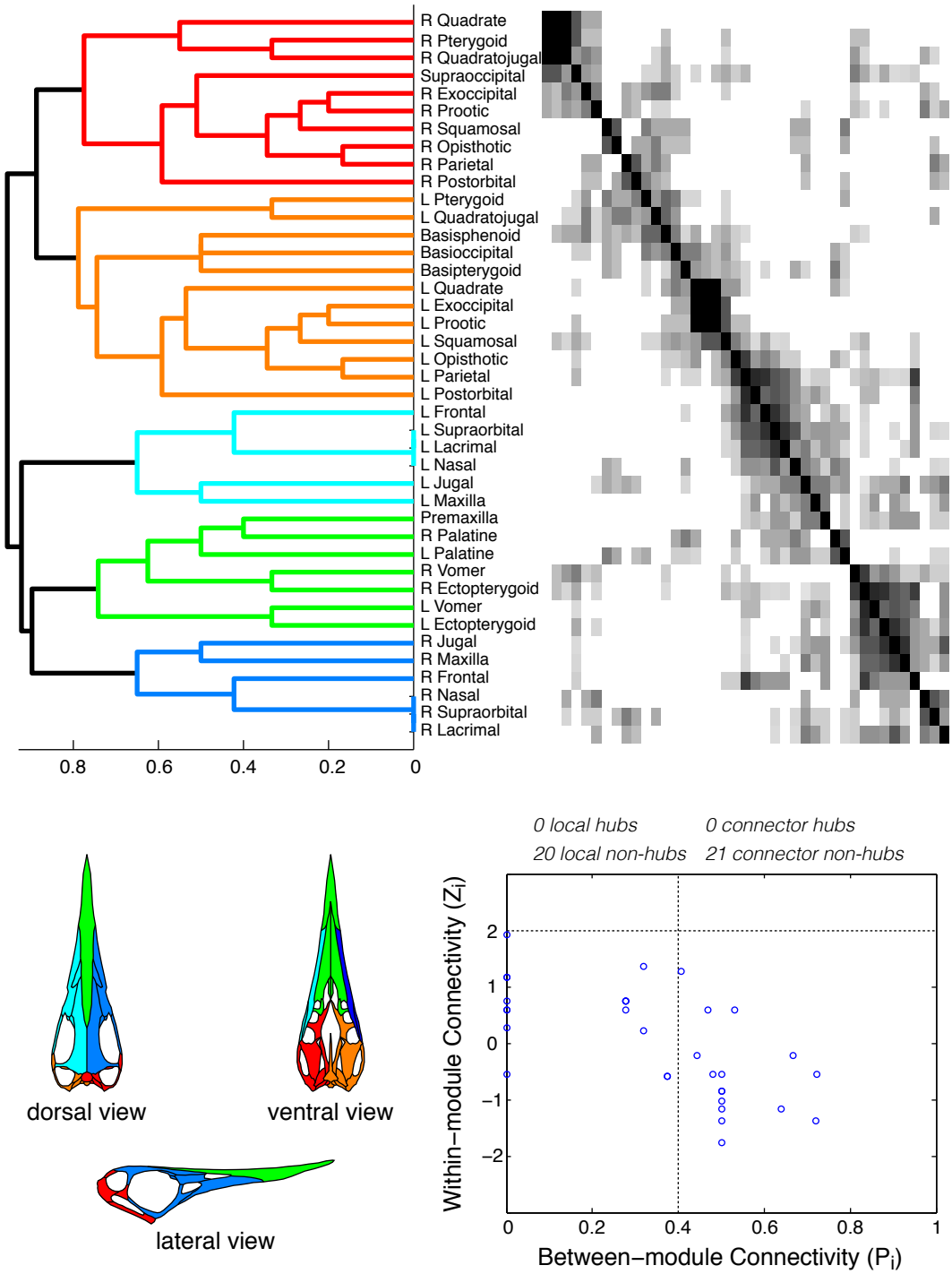

Figure 8.36: Connectivity modules in the skull of *Rhamphorhynchus muensteri*.

Crocodylus moreletii (Reptilia: Crocodylia)

Nodes	39
Links	97
Density	0.13
Clustering Coefficient	0.43
Shortest Path Length	2.62
Heterogeneity	0.33
Small-World	*Yes*
Modularity Q-value	0.48

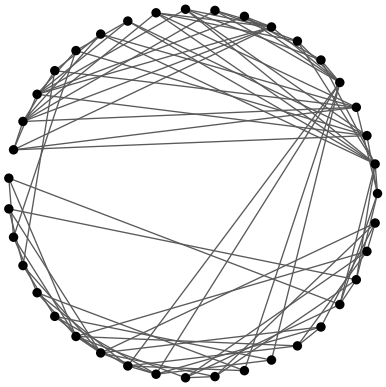

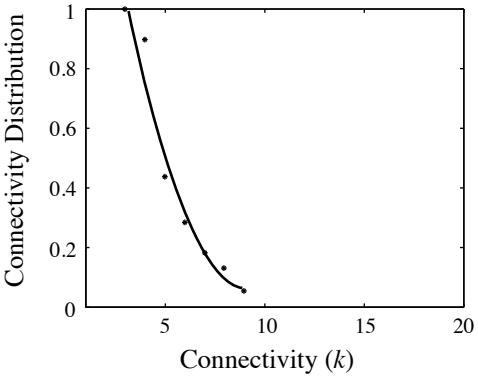

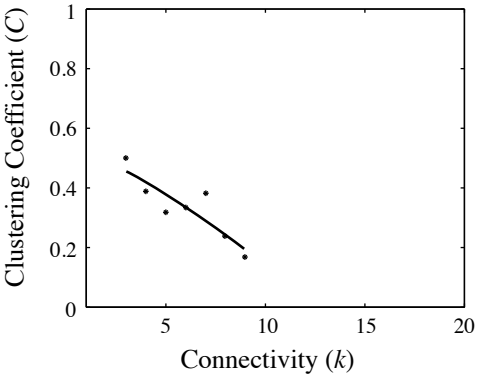

Best fit:

$P_{cum}(k) = 2.2 - 0.49\ k + 0.027\ k^2$

$\boldsymbol{r} = 0.98$ *(binomial)*

$\boldsymbol{r} = 0.97$ *(exponential)*

$\boldsymbol{r} = 0.94$ *(linear)*

$\boldsymbol{r} = 0.94$ *(power-law)*

Best fit:

$C(k) = 0.56 - 0.3\ k - 0.001\ k^2$

$\boldsymbol{r} = 0.88$ *(binomial)*

$\boldsymbol{r} = 0.88$ *(linear)*

$\boldsymbol{r} = 0.87$ *(exponential)*

$\boldsymbol{r} = 0.86$ *(power-law)*

Figure 8.37: Network analysis of the skull of *Crocodylus moreletii*.

Crocodylus moreletii (Reptilia: Crocodylia)

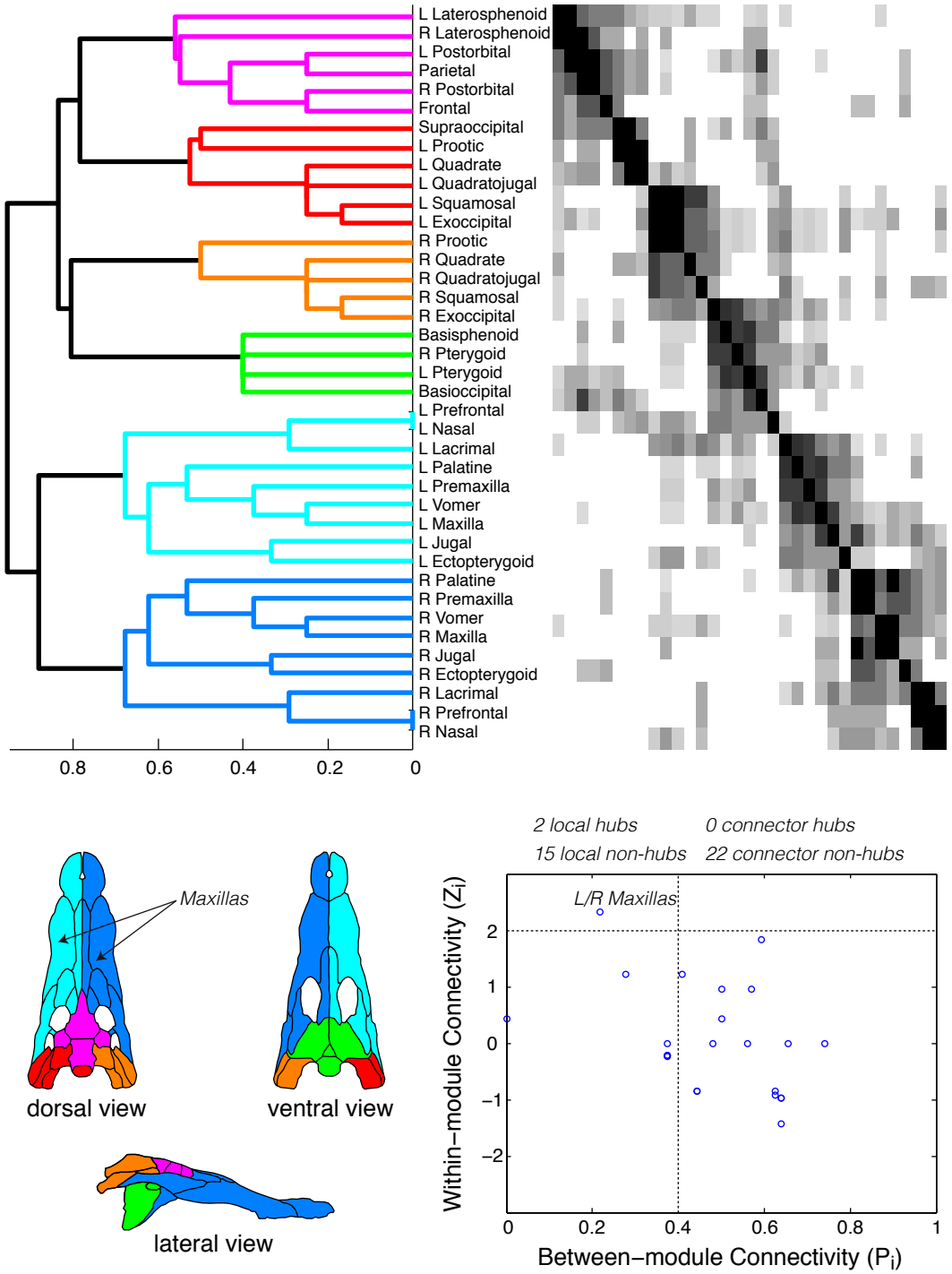

Figure 8.38: Connectivity modules in the skull of *Crocodylus moreletii*.

Stegosaurus armatus (Reptilia: Ornithischia)

Nodes	47
Links	114
Density	0.11
Clustering Coefficient	0.32
Shortest Path Length	2.89
Heterogeneity	0.34
Small-World	*Yes*
Modularity Q-value	0.47

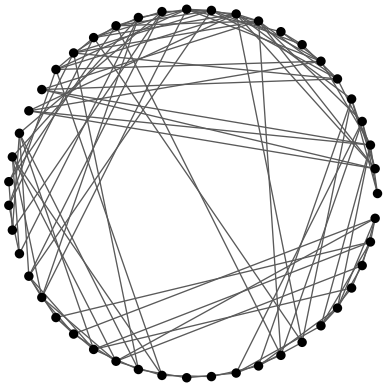

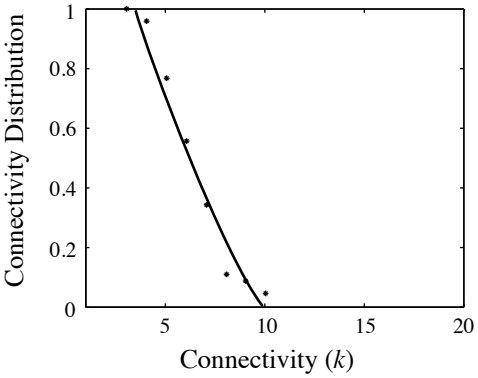

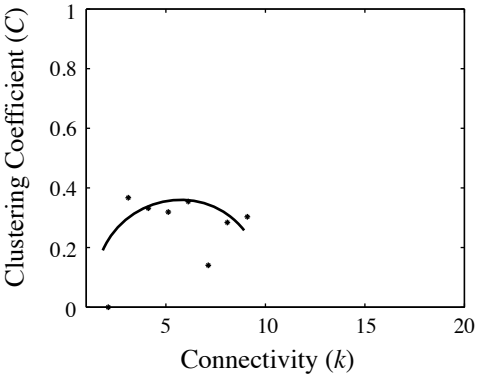

Best fit:

$P_{cum}(k) = 1.54 - 0.24\,k + 0.007\,k^2$

$\boldsymbol{r} = 0.98$ *(binomial)*

$\boldsymbol{r} = 0.98$ *(linear)*

$\boldsymbol{r} = 0.94$ *(exponential)*

$\boldsymbol{r} = 0.87$ *(power-law)*

Best fit:

$C(k) = -0.11 + 0.15\,k - 0.01\,k^2$

$\boldsymbol{r} = 0.53$ *(binomial)*

$\boldsymbol{r} = 0.32$ *(power-law)*

$\boldsymbol{r} = 0.27$ *(linear)*

$\boldsymbol{r} = 0.23$ *(exponential)*

Figure 8.39: Network analysis of the skull of *Stegosaurus armatus*.

Stegosaurus armatus (Reptilia: Ornithischia)

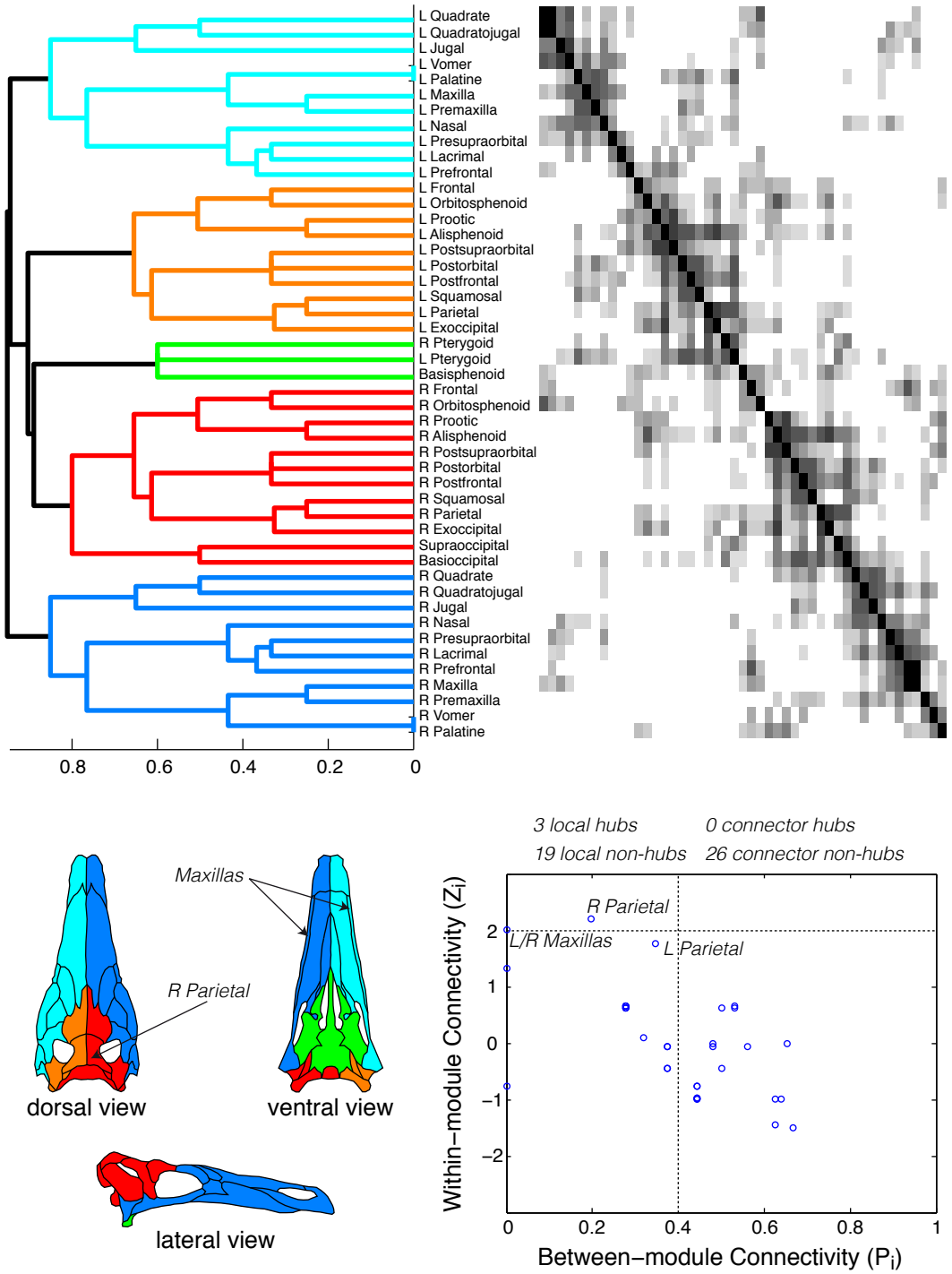

Figure 8.40: Connectivity modules in the skull of *Stegosaurus armatus*.

Corythosaurus casuarius (Reptilia: Ornithischia)

Nodes	33
Links	77
Density	0.15
Clustering Coefficient	0.43
Shortest Path Length	2.62
Heterogeneity	0.34
Small-World	*Yes*
Modularity Q-value	0.51

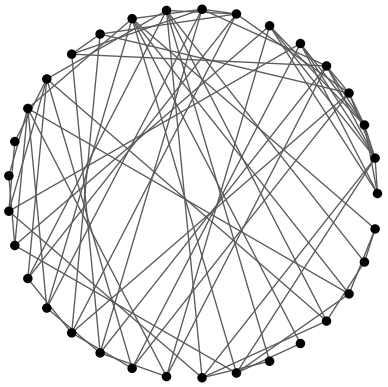

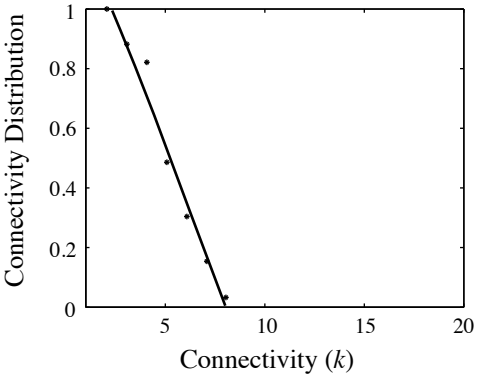

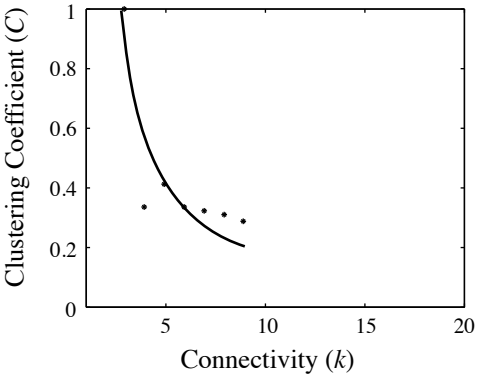

Best fit:

$P_{cum}(k) = 1.36 - 0.16\,k - 2.2\,k^{2}$

$\boldsymbol{r} = 0.99$ *(binomial)*

$\boldsymbol{r} = 0.99$ *(linear)*

$\boldsymbol{r} = 0.94$ *(exponential)*

$\boldsymbol{r} = 0.86$ *(power-law)*

Best fit:

$C(k) = 1.88\,k^{-1.07}$

$\boldsymbol{r} = 0.90$ *(power-law)*

$\boldsymbol{r} = 0.85$ *(binomial)*

$\boldsymbol{r} = 0.82$ *(exponential)*

$\boldsymbol{r} = 0.69$ *(linear)*

Figure 8.41: Network analysis of the skull of *Corythosaurus casuarius*.

Corythosaurus casuarius (Reptilia: Ornithischia)

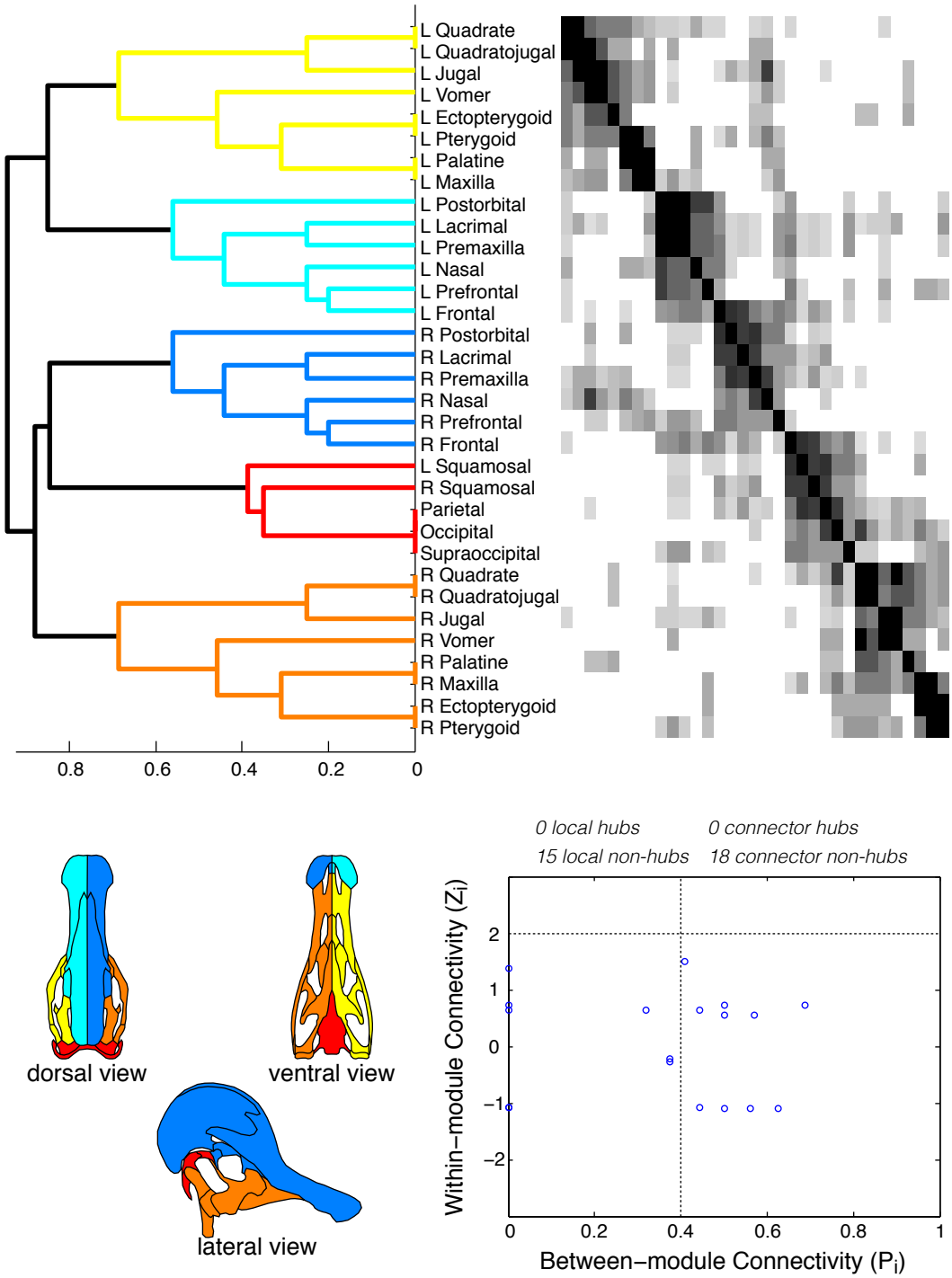

Figure 8.42: Connectivity modules in the skull of *Corythosaurus casuarius*.

Plateosaurus engelhardti (Reptilia: Dinosauria)

Nodes	49
Links	112
Density	0.10
Clustering Coefficient	0.34
Shortest Path Length	3.08
Heterogeneity	0.42
Small-World	*Yes*
Modularity Q-value	0.51

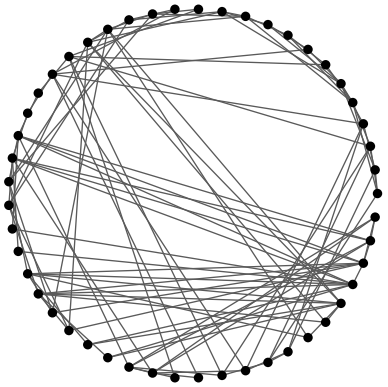

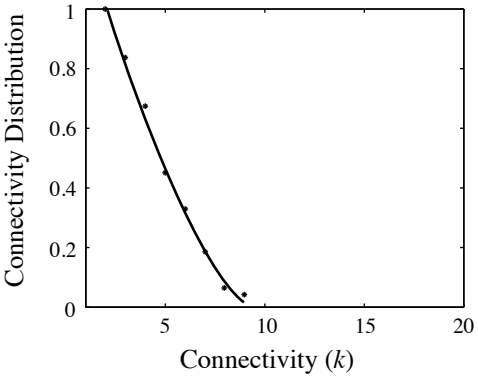

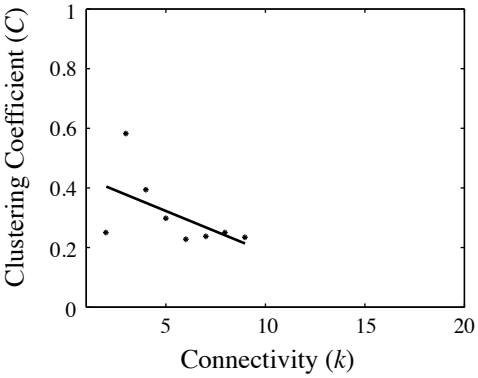

Best fit:

$P_{cum}(k) = 1.5 - 0.26\,k + 0.01\,k^2$

$\boldsymbol{r} = 0.99$ *(binomial)*

$\boldsymbol{r} = 0.99$ *(linear)*

$\boldsymbol{r} = 0.98$ *(exponential)*

$\boldsymbol{r} = 0.92$ *(power-law)*

Best fit:

$C(k) = 0.46 - 0.03\,k$

$\boldsymbol{r} = 0.54$ *(linear)*

$\boldsymbol{r} = 0.54$ *(binomial)*

$\boldsymbol{r} = 0.52$ *(exponential)*

$\boldsymbol{r} = 0.42$ *(power-law)*

Figure 8.43: Network analysis of the skull of *Plateosaurus engelhardti*.

Plateosaurus engelhardti (Reptilia: Dinosauria)

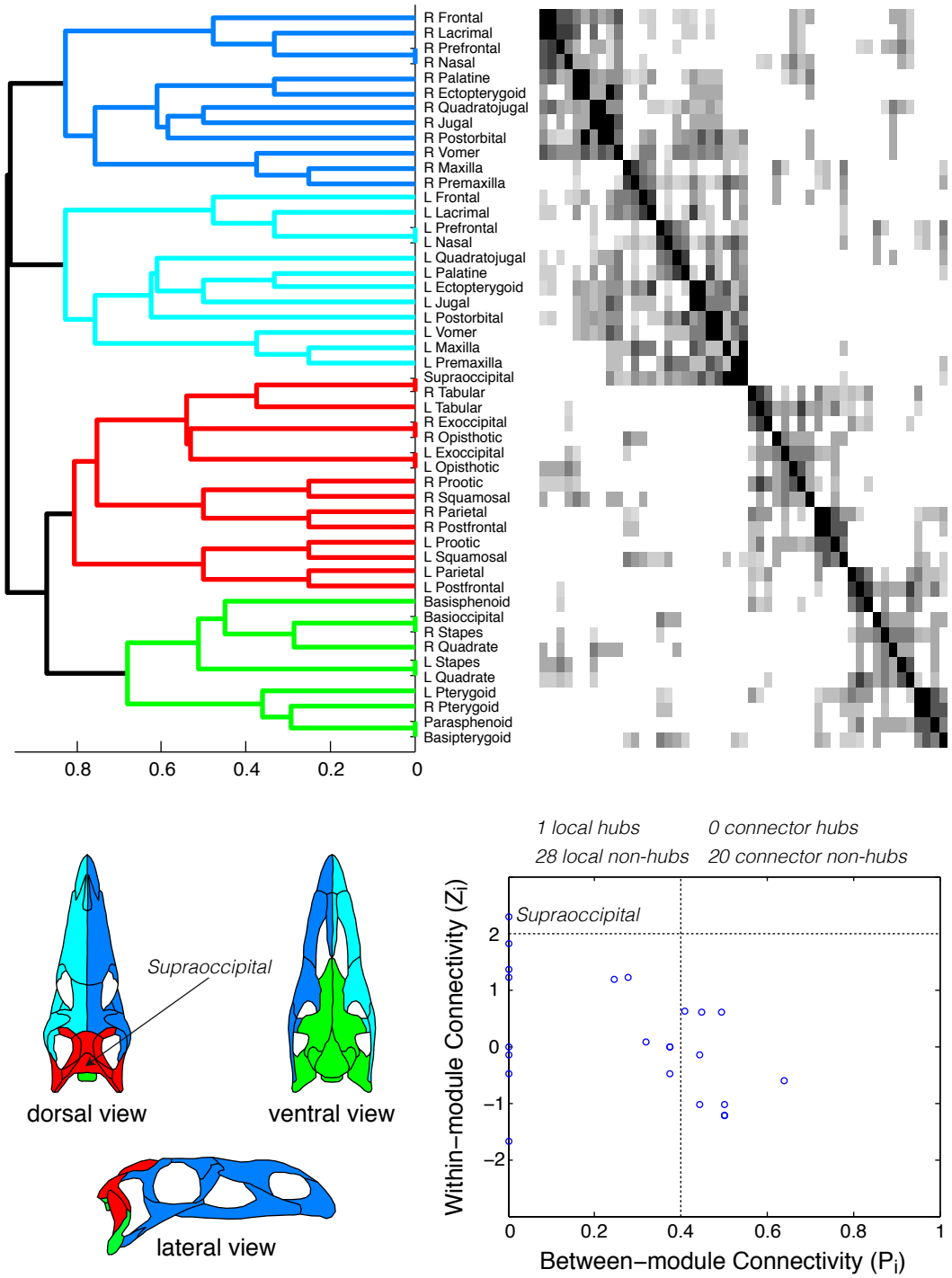

Figure 8.44: Connectivity modules in the skull of *Plateosaurus engelhardti*.

Dromaeosaurus albertensis (Reptilia: Dinosauria)

Nodes	41
Links	99
Density	0.12
Clustering Coefficient	0.29
Shortest Path Length	2.73
Heterogeneity	0.28
Small-World	*Yes*
Modularity Q-value	0.49

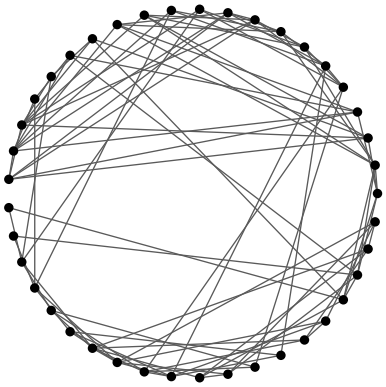

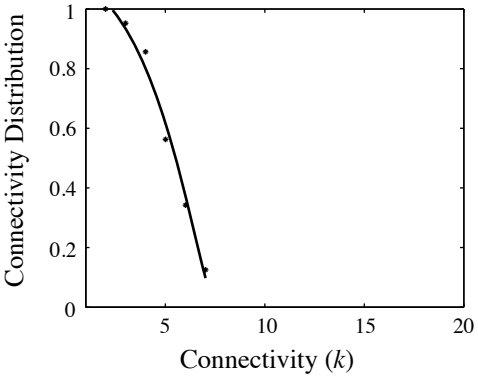

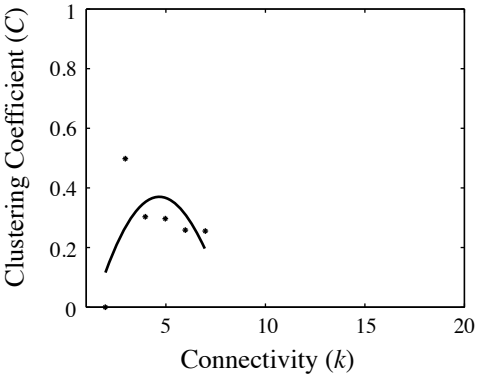

Best fit:

$P_{cum}(k) = 1.1 + 0.03\ k - 0.02\ k^2$

$\boldsymbol{r} = 0.99$ *(binomial)*

$\boldsymbol{r} = 0.97$ *(linear)*

$\boldsymbol{r} = 0.91$ *(exponential)*

$\boldsymbol{r} = 0.83$ *(power-law)*

Best fit:

$C(k) = -0.4 + 0.32\ k - 0.03\ k^2$

$\boldsymbol{r} = 0.61$ *(linear)*

$\boldsymbol{r} = 0.23$ *(power-law)*

$\boldsymbol{r} = 0.19$ *(linear)*

$\boldsymbol{r} = 0.15$ *(exponential)*

Figure 8.45: Network analysis of the skull of *Dromaeosaurus albertensis*.

Dromaeosaurus albertensis (Reptilia: Dinosauria)

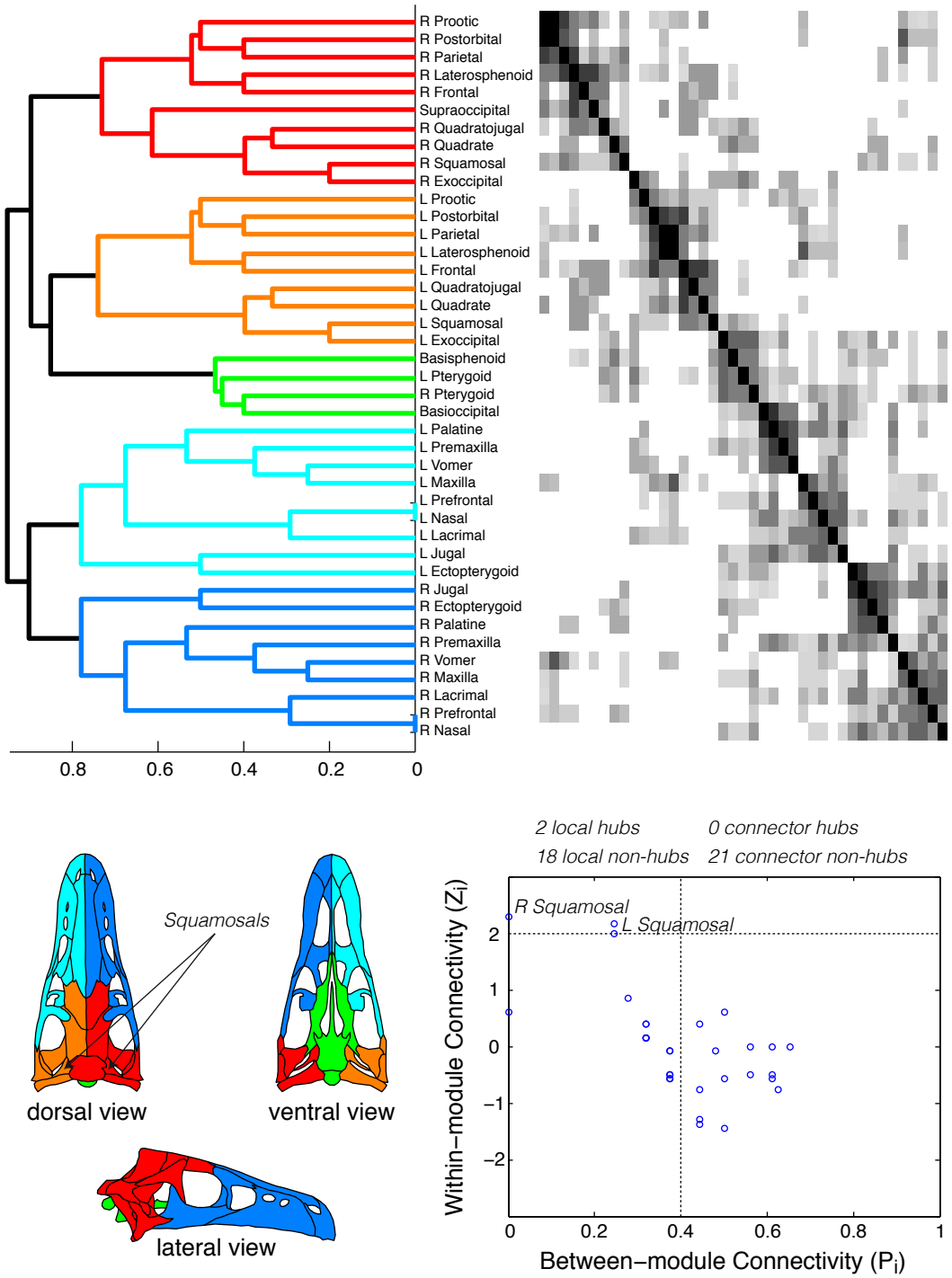

Figure 8.46: Connectivity modules in the skull of *Dromaeosaurus albertensis*.

Anser anser (Aves: Anseriformes), Adult

Nodes	18
Links	27
Density	0.18
Clustering Coefficient	0.38
Shortest Path Length	2.18
Heterogeneity	0.62
Small-World	*Yes*
Modularity Q-value	0.41

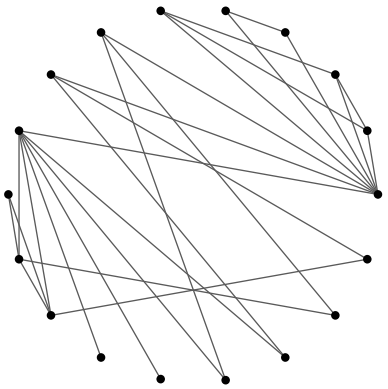

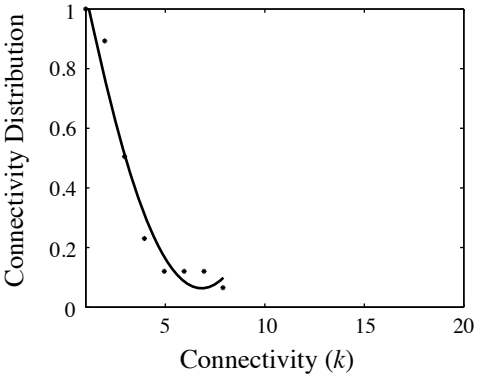

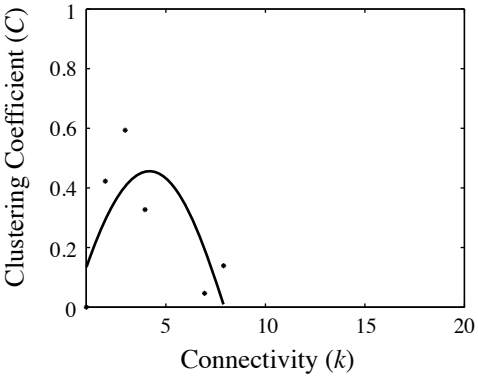

Best fit:

$P_{cum}(k) = 1.44 - 0.4\,k + 0.03\,k^2$

$\boldsymbol{r} = 0.98$ *(binomial)*

$\boldsymbol{r} = 0.97$ *(exponential)*

$\boldsymbol{r} = 0.91$ *(linear)*

$\boldsymbol{r} = 0.90$ *(power-law)*

Best fit:

$C(k) = -0.1 + 0.26\,k - 0.03\,k^2$

$\boldsymbol{r} = 0.73$ *(binomial)*

$\boldsymbol{r} = 0.31$ *(linear)*

$\boldsymbol{r} = 0.21$ *(exponential)*

$\boldsymbol{r} = 0.04$ *(power-law)*

Figure 8.47: Network analysis of the skull of *Anser anser*.

Anser anser (Aves: Anseriformes)

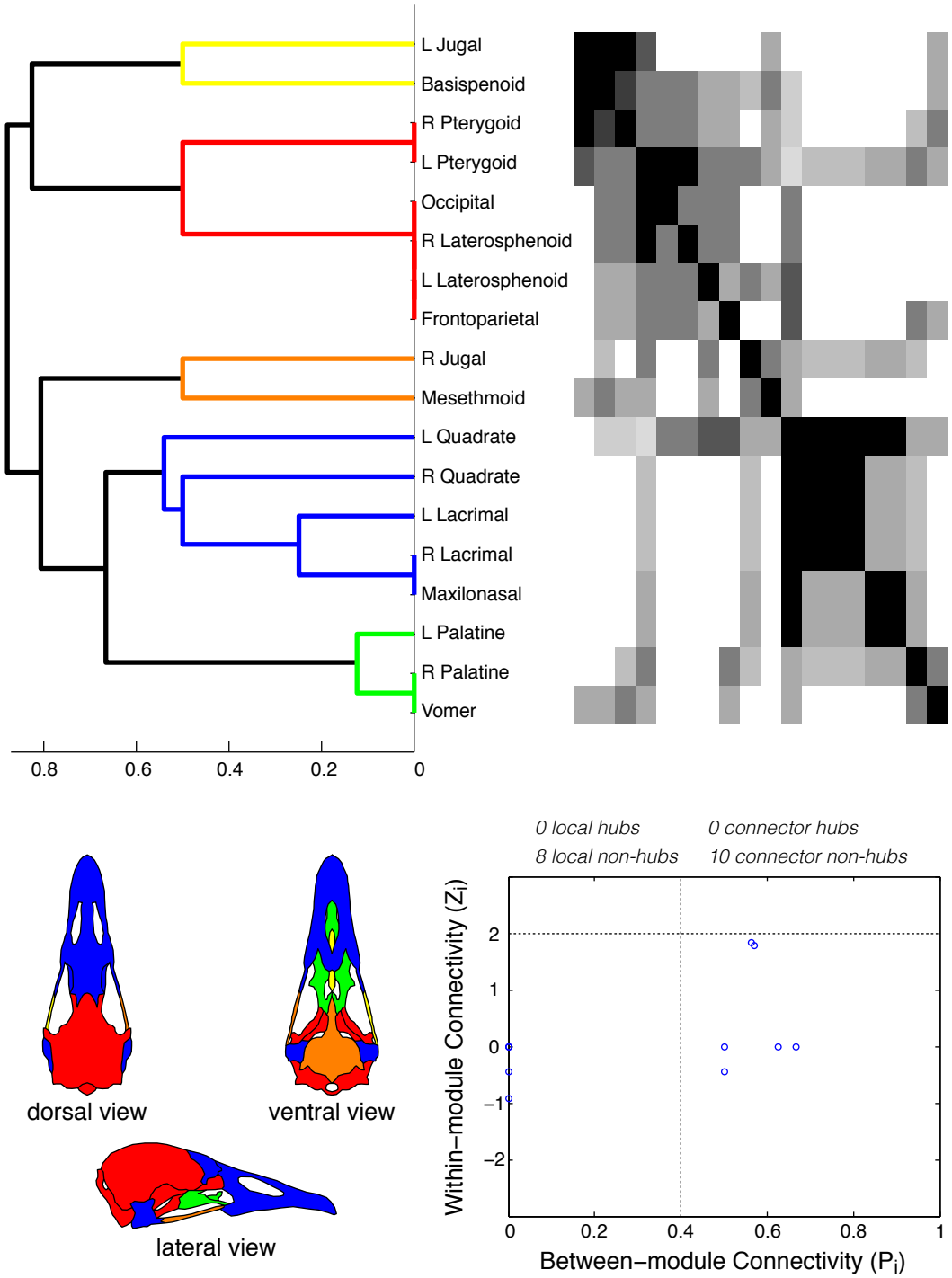

Figure 8.48: Connectivity modules in the skull of *Anser anser*.

Sphenodon punctatus (Reptilia: Rhynchocephalia)

Nodes	38
Links	78
Density	0.11
Clustering Coefficient	0.28
Shortest Path Length	2.85
Heterogeneity	0.33
Small-World	*Yes*
Modularity Q-value	0.47

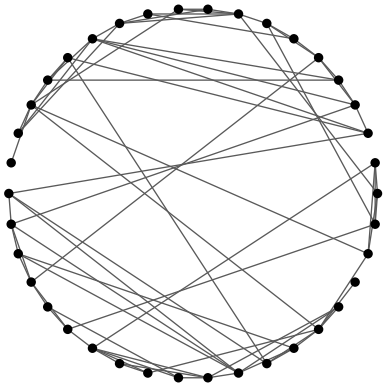

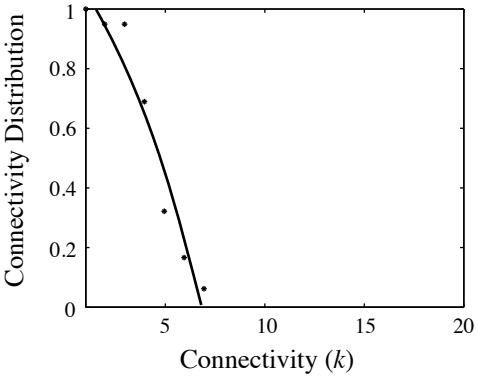

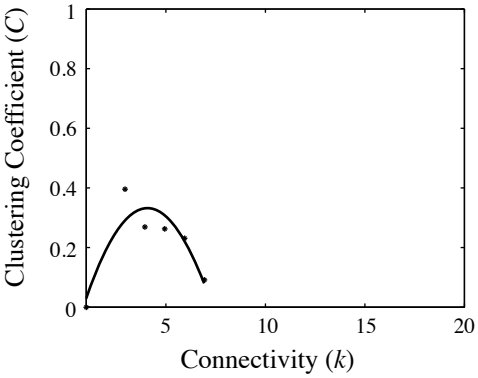

Best fit:

$P_{cum}(k) = 1.13 - 2.2\,k - 0.01\,k^2$

$\boldsymbol{r} = 0.97$ *(binomial)*

$\boldsymbol{r} = 0.96$ *(linear)*

$\boldsymbol{r} = 0.88$ *(exponential)*

$\boldsymbol{r} = 0.75$ *(power-law)*

Best fit:

$C(k) = -0.2 + 0.26\,k - 0.03\,k^2$

$\boldsymbol{r} = 0.91$ *(binomial)*

$\boldsymbol{r} = 0.25$ *(power-law)*

$\boldsymbol{r} = 0.13$ *(linear)*

$\boldsymbol{r} = 0.08$ *(exponential)*

Figure 8.49: Network analysis of the skull of *Sphenodon punctatus*.

Sphenodon punctatus (Reptilia: Rhynchocephalia)

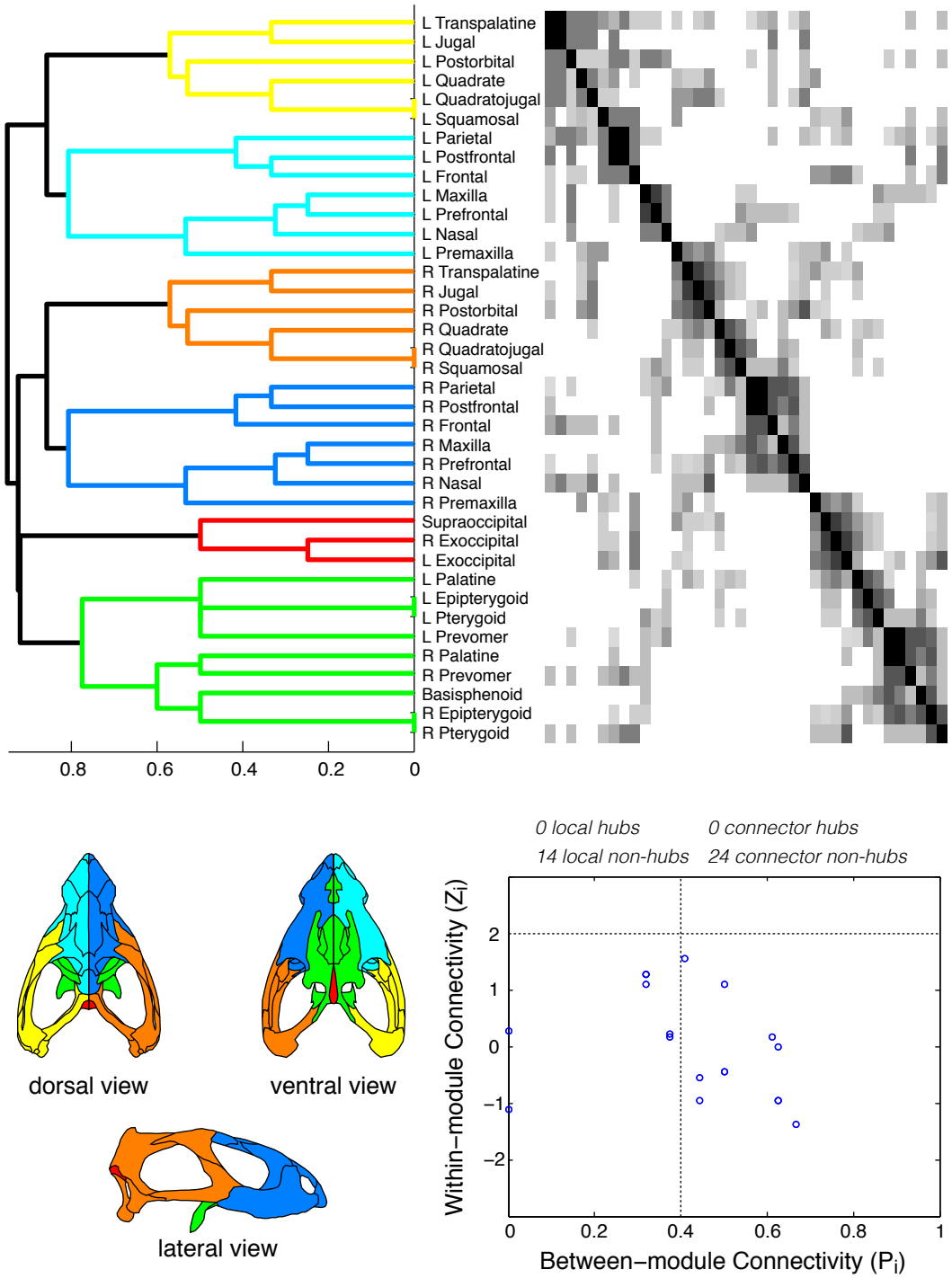

Figure 8.50: Connectivity modules in the skull of *Sphenodon punctatus*.

Iguana iguana (Reptilia: Squamata)

Nodes	42
Links	122
Density	0.14
Clustering Coefficient	0.47
Shortest Path Length	2.48
Heterogeneity	0.43
Small-World	*Yes*
Modularity Q-value	0.45

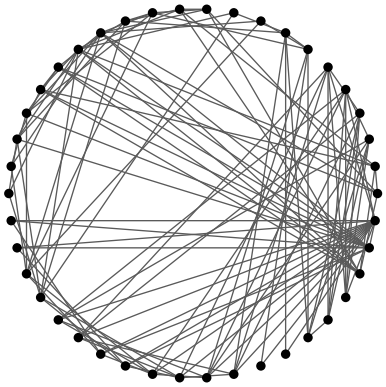

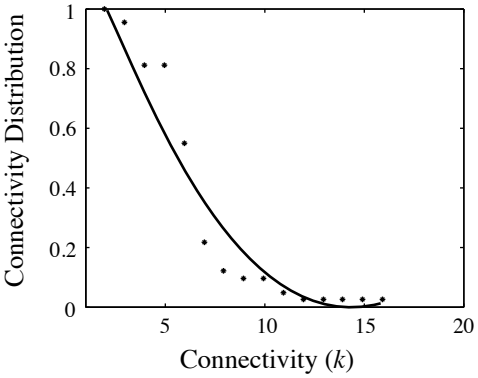

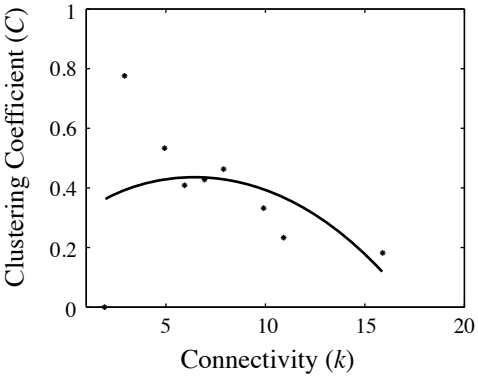

Best fit:

$P_{cum}(k) = 1.38 - 0.19\,k + 0.007\,k^2$

$\boldsymbol{r} = 0.96$ *(binomia)*

$\boldsymbol{r} = 0.94$ *(exponential)*

$\boldsymbol{r} = 0.89$ *(linear)*

$\boldsymbol{r} = 0.86$ *(power-law)*

Best fit:

$C(k) = 0.29 + 0.046\,k - 0.003\,k^2$

$\boldsymbol{r} = 0.45$ *(binomial)*

$\boldsymbol{r} = 0.31$ *(linear)*

$\boldsymbol{r} = 0.25$ *(exponential)*

$\boldsymbol{r} = 0.09$ *(power-law)*

Figure 8.51: Network analysis of the skull of *Iguana iguana*.

Iguana iguana (Reptilia: Squamata)

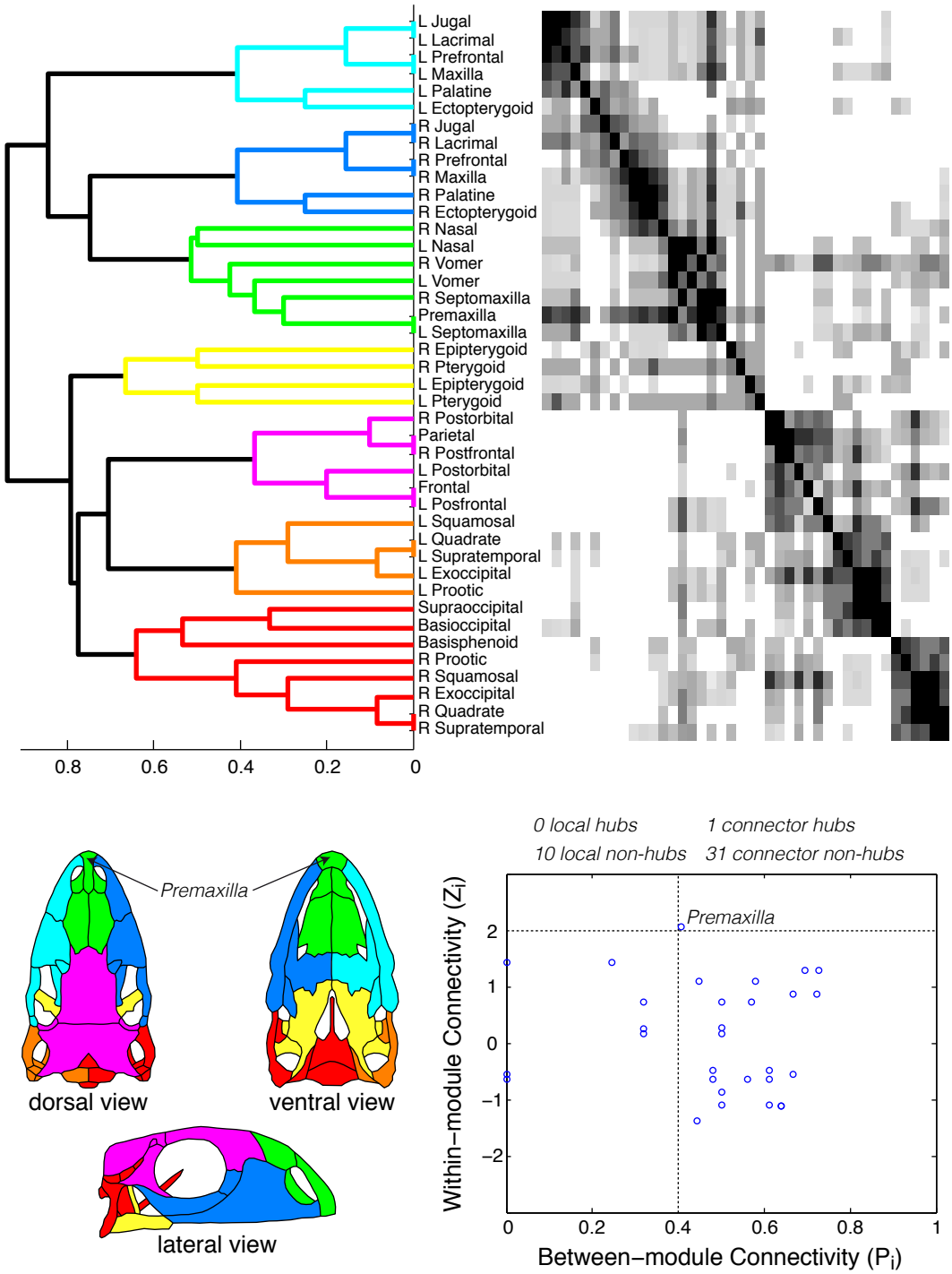

Figure 8.52: Connectivity modules in the skull of *Iguana iguana*.

Python regius (Reptilia: Squamata)

Nodes	35
Links	68
Density	0.11
Clustering Coefficient	0.46
Shortest Path Length	2.76
Heterogeneity	0.49
Small-World	*Yes*
Modularity Q-value	0.54

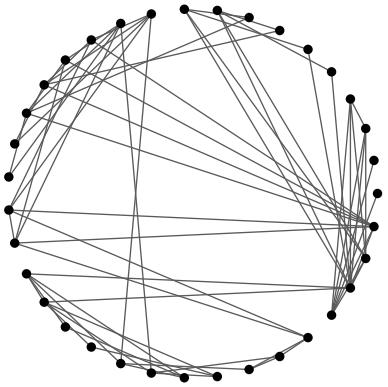

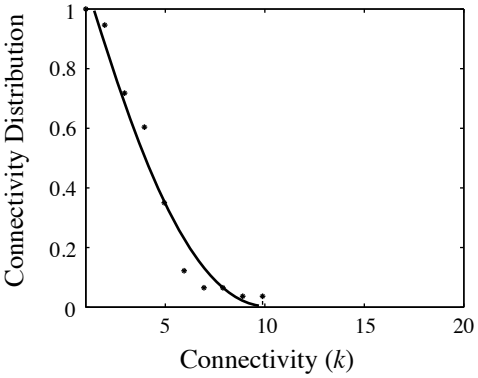

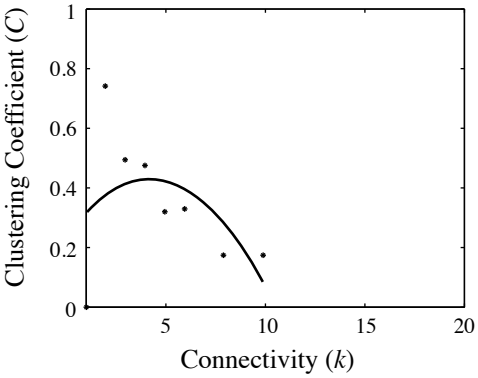

Best fit:

$P_{cum}(k) = 1.36 - 0.27\,k + 0.01\,k^2$

$\boldsymbol{r} = 0.98$ *(binomial)*

$\boldsymbol{r} = 0.96$ *(exponential)*

$\boldsymbol{r} = 0.95$ *(linear)*

$\boldsymbol{r} = 0.84$ *(power-law)*

Best fit:

$C(k) = 0.24 + 0.09\,k - 0.01\,k^2$

$\boldsymbol{r} = 0.50$ *(binomial)*

$\boldsymbol{r} = 0.33$ *(linear)*

$\boldsymbol{r} = 0.26$ *(exponential)*

$\boldsymbol{r} = 0.07$ *(power-law)*

Figure 8.53: Network analysis of the skull of *Python regius*.

Python regius (Reptilia: Squamata)

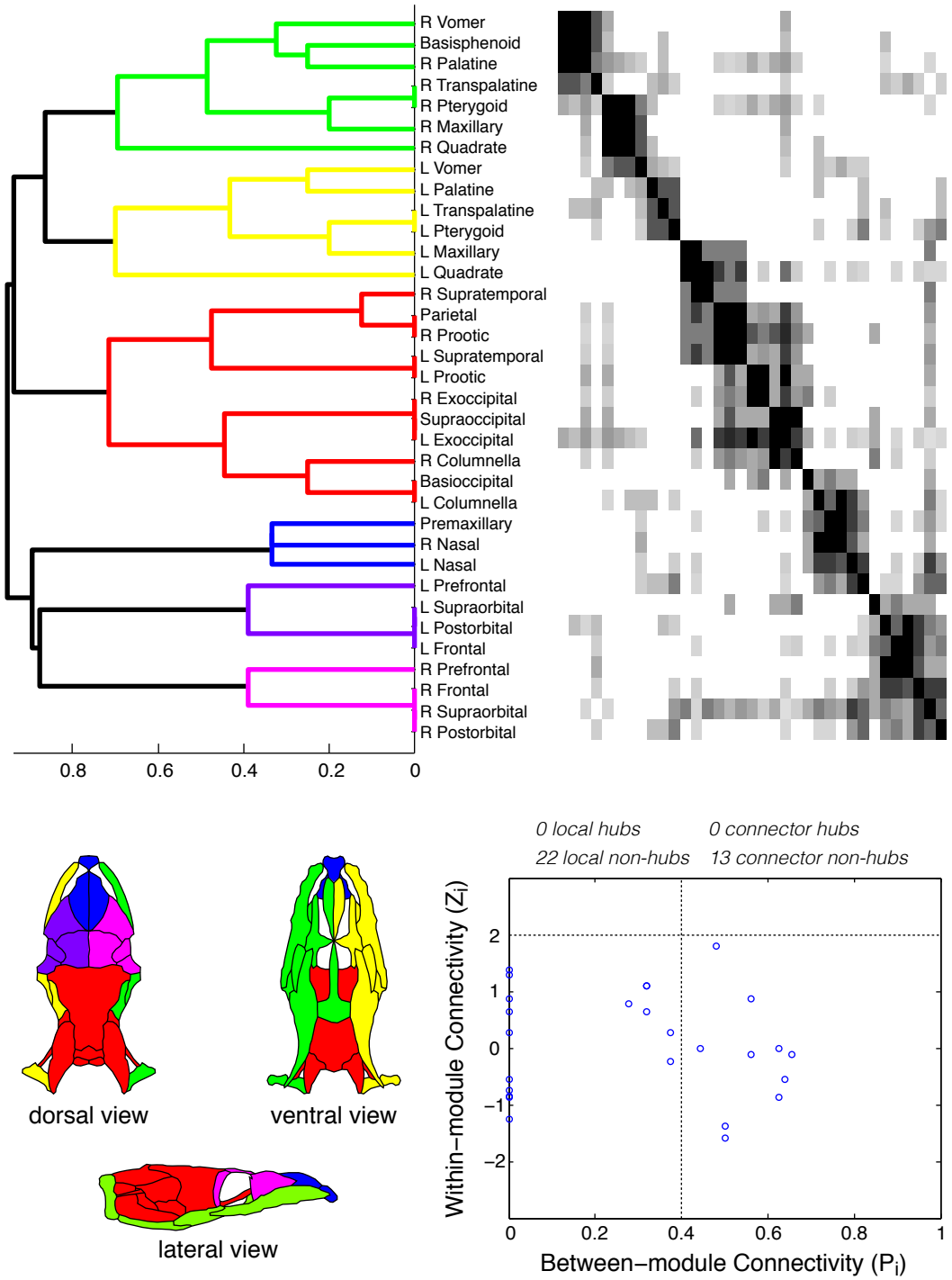

Figure 8.54: Connectivity modules in the skull of *Python regius*.

Hemitheconyx caudicinctus (Reptilia: Squamata)

Nodes	34
Links	72
Density	0.13
Clustering Coefficient	0.33
Shortest Path Length	2.70
Heterogeneity	0.39
Small-World	*Yes*
Modularity Q-value	0.48

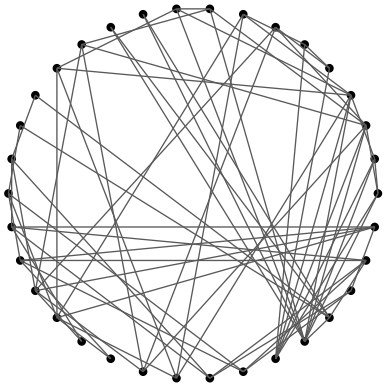

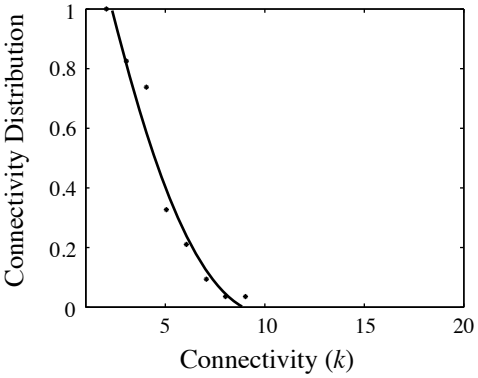

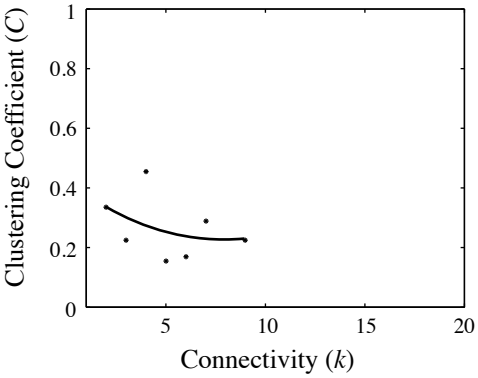

Best fit:

$P_{cum}(k) = 1.68 - 0.34\,k + 0.002\,k^2$

$\boldsymbol{r} = 0.98$ *(binomial)*

$\boldsymbol{r} = 0.96$ *(linear)*

$\boldsymbol{r} = 0.96$ *(exponential)*

$\boldsymbol{r} = 0.89$ *(power-law)*

Best fit:

$C(k) = 0.42 - 0.05\,k + 0.003\,k^2$

$\boldsymbol{r} = 0.38$ *(binomial)*

$\boldsymbol{r} = 0.37$ *(power-law)*

$\boldsymbol{r} = 0.36$ *(exponential)*

$\boldsymbol{r} = 0.35$ *(linear)*

Figure 8.55: Network analysis of the skull of *Hemitheconyx caudicinctus*.

Hemitheconyx caudicinctus (Reptilia: Squamata)

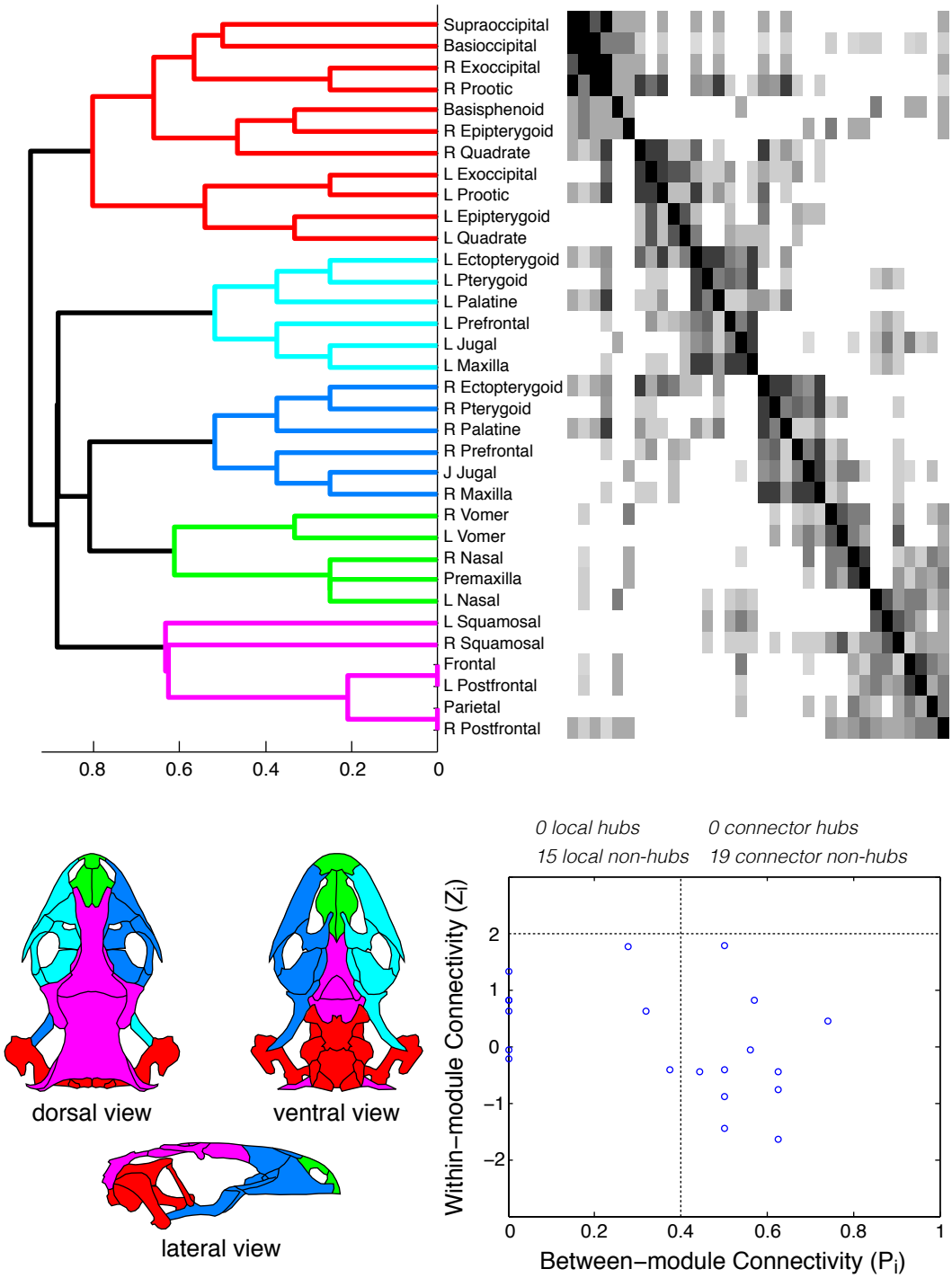

Figure 8.56: Connectivity modules in the skull of *Hemitheconyx caudicinctus*.

Tupinambis teguixin (Reptilia: Squamata)

Nodes	42
Links	94
Density	0.11
Clustering Coefficient	0.37
Shortest Path Length	2.81
Heterogeneity	0.42
Small-World	*Yes*
Modularity Q-value	0.47

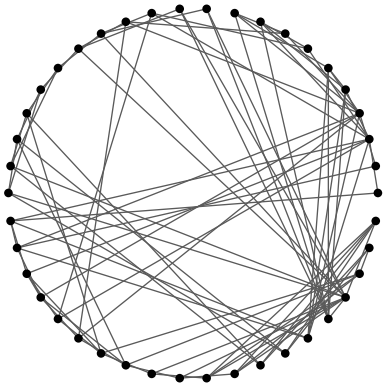

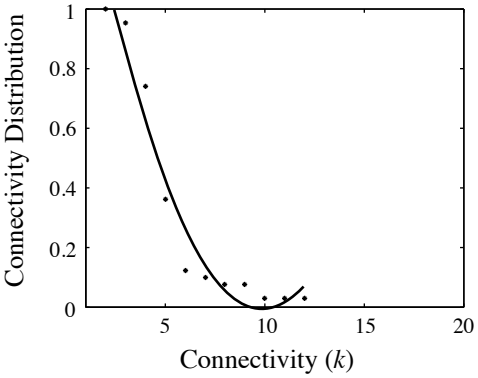

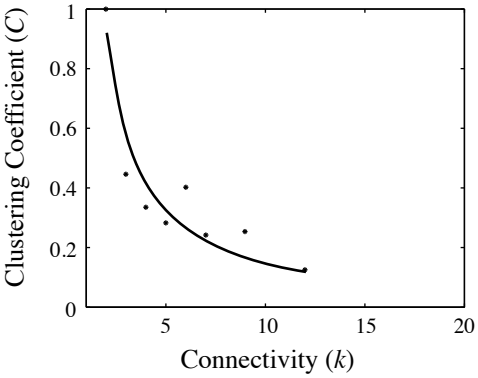

Best fit:

$P_{cum}(k) = 1.73 - 0.35\,k + 0.018\,k^{2}$

$\boldsymbol{r} = 0.98$ *(binomial)*

$\boldsymbol{r} = 0.96$ *(exponential)*

$\boldsymbol{r} = 0.89$ *(power-law)*

$\boldsymbol{r} = 0.88$ *(linear)*

Best fit:

$C(k) = 2.05\,k^{-1.15}$

$\boldsymbol{r} = 0.94$ *(power-law)*

$\boldsymbol{r} = 0.89$ *(exponential)*

$\boldsymbol{r} = 0.84$ *(binomial)*

$\boldsymbol{r} = 0.74$ *(linear)*

Figure 8.57: Network analysis of the skull of *Tupinambis teguixin*.

Tupinambis teguixin (Reptilia: Squamata)

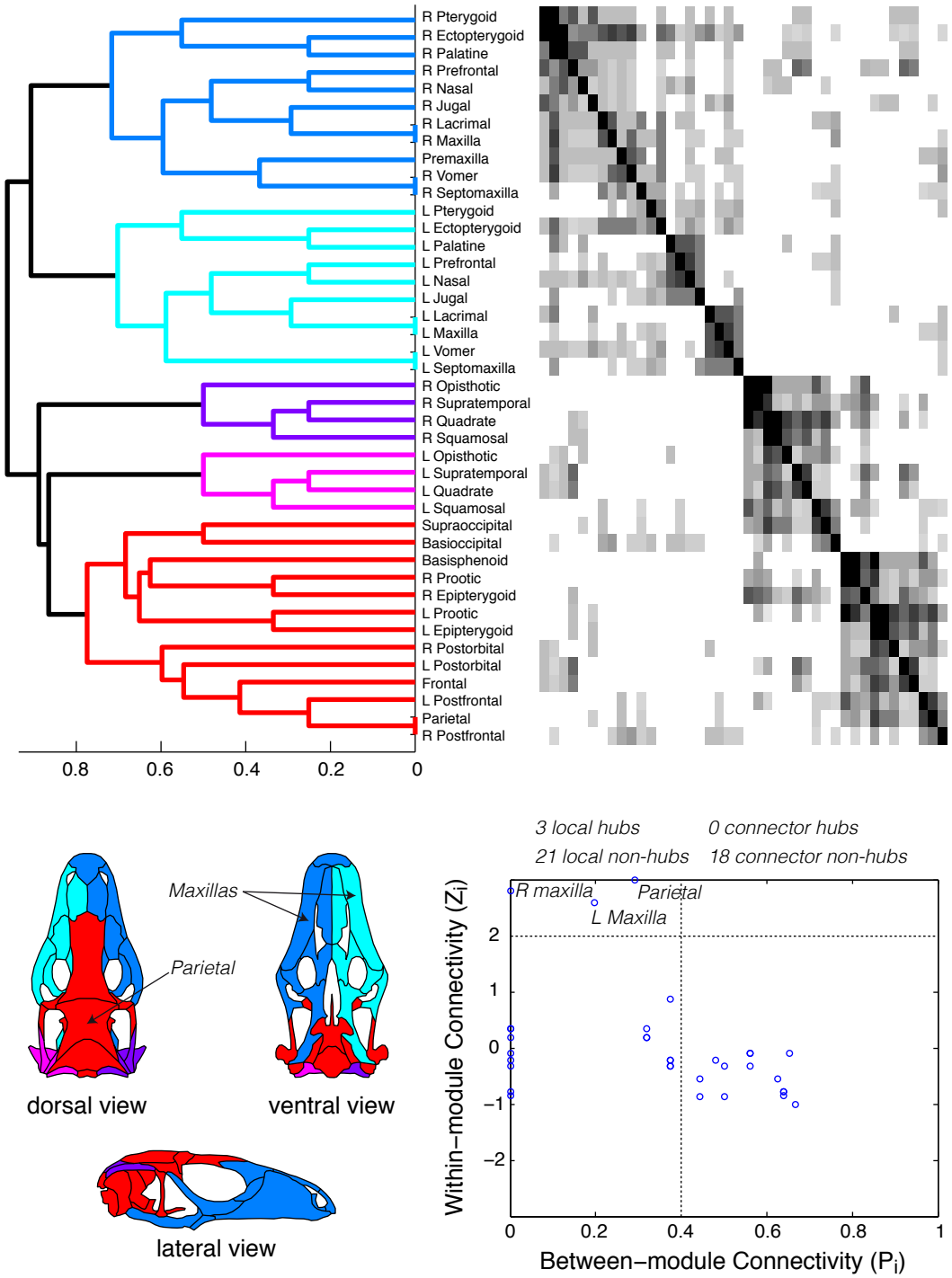

Figure 8.58: Connectivity modules in the skull of *Tupinambis teguixin*.

Diplometopon zarudnyi (Reptilia: Squamata)

Nodes	26
Links	57
Density	0.18
Clustering Coefficient	0.61
Shortest Path Length	2.52
Heterogeneity	0.44
Small-World	*Yes*
Modularity Q-value	0.38

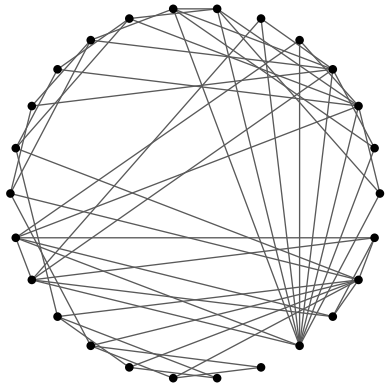

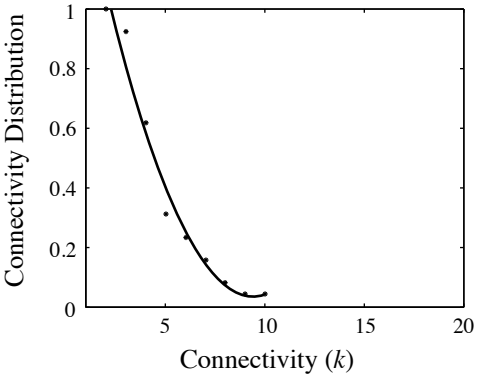

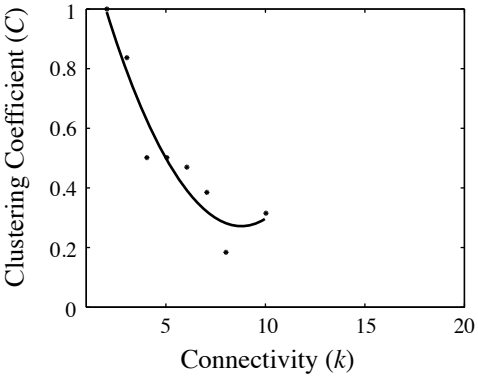

Best fit:

$P_{cum}(k) = 1.71 - 0.36\,k + 0.19\,k^2$

$\boldsymbol{r} = 0.99$ *(binomial)*

$\boldsymbol{r} = 0.97$ *(exponential)*

$\boldsymbol{r} = 0.94$ *(linear)*

$\boldsymbol{r} = 0.92$ *(power-law)*

Best fit:

$C(k) = 1.48 - 0.28\,k + 0.016\,k^2$

$\boldsymbol{r} = 0.96$ *(binomial)*

$\boldsymbol{r} = 0.95$ *(power-law)*

$\boldsymbol{r} = 0.95$ *(exponential)*

$\boldsymbol{r} = 0.88$ *(linear)*

Figure 8.59: Network analysis of the skull of *Diplometopon zarudnyi*.

Diplometopon zarudnyi (Reptilia: Squamata)

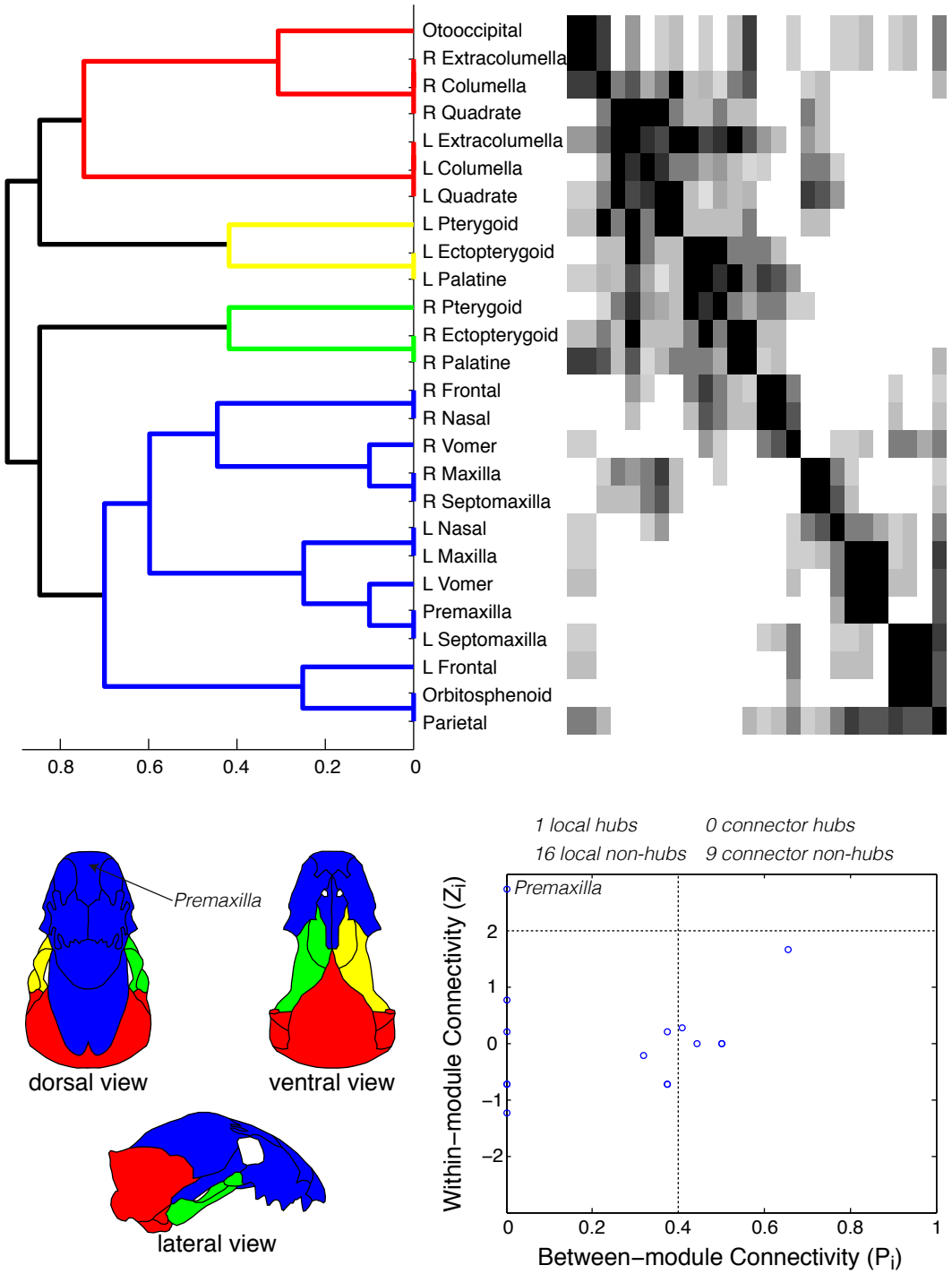

Figure 8.60: Connectivity modules in the skull of *Diplometopon zarudnyi*.

Stenocercus guentheri (Reptilia: Squamata)

Nodes	00
Links	000
Density	0.10
Clustering Coefficient	0.34
Shortest Path Length	2.90
Heterogeneity	0.45
Small-World	*Yes*
Modularity Q-value	0.49

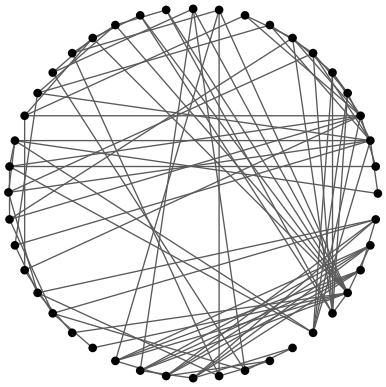

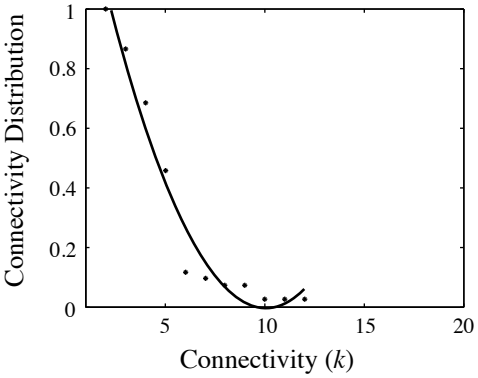

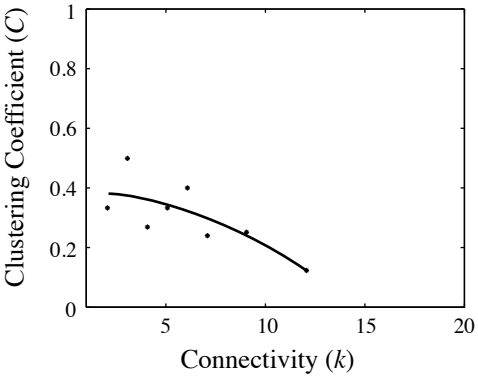

Best fit:

$P_{cum}(k) = 1.66 - 0.33\ k + 0.016\ k^2$

$\boldsymbol{r} = 0.98$ *(binomial)*

$\boldsymbol{r} = 0.97$ *(exponential)*

$\boldsymbol{r} = 0.91$ *(power-law)*

$\boldsymbol{r} = 0.98$ *(linear)*

Best fit:

$C(k) = 0.4 - 0.0005\ k - 0.002\ k^2$

$\boldsymbol{r} = 0.71$ *(binomial)*

$\boldsymbol{r} = 0.75$ *(linear)*

$\boldsymbol{r} = 0.71$ *(exponential)*

$\boldsymbol{r} = 0.60$ *(power-law)*

Figure 8.61: Network analysis of the skull of *Stenocercus guentheri*.

Stenocercus guentheri (Reptilia: Squamata)

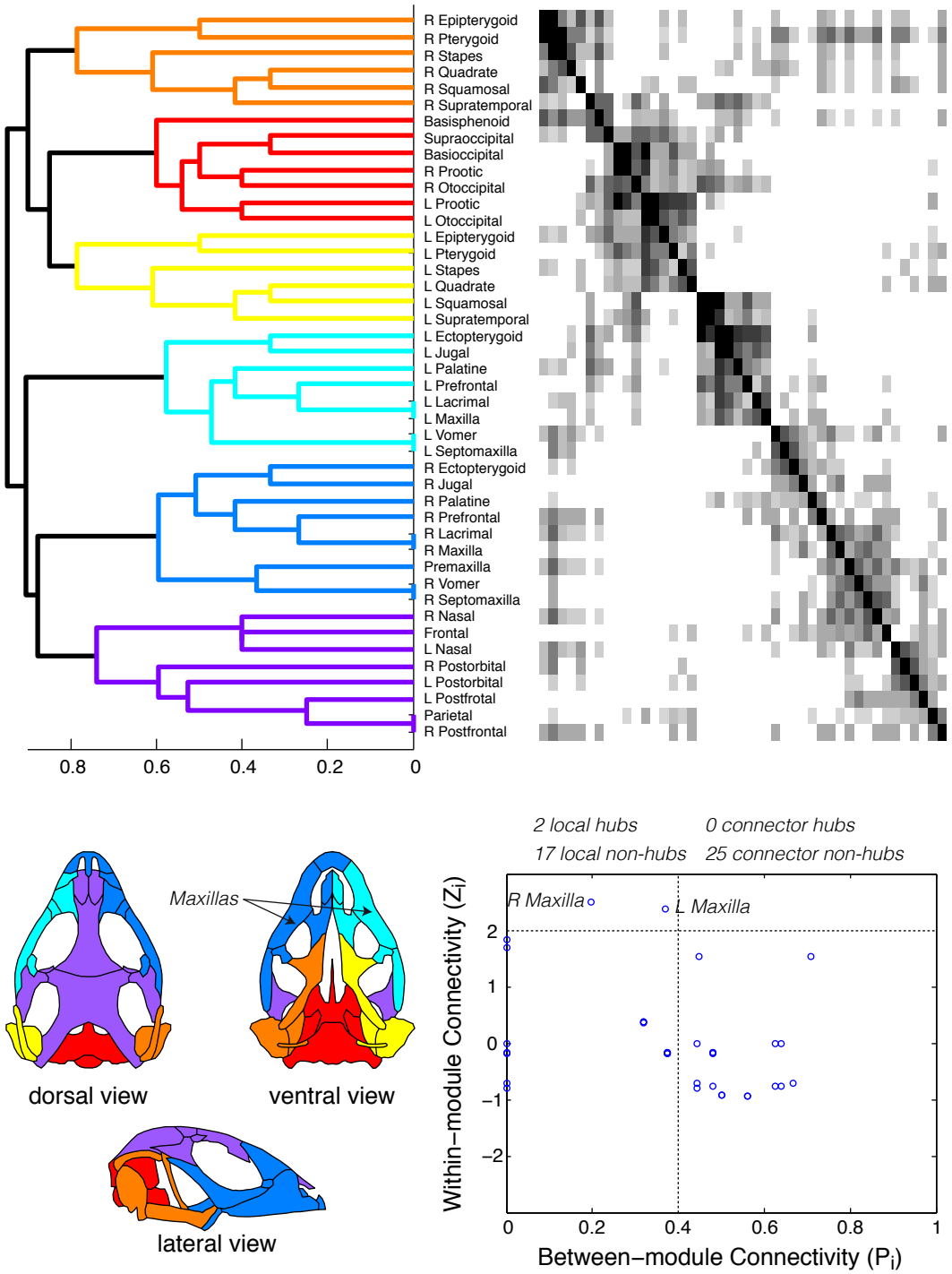

Figure 8.62: Connectivity modules in the skull of *Stenocercus guentheri*.

Varanus salvator (Reptilia: Squamata)

Nodes	42
Links	85
Density	0.10
Clustering Coefficient	3.19
Shortest Path Length	0.29
Heterogeneity	0.42
Small-World	*Yes*
Modularity Q-value	0.49

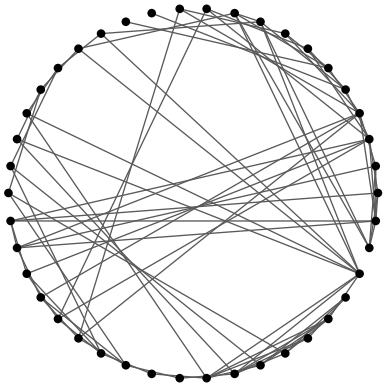

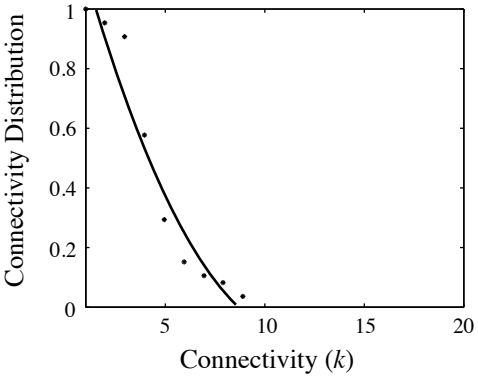

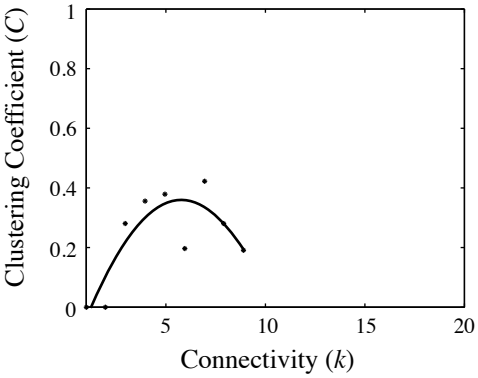

Best fit:

$P_{cum}(k) = 1.36 - 0.25\,k + 0.01\,k^2$

$\boldsymbol{r} = 0.97$ *(binomial)*

$\boldsymbol{r} = 0.96$ *(linear)*

$\boldsymbol{r} = 0.93$ *(exponential)*

$\boldsymbol{r} = 0.81$ *(power-law)*

Best fit:

$C(k) = -0.22 + 0.2\,k - 0.02\,k^2$

$\boldsymbol{r} = 0.84$ *(binomial)*

$\boldsymbol{r} = 0.53$ *(power-law)*

$\boldsymbol{r} = 0.52$ *(linear)*

$\boldsymbol{r} = 0.39$ *(exponential)*

Figure 8.63: Network analysis of the skull of *Varanus salvator*.

Varanus salvator (Reptilia: Squamata)

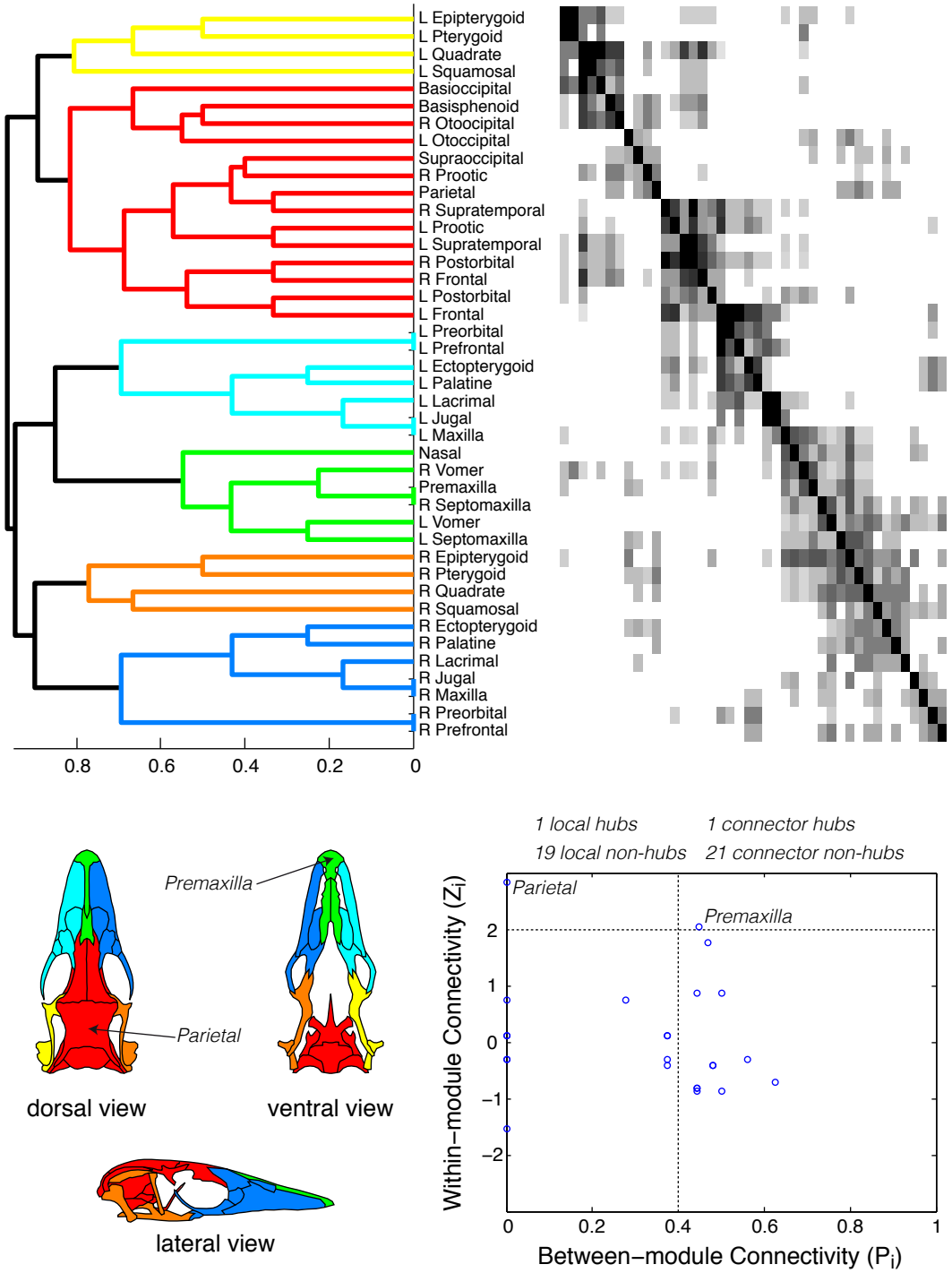

Figure 8.64: Connectivity modules in the skull of *Varanus salvator*.

Ennatosaurus tecton (Synapsida: Pelycosauria)

Nodes	52
Links	124
Density	0.09
Clustering Coefficient	0.36
Shortest Path Length	2.87
Heterogeneity	0.51
Small-World	*Yes*
Modularity Q-value	0.48

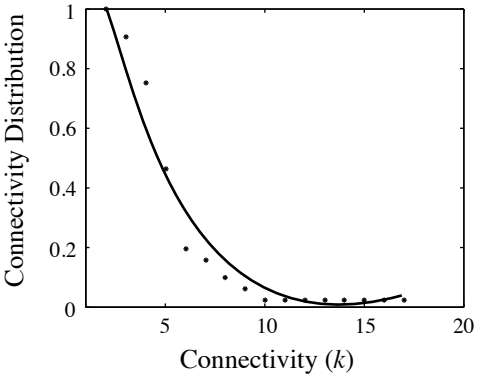

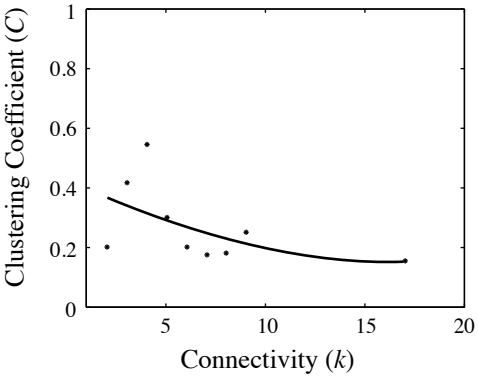

Best fit:

$P_{cum}(k) = 1.44 - 0.24\,k + 0.009\,k^2$

$\boldsymbol{r} = 0.98$ *(binomial)*

$\boldsymbol{r} = 0.97$ *(exponential)*

$\boldsymbol{r} = 0.92$ *(power-law)*

$\boldsymbol{r} = 0.82$ *(linear)*

Best fit:

$C(k) = 0.43 - 0.03\,k + 0.001\,k^2$

$\boldsymbol{r} = 0.52$ *(binomial)*

$\boldsymbol{r} = 0.52$ *(exponential)*

$\boldsymbol{r} = 0.50$ *(linear)*

$\boldsymbol{r} = 0.40$ *(power-law)*

Figure 8.65: Network analysis of the skull of *Ennatosaurus tecton*.

Ennatosaurus tecton (Synapsida: Pelycosauria)

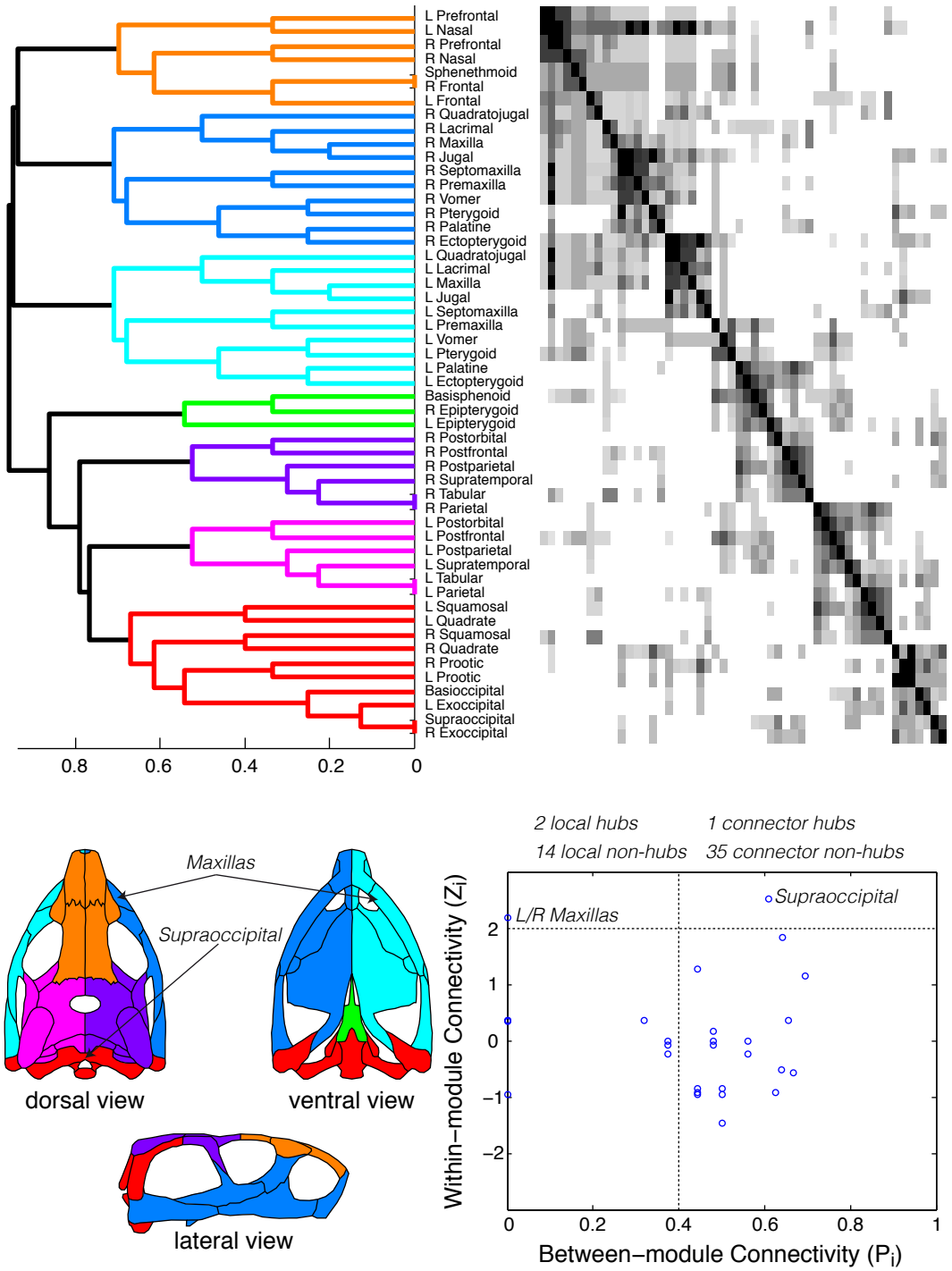

Figure 8.66: Connectivity modules in the skull of *Ennatosaurus tecton*.

Dimetrodon gigas (Synapsida: Pelycosauria)

Nodes	45
Links	111
Density	0.11
Clustering Coefficient	0.44
Shortest Path Length	2.71
Heterogeneity	0.39
Small-World	*Yes*
Modularity Q-value	0.47

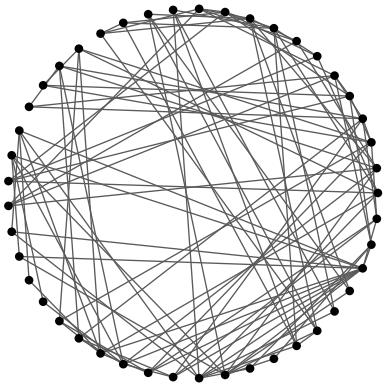

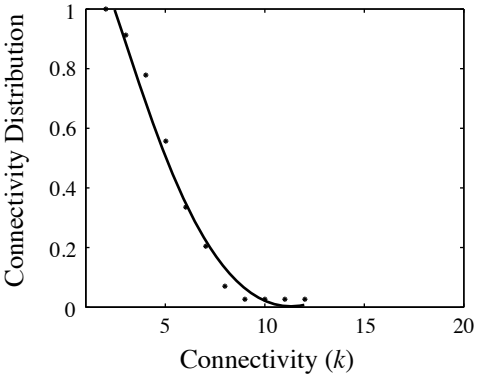

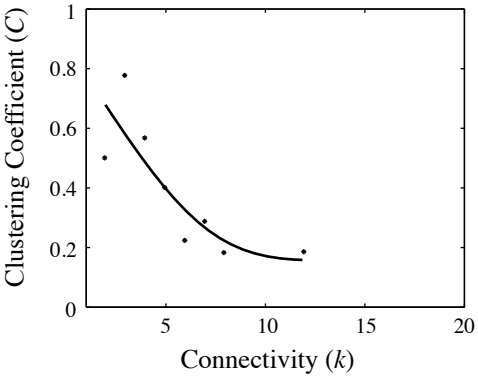

Best fit:

$P_{cum}(k) = 1.63 - 0.29\,k + 0.01\,k^2$

$\boldsymbol{r} = 0.99$ *(binomial)*

$\boldsymbol{r} = 0.96$ *(exponential)*

$\boldsymbol{r} = 0.94$ *(linear)*

$\boldsymbol{r} = 0.89$ *(power-law)*

Best fit:

$C(k) = 0.93 - 0.13\,k + 0.006\,k^2$

$\boldsymbol{r} = 0.84$ *(binomial)*

$\boldsymbol{r} = 0.82$ *(exponential)*

$\boldsymbol{r} = 0.78$ *(linear)*

$\boldsymbol{r} = 0.73$ *(power-law)*

Figure 8.67: Network analysis of the skull of *Dimetrodon gigas*.

Dimetrodon gigas (Synapsida: Pelycosauria)

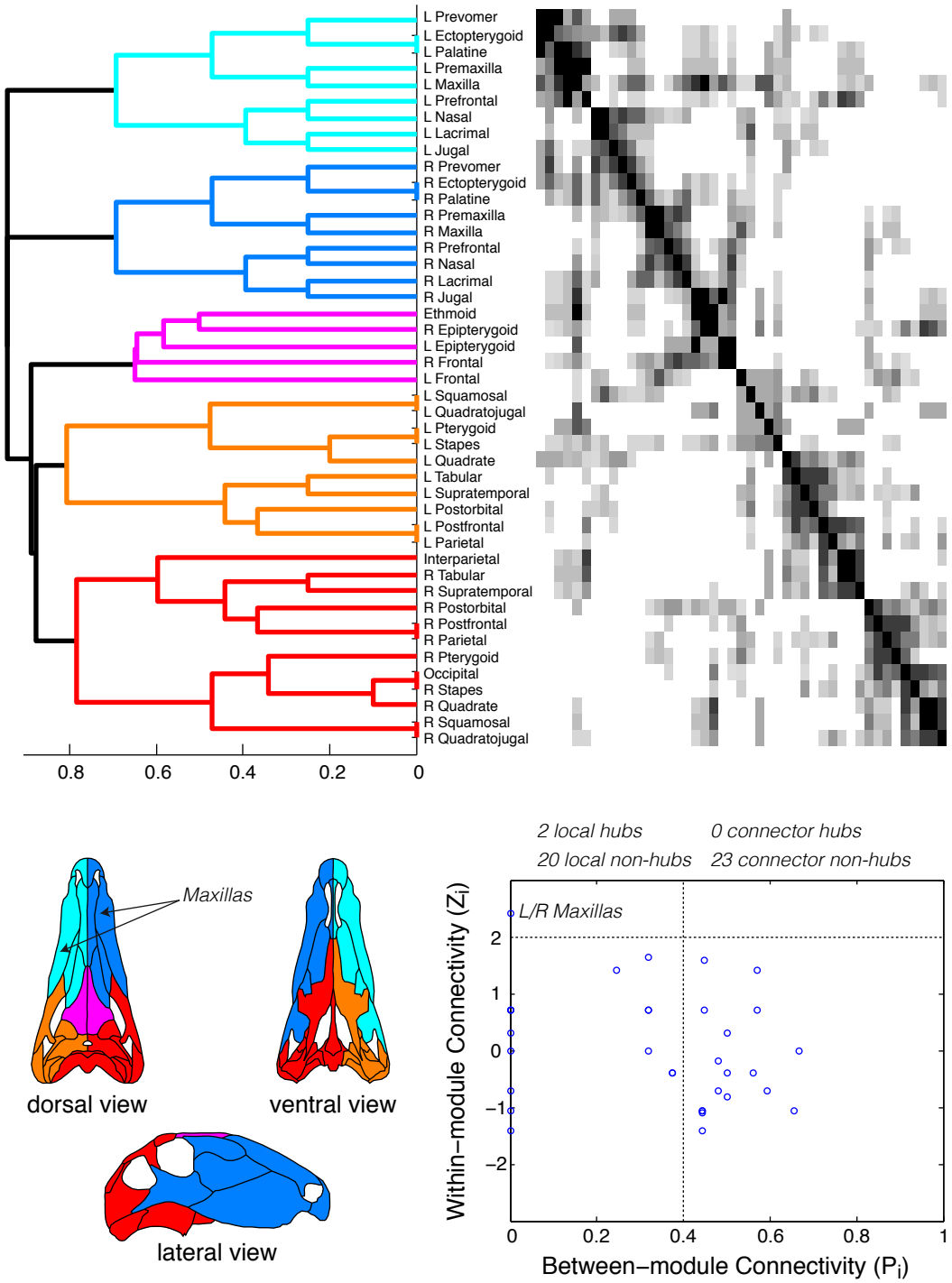

Figure 8.68: Connectivity modules in the skull of *Dimetrodon gigas*.

Jonkeria ingens (Synapsida: Therapsida)

Nodes	51
Links	130
Density	0.10
Clustering Coefficient	0.46
Shortest Path Length	2.75
Heterogeneity	0.50
Small-World	*Yes*
Modularity Q-value	0.46

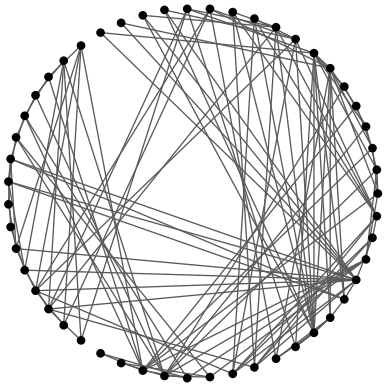

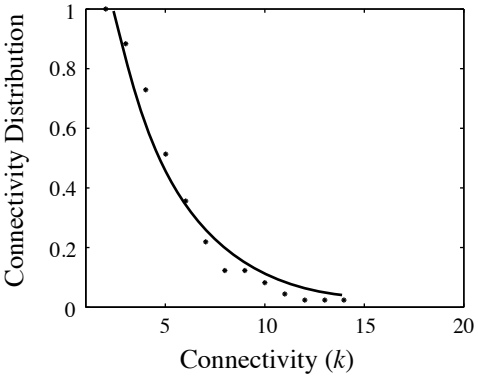

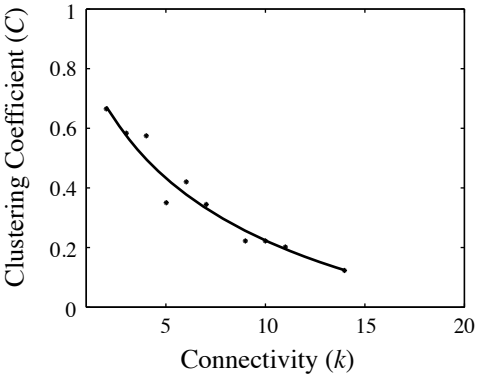

Best fit:

$P_{cum}(k) = 1.95\ e^{-0.29\,k}$

$\boldsymbol{r} = 0.98$ *(exponential)*

$\boldsymbol{r} = 0.92$ *(power-law)*

$\boldsymbol{r} = 0.92$ *(linear)*

$\boldsymbol{r} = 0.77$ *(binomial)*

Best fit:

$C(k) = 0.90\ e^{-0.14\,k}$

$\boldsymbol{r} = 0.98$ *(exponential)*

$\boldsymbol{r} = 0.97$ *(binomial)*

$\boldsymbol{r} = 0.95$ *(linear)*

$\boldsymbol{r} = 0.94$ *(power-law)*

Figure 8.69: Network analysis of the skull of *Jonkeria ingens*.

Jonkeria ingens (Synapsida: Therapsida)

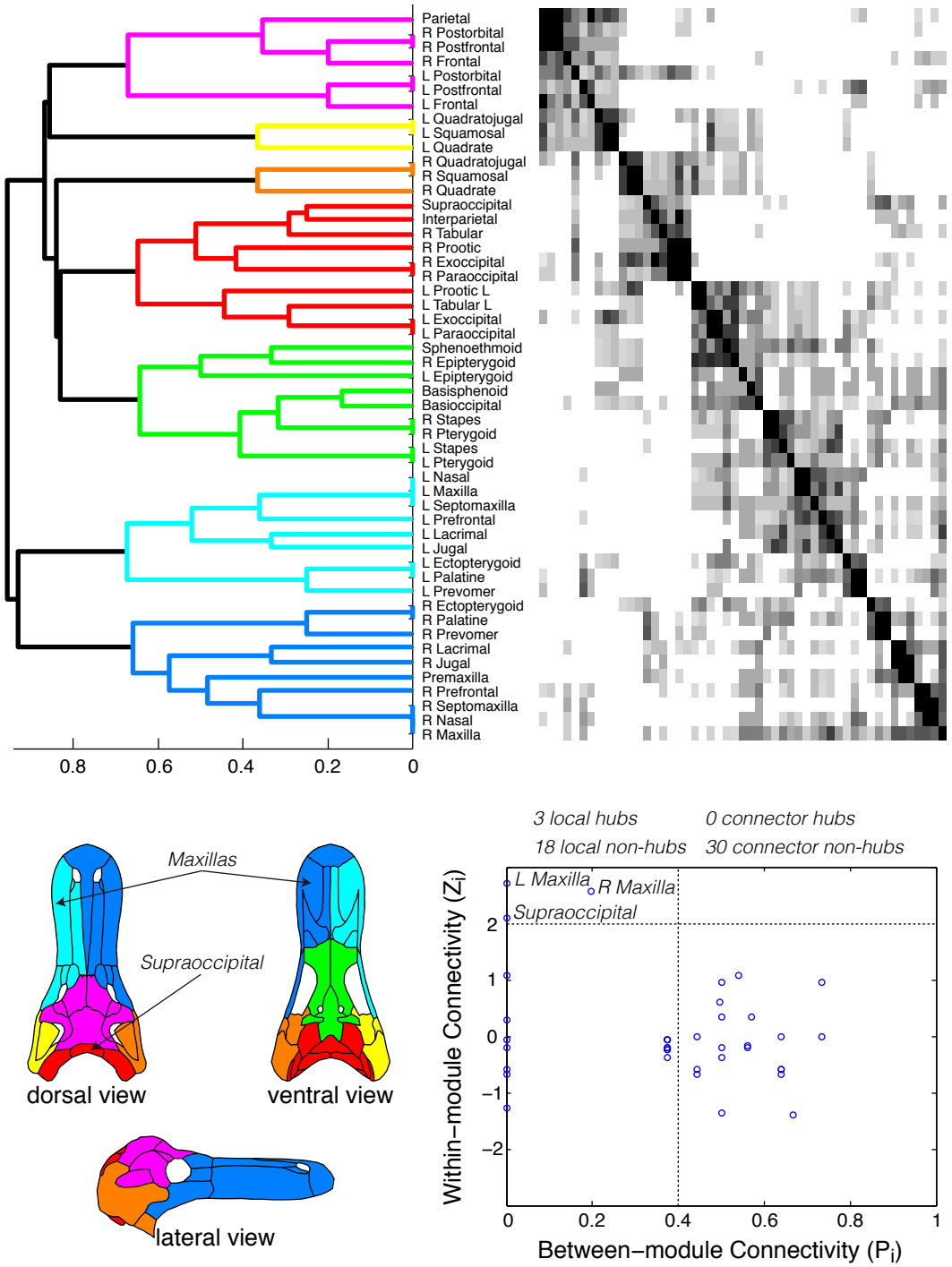

Figure 8.70: Connectivity modules in the skull of *Jonkeria ingens*.

Thrinaxodon liorhinus (Synapsida: Therapsida)

Nodes	44
Links	100
Density	0.11
Clustering Coefficient	0.40
Shortest Path Length	2.94
Heterogeneity	0.35
Small-World	*Yes*
Modularity Q-value	0.54

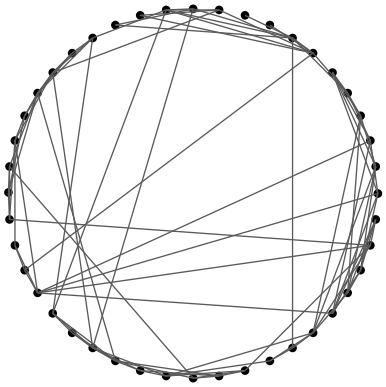

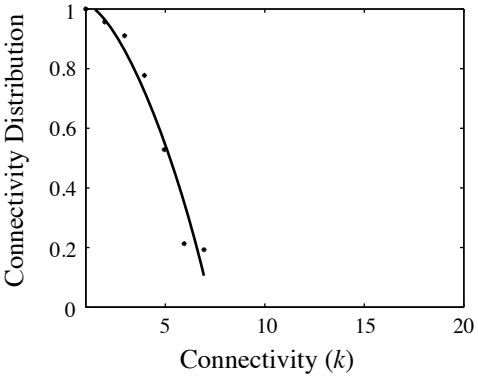

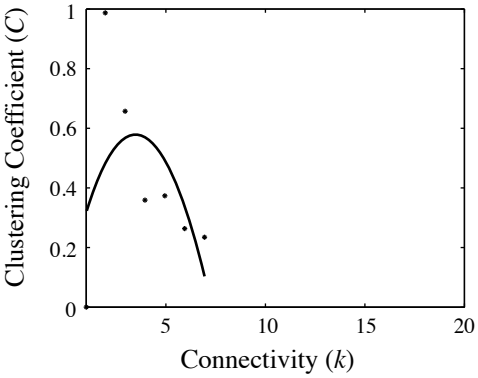

Best fit:

$P_{cum}(k) = 1.06 - 0.01\ k - 0.02\ k^2$

$\boldsymbol{r} = 0.98$ *(binomial)*

$\boldsymbol{r} = 0.97$ *(linear)*

$\boldsymbol{r} = 0.89$ *(exponential)*

$\boldsymbol{r} = 0.76$ *(power-law)*

Best fit:

$C(k) = 0.62\ e^{-0.1\ k}$

$\boldsymbol{r} = 0.86$ *(exponential)*

$\boldsymbol{r} = 0.86$ *(binomial)*

$\boldsymbol{r} = 0.85$ *(linear)*

$\boldsymbol{r} = 0.83$ *(power-law)*

Figure 8.71: Network analysis of the skull of *Thrinaxodon liorhinus*.

Thrinaxodon liorhinus (Synapsida: Therapsida)

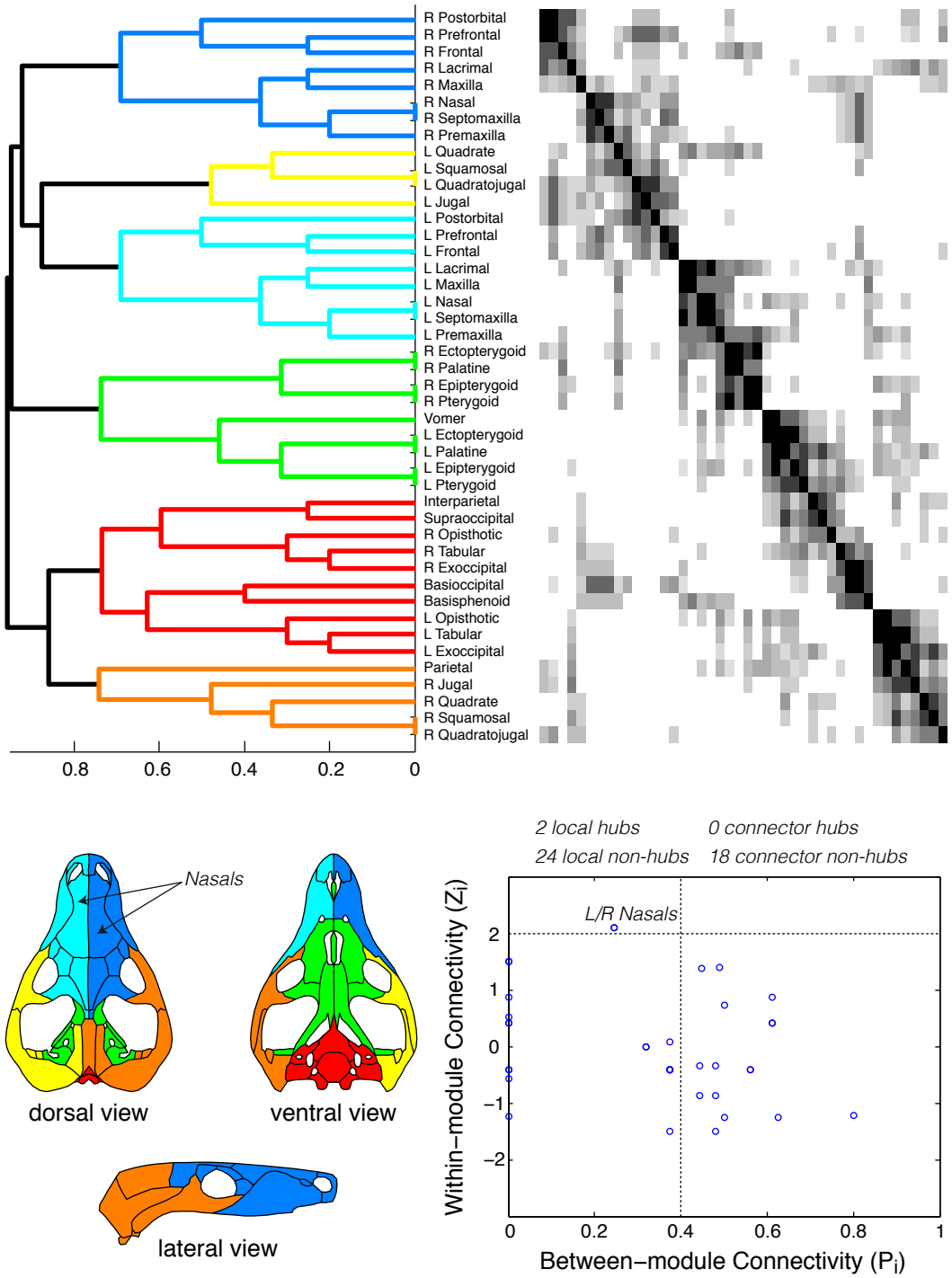

Figure 8.72: Connectivity modules in the skull of *Thrinaxodon liorhinus*.

Ornithorhynchus anatinus (Mammalia: Monotremata)

Nodes	26
Links	65
Density	0.20
Clustering Coefficient	0.55
Shortest Path Length	2.13
Heterogeneity	0.45
Small-World	*Yes*
Modularity Q-value	0.38

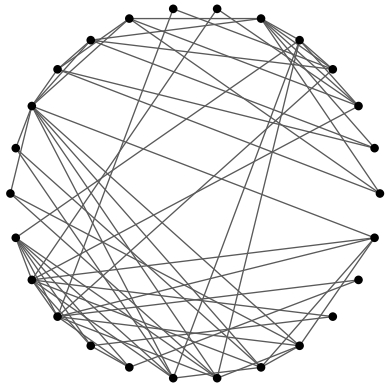

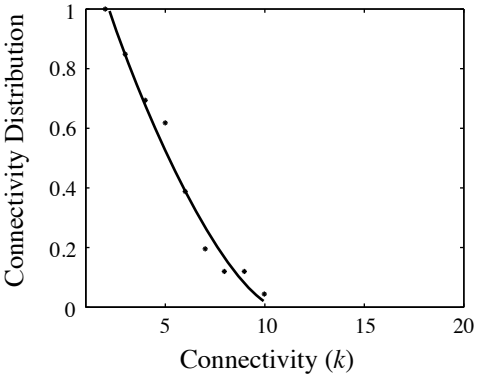

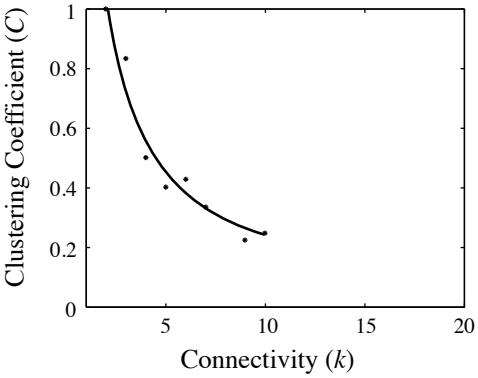

Best fit:

$P_{cum}(k) = 1.46 - 0.23\ k + 0.008\ k^2$

$\boldsymbol{r} = 0.99$ *(binomial)*

$\boldsymbol{r} = 0.98$ *(linear)*

$\boldsymbol{r} = 0.97$ *(exponential)*

$\boldsymbol{r} = 0.90$ *(power-law)*

Best fit:

$C(k) = 1.96\ k^{-0.91\ k}$

$\boldsymbol{r} = 0.98$ *(power-law)*

$\boldsymbol{r} = 0.97$ *(binomial)*

$\boldsymbol{r} = 0.97$ *(exponential)*

$\boldsymbol{r} = 0.89$ *(linear)*

Figure 8.73: Network analysis of the skull of *Ornithorhynchus anatinus*.

Ornithorhynchus anatinus (Mammalia: Monotremata)

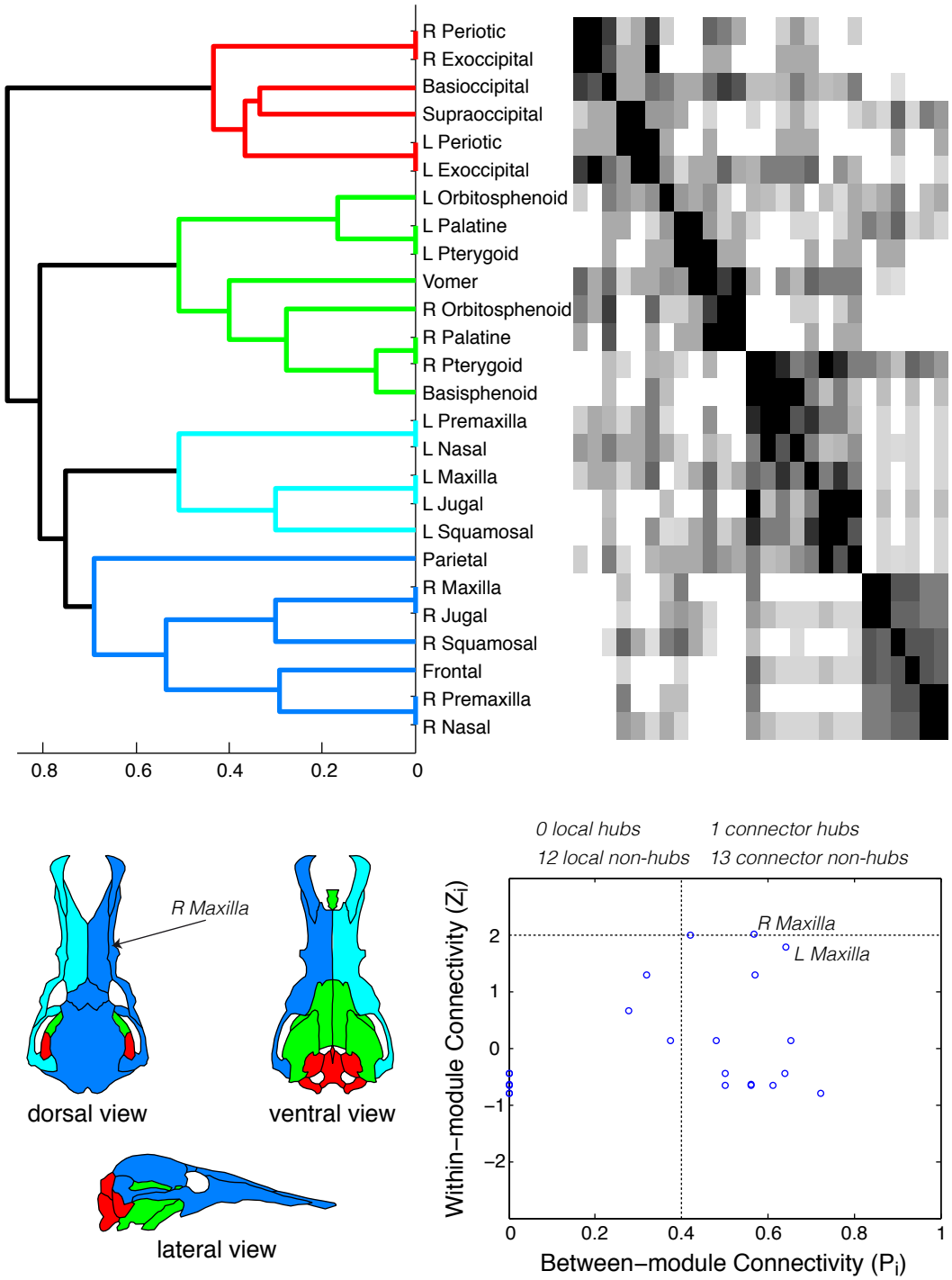

Figure 8.74: Connectivity modules in the skull of *Ornithorhynchus anatinus*.

Phascolarctos cinereus (Mammalia: Diprotodontia)

Nodes	31
Links	174
Density	0.19
Clustering Coefficient	0.47
Shortest Path Length	2.26
Heterogeneity	0.34
Small-World	*Yes*
Modularity Q-value	0.41

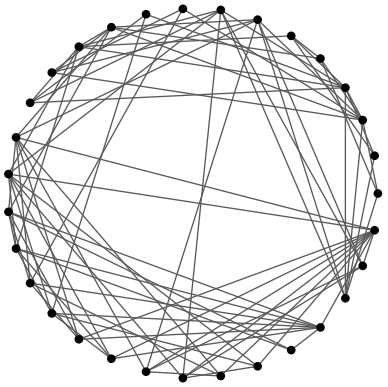

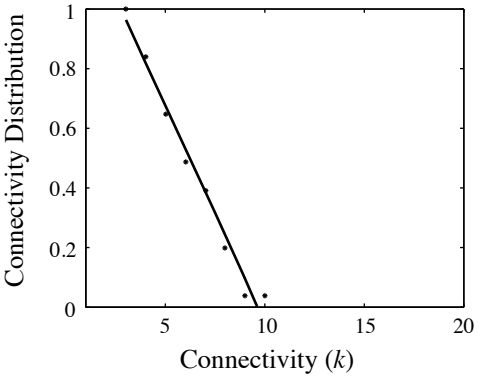

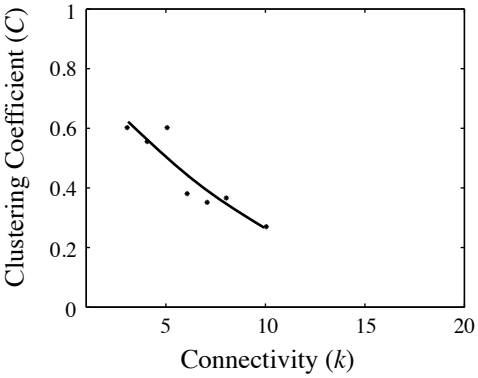

Best fit:

$P_{cum}(k) = -1.4 - 0.15\ k$

$\boldsymbol{r} = 0.99$ *(linear)*

$\boldsymbol{r} = 0.99$ *(binomial)*

$\boldsymbol{r} = 0.97$ *(exponential)*

$\boldsymbol{r} = 0.92$ *(power-law)*

Best fit:

$C(k) = 0.85 - 0.08\ k + 0.002\ k^2$

$\boldsymbol{r} = 0.92$ *(binomial)*

$\boldsymbol{r} = 0.92$ *(exponential)*

$\boldsymbol{r} = 0.92$ *(linear)*

$\boldsymbol{r} = 0.88$ *(power-law)*

Figure 8.75: Network analysis of the skull of *Phascolarctos cinereus*.

Phascolarctos cinereus (Mammalia: Diprotodontia)

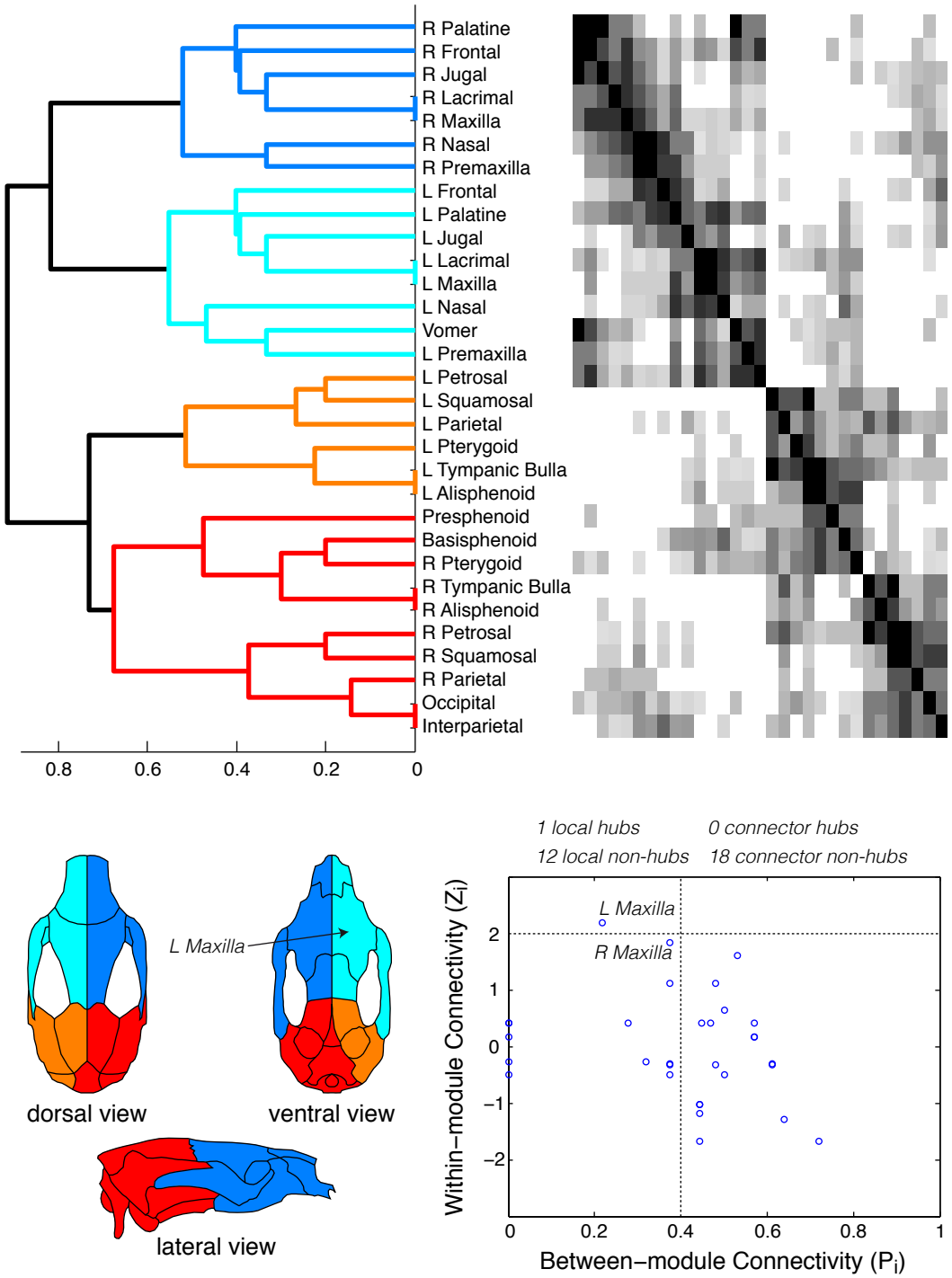

Figure 8.76: Connectivity modules in the skull of *Phascolarctos cinereus*.

Didelphis virginiana (Mammalia: Didelphimorpha)

Nodes	26
Links	66
Density	0.20
Clustering Coefficient	0.43
Shortest Path Length	2.14
Heterogeneity	0.39
Small-World	*Yes*
Modularity Q-value	0.40

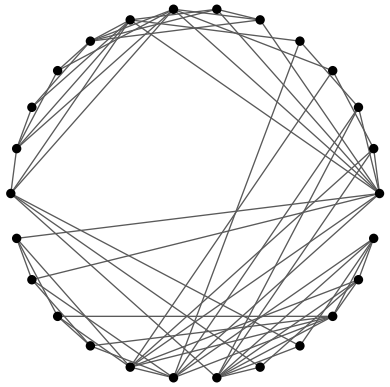

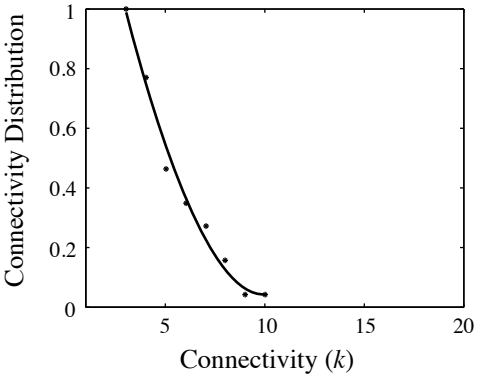

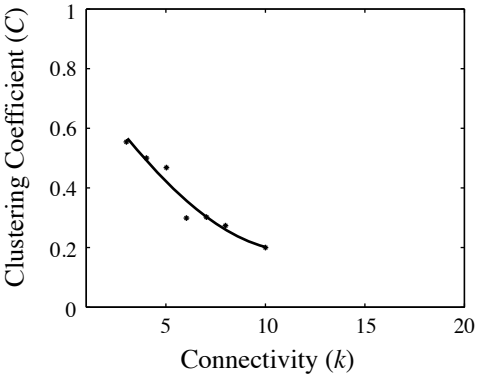

Best fit:

$P_{cum}(k) = 1.96 - 0.38\ k + 0.019\ k^2$

$\boldsymbol{r} = 0.99$ *(binomial)*

$\boldsymbol{r} = 0.99$ *(exponential)*

$\boldsymbol{r} = 0.97$ *(power-law)*

$\boldsymbol{r} = 0.96$ *(linear)*

Best fit:

$C(k) = 0.87 - 0.11\ k + 0.005\ k^2$

$\boldsymbol{r} = 0.97$ *(binomial)*

$\boldsymbol{r} = 0.97$ *(exponential)*

$\boldsymbol{r} = 0.95$ *(linear)*

$\boldsymbol{r} = 0.95$ *(power-law)*

Figure 8.77: Network analysis of the skull of *Didelphis virginiana*.

Didelphis virginiana (Mammalia: Didelphimorpha)

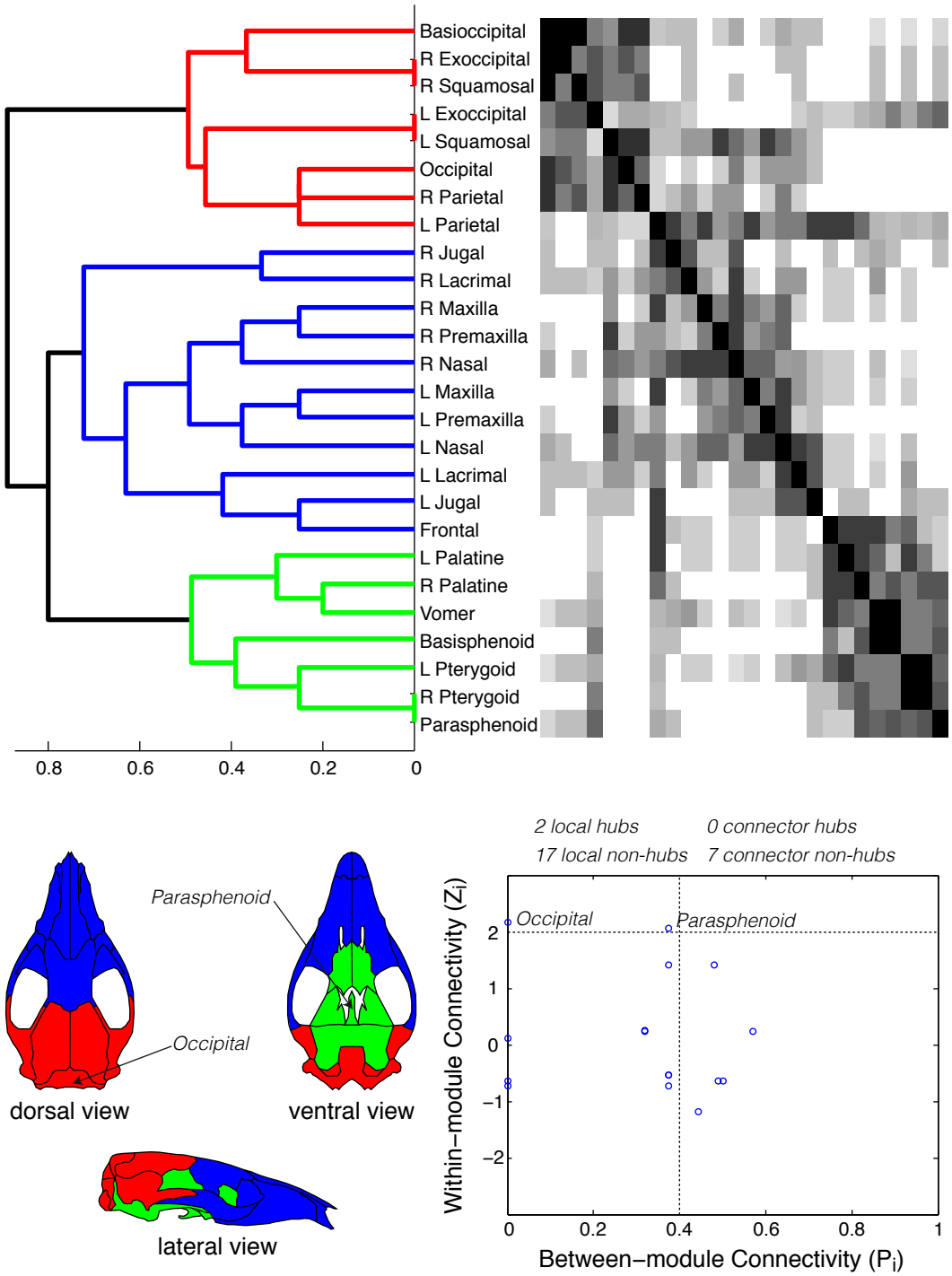

Figure 8.78: Connectivity modules in the skull of *Didelphis virginiana*.

Homo sapiens (Mammalia: Primates)

Nodes	21
Links	64
Density	0.30
Clustering Coefficient	0.63
Shortest Path Length	1.74
Heterogeneity	0.42
Small-World	*Yes*
Modularity Q-value	0.27

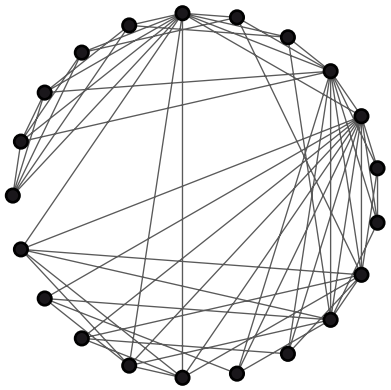

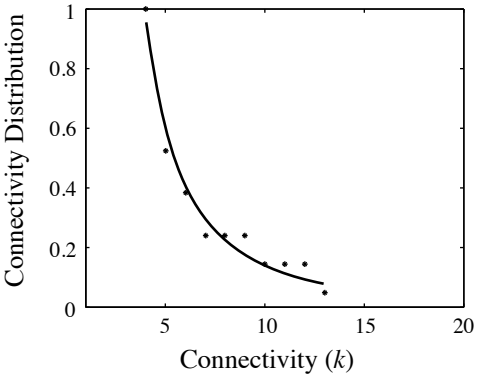

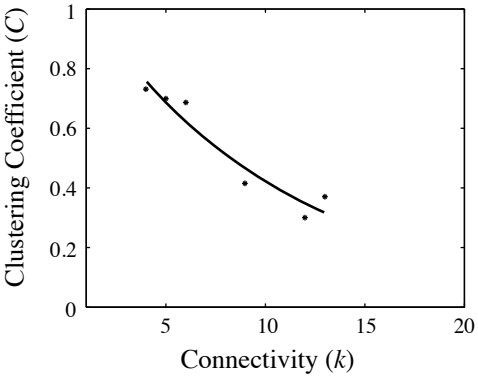

Best fit:

$P_{cum}(k) = 18.9 - k^{-2.15}$

r = 0.95 *(power-law)*

r = 0.93 *(exponential)*

r = 0.91 *(binomial)*

r = 0.84 *(linear)*

Best fit:

$C(k) = 1.79\ k^{-0.62}$

r = 0.82 *(exponential)*

r = 0.80 *(linear)*

r = 0.79 *(power-law)*

r = 0.79 *(binomial)*

Figure 8.79: Network analysis of the skull of *Homo sapiens*

Homo sapiens (Mammalia: Primates)

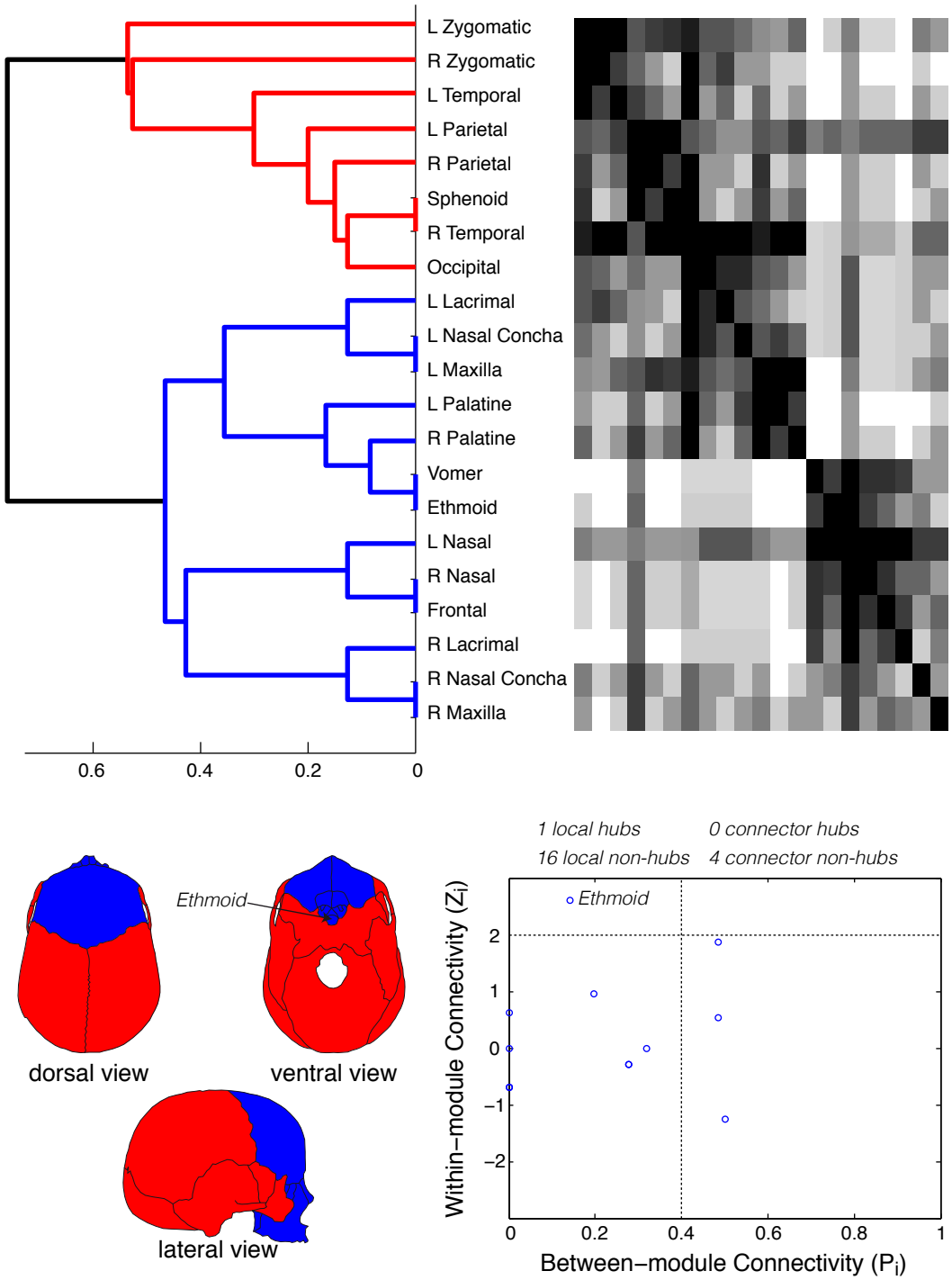

Figure 8.80: Connectivity modules in the skull of *Homo sapiens*.

Pteropus lylei (Mammalia: Chiroptera)

Nodes	21
Links	47
Density	0.22
Clustering Coefficient	0.53
Shortest Path Length	2.03
Heterogeneity	0.55
Small-World	*Yes*
Modularity Q-value	0.31

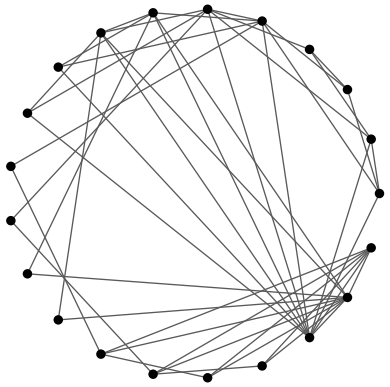

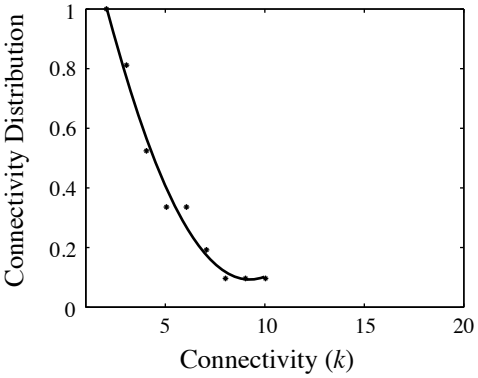

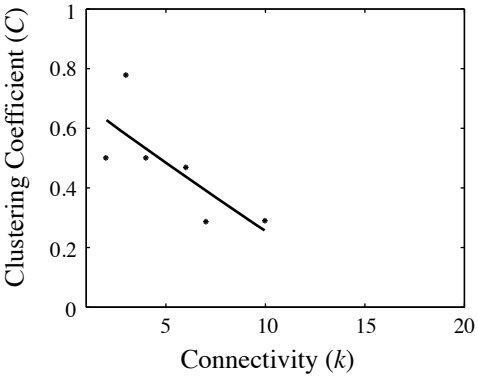

Best fit:

$P_{cum}(k) = 1.59 - 0.33\,k + 0.02\,k^2$

$\boldsymbol{r} = 0.99$ *(binomial)*

$\boldsymbol{r} = 0.99$ *(exponential)*

$\boldsymbol{r} = 0.96$ *(power-law)*

$\boldsymbol{r} = 0.93$ *(linear)*

Best fit:

$C(k) = 0.73 - 0.05\,k + 0.0005\,k^2$

$\boldsymbol{r} = 0.76$ *(binomial)*

$\boldsymbol{r} = 0.76$ *(linear)*

$\boldsymbol{r} = 0.74$ *(exponential)*

$\boldsymbol{r} = 0.65$ *(power-law)*

Figure 8.81: Network analysis of the skull of *Pteropus lylei*.

Pteropus lylei (Mammalia: Chiroptera)

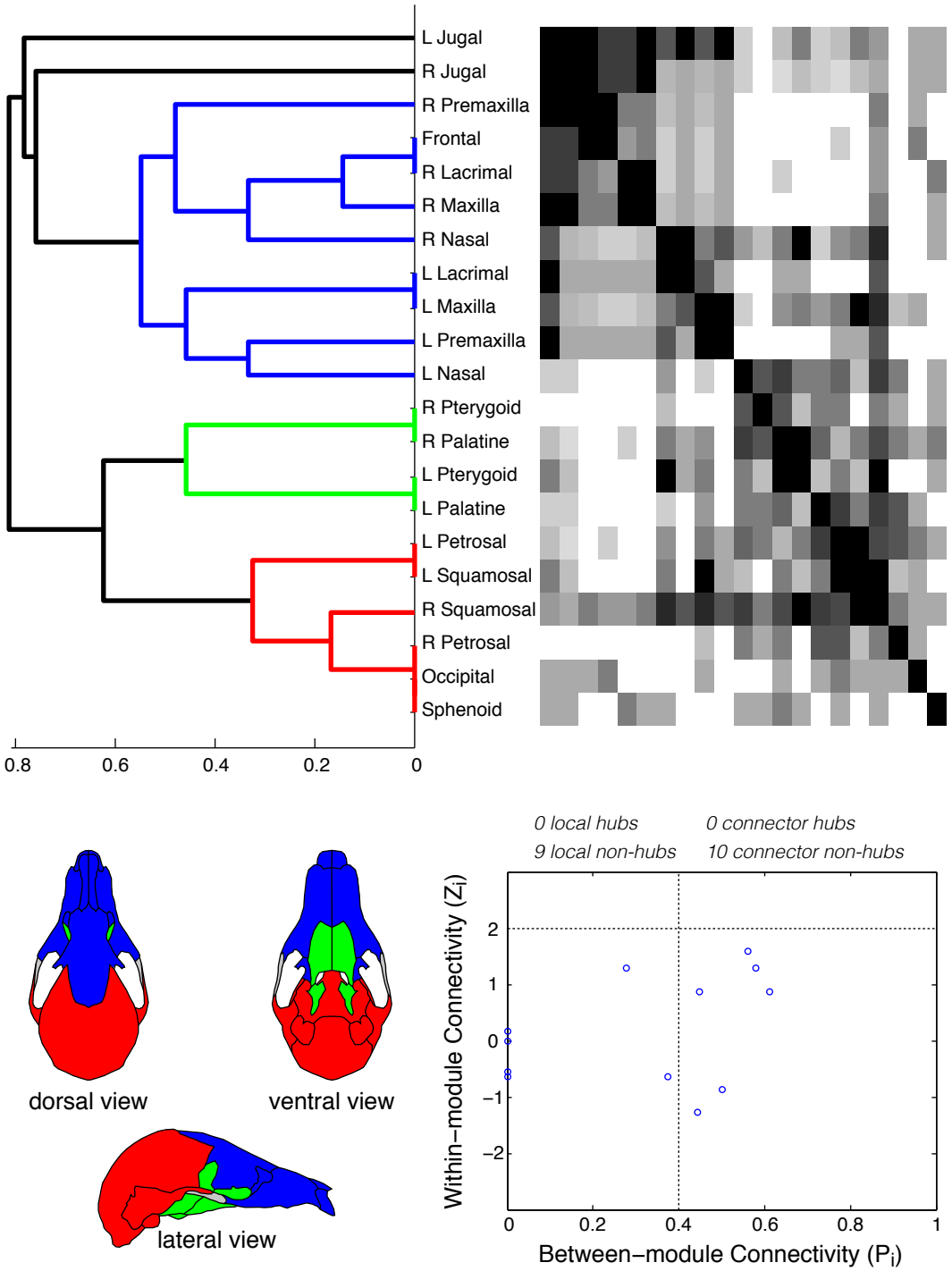

Figure 8.82: Connectivity modules in the skull of *Pteropus lylei*.

Mus musculus (Mammalia: Rodentia)

Nodes	28
Links	80
Density	0.21
Clustering Coefficient	0.46
Shortest Path Length	2.10
Heterogeneity	0.46
Small-World	*Yes*
Modularity Q-value	0.39

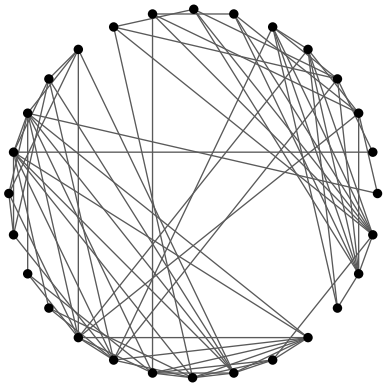

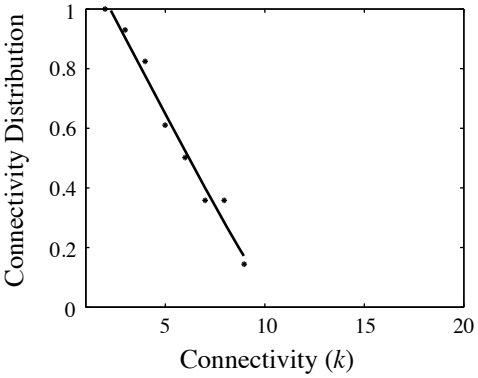

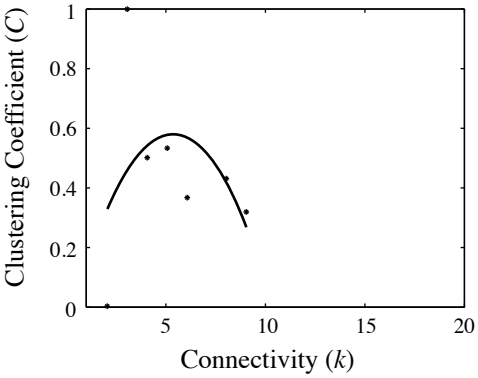

Best fit:

$P_{cum}(k) = 1.3 - 0.14\,k + 0.001\,k^2$

$\boldsymbol{r} = 0.99$ *(binomial)*

$\boldsymbol{r} = 0.99$ *(linear)*

$\boldsymbol{r} = 0.97$ *(exponential)*

$\boldsymbol{r} = 0.91$ *(power-law)*

Best fit:

$C(k) = -0.07 + 0.24\,k - 0.02\,k^2$

$\boldsymbol{r} = 0.41$ *(binomial)*

$\boldsymbol{r} = 0.10$ *(linear)*

$\boldsymbol{r} = 0.08$ *(exponential)*

$\boldsymbol{r} = 0.01$ *(power-law)*

Figure 8.83: Network analysis of the skull of *Mus musculus*.

Mus musculus (Mammalia: Rodentia)

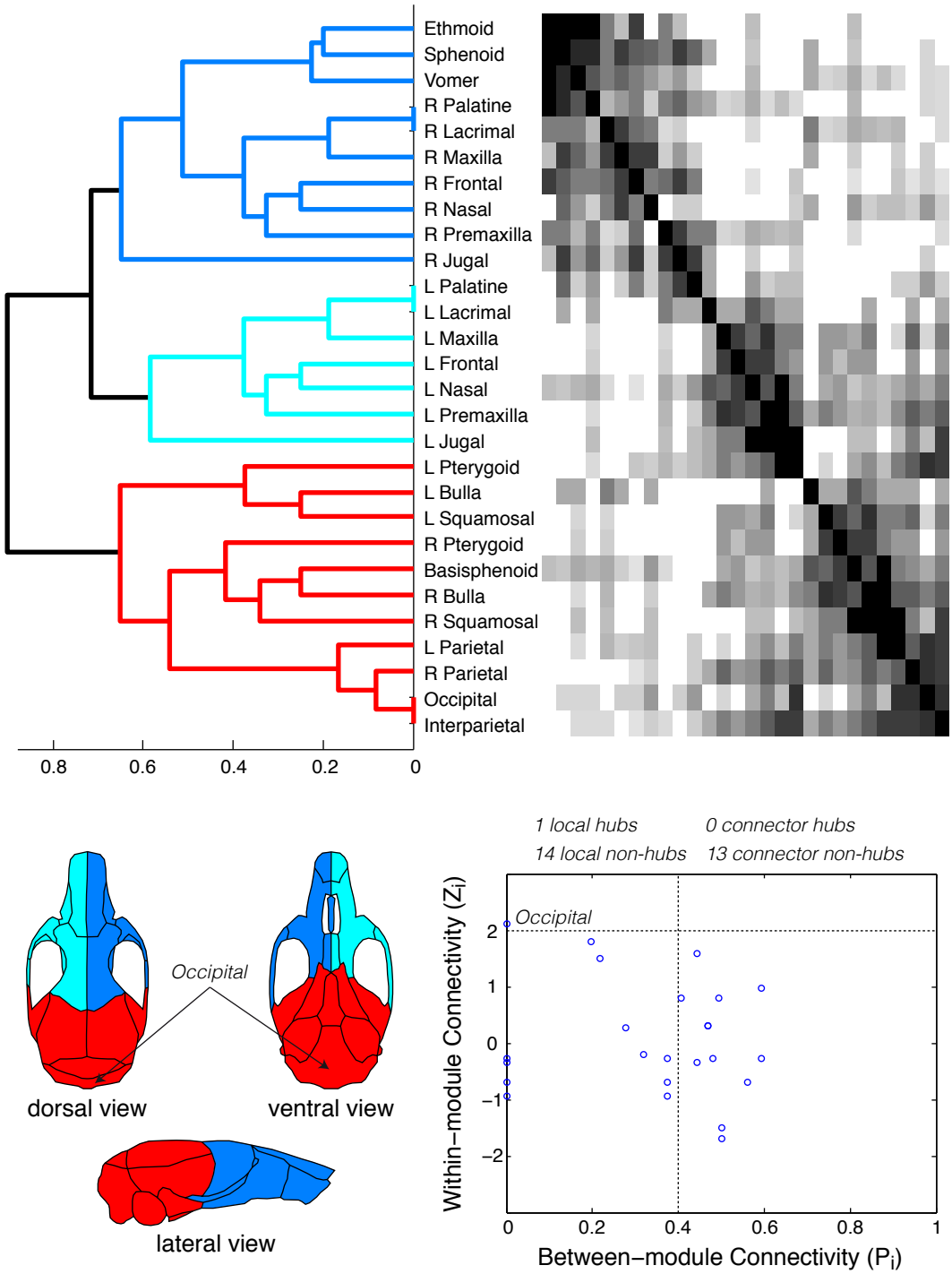

Figure 8.84: Connectivity modules in the skull of *Mus musculus*.

Canis lupus (Mammalia: Carnivora)

Nodes	29
Links	97
Density	0.22
Clustering Coefficient	0.60
Shortest Path Length	2.05
Heterogeneity	0.50
Small-World	*Yes*
Modularity Q-value	0.33

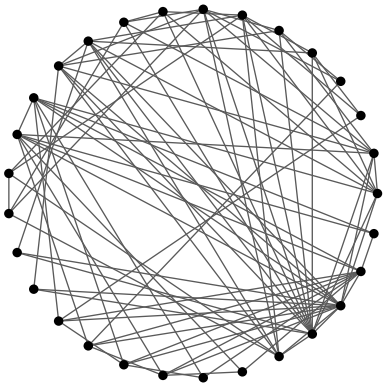

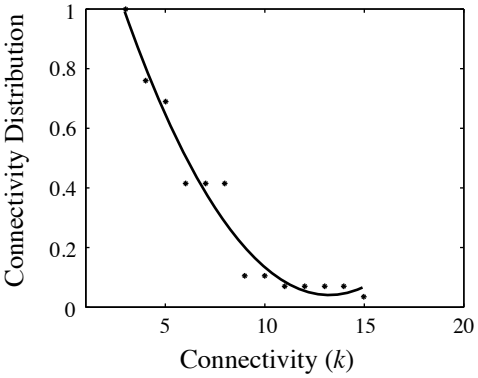

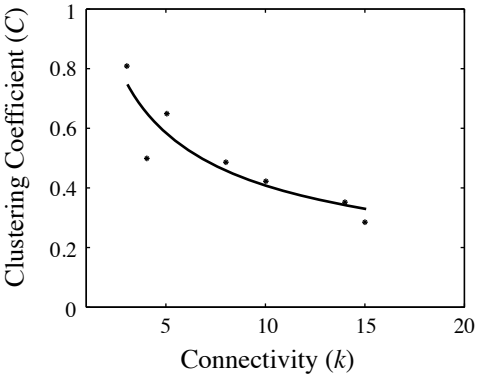

Best fit:

$P_{cum}(k) = 1.6 - 0.24\,k + 0.009\,k^{2}$

$\boldsymbol{r} = 0.98$ *(binomial)*

$\boldsymbol{r} = 0.98$ *(exponential)*

$\boldsymbol{r} = 0.95$ *(power-law)*

$\boldsymbol{r} = 0.91$ *(linear)*

Best fit:

$C(k) = 1.32\,k^{-0.5}$

$\boldsymbol{r} = 0.91$ *(power-law)*

$\boldsymbol{r} = 0.90$ *(exponential)*

$\boldsymbol{r} = 0.90$ *(binomial)*

$\boldsymbol{r} = 0.88$ *(linear)*

Figure 8.85: Network analysis of the skull of *Canis lupus*.

Canis lupus (Mammalia: Carnivora)

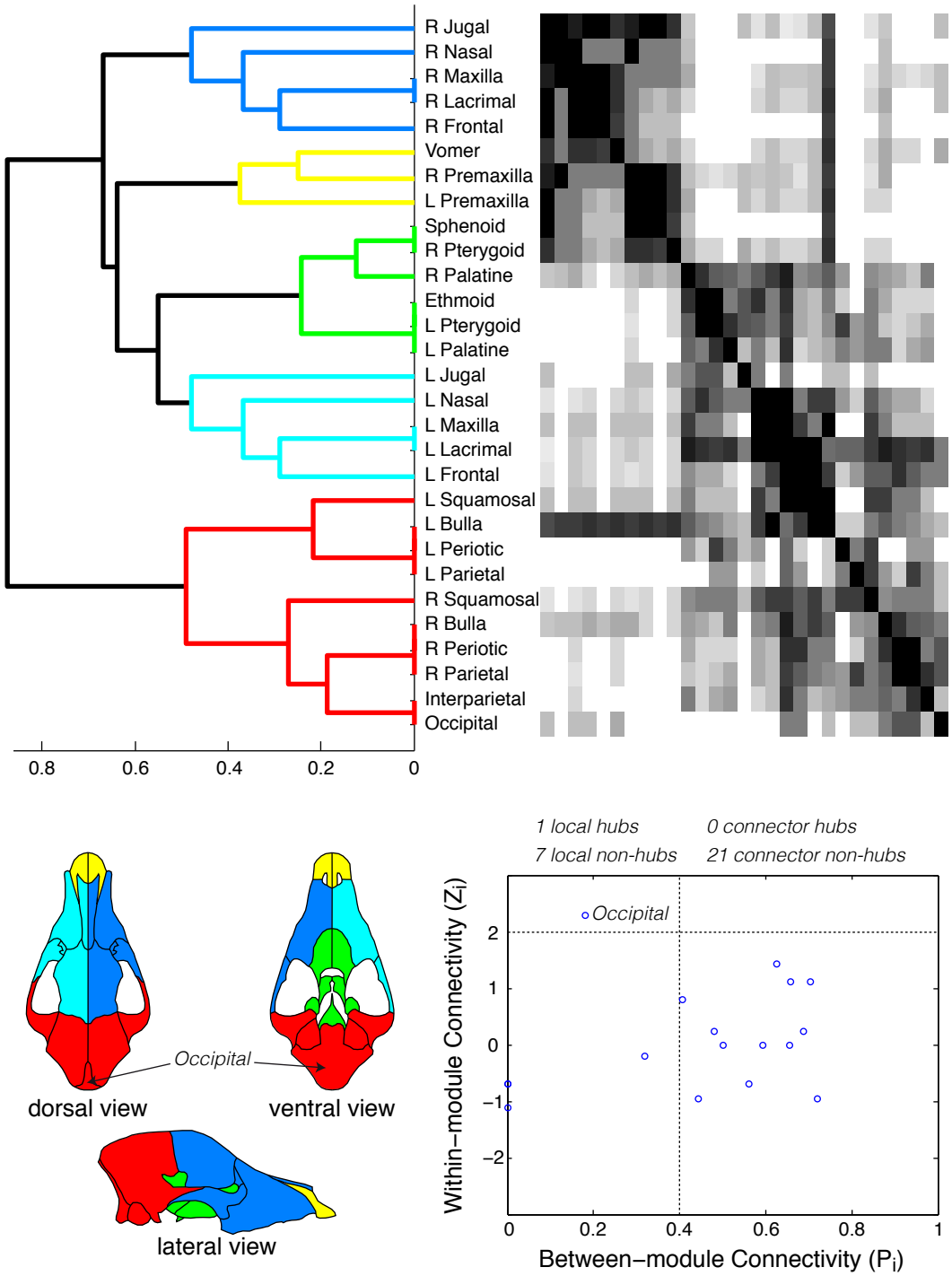

Figure 8.86: Connectivity modules in the skull of *Canis lupus*.

Tursiops truncatus (Mammalia: Cetacea)

Nodes	32
Links	99
Density	0.20
Clustering Coefficient	0.51
Shortest Path Length	2.19
Heterogeneity	0.49
Small-World	*Yes*
Modularity Q-value	0.32

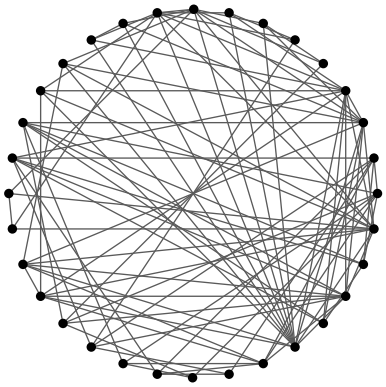

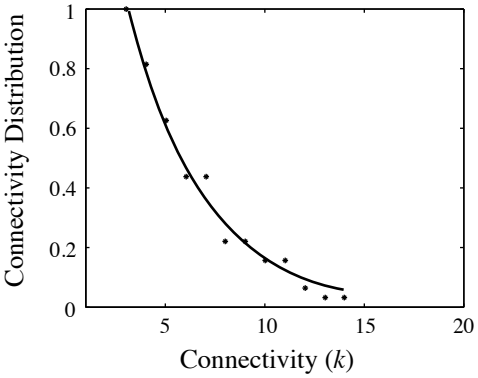

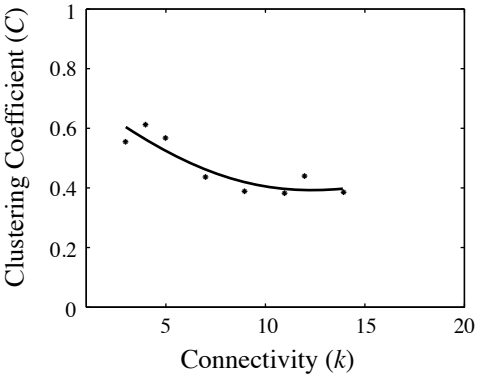

Best fit:

$P_{cum}(k) = 2.3\ e^{-0.26\,k}$

$\boldsymbol{r} = 0.99$ *(exponential)*

$\boldsymbol{r} = 0.99$ *(binomial)*

$\boldsymbol{r} = 0.96$ *(power-law)*

$\boldsymbol{r} = 0.94$ *(linear)*

Best fit:

$C(k) = 0.76 - 0.06\,k + 0.002\,k^2$

$\boldsymbol{r} = 0.90$ *(binomial)*

$\boldsymbol{r} = 0.88$ *(power-law)*

$\boldsymbol{r} = 0.87$ *(exponential)*

$\boldsymbol{r} = 0.85$ *(linear)*

Figure 8.87: Network analysis of the skull of *Tursiops truncatus*.

Tursiops truncatus (Mammalia: Cetacea)

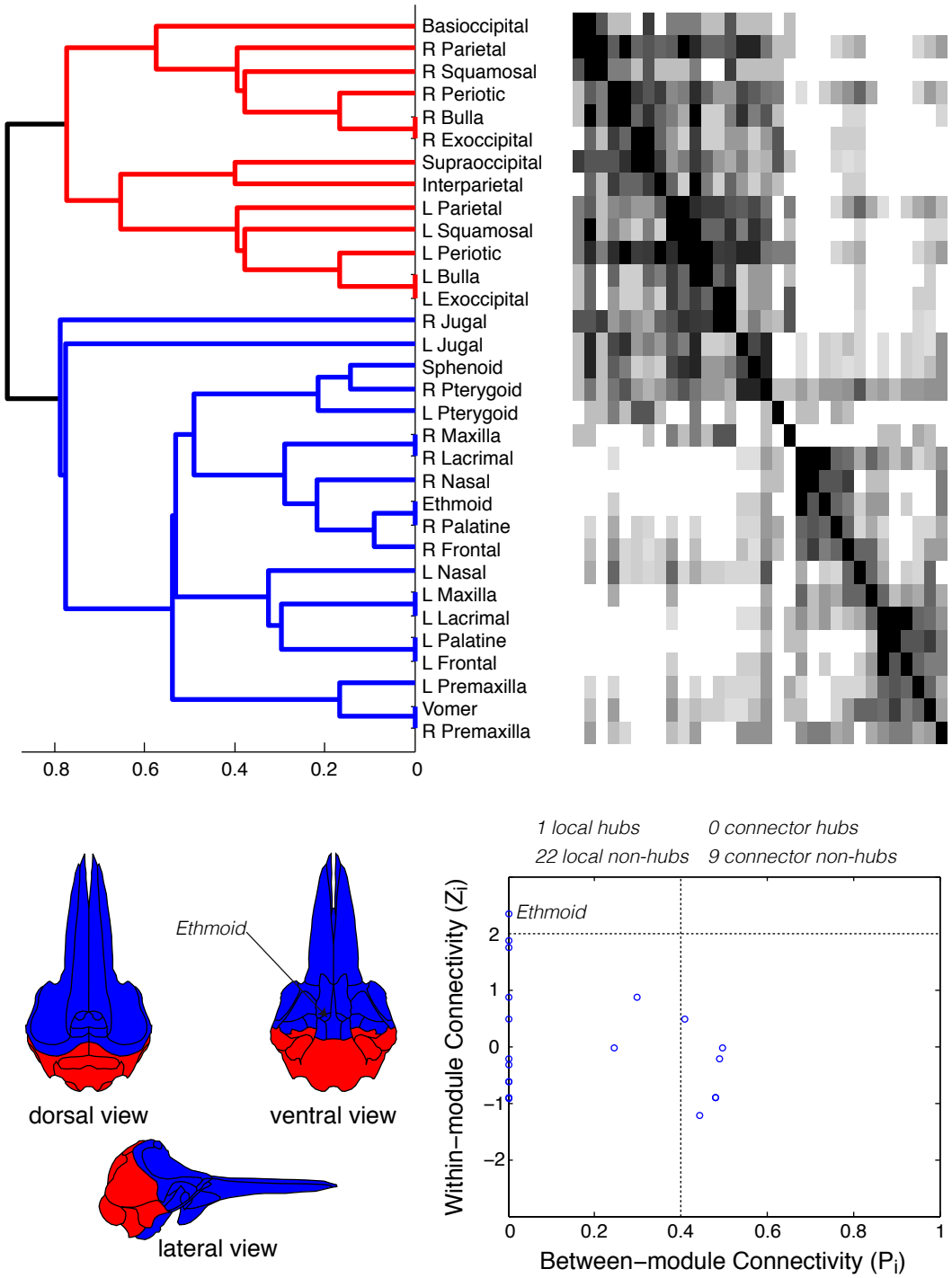

Figure 8.88: Connectivity modules in the skull of *Tursiops truncatus*.

9

Evolutionary Trends in the Tetrapod Skull

This chapter has been published as:

Esteve-Altava, B., Marugán-Lobón, J., Botella, H., and Rasskin-Gutman, D. (2013). Structural Constraints in the Evolution of the Tetrapod Skull Complexity: Williston's Law Revisited Using Network Models. *Evolutionary Biology*, 40:209–219.

Esteve-Altava, B., Marugán-Lobón, J., Botella, H., and Rasskin-Gutman, D. (2013). Random Loss and Selective Fusion of Bones Originate Morphological Complexity Trends in Tetrapod Skull Networks. *Evolutionary Biology*, doi 10.1007/s11692-013-9245-4.

9.1 Structural Constraints in the Evolution of the Tetrapod Skull Complexity: Williston's Law Revisited Using Network Models

Abstract — Ever since the appearance of the first land vertebrates, the skull has undergone a simplification by loss and fusion of bones in all major groups. This well-documented evolutionary trend is known as "Williston's Law". Both loss and fusion of bones are developmental events that generate, at large evolutionary scales, a net reduction in the number of skull bones. We reassess this evolutionary trend by analyzing the patterns of skull organization captured in network models in which nodes represent bones and links represent suture joints. We also evaluate the compensatory process of anisomerism (bone specialization) suggested to occur as a result of this reduction by quantifying the heterogeneity and the ratio of unpaired bones in real skulls. Finally, we perform simulations to test the differential effect of bone losses in skull evolution. We show that the reduction in bone number during evolution is accompanied by a trend toward a more complex organization, rather than toward simplification. Our results indicate that the processes by which bones are lost or fused during development are central to explain the evolution of the morphology of the skull. Our simulations suggest that the evolutionary trend of increasing morphological complexity can be caused as a result of a structural constraint, the systematic loss of less connected bones during development.

Introduction

One of the best-documented trends in vertebrate evolution is the reduction in number of skull bones, also known as Williston's law (Gregory, 1935, see also 1.2.1). For instance, the mammalian skull lacks bones that are characteristically present in ancestral forms, such as the pre- and post-frontals, postorbitals, and quadratojugals, and has also new bones that have appeared from the fusions of others, such as the occipital and the sphenoid (Sidor, 2001). Similar patterns of bone loss have been reported in other lineages, including snakes, lizards, birds, and turtles (Goodrich, 1958; Estes, 1961; Gaffney, 1979; Carroll, 1988; Rieppel, 1993; Laurin, 1996; Sereno, 1997; Kardong, 2005).

This reduction of the number of skull bones in vertebrates has been interpreted as an evolutionary trend toward simplification of skull architecture, associated to a decrease

in complexity (Hildebrand, 1988, Chapter 8). Sidor (2001) argued that this reduction is phylogenetically sound in synapsids, interpreting that simplified, compact skulls are selectively advantageous. At the same time, developmental constraints that facilitate the loss and fusion of bones, and others that prevent the formation of new ossification centers, favor this trend. A constraint that can cause an evolutionary reduction in number of skull bones is related to changes in the developmental timing of suture formation (Depew et al., 2008); both losses and fusions are caused by either lack of formation of ossification centers or premature closures of suture joints.

The difficulty of measuring and comparing morphological complexity in the skull across lineages hampers the evolutionary study of complexity at large-scales. According to Gregory (1934), a greater complexity of individual bones compensates for the reduction in number. Gregory called this compensation *"anisomerism"*, a trade-off process that generates more specialized, different anatomical elements, as a result of this reduction in number. The opposite process, *"polysomerism"*, accounts for a pattern of less specialized, similar anatomical elements (Gregory, 1934).

A simple and operative way to study this general trend in major groups of vertebrates is by defining skull complexity as a function of the number of bones (Sidor, 2001); however, this approach is limited (for a thorough discussion see McShea, 1991, 1996, 1998). In order to circumvent these limitations, we represent each vertebrate skull as a network of connected bones using network analysis to detect changes in their structural arrangement (Fig. 9.1). This method provides an operative framework for the early comparative anatomy ideas of Geoffroy Saint-Hilaire's principle of connections (Riedl, 1978; Le Guyader, 2003). Its output yields connectivity patterns among individual bones, within bone groups, as well as statistical signals of morphological complexity.

Recent analyses of complexity trends in many biological systems using network theory demonstrate that complexity can be quantified more accurately as a function of the relational properties of the system's components than as the number of elements (Sporns, 2002; Newman and Forgacs, 2005; Proulx et al., 2005; Newman et al., 2006; Mason and Verwoerd, 2007; Dunne et al., 2008a; Knight and Pinney, 2009). These methods can also be applied to the study of morphological complexity in anatomical systems (Rasskin-Gutman, 2003; Esteve-Altava et al., 2011). Here, morphological complexity is quantified as a function of the pattern of organization of the skull, in which bones and suture joints are modeled as the nodes and links of a network. Using this framework, we have reassessed Williston's Law in the tetrapod skull.

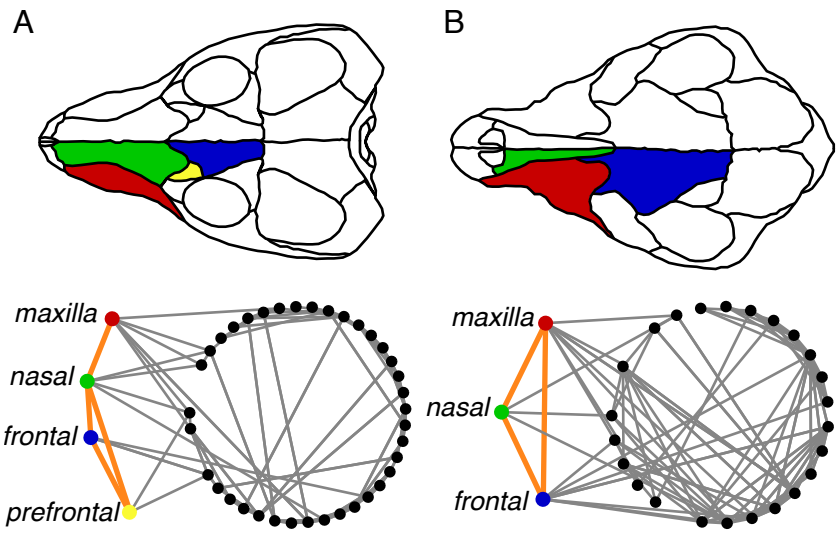

Figure 9.1: Example of how connectivity relationships among bones can change between evolutionary related species in a schematic skull representation of A) an extinct therapsid, *Thrinaxodon liorhinus*, and B) a modern mammal, *Canis lupus*. The left frontal, maxilla, nasal, and prefrontal have been highlighted with colors; *blue*, *red*, *green*, and *yellow*, respectively, to show changes in the local connectivity pattern as a result of prefrontal bone loss. A new connection appears between the frontal and the maxilla as a consequence of the prefrontal loss.

Morphological complexity was quantified with three different well-established network statistics: the density of connections, the characteristic path length ($\overline{L}$), and the cluster coefficient ($\overline{C}$). These statics have been used before to approach complexity in other biological systems, in different ways. For example, density has been used in ecological network models to analyze complex functional responses (Dunne et al., 2008a,b) We used density as a direct measure of complexity; the more connected a network, the more complex its organization. $\overline{L}$ is often used to estimate the speed of information flow between the nodes of a network associated to complex organizations (Xu et al., 2011). This flow depends on the nature of each type of network; for instance, the Internet transmits data, a food web transmits biomass, and the brain transmits electric impulses. For instance, in skull networks this flow could be equated to the diffusion of stress forces acting on skull bones (Moazen et al., 2009). Accordingly, we used $\overline{L}$ as an estimate of complexity in terms of efficiency for spreading biomechanical forces as well as molecular signals between skull bones. Finally, $\overline{C}$ measures the presence of loops of connections between

elements (triangular motifs), which promotes functional and structural correlations between connected parts as a result of the formation of clusters (Dorogovtsev and Mendes, 2003). We interpret the presence of cluster coordinate responses in varying traits as an indication of morphological integration and modularity (Olson and Miller, 1958; Chernoff and Magwene, 1999; Magwene, 2008); using $\overline{C}$ as an estimate of complexity as it relates to patterns of integration among skull bones. In summary, we have assessed changes in structural patterns in the tetrapod skull with three complementary qualities of morphological complexity captured by well-established network statistics: structural organization (density), functional efficiency ($\overline{L}$), and integration ($\overline{C}$).

The compensatory process of anisomerism proposed by Gregory (*op. cit.*) is far more complicated to capture than skull complexity by means of network statistics because its effects occur mainly at the level of bones, not across the entire skull. Gregory's basic definition of anisomerism refers to structural similarity among elements. In a network context, an easy way to estimate this similarity among bones is to compare the number of connections they have. Therefore, we quantified anisomerism as connectivity heterogeneity (H) according to Horvath and Dong (2008). In addition, we also estimated the relative number of unpaired bones (UBR) as a side-measure of anisomerism, for two reasons: (1) they appear in evolution from the fusion of two or more pre-existing bones, which is one of the proposed causes of Williston's law, and (2) they are among the most modified, specialized bones.

Here, we test whether the evolutionary trend toward reduction in number of skull bones simplifies the skull structure or rather makes it more morphologically complex. To do so, we first quantified skull complexity using network statistics. Then we tested if there is a correlation between the number of skull bones, morphological complexity, and anisomerism in a phylogenetic context. Finally, we analyzed different scenarios of bone number reduction: selective loss of most connected bones, selective loss of less connected bones, and random losses in order to check which scenario is more suitable to generate trends in complexity during evolution.

Materials & Methods

The materials and methods used to build and analyze skull networks, as well as the phylogenetic context, have been described in Chapters 4, 6, and 7. Here, I shall describe only the specific analysis performed for this publication.

Tests of Robustness

We studied the response of skull complexity to the loss of bones with a simulation that iteratively removed network nodes, measuring complexity after each node removal. This kind of simulation has been used to study network resilience to selective versus random deletions (Albert et al., 2000).

We performed node removal under three different likely evolutionary scenarios: (1) random loss of bones, (2) selective loss of highly connected bones, and (3) selective loss of poorly connected bones. In a scenario of random losses all bones can be lost with same probability. In selective loss scenarios there is a bias in favor of losing either highly connected or poorly connected bones (ties were solved at random). We simulated 10,000 iterations of sequential losses for each skull and scenario.

Results

Complexity and Anisomerism

The morphological complexity in the tetrapod skull showed a significant correlation with the number of bones: Negative in density and $\overline{C}$, and positive in $\overline{L}$ (Table 9.1). This indicates that the reduction in bone number correlates with an increase in complexity. Figure 9.2 shows scatter plots for density, $\overline{L}$, and $\overline{C}$ along with the estimations of circular, random, and Gabriel simulations. Considering the three statistics together, the organization of skull networks clearly differs from the three theoretical models.

Whereas H did not show a significant correlation with bone number reduction, UBR did it (Table 9.1). Thus, there is no evidence of increase in heterogeneity for all skull bones; in this respect skull networks do not differ from Gabriel networks (Fig. 9.3A). However, as predicted by the anisomerism hypothesis, if we consider only the relative amount of unpaired bones, the reduction in the number of bones occurs simultaneously with an increase in complexity and specialization of individual bones, (Fig. 9.3B). In other words, bone number reduction is linked to skull specialization as a result of the appearance of new unpaired bones, which occur from the fusion of ancestral paired ones.

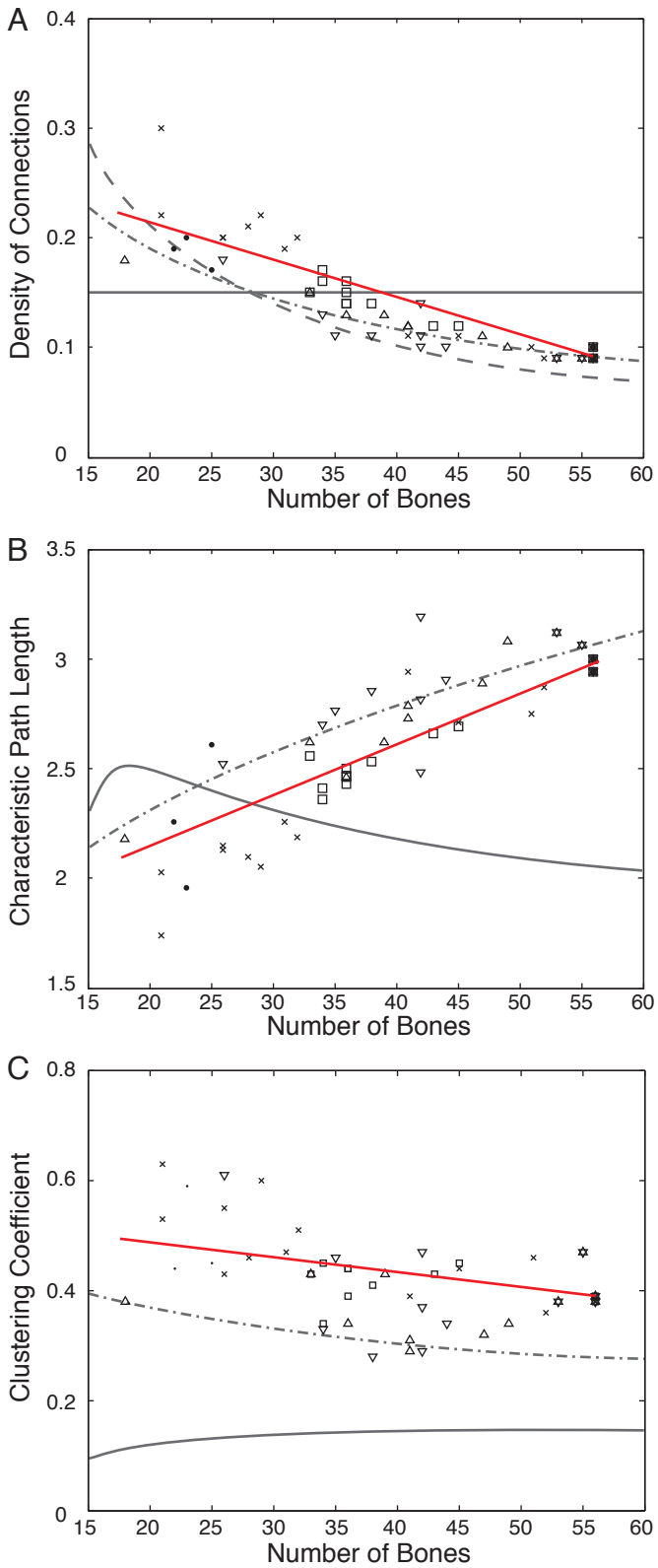

Figure 9.2: Correlation of bone number reduction with morphological complexity measured with different network statistics. *Red line* indicates regression slope, *gray lines* indicate the estimations for theoretical models: *solid*, Erdös, & Renyí random network; *dashed* regular circular network; *dot-dashed* Gabriel network. A) The density of connections shows a clear increasing trend as the bone number diminishes. In contrast, density does not vary with bone number in the random model. The circular and Gabriel model show a similar behavior than skull networks, but underestimate density. B) The characteristic path length shows a decreasing trend with bone number reduction. The random model has a completely different behavior, while the Gabriel model shows a similar decay but mostly overestimate $\overline{L}$. The circular model has $\overline{L}$ values out of range and is not shown here. C) The clustering coefficient shows a slightly increasing with bone number reduction. Both the random and the Gabriel models strongly underestimate $\overline{C}$ when comparing with real skull networks. The circular model has a constant $\overline{C}$ equal to 0 and it is not shown. Legend: *Crosses* for synapsids, *squares* for anapsids, *up-triangles* for archosaurs, *down-triangles* for lepidosaurs, and *dots* for amphibians.

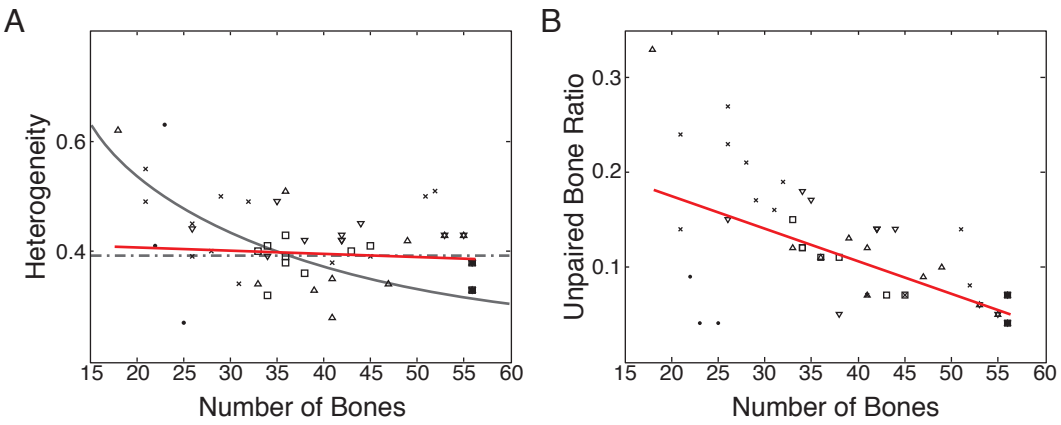

Figure 9.3: Relationship between bone number reduction and anisomerism. A) The heterogeneity of skull networks does not show correlation with bone number and behaves as the Gabriel model. In contrast, the random model shows an increase in H as the number of bones decrease. In the circular model H is constant. C) The relative number of unpaired bones is reduced as the number of bones increases. This suggests a relationship between fusion events and bone number. Legend and symbols as in Fig. 9.2.

Table 9.1: Pearson Product-Moment Correlation Coefficient for the five network statistics.

	Density	$\overline{L}$	$\overline{C}$	*H*	*UBH*
Pearson's r	-0.827	0.797	-0.302	-0.078	-0.558
p-value: 2-tailed	4.46^{-12}	9.8^{-11}	0.046	0.613	8.24^{-5}

Skull Robustness to Bone Losses

The robustness test yielded different results depending on the way we removed bones (Fig. 9.4). A sequential removal of bones at random did not cause a net change in density, $\overline{L}$, and $\overline{C}$. Only after removal of the 15% of bones there was a slight loss of complexity. In contrast, a selective removal of the most connected bones generated a rapid loss of complexity, while a selective removal of the less connected bones had the opposite effect; a slow increase of network complexity. This indicates that skull networks are robust to random losses, but fragile to selective losses of highly connected bones. Moreover, we found that a selective loss of poorly connected bones promoted an increase of complexity; density and $\overline{C}$ increase, and $\overline{L}$ decreases.

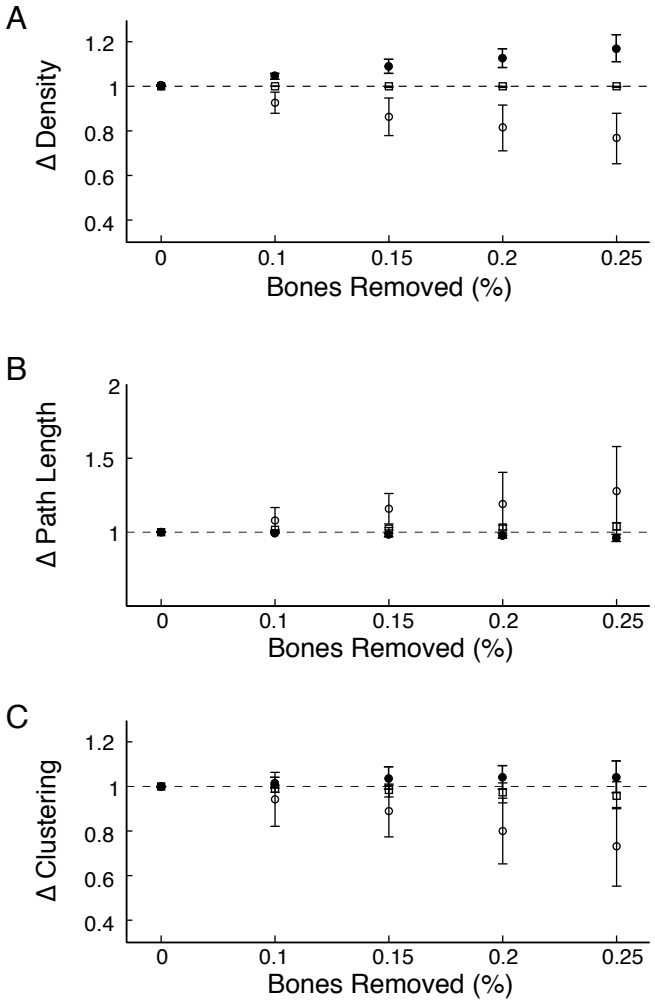

Figure 9.4: Simulation of skull network complexity response after bone losses. Bones were removed sequentially according to three different scenarios: random removal of bones, *squares*; selection of more connected bones, *circles*; and selection of less connected bones, *dots*. The three complexity parameters: A) density of connections, B) characteristic path length, and C) clustering coefficient shows the same behavior in each scenario. Skulls show a high robustness to losses of bones at random (complexity parameters barely change until more than the 15% of bones are lost). In contrast, skulls are very sensitive to connectivity-selective losses. The loss of a highly connected bone weakens skull structure and makes complexity measures drop. Accumulation of such losses eventually destroys the complexity of the network. On the other hand, the loss of a poorly connected bone increases skull complexity. Of the three scenarios, selective loss of poorly connected bones (along with fusions) is the only scenario that explains the observed evolutionary pattern.

Discussion

Largely inspired by Williston's work (1914), Gregory et al. (1935) showed that the vertebrate skull has undergone a general process of bone number reduction along with a functional specialization of each individual bone. This evolutionary trend was incorporated and accepted into general anatomical knowledge under the name of Williston's law. This law has been entrenched with the idea that the vertebrate skull has suffered an evolutionary simplification (Williams, 1966; Sidor, 2001) according to the classical assessment of morphological complexity as the number of distinct anatomical elements (Bonner, 1988; McShea, 1991; Valentine et al., 1994).

Our results indicate that there is an increase of morphological complexity in the tetrapod skull associated with the reduction in number of skull bones during its evolution. An evolutionary pattern of skull complexity increase is even clearer if we carry out pairwise comparison of basal and modern forms (see Supplementary Material), such as from *Seymouria* and *Ichthyostega* to all living species, from *Procolophon* and *Proganochelys* to modern turtles, from *Petrolacosaurus* and *Younginia* to archosaurs and lepidosaurs, or from basal synapsids to modern mammals. In all, there is a reduction in the number of bones that is correlated with a relative increase of the number of suture relations (density), an increase in the structural proximity of bones ($\overline{L}$), and proliferation of triangular motifs of integration ($\overline{C}$).

The behavior of complexity estimates might be a consequence of differential rates of losses and fusions during skull evolution. For instance, an over-fusion of bones, especially along the midline, generates redundant connectivity patterns. In basal synapsids the palate is composed of three paired elements (vomers, palatines, and maxillae); each one connects to its contralateral pair, as well as to the other bones of the same side, generating rectangular motifs. After the fusion of vomers, rectangular motifs lead to triangular motifs; hence, the new unpaired vomer connects to two bones already connected (paired palatines and maxillae), and $\overline{C}$ increases in the skull network.

On the other hand, it is known that the loss of bones provokes the reoccupation by other bones of the space left open (Girgis and Pritchard, 1958; Mabbutt and Kokich, 1979; Hall, 2005); thus, new connections can form within this space by bones that, otherwise, were not previously connected. Because of this mechanism, a reduction in the bone number increases the density of connections provoking that distant bones now get closer; in contrast to fusions, this does not generate more triangulations. Therefore, the way in which the connections of the skull are reorganized after losses and fusions is what causes

the observed pattern of complexity; which is different from that expected in theoretical models.

Morphological Complexity and Anisomerism

Originally proposed by Gregory (1934), anisomerism is the process that guides reduction in number of skull bones by controlling developmental growth rates akin to heterochrony. For Gregory, reduction in number and differentiation of parts was one and the same evolutionary and developmental process. We find no support for a relationship between the reduction of the number of bones and anisomerism (bone's individual complexity). This could be due to the difficulty of capturing anisomerism with a parameter (H) that does not describe individual bones.

However, the relative amount of unpaired bones does increase with bone number reduction suggesting that, indeed, there is an emergence of more specialized and differentiated bones after fusions, as predicted by the anisomerism hypothesis. This observation clearly stresses the relationship between fusion events during development and the evolutionary trend in skull bone number reduction (Aldridge et al., 2002; Richtsmeier et al., 2006).

Structural Constraints in Bone Loss and the Increase of Skull Complexity

The robustness simulation indicates that skull morphological complexity might vary after bone losses, according to the number of connections of each of the lost bones. This is a biased process; other things being equal, the loss of less connected bones will be more likely than the loss of highly connected ones, and indeed it is (Benton, 1990, p. 297). Moreover, losses of less connected bones cause a net increase of morphological complexity in the skull (density and $\overline{C}$ increase, and $\overline{L}$ decreases).

This prompts two conclusions: (1) that connectivity, indeed, matters, as daringly pointed out by Saint-Hilaire, and (2) that not all the bones are equally important in maintaining skull structure. Thus, the structural stability of the skull against externally driven (environmental) or inherited bone losses varies according to the connectivity of the affected bones. Therefore, highly connected bones might have a primary role in shaping the skull with a robust internal organization. The structure would tend to collapse if these bones are lost.

Less connected, small bones often develop from single ossification centers (Rice, 2008); and when these centers are lost, entire bones also disappear. These losses have minor effects upon skull architecture, because the compensatory growth of other bones can fill

the space of the lost bone (Hall, 2005). In contrast, more complex, specialized bones are seldom lost because they originated from fusion of several (sometimes many) centers of ossification (Koyabu et al., 2012), and would be hard to replace completely. The way most skull bones develop, by iterative fusion of ossification centers, would prevent the loss of complex, and more connected bones, whereas it would facilitate the loss of simple, less connected bones.

The observation that the developmental losses of less connected bones are responsible for this evolutionary trend in skull complexity emphasizes the relationship between connectivity of bones and their structural importance, or burden-rank (Riedl, 1978). The concept of burden was originally proposed as an organismic developmental constraint as a result of an increase in hierarchically nested constraints on traits during evolution (Schoch, 2010); more connections entail more developmental dependences with other bones. In this context, the concept of burden explains the relationship between structural robustness and connectivity and the evolutionary trend in skull morphological complexity.

Concluding Remarks

The reduction in the number of skull bones during vertebrate evolution has been interpreted as an evolutionary trend toward simplification as a consequence of selective advantages for more simplified, compact skulls. However, our results show that the reduction in bone number is not accompanied by a simplification of the skull; rather, there is an increase in the complexity of the connectivity patterns that organize the skull architecture as a consequence of how skull development buffer the harmful effects of bone losses and fusions. Our network simulations strongly suggest that a possible cause behind Williston's Law is a structural constraint by which less connected bones are more likely to be lost, shaping a general evolutionary trend toward higher skull complexity.

Supplementary Materials

We studied the evolution of the skull bone number and complexity estimates in our sample by a squared-change parsimony optimization (Maddison, 1991) on our calibrated phylogeny (see Fig. 9.2). Parsimony optimization renders estimation values for the root of the tree. The confidence intervals 95% (CI) for the root node values were generated using independent contrasts (Midford et al., 2003). To obtain the CI of internal nodes we rerooted the tree on each of the branches as described in Laurin (2004). This analysis was performed in Mesquite.

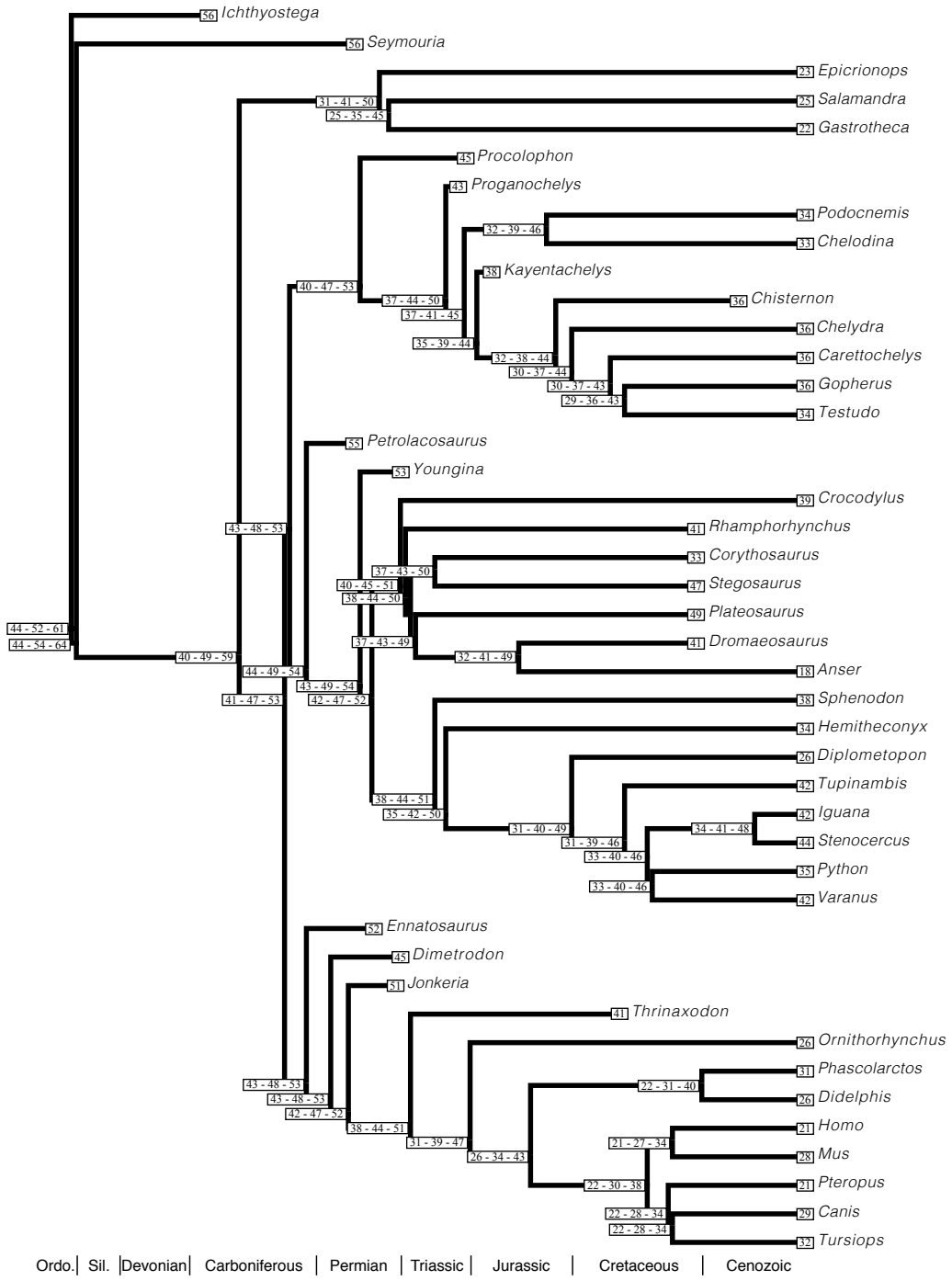

Figure 9.5: Parsimony optimization and CI 95% for the number of bones

Figure 9.6: Parsimony optimization and CI 95% for the density.

Figure 9.7: Parsimony optimization and CI 95% for the shortest path length.

Figure 9.8: Parsimony optimization and CI 95% for the clustering coefficient.

Figure 9.9: Parsimony optimization and CI 95% for the heterogeneity.

Figure 9.10: Parsimony optimization and CI 95% for the unpaired bone ratio.

9.2 Random Loss and Selective Fusion of Bones Originate Morphological Complexity Trends in Tetrapod Skull Networks

Abstract — The tetrapod skull has undergone a reduction in number of bones in all major lineages since the origin of vertebrates, an evolutionary trend known as Williston's Law. Using connectivity relations between bones as a proxy for morphological complexity we showed that this reduction in number of bones generated an evolutionary trend toward more complex skulls. This would imply that connectivity patterns among bones impose structural constraints on bone loss and fusion that increase bone burden due to the formation of new functional and developmental dependencies; thus, the higher the number of connections, the higher the burden. Here, we test this hypothesis by exploring plausible evolutionary scenarios based on selective vs. random processes of bone loss and fusion. To do this, we have built a computational model that reduces iteratively the number of bones by loss and fusion, starting from hypothetical ancestral skulls represented as Gabriel networks in which bones are nodes and suture connections are links. Simulation results indicate that losses and fusions of bones affect skull structure differently whether they target bones at random or selectively depending on the number of bone connections. Our findings support a mixed scenario for Williston's Law: the random loss of poorly connected bones and the selective fusion of the most connected ones. This evolutionary scenario offers a new explanation for the increase of morphological complexity in the tetrapod skull by reduction of bones during development.

Introduction

In the early 19$^{\text{th}}$ century, Étienne Geoffroy Saint-Hilaire proposed the principe des connexions as a methodological rule to study animal form (Geoffroy Saint-Hilaire, 1818). Other notable naturalists before Geoffroy, such as Pierre Belon and Johann Wolfgang Goethe, also made use of this principle as a way to recognize similarities, a tradition that goes back to Aristotle. However, Geoffroy was the first to establish connections as an operational criterion to identify morphological similarity among different anatomical parts by means of their structural relations to other parts, rather than by their shape and function. Thus,

Geoffroy's principle of connections formalized the intuitive notion of similarity then in vogue and opened up a new research program in pure morphology at the structural level (Appel, 1987; Le Guyader, 2003; Ochoa and Barahona, 2009; Nuño de la Rosa, 2012).

Several conceptual frameworks were later proposed for the use of connectivity relations in anatomical systems: Woodger's *structural correspondence*, Rashevsky's *bio-topological principle*, and Riedl's *diagrammatic morphotype* (see 2.2). However, they were too general to be systematically applied to study practical morphological problems. Another, more quantitative way to address connectivity relations in anatomical systems within a precise operational framework, using Network Theory, was also laid out (Rasskin-Gutman and Buscalioni, 2001; Rasskin-Gutman, 2003). We have argued elsewhere that patterns of bone sutures in the skull can also be characterized as networks, in which nodes represent bones and links represent suture connections. The analysis of these networks in tetrapod skulls might revealed evolutionary patterns in morphological complexity, integration, modularity, and phenotypic stability (Esteve-Altava et al., 2011).

The tetrapod skull has undergone many different lineage-specific morphological changes during its evolution; for example, enlargement and shortening of the rostrum in humans and porpoises (Lieberman, 1998; Galatius et al., 2010), miniaturization in lizards and amphibians (Rieppel, 1984; Trueb and Alberch, 1985; Laurin, 2004), and expansion of the cranial vault in birds (Marugán-Lobón and Buscalioni, 2003; Bhullar et al., 2012). In addition to these specific trends, a general pattern has occurred in all major lineages since the origin of the vertebrate skull: the reduction in number of skull bones (see Table 1.1). Williston (1914) first described this trend in his studies on Permian reptile skulls; later, Gregory (1935) generalized it to all tetrapods, suggesting that loss and fusion of bones were the mechanisms underlying the establishment of this evolutionary pattern. Gregory paid homage to Williston by naming this evolutionary trend Williston's Law (see 1.2.1).

The reduction in the number of elements, as it occurs in Williston's Law, has also been proposed as a general mechanism to retain highly complex and functional biological systems throughout evolution, *"complexity by subtraction"* (McShea and Hordijk, 2013); this notion of complexity uses a standard definition of morphological complexity as number of part types (McShea, 1996). Using this metrics, Sidor (2001) concluded that Williston's Law is an evolutionary trend toward skull simplification in synapsids. Our view on morphological complexity also includes number of bones (part types) as model parameters, but the focus is on measuring complexity as connectivity relations between the bones using a series of complementary network parameters: density of connections, characteristic path length, clustering coefficient, and heterogeneity (see 5.2). These parameters capture not

only the number of part types in the skull, but also their local and overall organization (i.e., their connectivity pattern).

Using this new morphological complexity metrics, we showed in 9.1 that this reduction in bone number generates an evolutionary trend toward more complex skulls. In addition, we concurred with Gregory about the importance of losses and fusions of bones as evolutionary mechanisms producing the diversity of extant and extinct skull forms. Moreover, the use of connectivity patterns to quantify morphological complexity suggested that the selective loss of poorly connected bones, alongside new unpaired bone formation by fusion, is responsible for this evolutionary trend. We concluded that the connectivity pattern among skull bones is a source of structural constraints on the loss and fusion of individual bones. Conversely, both mechanisms imposed new constraints on the modification of the connectivity pattern of the entire skull, for example, by increasing the number of connections of bones originated by fusions. The underlying developmental basis for this structural constraint is due to the increase in functional and developmental dependencies, which arises with the establishment of connections among bones (Esteve-Altava et al., 2013a, see also 5.2.2), an evolutionary concept known as developmental burden (Riedl, 1978). Other authors have also suggested similar constraint relationships in more general biological contexts, such as Wimsatt's generative entrenchment (Wimsatt, 1986). Since the number of connections of a given bone (i.e., dependencies) characterizes the amount of burden carried by that bone, we suggested in the previous section that the higher the burden the less likely the bone will be lost during evolution.

Here, we address this hypothesis by analyzing the effect of random and selective losses and fusions of bones. To do so, we have built a computational model of skull evolution that simulates Williston's Law-like evolutionary patterns, from hypothetical ancestral skulls. We have used Gabriel networks (Gabriel and Sokal, 1969, 1980) as a null model to analyze growth rules and constraints that might be involved in producing connectivity patterns during evolution. Then, we compared the complexity measures of the ancestral and derived simulated networks with those of empirical skull networks from all major tetrapod groups (see 6.2). Our aim is to explore selective vs. random processes of bone loss and fusion mechanisms as plausible evolutionary scenarios. We evaluate three different processes by which the computational model picks a specific bone to be lost or fused: (1) selection of the least connected (L), (2) selection of the most connected (M), and (3) random selection (R). The combination of these mechanisms produces nine different scenarios to be evaluated: LL, LM, LR, ML, MM, MR, RL, RM, RR, in which the first letter is for loss mechanism and the second for fusion mechanism. We also systematically evaluate a series of initial

conditions that constrain the model: (1) spatial boundary of the including space, (2) loss to fusion ratio, and (3) number of unpaired bones.

Materials & Methods

The computational model that simulates skull evolution has been described in 6.2.

A full parameter space exploration has been carried out after discretizing the three initial conditions: spatial boundary of the including space, lost to fusion ratio (*l:f*), and number of unpaired bones (Fig. 9.11). Four different initial spatial boundaries (i.e., 3D Euclidean space where bones are initially positioned) were used: cubic (1x1x1); and three different rectangular prisms, long (1x1x2), flat (2x1x2), and flat and long (2x1x4). The *l:f* ranges from 0 for only fusions to 1 for only losses, and it was sampled in intervals of 0.1. The initial number of bones was 30 paired bones (60 total) plus 1 to 7 unpaired bones. In total, 2,772 combinations of scenarios and initial conditions were evaluated by running 1,000 simulations for each combination.

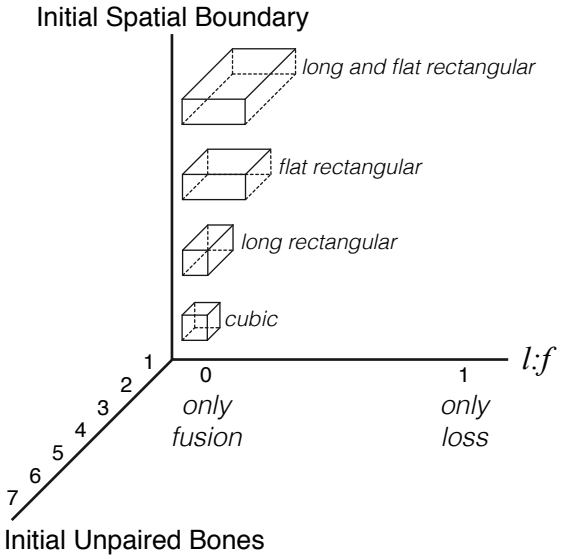

Figure 9.11: Parameter space definition for the three initial conditions: *l:f*, number of unpaired bones, and initial spatial boundary. The number of unpaired bones defines the total initial number of skull bones as 30 paired (60 total) plus 1 to 7 unpaired bones. For each scenario, we ran 1,000 simulations for each possible combination (2,772) in this parameter space.

Comparing Simulated and Real Skull Networks

The evolutionary path of each hypothetical ancestral skull network was traced in the simulation by quantifying four network parameters: density of connections, characteristic path length, clustering coefficient, and heterogeneity. These network parameters are complementary estimates of morphological complexity, in terms of how many connections are actually formed and the complexity of their arrangement pattern in the skull. These parameters are extensively explained in Chapter 4.

Each reduction step during a simulation run generates a new derived network with fewer bones, for which the above explained network parameters are quantified. After 1,000 simulations, we computed the mean and STD for each network parameter. Results are shown as error bar diagrams representing two STD from the mean value versus number of bones. In order to evaluate the fit of each scenario to the empirical data, we counted the number of real skull networks that fall within the error bars range for all four parameters at the same time. Each skull network that meets this requirement is considered as a data match. The number of data matches for the whole empirical sample (44 skull networks, see Chapter 8) defines how well each combination of scenario and set of initial conditions fits the data. Combinations with 36 or more data matches (more than 80% of fit) define what we call 'plausible scenarios'.

Results

After full exploration of the parameter space, results for each combination of scenario and set of initial conditions range from 0 to 38 data matches. Table 9.2 shows the number of plausible scenarios for all possible scenarios, itemized by the initial spatial boundary condition.

Results indicate that all scenarios with selection of the least connected bones to be lost or fused (LL, LM, LR, ML, and RL) have less than 80% of fit (i.e., fewer than 36 matches out of 44), which indicates that if these processes are present no plausible scenarios are generated. In contrast, when the mechanism for fusion of bones is the selection of the most connected ones, MM and RM, the greatest number of plausible scenarios occurs, 11 and 17, respectively.

Table 9.2: Number of plausible scenarios for all scenarios in each initial spatial boundary.

Loss	**Fusion**	**Abbrv**	**1x1x1**	**1x1x2**	**2x1x2**	**2x1x4**	**Total**
Least	Least	LL	0	0	0	0	0
Least	Most	LM	0	0	0	0	0
Least	Random	LR	0	0	0	0	0
Most	Least	ML	0	0	0	0	0
Most	Most	MM	7	0	4	0	11
Most	Random	MR	1	3	4	0	8
Random	Least	RL	0	0	0	0	0
Random	Most	RM	4	6	7	0	17
Random	Random	RR	0	0	5	0	5

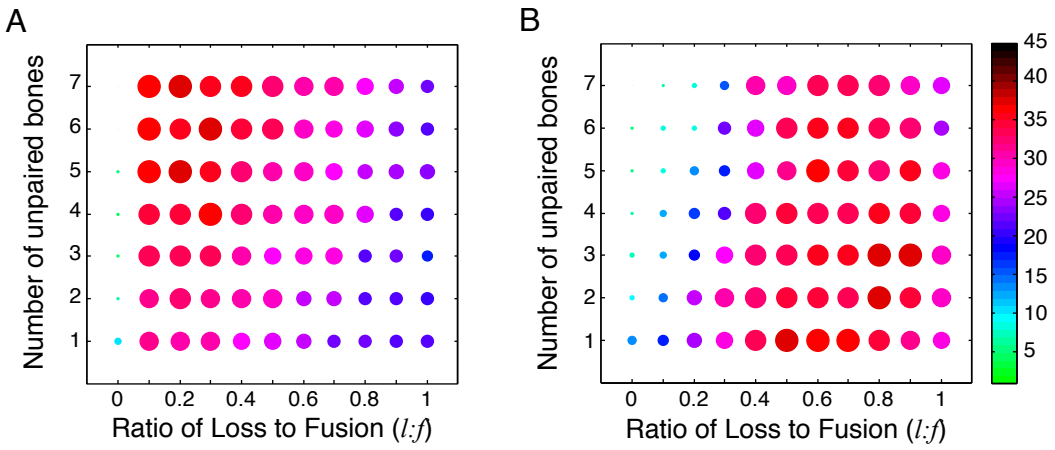

Figure 9.12: Number of matches (color bar) in the parameter space for scenarios cubic MM and flat rectangular RM. (A) The MM scenario shows higher matches for lower values of *l:f*, except for only fusions ($l{:}f = 0$), and higher number of unpaired bones. (B) The RM scenario shows higher matches for higher values of *l:f*, except for only losses ($l{:}f = 1$), and lower number of unpaired bones. The two scenarios have opposite optimal initial conditions due to differences in the process of picking bones to be lost (selection of most connected vs. random selection) and the shape of the initial spatial boundary (cubic vs. flat rectangular). Color bar and marker size indicate the number of matches.

Selective Scenarios

For the MM scenarios the best initial spatial boundary is the cubic one, with 7 plausible scenarios. Figure 9.12A shows how this highly selective scenario varies in number of matches according to *l:f* and initial number of unpaired bones. Higher numbers of matches occur between $l{:}f = 0.4$ (40% loss, 60% fusion) and $l{:}f = 0.1$ (10% loss, 90% fusion), and an initial number of unpaired bones between 4 and 7.

Mixed Scenarios

For the RM scenarios the best initial spatial boundary is the flat rectangular one, with 7 plausible scenarios. Figure 9.12B shows how this mixed scenario varies in number of matches according to the *l:f* and initial number of unpaired bones. Higher numbers of matches occur between $l{:}f = 0.5$ (50% loss, 50% fusion) and $l{:}f = 0.9$ (90% loss, 10% fusion), and an initial number of unpaired bones between 1 and 5.

Within the RM scenarios, the best overall plausible scenario occurs for the following conditions: $l{:}f = 0.7$ (70% loss, 30% fusion), 2 initial unpaired bones, and a cubic spatial boundary, which shows the highest number of matches, 38. Figure 9.13 plots all empirical skull networks on the average values of each network parameter estimated for 1,000 simulations.

Discussion

We have shown that complexity in connectivity patterns among skull bones (i.e, number of connections and their organization) increases in every evolutionary scenario of bone number reduction by loss and fusion of bones. This increase in morphological complexity varies in a wide range below and above the actual increase that we have measured previously (see 9.1). Thus, how each scenario fits our empirical sample depends on which processes have been involved, selective or random, as well as the fine-tuning of the initial conditions of the model: spatial boundary of the including space, loss to fusion ratio, and number of unpaired bones. The main finding in this study is that Williston's Law is a trend guided by a structural constraint: the random loss of poorly connected bones and the selective fusion of the most connected ones. This evolutionary scenario highlights the importance of bone reduction mechanisms to explain morphological complexity (see McShea and Hordijk, 2013, for a general discussion of *"complexity by subtraction"*).

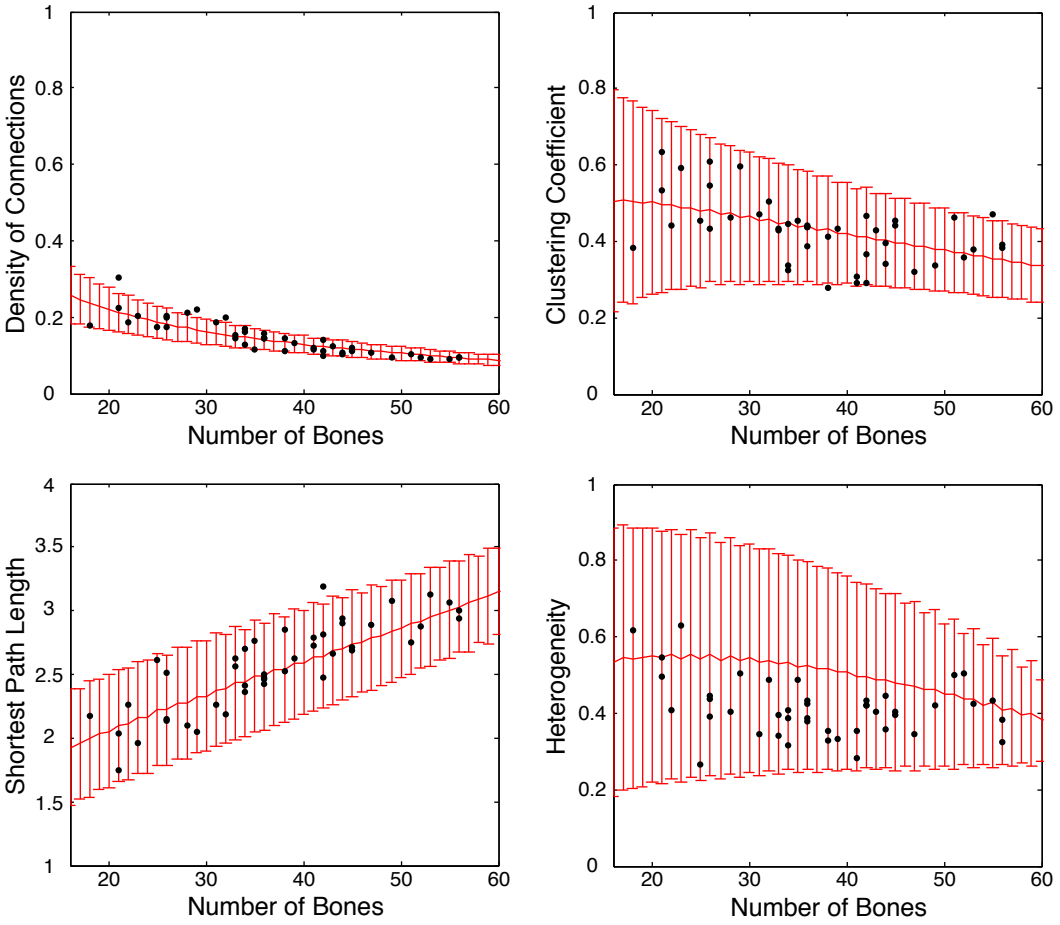

Figure 9.13: Data matches (38; 86%) of the best overall plausible scenario for the four network parameters used to evaluate the fit of the model: density of connections, characteristic path length, clustering coefficient, and heterogeneity. Red line indicates average values of 1,000 iterations and error bars represent 2 STD.

Our results further indicate that neither the selective loss nor the selective fusion of the least connected bones can fully explain the evolution of morphological complexity in Williston's Law. In all these scenarios (LL, LM, LR, ML, and RL) new connections appear among bones, over-increasing the complexity of the simulated skull networks; thus, no plausible generated scenarios can account for Williston's Law under these circumstances. In contrast, two scenarios involving the selective fusion of the most connected bones produce a higher number of plausible scenarios: one with selective loss of the most connected

bones (MM) and one with random bone loss (RM). Hereafter, we refer to these two types of plausible scenarios as 'selective' and 'mixed' scenarios, respectively.

In selective scenarios, loss and fusion of bones have opposite effects. The loss of the most connected bones reduces complexity because, on average, more connections are lost than re-wired among neighboring bones. On the other hand, fusion of the most connected bones increases morphological complexity because the new fused bone ends up being hyper-connected after inheriting the connections of all the bones involved in the fusion event. In these scenarios, both mechanisms are balanced for low values of *l:f*, that is, loss is less frequent than fusion (40% loss or less, 60% fusion or more). A higher frequency of fusion events buffers the decrease of complexity due to losses, and also produces some plausible scenarios with good fits to empirical data. However, the prevalence of this selective scenario would suggest that fusions have been more frequent than losses during the evolution of the skull, but mixed scenarios suggest a different story.

In mixed scenarios, loss of bones occurs at random. However, a random pick does not mean that all bones are lost with equal probability whether they are highly or poorly connected. This is because, as in empirical skull networks (see Chapter 8), simulated Gabriel networks have right-skewed distributions of connections, such as binomial decay, uniform decay, exponential decay, and power-law (see 6.1.7). This indicates that most bones have fewer connections than the average, while a few bones have most of the network connections. As a consequence, poorly connected bones are more easily picked than highly connected ones, even when this is done at random. In mixed scenarios, loss of bones also increases morphological complexity. Here, the range of *l:f* that produces the highest number of data matches (shown in Fig. 9.12B) is biased toward more proportion of losses than fusions (50% loss or more, 50% fusion or less). Furthermore, the best overall plausible scenario simulated is a mixed scenario with $l{:}f = 0.7$ (70% loss, 30% fusion). As Table 1.1 shows, the number of lost bones compiled from mainstream literature is slightly higher than the number of fused bones in tetrapods. However, to determine if a bone has been lost rather than fused in the fossil record is very difficult. Nevertheless, the proportion of bone loss and fusion in the literature seems to better support mixed scenarios than selective ones (i.e., slightly more loss than fusion of bones). It is worth noting that for both, selective and mixed scenarios, the most extreme ratios of loss to fusion events (i.e., only loss or only fusion) show a significant decrease in number of data matches; this suggest that, whatever the scenario, both losses and fusions mechanisms are necessary to evolve complex skull networks.

The optimal initial spatial boundary is also different for selective and mixed scenarios. A cubic boundary is preferred in selective scenarios, while a long rectangular boundary is preferred in mixed scenarios. However, this result has much to do with the Gabriel rule that we used to build theoretical ancestral skull networks. Gabriel networks capture an important developmental constraint: the impossibility of creating a suture contact between distant bones. This is not due to the physical distance between ossification centers, but rather to the presence of obstacles between them: cavities, openings, organs, as well as other bones. Thus, in spaces in which one or more axes are more prevalent, such as in flat (2x1x2) and long and flat (2x1x4) prisms, the Gabriel rule imposes too strong constraints on connectivity (Gabriel and Sokal, 1980). For instance, positioning bones along a very long axis will prevent most of the connections between them, since many bones will fall within the intersection sphere of others. As a consequence, those spaces that are more uniform in the three body axes, such as the cubic (1x1x1) and the long rectangular (1x1x2), are the least restrictive of all spatial boundaries; the latter being the optimal in mixed scenarios. Furthermore, the flat rectangular boundary resembles more the shape of the skull in basal tetrapods, such as *Acanthostega*, *Ichthyostega* or *Seymouria*.

The initial number of unpaired bones also shows different optimal values for each scenario. In selective scenarios, this number ranges from 4 to 7, which is above the estimated average values for the reconstructed last common ancestor using parsimony optimization (see Fig. 9.10). In mixed scenarios, there is a preference for lower numbers of unpaired bones, from 1 to 5, that is, below the average for the reconstructed last common ancestor. Furthermore, the best overall plausible scenario simulated is a mixed scenario with 2 initial unpaired bones, which is what is found in some basal tetrapods, such as Seymouria baylorensis (Laurin, 1996) or in basal bony fishes (Claeson et al., 2007). Thus, the preference for a low number of unpaired bones further reinforces the plausibility of mixed scenarios.

In addition, the plausibility of mixed scenarios is further supported by a series of arguments. The loss of poorly connected bones, rather than of the most connected ones, has a sound biological explanation due to the many developmental and functional roles of suture connections as sites of bone growth (Rice, 2008, see also 1.1.2), cranial bone movements (Jaslow, 1990), and strain sinks (Rafferty et al., 2003). Thus, bones with a high number of connections carry a higher developmental burden within the skull structure than poorly connected ones do. As a consequence, highly connected bones tend to be preserved during evolution, while the loss of poorly connected ones is less constrained, as is predicted given their lower burden (Riedl, 1978; Schoch, 2010; Esteve-Altava et al.,

2013c,a). Finally, the higher the number of suture connections, the higher the chance of undergoing a fusion event of bones, explaining the preference for fusions of the most connected ones.

Concluding Remarks

Computational models based on networks, like the one presented here, demonstrate their usefulness in unveiling plausible mechanisms underlying evolutionary trends such as Williston's Law. These models offer the opportunity to reproduce structural constraints and processes that might have taken place during skull evolution. Here, we have used a computational model to assess the likelihood of some bones, and not others, to be lost or fused according to their number of connections, as well as the initial conditions that facilitated these two mechanisms.

Our findings support a mixed scenario for Williston's Law: the random loss of poorly connected bones and the selective fusion of the most connected ones. Specifically, the model suggests the following optimal evolutionary conditions: (1) an initial spatial boundary unconstrained and uniform in the three body axes, (2) a low number of initial unpaired bones, and (3), on average, bone losses should be slightly higher than bone fusions. These conditions seem to be optimal to facilitate the evolution of the tetrapod skull in which the reduction in number of bones promotes an increase in morphological complexity.

10

Network Modularity in the Tetrapod Skull

10.1 Evolutionary Patterns in Skull Network Modularity

Abstract – The organization of connectivity patterns in tetrapod skulls is small-world, a type of organization between randomness and regularity that promotes the formation of connectivity modules. Here, modularity has been analyzed at a pure structural level using network tools. Connectivity modules have been defined as highly connected groups of bones and identified using an agglomerative hierarchical method. This analysis reveals three types of modules: bilateral, specular, and asymmetric specular. *Bilateral modules* group together bones from the left and right sides in the same module. *Specular modules* group bones of only one side, left or right; for each specular module there is a contralateral module that groups the same bones but from the other side. *Asymmetric specular modules* group paired bones from only one side (as in specular modules), but they also include one or more unpaired bones; this makes these modules asymmetric in relation to their contralateral specular modules. A series of generalizations can be inferred from the comparative analysis of connectivity modules in tetrapod skulls. (1) Bilateral modules occur more frequently around highly connected unpaired bones, which is common in posterior and palatal regions of the skull. (2) Specular modules occur when there are not unpaired bones in a region, or, if there are, they do not have enough connections to integrate both sides; when this happens, these unpaired bones are grouped with one of the specular modules and form an asymmetric specular module. (3) Left and right specular modules tend to have symmetric organizations in their hierarchical grouping of their bones. (4) Most bones (74%) divide their connections into different modules; among them, the 60% act as connectors (50% of the total number of bones). (5) The hierarchical formation of modules tend to follow an order in the process of grouping bones, following the three body axes: antereoposterior, left-right, and dorsoventral. No other common organization patterns of connectivity modules have been found.

Introduction

Morphological modules arise by the combination of different morphogenetic processes such as genetic regulatory networks, developmental constraints, and epigenetic factors (Santagati and Rijli, 2003; Martínez-Abadías et al., 2009; Percival and Richtsmeier, 2011). As a

consequence, a harmonious functioning structure is built at genetic, developmental, phenotypic, and evolutionary scales. Current morphological sciences are concerned with the role that integration and modularity play in the organization and evolution of organismal forms (Klingenberg, 2010). Since integration brings about the notion of correlation between traits (Olson and Miller, 1958), morphometric tools and statistics have been considered to be the most adequate tools with which to study skull morphological integration (Roth and Mercer, 2000). Conceptually, integration and modularity are strongly linked concepts; so much so that modules are defined as groups of elements more integrated between them than to other groups (Schlosser and Wagner, 2004; Callebaut and Rasskin-Gutman, 2005; Wagner et al., 2007). However, defining boundaries between morphological modules with morphometric tools has remained a challenge because (1) in different studies morphometric proxies are operationally different (i.e., different landmarks), (2) the targets of study are different (i.e., different species or experimental models), and (3) the precise definition of modules depends on very specific criteria (Klingenberg, 2008; Martínez-Abadías et al., 2012).

Different criteria can identify different classes of modules in the skull: functional modules group bones that interact to perform a specific function; genetic modules group bones controlled by the same genetic regulatory network; developmental modules group bones under control of the same genetic and epigenetic factors in development and morphogenesis; variational modules group bones with coordinated changes in shape and size; and finally, evolutionary modules group bones with evolutionary continuity following some of the previous criteria. Furthermore, for some criteria bones are not the structural units that compose modules; thus, for the same bone, some parts belong to one module, while other parts belong to another module. For instance, the frontal bone in humans using a functional criterion is in part facial in part neurocranial (Martínez-Abadías et al., 2012). These difficulties increase when one approaches modularity and integration from an evolutionary perspective due to the lack of a unified operational framework suitable to broader scales; i.e. comparing skulls from distant-related species, anatomies from different biological kingdoms, or even systems up or down the morphological scale.

At a connectivity level, we use a structural criterion to identify morphological modules: the organization of connections between bones (see 3.4). In this context, a connectivity module is defined as a highly connected group of bones. In addition, this approach allows to identify hierarchical organization when nodes within modules tend to group in highly clustered sub-modules or blocks. In modular, hierarchical networks, the participation of each bone in the organization of modules can be characterized as a function of their

connectivity within and between modules, thus, defining structural-connectivity roles (see 5.2). Some bones are keystones that hold together all the bones in a module by having their high number of connections within the module (*local hubs*), while some other bones are also highly connected but their connections are shared between modules (*connector hubs*). Finally, most bones are scarcely connected both within and between modules (*local* and *connector non-hubs*). Here, I discuss the result of the modularity analysis for each skull network. I paid special attention to the relationship between (1) unpaired bones, (2) their role as hub and/or connector, and (3) their participation in the formation of connectivity modules.

Material & Methods

The grouping method used to analyze modularity in skull networks has been described in Chapter 4. This method is based on a definition of connectivity module as a group of bones more connected to bones within the group than to other bones outside the group. To identify such groups, an agglomerative hierarchical cluster analysis was carried out using the topological overlap between bones as the measure of similarity between their connectivity patterns (i.e., number and correspondence of neighbors). Finally, ZP spaces have been analyzed for each skull network, for which the relative amount of local hubs, connector hubs, local non-hubs, and connector non-hubs has been calculated (see 4.1.2 and 5.2.2).

Results & Discussion

The results reveal three types of connectivity modules: bilateral, specular, and asymmetric specular. *Bilateral modules* group together bones from the left and right sides in the same module. *Specular modules* group bones of only one side, left or right; for each specular module there is a contralateral module that groups the same bones from the other side. *Asymmetric specular modules* group paired bones from only one side (as in specular modules), but they also include one or more unpaired bones; this make these modules asymmetric in relation to their contralateral specular modules. Since the grouping method used do not set any a priori preference on which bones are grouped, all three types of module structures are possible. These categories differentiate skull regions with enough connectivity integration to group both sides and the strength of unpaired bones to do so.

Stem Tetrapoda

The skull of stem tetrapods (Figs. 8.2 and 8.4) has many paired bones and a few unpaired bones. In general, unpaired bones are grouped only in bilateral modules, except the internasal in *Ichthyostega*. In regions free of unpaired bones, paired bones are grouped in specular modules; usually, paired bones in these specular modules can also act as local hubs. While connector hubs are absent in both skulls, connector non-hubs represent the 48% of bones in *Ichthyostega* and the 34% in *Seymouria*.

Modern Amphibia

Modern amphibians (Figs. 8.6, 8.8, and 8.10) have only a few number of unpaired bones (although some are massive in size), which originated by fusion of paired and unpaired bones in the midline. Fusions are more common in the posterior palatal and vault regions of the skull. However, these massive unpaired bones do not always have enough connections to integrate bones of both sides in one bilateral module (e.g., the *os basale* in *Epicrionops* or the parasphenoid in *Salamandra* and *Gastrotheca*); as a consequence, bones are grouped in asymmetric specular modules. In addition, these modern amphibians lack hub bones; thus, all their unpaired bones act as connector non-hubs, while most paired bones act as connector non-hubs.

Anapsida

Anapsids (Figs. 8.12, 8.14, 8.16, 8.18, 8.20, 8.22, 8.24, 8.26, 8.28, and 8.30) have four or five modules, which can be bilateral, specular or asymmetric specular. In general, each specular module shows the same hierarchical structure of cluster formation within the dendrogram; this similar internal structure between specular modules is only slightly modified in some asymmetric specular modules with a few number of unpaired bones (e.g., in left and right posterior modules in *Carettochelys*). In basal anapsids (*Procolophon* and *Proganochelys*), in which vomers are paired, rostral specular modules show two internal blocks: one groups dorsal rostral bones and the other ventral palatal ones. In contrast, in some bilateral modules, internal blocks group left and right bones separately. Moreover, the formation of bilateral modules is not exclusively related to the presence of unpaired bones; thus, some bilateral modules are formed without any unpaired bone, such as modules grouping roof bones in *Podocnemis*, *Chisternon*, and *Carettochelys*. In modern anapsids, the fusion of the paired vomers is related to the formation of bilateral modules grouping rostral or palatal bones. In general, all these modern forms show rostro-palatal

modules well integrated by a local hub bone, being the most common the unpaired vomer. In contrast, in basal forms, vomers are paired bones that never act as hubs. Both paired and unpaired bones can act as local hubs in bilateral modules. However, unpaired bones act often as connector or local non-hubs. They do so in bilateral modules, as well as, sporadically, in asymmetric specular modules. In addition, one-side paired bones can act also as hubs in some asymmetric specular modules. The relative number of connector bones is less variable than in amphibians, ranging from 40% to 65%.

Basal Diapsida

Basal diapsids (Figs. 8.32 and 8.34) have a high number of modules; all types are present, bilateral, specular, and asymmetric specular. Left and right specular modules have the same hierarchical structure of cluster formation within the dendrogram. Usually, unpaired bones are integrated in bilateral modules, but it can be otherwise, for example, the right lateral-roof module in *Petrolacosaurus* (in orange). In addition, there are also bilateral modules without unpaired bones: the anterior-roof module in *Petrolacosaurus* (in purple) and the palatal module in *Youngina* (in green). Thus, unpaired bones can act as local hubs, local non-hubs, and connector non-hubs.

Archosaurs

The skulls of Archosaurs (Figs. 8.36, 8.38, 8.40, 8.42, 8.44, 8.46, and 8.48) have the three types of connectivity modules, as in basal diapsids; the presence of asymmetric specular modules is quite common. Left and right specular modules have the same hierarchical structure of cluster formation within the dendrogram. Even asymmetric specular modules show a high degree of symmetry in their hierarchical structure of clusters. In general, the rostral region is free of unpaired bones and bones are grouped in specular modules; however, the unusual presence of unpaired bones is related to the formation of bilateral modules (e.g., *Rhamphorhynchus* and *Anser*). In addition, the presence of hub bones is not generalized in archosaurian skulls; usually, paired bones grouped in specular modules act as local hubs, such as maxillas in *Crocodylus*, parietals in *Stegosaurus*, and squamosals in *Dromaeosaurus*. In general, unpaired bone act as local or connector non-hubs either in bilateral (mostly) or in specular asymmetric modules. As in anapsids and basal diapsids, unpaired bones acting as local non-hubs appear mostly in bilateral modules; as an exception, the basisphenoid and basioccipital in *Rhamphorhynchus* act as connector non-hubs. In fact, connector non-hubs represent around 50% of all archosaurian skulls bones.

Birds are a special case within archosaurs because of an over-fusion of bones that produces massive unpaired bones, which affects the formation of connectivity modules. Thus, some uncommon connectivity modules group one-side paired bone and a massive unpaired one, namely: the left jugal-basisphenoid module (in yellow) and the right jugal-mesethmoid module (in orange). In addition, the skull of *Anser* lacks hub bones; thus, unpaired bones act either as local or connector non-hubs in bilateral or asymmetric specular modules.

Lepidosaurs

Lepidosaurian skulls (Figs. 8.50, 8.52, 8.54, 8.56, 8.58, 8.60, 8.62, and 8.64) show the three types of connectivity modules (often in the same skull). In general, left and right specular modules have the same hierarchical structure of cluster formation within the dendrogram. Modules in one side are usually subdivided into roof and rostral blocks, such as in the rostral (blue) module in *Sphenodon*. In asymmetric specular modules, unpaired bones often do not break totally the internal symmetry between left and right modules; instead, unpaired bones are grouped in semi-independent small blocks (e.g., in *Tupinambis*, the unpaired premaxilla form a block with left septomaxilla and vomer). As it occurs in some diapsids and amphibians, over-fusion of bones produce massive unpaired bones, which are grouped within bilateral modules (e.g., in *Diplometopon* and *Varanus*). These massive unpaired bones, such as occipital, frontal, or parietal rarely make hub bones (e.g., in *Diplometopon*). In addition, the presence of hub bones varies from none to three; all hubs are local hubs except the unpaired premaxilla in *Iguana*, which act as a connector hub in a bilateral module. Maxillas in specular modules, as well as the unpaired premaxilla and parietal in bilateral modules, are the most common local hubs.

Basal Synapsida

The skulls of basal synapsids (Figs. 8.66, 8.68, 8.70, and 8.72) have the three types of connectivity modules. Specular modules show the same hierarchical structure of clusters between left and right modules, even if unpaired bones are present and asymmetric specular modules are formed; as in diapsids, these rarely change blocks within the modules. Internal hierarchical symmetry occurs also within bilateral modules, for example, in the roof module in *Jonkeria* (in purple). Similarities in cluster formation between specular modules, as well as within bilateral modules are clearer than in diapsids and anapsids. As in basal turtles, the vomer is a paired bone; thus, the most anterior region of the skull is

often free of unpaired bones unless the premaxilla is also an unpaired bone as in *Jonkeria*. As a consequence, most anterior regions of the skull (face and palate) have specular modules, while most posterior regions (roof and vault) have asymmetric specular or bilateral modules. For instance, the presence of an unpaired vomer in *Thrinaxodon* is related to the formation of a bilateral module grouping palatal bones; in contrast, other unpaired bones, such as the parietal in the roof, fail to group together left and right side bones. The formation of a bilateral vault module is a common feature in all basal synapsids, while *Enannatosaurus*, *Jonkeria*, and *Thrinaxodon* show also a similar palatal bilateral module. In addition, all skulls have hubs; left and right maxillas act often as local hubs in both contralateral specular modules. This role is taken by the nasals in *Thrinaxodon*. The skull of *Ennatosaurus* is the only one with a connector hub, the supraoccipital, which integrate the vault bilateral module. In general, unpaired bones act as local non-hubs, while between 41% and 67% of the total number of bones for the four skulls act as connector non-hubs.

Modern Mammals

Modern mammals (Figs. 8.74, 8.76, 8.78, 8.80, 8.82, 8.84, 8.86, and 8.88) show the three types of modules, although this is the only group in which some skulls have only bilateral modules. In general, modules delimit well three skull regions: rostrum, vault, and palate. Palatal bones can be grouped either in a module or in a block within a bigger bilateral module.

The hierarchical clustering in mammalian skulls shows a clear pattern of grouping according to the position of bones along the three main body axes. According to this pattern, bones that are grouped first in the hierarchy are dorsal or ventral bones from the same side, which form small blocks. Then, these ventral and dorsal blocks of the same side group together, in turn, to form bigger blocks. Finally, left and right contralateral blocks group into an anterior or posterior bilateral module. This extreme case, in which two-module partition is the best one, only occurs in *Homo* and *Tursiops*; however, more relaxed examples can be observed in the dendrogram of all tetrapod skull networks. When anterior bones are grouped into two asymmetric specular modules (e.g., in *Ornithorhynchus*, *Phascolarctos*, and *Mus*), they have a similar hierarchical structure of cluster formation within the dendrogram. In all modules, unpaired bones are grouped in the dendrogram after paired bones, which are grouped first; thus, the inclusion of unpaired bones do not have consequences in the formation of bilateral or asymmetric specular modules. However,

not all connectivity modules show this internal hierarchical organization; instead, some modules group bones sequentially, for example, in the cranial module of *Homo* (in red).

The only case in which some bones have been left out of any connectivity module occurs also in mammals. In *Pteropus*, the hierarchical clustering groups jugal bones as the last elements of the dendrogram, just before the first branching point of the dendrogram (viewed from left to right). However, the optimal modularity Q-value is for the five-modules partition: (1) cranial (in red), (2) palatal (in green), (3) rostral (in blue), (4) right jugal, and (5) left jugal. The morphological reason is that both jugals are poorly connected to the skull (two connections) as well as to any particular module (one connection to each one); as a consequence of this weak integration, jugals are grouped late in the dendrogram. When integration between and within modules is evaluated in each branching point, having two modules (rostral plus jugals and palatal plus cranial) produces a less integrated structure than letting jugals out of any module (because they take more integration than they add). A clear counter-example is found in *Tursiops*. Here, jugal bones are also grouped late in the clustering process; however, they add more integration to the rostral module in *Tursiops* than they do in *Pteropus*, because they contact with two connections instead of only one to this module. Since a two-module partition is the optimal one, jugals are grouped within the rostral module.

The presence of hub bones is common in mammals. Most local hubs are also unpaired bones such as the ethmoid and the occipital; the only connector hub is the right maxilla in *Ornithorhynchus*. In general, most unpaired bones act as connector non-hubs, although the relative number of connector non-hubs is similar to that of other groups (between 46% and 72%) except for those skulls that show a clear two-module partition, one anterior and one posterior, which have an unusual small number of connector bones (19% in *Homo* and 28% in *Tursiops*).

Concluding Remarks

Tetrapod skulls vary in the number of connectivity modules, from two to seven, as well as the type of modules they have: bilateral, specular, or asymmetric specular. In general, grouping bones in bilateral or specular modules depends on the presence and connectivity patterns of unpaired bones. Bilateral modules without unpaired bones are very rare (e.g., in *Podocnemis*). Thus, unpaired bones and bilateral modules do not always go hand in hand; the presence of unpaired bones that did not integrate together left and right side bones is related to the formation of asymmetric specular modules. Since unpaired bones

appear more frequently in posterior and palatal regions (e.g., basioccipital, basisphenoid, parasphenoid, supraoccipital), bilateral modules are also more frequent there (i.e., cranial vault and palatal modules). Thus, skull regions lacking unpaired bones often have left and right specular modules. These specular modules have the same (or very similar) hierarchical structure of cluster formation within the dendrogram; in other words, the order in which bones are grouped hierarchically within left and right modules is the same.

The presence or absence of hub bones varies in each skull; some have several, others have none. On average, 50% of skull bones act as connectors; particular values range from 19% to 78% in different species. A high number of connectors can be related to the formation of big modules with many boundary bones between them or, on the other hand, many small modules whose bones are connected to several different modules at the same time.

In general, the hierarchical formation of modules tend to follow an order in the process, by which bones are grouped together according to the three body axes: dorsoventral, left-right, and anteroposterior. The first branching events (i.e., reading the dendrogram from left to right) separate anterior and posterior skull bones. Subsequent branching events separate left and right groups of bones. The last branching events separate bones from dorsal and ventral areas. This hierarchically idealized grouping pattern (Fig. 10.1) is modified in each skull depending on its specific overall connectivity pattern as well as the presence of unpaired bones. Moreover, this grouping pattern further suggests a relative 'order of importance' of each body axis in the formation of connections between neighbor bones during skull ontogeny and suture growth. This last conclusion is further analyzed in the next section using artificial manipulation of connectivity patterns in *Kayentachelys* and *Homo*.

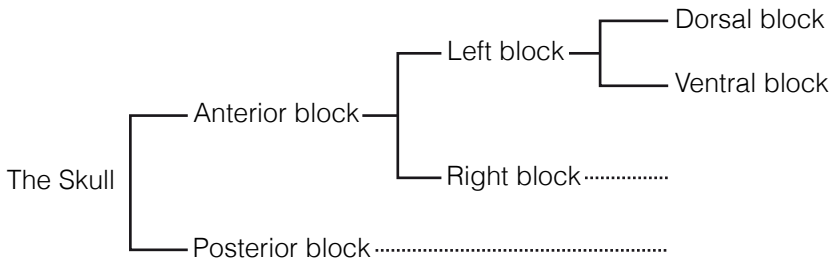

Figure 10.1: Generalized rule of connectivity modules formation according to bone position along the three body axes. The hierarchical grouping of skull bones in blocks within blocks during the formation of connectivity modules follows a particular order according to the three body axes. Dorsal and ventral neighbor bones are grouped together first in the dendrogram. Then, dorsal and ventral blocks in each skull side are grouped into left and right symmetric blocks. Finally, these left and right blocks are grouped into anterior and posterior blocks. Dashed lines indicate equivalent block formation.

10.2 Artificial Manipulation of Connectivity Patterns

Abstract – Two skull networks have been artificially manipulated disjoining one or more unpaired bones and evaluating the effect in the modular organization of skulls due to changes in connectivity patterns. The result of this theoretical experiment suggests that the presence of unpaired bones affects the order of grouping of bones in nested blocks, modules, and bigger partitions. First, bones form groups according to their position along the dorsoventral axis; then, these groups form blocks that bring together left and right groups of bones; finally, these blocks form modules that bring together anterior and posterior blocks. Thus, the skull is often divided in anterior and posterior modules when unpaired bones are present. The lack of unpaired bones reverses this order causing the formation of different connectivity modules; specular modules separating right and left groups of bones are formed more frequently. This order highlights the relative importance of each body axis in the formation of connections between neighbor bones, suggesting the presence of differential maturation patterns determining the connections between bones (formation of sutures) along each of the three body axes.

Introduction

The comparative analysis of modularity has shown that the formation of any type of connectivity module in one particular region of the skull depends entirely on the overall connectivity pattern of the skull. Thus, connectivity modules (bilateral, specular, or asymmetric specular) are emergent patterns of organization (see 10.1). The participation of unpaired bones in the integration of left and right sides is ambiguous. Bones form a bilateral module when the left and right sides are more integrated together than separately. However, the formation of bilateral modules without unpaired bones (e.g., the module that groups frontal bones in *Podocnemis unifilis*, *Chisternon undatum*, and *Carettochelys insculpta*) confirms that their presence is not always needed. In this section, the formation of connectivity modules is analyzed from an evolutionary perspective using two theoretical experiments of artificial unpaired bones formation in skull networks.

The first experiment studies the formation of a bilateral module in turtles in the anterior region of the face and palate (see Chapter 8, pages 101 to 119). In basal anapsids and testudines, such as *Procolophon* and *Proganochelys*, the vomers are two paired bones; these skulls show the formation of two specular connectivity modules in this anterior

region. During the evolution of turtles, both in pleurodires and in cryptodires, the two vomers fuse in the midline to form an unpaired bone. At the same time, a bilateral module combining both specular modules is formed in those turtles with an unpaired vomer. In this experiment, the skull network of a basal turtle, *Kayentachelys aprix*, has been manipulated to reconstruct the ancestral condition of the vomer as a paired bone. The connections of the vomer have been rearranged as it were two vomers: left and right.

The second experiment analyzes a more dramatic (unreal) scenario: the disjoint of all unpaired bones in the skull of *Homo sapiens*. A network model of the human skull has been built with all bones paired; connections have been rearranged for all bones reconstructing this new situation. This example will serve to highlight the relationship between modularity and body axes, together with unpaired bones, in the formation of modules along the anteroposterior axis and specular modules along the left-right axis.

Materials & Methods

Two skulls were selected for these theoretical experiments: a fossil skull of a basal turtle and the human skull (described in Chapter 8). The skull of *Kayentachelys aprix* represents Early Jurassic turtles with a fused vomer. This skull, still resembles to a great extent that of *Proganochelys*, a more basal turtle of the Late Triassic, in which the vomer is still formed by a pair of bones. The skull of *Homo sapiens* was selected for the medical relevance of their premature fusions in newborns (see Chapter 12). Two new hypothetical skull networks were built: one for *Kayentachelys* with a paired vomer and one for *Homo* with all bones paired. The same modularity analysis described in the previous section was performed for these networks.

Results & Discussion

Kayentachelys

Disjoining the unpaired vomer in one left and one right vomer in the skull of *Kayentachelys* produces a split in two specular modules of the anterior bilateral faciopalatal module (Fig. 10.2). Only frontal bones change their assignment, being grouped now in more posterior specular modules. The hierarchical structure of the other modules is the same as in the original skull. However, the order in which bones are grouped in some regions regarding the three body axes changes with and without the unpaired vomer. With an unpaired vomer, bones are generally grouped first in dorsoventral blocks, then in left-right

partitions, and finally in anteroposterior partitions; thus, a bilateral module is formed in the anterior facial region of the skull. With paired vomers, the order in which bones are grouped changes, first in dorsoventral blocks, then in anteroposterior modules, and finally in left-right partitions; thus, two specular modules appear now in the anterior region of the skull. This result points out the importance of the unpaired vomer in the formation of this anterior bilateral module during the evolution of turtles skull modularity.

Homo

Disjoining all unpaired bones in two paired bones in the skull of *Homo* causes a totally different modular organization. The original division in two bilateral modules along the anteroposterior body axis has been replaced by a four-module division, in which bones are first divided along the left-right axis and then the anteroposterior axis (Fig. 10.3). This extreme example points out the importance of unpaired bones in the modular division of skulls along the three main body axis. In absence of unpaired bones, bones tend to group in left and right specular modules. The presence of originally unpaired bones, such as (in part) the sphenoid and the occipital, or unpaired bones formed by midline fusions, such as the frontal and the vomer, generates the formation of bilateral modules.

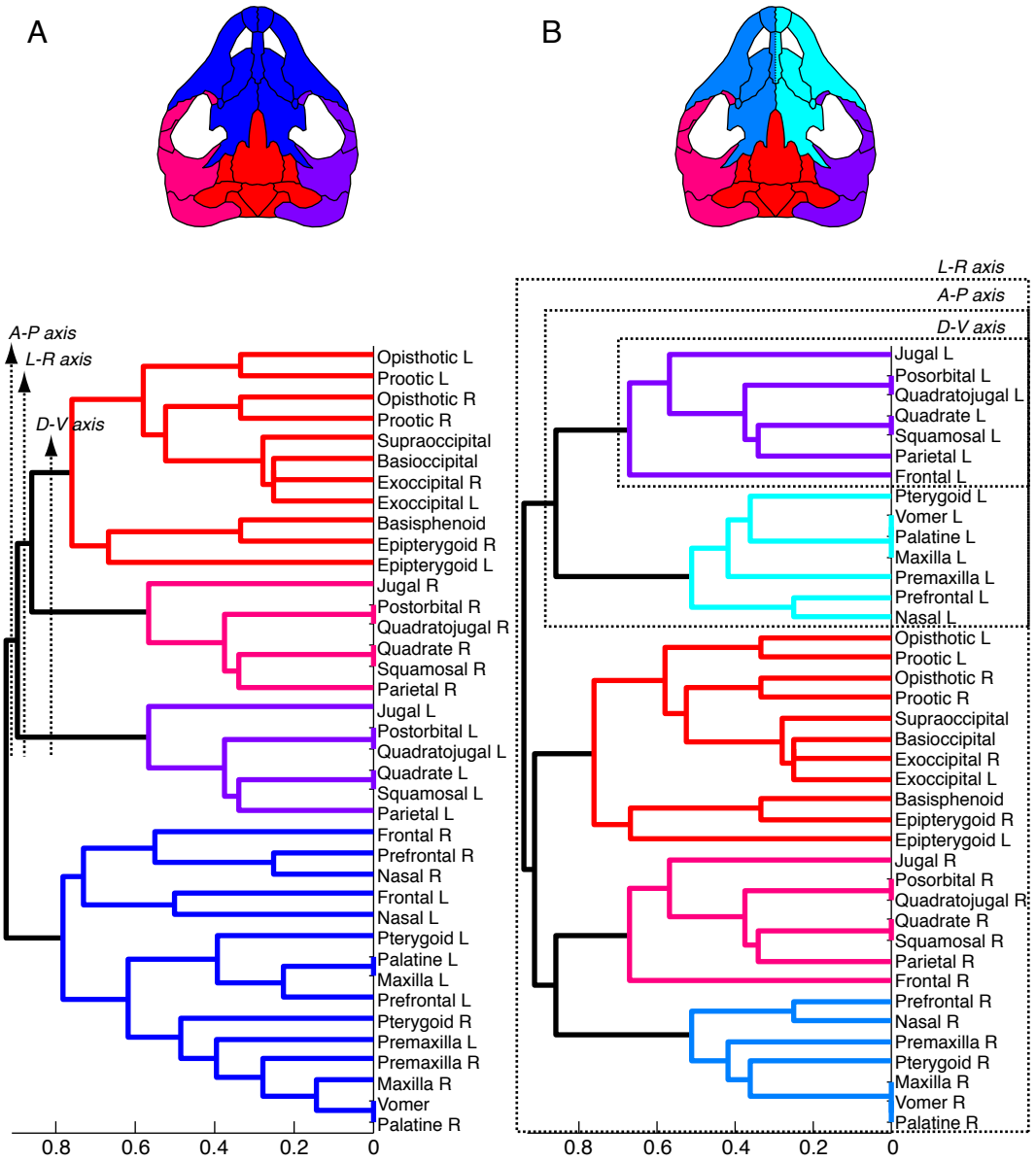

Figure 10.2: Artificial disjoining of the vomer in *Kayentachelys aprix*. A) Empirical skull network, the bones of the anterior region of the face and palate form a bilateral module that includes the unpaired vomer (in blue). B) Skull network with an artificially disjointed vomer, the same bones now form two specular modules, except frontals, which are instead grouped in other, posterior specular modules. The formation of two anterior specular modules is a feature observed in basal turtles, prior to the evolutionary fusion of the vomer.

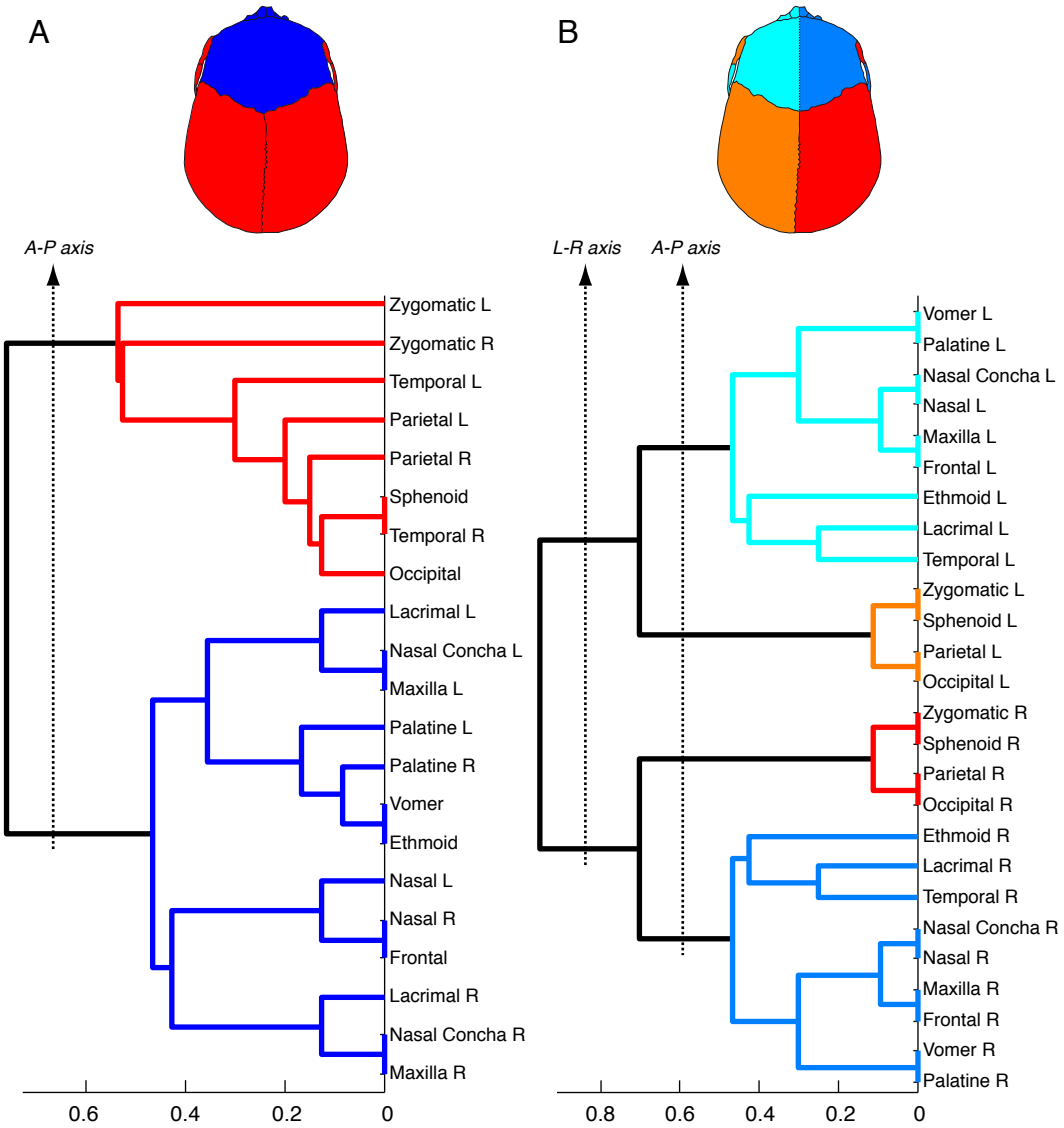

Figure 10.3: Artificial disjoining of the skull in *Homo sapiens*. A) Original skull modularity with one anterior and one posterior bilateral module. B) After disjoining unpaired bones, modules are separated in two specular left and right modules, emphasizing the importance of the anteroposterior body axis in bilateral module formation.

Concluding Remarks

Unpaired bones have an important role in the formation of bilateral modules. The presence or absence of unpaired bones determines the formation of bilateral or specular modules in particular regions of the skull. The artificial manipulation of unpaired bones shows that they also affect the order in which bones are grouped in nested blocks, modules, and bigger partitions regarding the three main body axes (Fig. 10.4). First, bones form groups according to their position along the dorsoventral axis; then, these groups form blocks that bring together left and right groups of bones; finally, these blocks form modules that bring together anterior and posterior blocks. Thus, the skull is often divided in anterior and posterior modules when unpaired bones are present. The lack of unpaired bones reverses this order causing the formation of different connectivity modules; specular modules separating right and left groups of bones are formed more frequently. Furthermore, this order reveals a possible relative importance of each body axis in the formation of connections between neighbor bones, suggesting the presence of differential maturation patterns determining the connections between bones (formation of sutures) along each of the three body axes. The formation of new unpaired bones during the evolution of the skull in different lineages is responsible for changes in their modular organization due to changes in overall connectivity patterns.

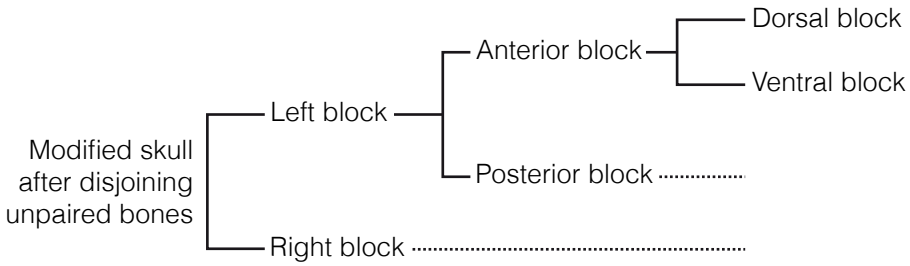

Figure 10.4: Modification of the generalized rule connectivity modules formation. The hierarchical grouping order when unpaired bones are absent differs from that showed in Fig. 10.1. The main shift in connectivity modules formation, due to disjoining unpaired bones, is that anterior and posterior blocks of bones are formed before than left and right side blocks, which, together with higher modularity Q values, promotes the formation of only specular modules in modified skulls.

11

Theoretical Morphology and Morphospaces

This chapter has been published as:

Esteve-Altava, B. and Rasskin-Gutman, D. (2013). Theoretical Morphology of Tetrapod Skull Networks. *Comptes Rendus Palevol*, accepted.

11.1 Theoretical Morphology of Tetrapod Skull Networks

Abstract – Network models of the tetrapod skull in which nodes represent bones and links represent sutures have recently offered new insights into the structural constraints underlying the evolutionary reduction of bone number in the tetrapod skull, known as Williston's Law. Here, we have built null network model-derived generative morphospaces of the tetrapod skull using random, preferential attachment, and geometric proximity growth rules. Our results indicate that geometric proximity is the best null model to explain the disparity of skull structures under two structural constraints: bilateral symmetry and presence of unpaired bones. The analysis of the temporal occupation of this morphospace, concomitant with Williston's Law, indicates that the tetrapod skull has followed an evolutionary path toward more constrained morphological organizations.

Introduction

The evolution of the tetrapod skull has been extensively studied in comparative morphology. In the early 20^{th} century, a pivotal analysis of changes in the number and complexity of skull bones in the evolution of Permian reptiles formed the basis for what is now known as the Williston's Law: an evolutionary trend in tetrapods toward reduction in the number of skull bones (see 1.2.1). Three complementary causal factors have been proposed to explain the reduction in the number of bones and sutures during tetrapod skull evolution (Sidor, 2001): (1) natural selection favoring more rigid, boxy skulls that improved functional and biomechanical integration in terrestrial vertebrates; (2) developmental and statistical constraints favoring the loss of bones rather than their new formation; and (3) unlikeliness of new bone formation by either genetic or epigenetic mechanisms (see also Rasskin-Gutman and Esteve-Altava, 2008, and references therein, for a review of external and internal processes related to evolutionary trends). Although reversions of Williston's Law are theoretically possible, for example, due to paedomorphosis in the patterns of cranial suture closure, this mechanism has not been reported at a broad scale as a sustained evolutionary process (but see Wilson and Sánchez-Villagra, 2009; Koyabu et al., 2011, for insights on heterochronic shifts in ossification and fusion sequences in mammals). Recent studies on the evolution of the skull have focused on the analysis of morphological integration and modularity in different groups, such as: hominids (Bastir, 2008; Mitteroecker and Bookstein, 2009; Mitteroecker et al., 2012), mammals (Couly et al., 2007; Goswami

et al., 2009; Porto et al., 2009), and birds (Marugán-Lobón and Buscalioni, 2003, 2009; Bhullar et al., 2012; Klingenberg and Marugán-Lobón, 2013). In addition, the importance of cranial anatomy at all levels of organization has prompted the comparative and evolutionary analysis of gene regulatory networks (Chase et al., 2002; Haberland et al., 2009) and developmental origin of skull embryonary cells (Couly et al., 1993; Santagati and Rijli, 2003), as well as biomechanics and functional morphology (Rafferty et al., 2003; Moazen et al., 2009). These studies show that although the organization of the skull is modular at the genetic, developmental, functional, and morphological level, it still retains a tight integration of parts. As a consequence, the bony elements of the skull, which derive from multiple developmental and evolutionary origins, carry many coordinated functions (e.g., protection and hosting of sensory organs and the brain, feeding, or breathing). To which extent this multi-functional, highly integrated, and modular anatomical structure has occupied the morphospace of all possible tetrapod forms is missing in this picture. Here, we will try to answer this question duly by exploring theoretical morphospaces using network theory; with these tools we can simulate millions of networks that represent possible skulls at a broad macroevolutionary scale, using different null models of growth.

Theoretical Morphology and Networks

Theoretical morphology appeared in the 1960s beginning with the seminal work of David Raup on the accretionary growth of coiling shells (Raup, 1961, 1962, 1966, 1967, 1968). This methodological approach is based on the construction of a space of possible forms by using a set of generative rules that are formal abstractions of growth patterns (for recent extensive reviews of theoretical morphology and morphospaces see Dera et al., 2008; McGhee, 1998, 2007). An empirical morphospace including both extinct and extant forms is subsequently superimposed onto the theoretical morphospace; as a result of this mapping, real forms can be analyzed against a background of possible and impossible forms, obtaining a more general picture of how real forms are distributed in nature (Fig. 11.1).

The dimensions of a morphospace are timeless; this makes theoretical morphology suitable to frame evolutionary patterns of morphological change (McGhee, 1998). A theoretical morphospace describes (or puts into relation) organismal forms with one basic assumption: the morphospace is not occupied uniformly (Rasskin-Gutman and De Renzi, 2007). If the models to generate these forms are carefully chosen, distances among forms and trajectories of occupation within the theoretical morphospace will inform us about

underlying causes in development and evolution (Mitteroecker and Huttegger, 2009).

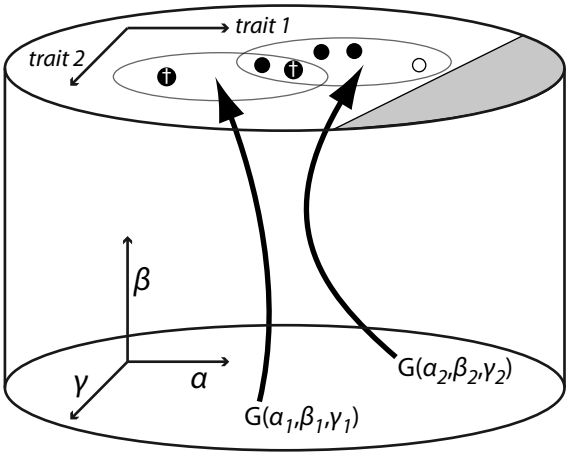

Figure 11.1: Analysis of form using theoretical morphospaces. The empirical morphospace of morphological traits is mapped onto the broader framework provided by the theoretical construction, in which possible and impossible forms can be generated. Below, a hypothetical three-dimensional parameter space (α, β, γ) from which a generative rule, G, explicitly build parameter-specific regions of theoretically possible forms in the plane above. Above, the theoretical space is divided in possible regions (white) and theoretically impossible regions (grey) given the assumptions of the model. Each set of parameters for the generative rule can produce possible forms (circles), which, in the ideal case, match the empirical ones, including those that exist (black dots), have existed in the past (crossed dots), or are functionally unviable (empty dots). Modified after Rasskin-Gutman (2005).

In theoretical morphology, the distinction between possible and impossible forms depends on which generative rule is chosen to build the theoretical morphospace. Given a set of parameters, there always will be forms that are impossible either because the generative rule cannot make them or because the combination of those parameters is meaningless. For example, if we consider, by definition, that skull networks cannot be disconnected, then any combination of parameters for each null model that would grow disconnected networks has to be treated as impossible. Also note that we do not impose functional constraints on the exploration of the skull network morphospace, this means that what is biologically possible is a subset of the formally possible, which might be further constrained by functional requirements. Moreover, the set of rules based on morphogenetic

processes converts a generative morphospace in a hypothesis of developmental constraint (Rasskin-Gutman, 2003; Rasskin-Gutman and Izpisua-Belmonte, 2004). Indeed, this is how we should look at the null models presented here (see also 6.1).

The articulation of skull bones was first analyzed in a theoretical morphology framework in Rasskin-Gutman (2003). There, only 2D bone connectivity networks were studied from data taken from skull diagrams in lateral view. The exploration of the possible connections among skull bones was carried out using a computational model based on cellular automata, an approach that uses stochastic rules to generate connectivity patterns. These changed sequentially, following a constraint specified as a computational goal: a specific connectivity distribution and a fixed number of bones. Here, we analyze full 3D connectivity information of all bone sutures for each skull in the sample. To explore the theoretical morphospace we use null models of network growth. In general, null models are idealized representations of strategies and scenarios for a given phenomenon that also provide a comparative baseline to analyze other models (Nitecki and Hoffman, 1987). Even assuming that there is not a one-to-one mapping between the network growth rule and its properties (Fox-Keller, 2005), null network models are useful heuristic tools in biology (Watts and Strogatz, 1998; Barabási and Albert, 1990). We show that the properties of these null network models, when compared with empirical skull networks reveal plausible mechanisms of network formation in evolution. Furthermore, the analysis of the growth rules and constraints that form connectivity patterns in networks can be interpreted as developmental mechanisms that impinge on skull evolutionary dynamics.

We built four null network model-derived generative morphospaces based on different growth assumptions about how bone connections are established during skull formation: at random, by preferential attachment, and using two different geometric proximity assumptions (see 6.1). Each model of network growth proposes competing sets of structural constraints that might have been in place during the evolution of the tetrapod skull. The fit of skull networks to the random model would suggest absence of constraints on the formation of connections among bones. This would mean that there would be a decoupling between any evolutionary trend on skull connectivity and their underlying developmental constraints. In other words, skull connectivity trends would be exclusively due to non-developmental factors. On the other hand, the fit to the preferential attachment model would suggest that the number of connections is the main constraint in establishing new connections; thus, some bones would have a growth pattern allowing them to make contact with more and more bones as they become ossified. As far as we know, no developmental mechanism would favor this kind of preferential attachment growth. Finally, the fit to the

geometric proximity models would indicate that the key factor constraining the formation of skull suture connections is the relative spatial proximity of all ossification centers. This would further suggest that changes in genetic regulatory networks that determine bone position in the developing skull (i.e., migration, determination, and differentiation of bone precursors), as well as their epigenetic regulation, could cause evolutionary changes on the formation of connections among skull bones.

We have used these four null models to build generative morphospaces, analyzing their occupation using an empirical sample of real tetrapod skull networks. The results of this approach will be used to address the following questions: (1) how does the number of connections vary in relation to the number of bones; (2) how is this variation distributed across geological time; and, most importantly, (3) which growth rules are more likely to have been involved in producing the disparity of skull structures found in nature?

Material & Methods

Skull network models are a morphological abstraction of the structure of the suture patterns of the skull in which each bone is a node and each suture connection is a link of the network. Methods to build skull network models have been extensively discussed in Chapter 4. In the following sections, we will describe the process of construction of generative morphospaces using null network models and the empirical sample used here to analyze the morphospace occupation.

Boundaries of the Morphospace Based on Network Models

We have built four generative morphospaces for two morphological traits: number of bones (N) and total number of suture connections between bones (K). These traits correspond to basic descriptors of network models: number of nodes and links. The ratio between the actual number of connections and the maximum theoretical possible, $K/N(N\text{-}1)$, defines the density of the network.

We have set the space of possible networks by imposing the following restrictions (Fig. 11.2): (1) redundant connections between bones, loops, are not considered (region **a** in Fig. 11.2), this generates an upper limit for possible theoretical networks given by a value of density = 1 (boundary **b** in Fig. 11.2); (2) bones cannot be disconnected (region **c** in Fig 11.2), and (3) $K > N–1$ in all instances, setting the minimum threshold of disconnectivity (boundary **d** in Fig. 11.2). These restrictions define the boundaries that constraint

the space of modeled skull networks for all generative morphospaces (region **e** in Fig. 11.2).

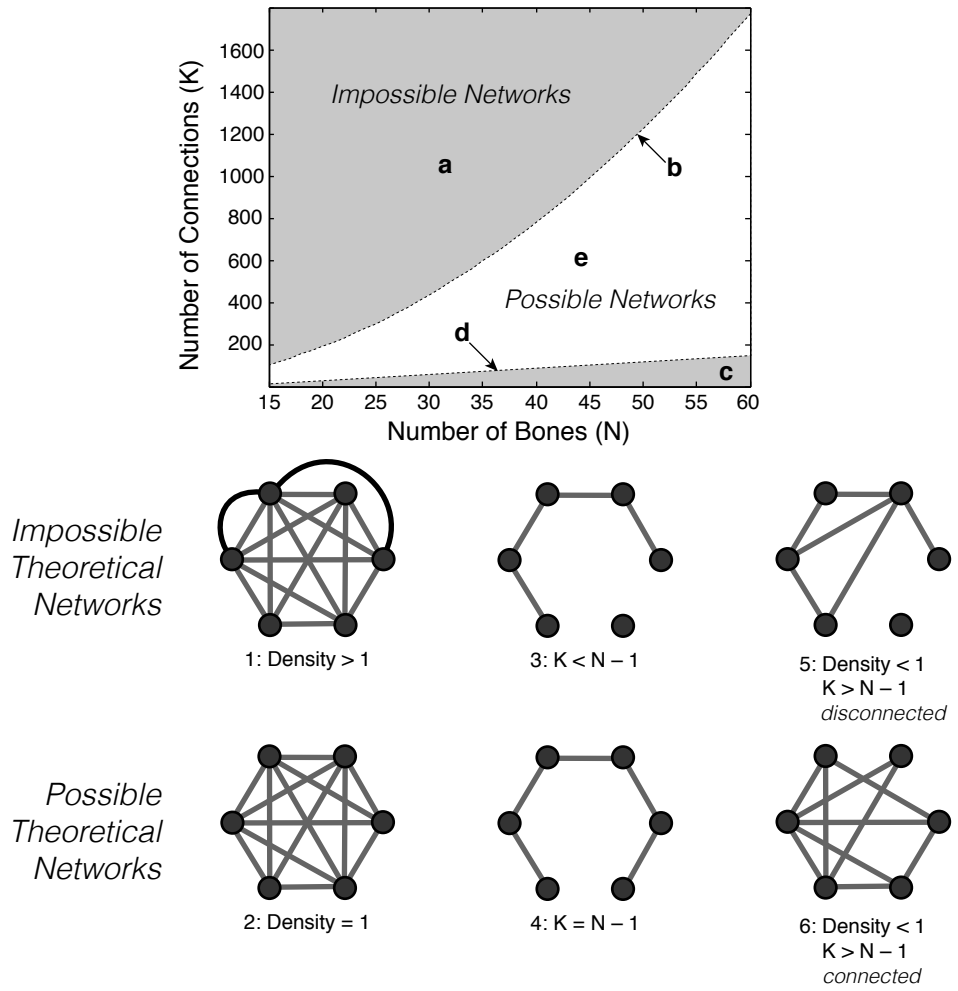

Figure 11.2: Boundaries constraining the theoretical morphospace of skull networks. Possible skull networks occupy the white region between both boundaries, whereas the grey regions contain only impossible networks. Based on measures of density, number of connections (K), and number of bones (N), five regions **a**-**e** can be differentiated within the morphospace: **a**, includes impossible regions with redundant connections (type 1); **b**, includes possible, totally connected networks (type 2); **c**, includes impossible, disconnected networks (type 3); **d**, includes possible networks of minimal connectivity (type 4); and **e**, includes most possible networks found in nature (type 6), but also some special impossible networks (type 5).

Building Generative Morphospaces

We built four generative morphospaces: random, preferential, proximal, and symmetric proximal, using different null network models (Table 11.1). Each morphospace is based on a growth rule that uses different sets of parameters. Different parameter values generate different regions for each morphospace, exhibiting different degrees of overlapping. The regions generated for different values of the generative parameter delimit restricted morphospace regions, while the sum of all restricted regions configures an extended morphospace region. To set the upper and lower boundaries for each generative morphospace, the maximum and minimum values of K were calculated by simulating 10,000 networks for each value of N, ranging from 15 to 60.

Table 11.1: Properties of the four generative morphospaces.

Morphospace	**Growth Rule**	**Parameters**
Random	Random Linkage	$p = \{0.1, 0.2, 0.3\}$
Preferential	Preferential Attachment	$m = \{1, 2, 3, 4, 5, 6\}$
Proximal	Proximity Constraint	x, y, z = random
Symmetric Proximal	Proximity Constraint	y, z = random x = bilateral symmetry *unpaired nodes* = {0-7}

The Random morphospace is based on the classic model of Erdös and Rényi (1959), in which connections between nodes are established by random linkage (see 6.1.2). In this model, networks are built by taking a given number of nodes (N) and connecting each pair with probability p. The choice about whether or not to connect two nodes is made independently for each pair of nodes. In random networks, all connections are equally probable and there are no constraints to connectivity. Thus, the density of the generated networks depends directly on the linkage probability: if $p = 0$ the random model will generate a totally disconnected network; if $p = 1$, it will generate a complete network, where all nodes are mutually connected; and, for a large N the average connectivity of the network is $p(N–1)$. In real skull networks p is calculated as the ratio between the average number of connections, $\overline{k_i}$, for all nodes and the total number of bones, N. For example, in the human skull network $\overline{k_i} = 6.04$ and $N = 21$, so $p = 0.28$. In the empirical

sample, p ranges approximately from 0.1 to 0.3; thus, we have constructed the Random morphospace for values of p equal to 0.1, 0.2, and 0.3.

The Preferential morphospace is based on the model proposed by Barabási and Albert (1990) to generate scale-free networks by preferential attachment (see 6.1.5). Networks are built starting from a small number of nodes (we used $N = 10$), to which new nodes are iteratively added. New nodes introduce a fixed number of new connections (m), connecting the new nodes to old nodes already present in the network. When choosing the old nodes to which the new node connects, those with a higher number of connections are chosen preferentially. Thus, nodes with more connections have a higher probability to attach new connections (*"the rich get richer"*), in contrast with the random model, in which all nodes have the same probability to connect. We have constructed the Preferential morphospace for values of m between 1 and 6, which cover the range of average number of connections per node in all empirical skull networks.

The Proximal morphospace is based on the model proposed by Gabriel and Sokal (1969), which imposes spatial constraints to connectivity according to node geometric proximity (see 6.1.6). Here, networks are built by positioning a given number of nodes uniformly at random in a Euclidean space; each pair of nodes is connected if, and only if, the sphere whose diameter is the line between both nodes does not have any other node within its volume. In contrast with the previous null network models, proximity networks are spatially constrained: two nodes only connect if they satisfy a geometric requirement. We have built the Proximal morphospace by placing all nodes at random within a cubic space of size 1.

In addition, we have modified the model of Gabriel and Sokal to build a Symmetric Proximal morphospace, which introduces two additional constraints based on real skull anatomy: (1) the symmetric positioning of bones along a left-right axis (bilateral symmetry) and (2) the presence of unpaired bones positioned in the midline of this axis (see 6.1.7). We built the Symmetric Proximal morphospace for 0 to 7 unpaired nodes, while the remaining nodes were paired.

Empirical Sample of Skull Network Models

An empirical sample of 53 skull networks has been used to explore their occupation within each generative morphospace. The sample includes 44 network models of adult tetrapod skulls (see details in Chapters 7 and 8). Two basal amphibian skulls have been added to this sample: *Brachydectes sp.* (40 bones, 81 connections, Carboniferous; from Marjanovic and Laurin, 2008) and *Pantylus sp.* (51 bones, 146 connections, Permian; from

Romer, 1969). In addition, seven network models of human newborn skulls were built; the normal human skull at birth and six nonsyndromic craniosynostosis conditions in which premature fusion of the following sutures occur: metopic, sagittal, hemicoronal, bicoronal, lambdoidal, and lambdoidal plus occipitomastoid (see 12.2). The inclusion of these six pathological human skulls broadens the empirical sample with developmentally possible forms, challenging the limits of each generative morphospace. All these skulls were selected to show a wide diversity of tetrapod forms, including extinct basal forms. It is also worth noting that the identification of bones and suture connections is a very hard task in extinct species due to preservation problems in fossil skulls; in these cases, bones and connections have been quantified according to expert descriptions in the literature and personal judgment (see 5.1).

Temporal Occupation

Empirical skull networks have been mapped onto each generative morphospace in order to analyze their occupation. Additionally, a temporal analysis of the morphospace occupation has been carried out for the generative morphospace that shows the best fit to the empirical sample. We have used seven time intervals: Devonian, Carboniferous, Permian, Triassic, Jurassic, Cretaceous, and Cenozoic. Temporal occupation for each empirical skull network was taken at the genus level using origin and extinction occurrence from the Paleobiological Database (available at http://paleodb.org). Extant genera without known fossil record were marked as originating in the Cenozoic.

Results

Coverage of the Theoretical Morphospace

Generative morphospaces cover the theoretical morphospace distinctively; in addition, each type of morphospace behaves differently when varying their parameter values (Fig. 11.3). The Random and the Preferential morphospaces include all empirical networks, as parameters p and m vary for 0.1 to 0.3 and from 1 to 6, respectively. However, within these restricted regions some areas remain unoccupied by empirical data. In contrast, Proximal morphospaces only generate networks in a limited constant region, which are almost uniformly occupied by empirical data. In the Symmetric Proximal morphospace, its form is prominently narrower for lower values of N and K than for higher values; consequently, the occupation is more scattered as the values of N and K increase.

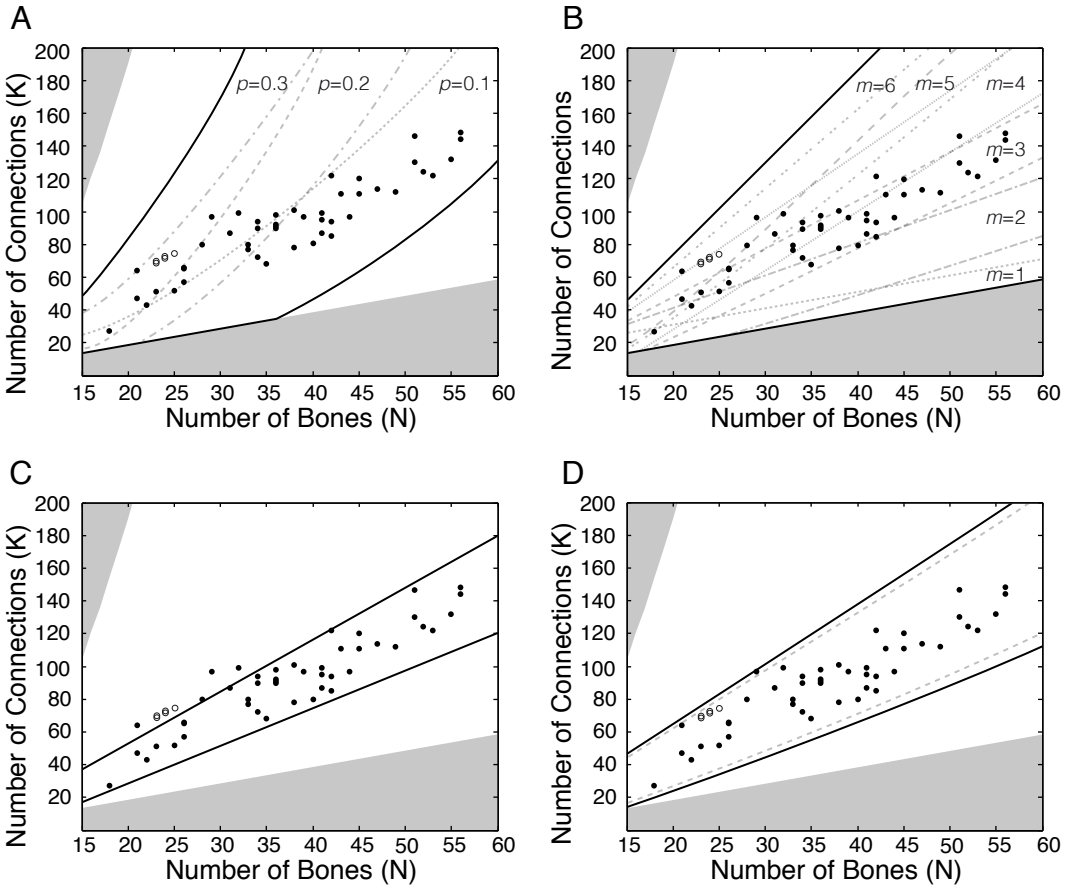

Figure 11.3: Coverage of the theoretical morphospace by the four generative rules. In grey, the region of impossible forms; in white, the region of possible forms, which each model covers distinctively. Solid dots, adult empirical skull networks; empty dots, human newborns. For each morphospace, the regions generated for different values of the generative parameter delimit restricted morphospace regions (grey line patterns), while the sum of all restricted regions configures an extended morphospace region (black continuous lines). A) The Random morphospace; forms can be generated in three restricted regions according to the probability value, p. B) The Preferential morphospace; forms can be generated in six restricted regions according to the number of new connections introduced for new nodes as the network grows, m. C) The Proximal morphospace; forms can be generated within a unique, uniform restricted region. D) The Symmetric Proximal morphospace; here the restricted and extended regions are almost identical. In all models, the distribution of K for each N is normal around the mean value.

The occupation of the Random morphospace varies in each restricted region, according to the probability value (Fig. 11.3A): $p = 0.1$ (58%); $p = 0.2$ (49%); and $p = 0.3$ (21%). In the Preferential morphospace, occupation also varies in each restricted region, according to the number of new connections introduced for new nodes as the network grows (Fig. 11.3B): $m = 1$ (2%); $m = 2$ (9%); $m = 3$ (68%); $m = 4$ (55%); $m = 5$ (26%); $m = 6$ (17%). In addition, for each set of parameters there are different areas of non-occupation; for example, for values of $p = 0.2$ and 0.3 the Random Morphospace is occupied by forms that are over-connected when compared with real skull networks; and for $p = 0.1$ the smaller networks generated by this morphospace are under-connected. For the Preferential morphospace, most areas generated for $m = 1$, 2, 5, and 6 are empty, while the empirical sample occupies more uniformly the areas generated for $m = 3$ and 4. Finally, for $m = 1$ and 2, the generated networks are under-connected for their size, whereas for $m = 5$ and 6 the generated networks are over-connected for their size when they are compared with real skull networks.

Morphospaces generated with spatial constraints are more uniformly occupied. The Proximal morphospace includes 42 out of 53 skull networks (79%) inside its boundaries (Fig. 11.3C); some skulls such as all human newborns and some modern mammals that possess a relatively high density of connections (*Homo sapiens*, *Mus musculus*, *Canis lupus*, and *Tursiops truncatus*) fall outside this morphospace. The Symmetric Proximal morphospace includes all empirical skull networks in its extended region and all but one (*Canis lupus*) in the overlap region of all its restricted regions (Fig. 11.3D).

Temporal Occupation of the Theoretical Morphospace

To analyze the temporal occupation of the empirical sample of skull networks within the theoretical morphospace, we have used the extended Symmetric Proximal morphospace. This generative model fits the empirical data well, including the human pathological forms. Early tetrapod skulls occupy the wider region of the morphospace during the Devonian and Carboniferous Periods. Temporal occupation changes toward the narrower area of the morphospace as the wider area (i.e., higher values of N and K) begins to empty out during the Mesozoic, being completely unoccupied in the Cenozoic (Fig. 11.4).

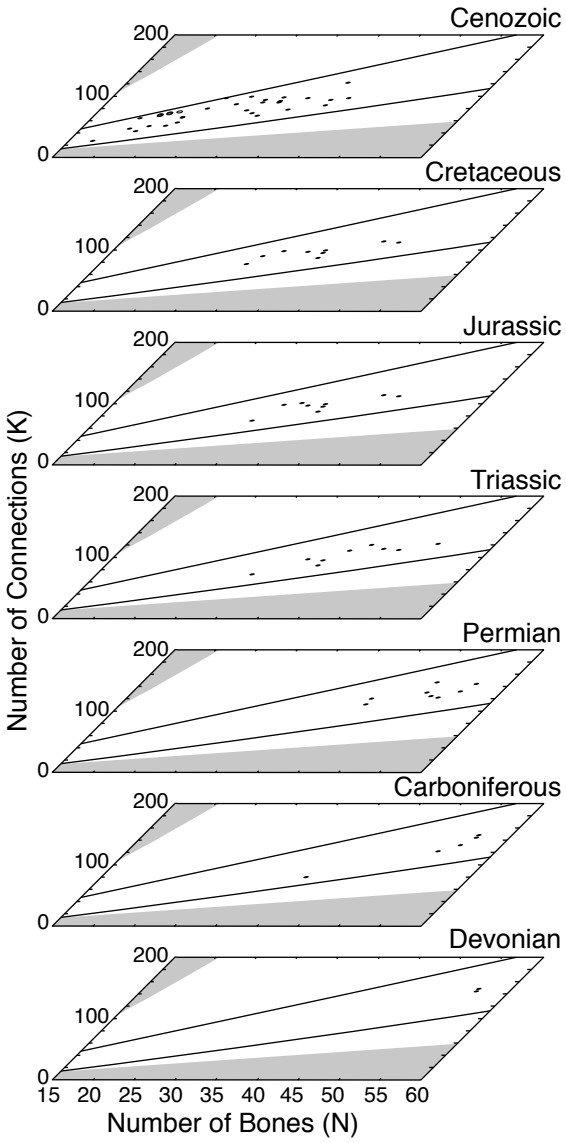

Figure 11.4: Temporal occupation of the theoretical morphospace. Black lines delimit the area generated by the Symmetric Proximal morphospace. Skull networks of major groups originate in the wider area of the morphospace (right; higher N and K), in which the disparity of networks is potentially greater; after the Devonian, all groups evolved toward the narrower part of the morphospace (left; lower N and K), in which the potential disparity of skull networks is lower. By the Cenozoic, the area where skulls originated is empty.

Discussion

We have built four null network model-derived generative morphospaces using three growth rules: randomness, preferential attachment, geometric proximity, and symmetric geometric proximity. By mapping an empirical sample of skull networks onto these morphospaces, we have assessed their plausibility as developmental processes involved in the formation and evolution of the tetrapod skull. Our results indicate that geometric proximity is the best model to explain the disparity of skull structures found in tetrapods. This can only happen when bones are positioned in such a way that bilateral symmetry is kept and only a few of them are unpaired, which is the case of the Symmetric Proximal morphospace. Further analysis of the temporal occupation of this network morphospace reveals that early skulls, for all major groups, originated in the wider area of the morphospace, in which the variability is potentially greater. Subsequently, skull networks have evolved toward the narrower area of the morphospace, in which the potential skull variability is lower. This fits Williston's Law because the wider area represents skulls with higher number of bones and connections, whereas the narrower area represents skulls with fewer bones and connections (but showing higher density or complexity).

Our results do not support random and preferential growth rules as plausible processes of skull network formation. The analysis of the occupation of these morphospaces show that: (1) different skulls need different values for basic generative parameters, which are linked to their number of bones without any developmental or phylogenetic basis; and (2) their extended regions cover the full range of possible forms, which clearly limits their explanatory power. A common characteristic of both morphospaces is that none of their restricted regions can include completely the empirical sample of skull networks; full sample inclusion occurs only when taking all extended regions. This result entails that if skull structure (as modeled by networks) were produced by random or preferential mechanisms for establishing connections between bones, then the basic generative parameters (p and m, respectively) would have to vary in each case to produce different skulls. Furthermore, these two models can cover the full range of possible network forms by using more values for p and m; increasing these parameters increases the number of connections available in relation with the number of bones. Since extended regions in the Random and the Preferential morphospace cover all the space of possible forms, the bounded pattern of occupation of the empirical skull networks would need additional explanation. As a consequence, the biological predictions of these models cannot be supported. This suggests that suture connection formation is constrained by specific developmental mechanisms in

the tetrapod skull, coupling development with evolutionary trends (Rasskin-Gutman and Esteve-Altava, 2008). In addition, the number of connections, solely, cannot guide the establishment of new connections via specific growth patterns in the tetrapod skull.

In contrast, geometric proximity rules are well supported by our results. Even though, in these models, the positioning of bones imposes physical constraints for establishing bone connections during skull growth, they are able to generate highly bounded regions of the theoretical morphospace, which fit the empirical data very well. Thus, the Proximal morphospace includes most of the real skull networks, except several skulls that have a higher number of connections (and consequently, more density) than expected for their number of bones, namely, *Homo sapiens*, *Mus musculus*, *Canis lupus*, *Tursiops truncatus*, and human newborn skulls with craniosynostosis. The addition of a bilateral symmetry constraint to the model allows the coverage of the Symmetric Proximal morphospace to include all skulls of the empirical sample.

The different occupation of the Proximal and the Symmetric Proximal morphospace can be better understood if we interpret nodes in growing networks as analogous to ossification centers in skulls. For these null models, this interpretation implies also an idealized mechanism of homogeneous bone growth both in speed and direction. This is so because by connecting nodes using the Gabriel & Sokal model we are assuming that each node is a center of growth that extends spatially until it contacts another growth front. Since some empirical skulls are not included in the Proximal morphospace, this indicates that this model is unable to predict some connections between bones. These skulls deviate from the growth assumptions of this null model because some of their bones might grow in size, have more irregular shapes, or have different developmental timing (Schoch, 2006; Wilson and Sánchez-Villagra, 2009; Wilson et al., 2010; Koyabu et al., 2011). However, all real skull networks are included in the Symmetric Proximal morphospace, in which bone position is more realistic: two sets of bones with bilateral symmetry and a few unpaired bones in the middle. This suggests that those hypothetical bones able to overcome geometric constraints in the Proximal morphospace might just be unpaired bones with a privileged position that allows them to connect to many paired bones. As a consequence, the best null model to predict the formation of the skull structure is based on a mechanism by which bones establish suture connections according to their geometric distance; furthermore, the skull bilateral symmetry as well as the presence of a few unpaired bones is essential.

The generative region in the Symmetric Proximal morphospace is narrower for lower values of N and K than for higher values. Thus, it shows a variation in the range of the

number of connections for skulls with lower or higher number of bones. As a consequence, there are more structural configurations of skull networks (i.e., disparity) available in the wider area of the morphospace than in the narrower area; in contrast, in the narrow area, the variability of theoretically possible skull networks is lower, that is, more constrained. Moreover, early tetrapod skulls that originated during the Devonian and Carboniferous Periods only occupy the region of the morphospace characterized by a high number of bones. Throughout the Mesozoic, the occupation shifts toward narrower areas of the morphospace; that is, skulls reduce their numbers of bones, following Williston's Law. As skull bone number decreases in early tetrapod evolution, the wider area of the morphospace begins to empty out, while that narrower area begins to fill in with more derived skull forms during the Cenozoic. Thus, the occupation of the theoretical morphospace suggests that the tetrapod skull has evolved toward more constrained morphological organizations. It is worth noting also that this directional pattern of occupation is convergent in all major groups and all measures of structural complexity increase over time (see 9.1).

Generative morphospaces, as hypotheses of developmental constraints, have allowed us to show a directional pattern of morphospace occupation in macroevolutionary time scales, further suggesting that the tetrapod skull has evolved in most lineages under the influence of structural constraints acting on the formation of new patterns of connectivity. These structural constraints are also related with mechanisms that favor the random loss of poorly connected bones and the selective fusion of the most connected ones, incidentally increasing morphological complexity, and providing a mechanistic basis for Williston's Law (see Chapter 9). Taken together, these results suggest an evolutionary scenario in which a structural constraint imposed by bilateral symmetry and geometric proximity between skull bones has been operating, favoring bone loss and fusion, creating highly connected unpaired bones in the midline.

12

The Human Skull Network

First section of this chapter has been published as:

Esteve-Altava, B., Marugán-Lobón, J., Bastir, M., Botella, H., and Rasskin-Gutman, D. (2013). Grist for Riedl's mill: A network model perspective on the integration and modularity of the human skull. *Journal of Experimental Zoology Part B (Molecular and Developmental Evolution)*, doi 10.1002/jez.b.22524.

12.1 Grist for Riedl's Mill: A Network Model Perspective on the Integration and Modularity of the Human Skull

Abstract – Riedl's concept of burden neatly links development and evolution by ascertaining that structures that show a high degree of developmental co-dependencies with other structures are more constrained in evolution. The human skull can be precisely modeled as an articulated complex system of bones connected by sutures, forming a network of structural co-dependencies. We present a quantitative analysis of the morphological integration, modularity, and hierarchical organization of this human skull network model. Our overall results show that the human skull is a small-world network, with two well-delimited connectivity modules: one facial organized around the ethmoid bone, and one cranial organized around the sphenoid bone. Geometric morphometrics further support this two-module division, stressing the direct relationship between the developmental information enclosed in connectivity patterns and skull shape. Whereas the facial module shows a hierarchy of clustered blocks of bones, the bones of the cranial modules show a regular pattern of connections. We analyze the significance of these arrangements by hypothesizing specific structural roles for the most important bones involved in the formation of both modules, in the context of Riedl's burden. We conclude that it is the morphological integration of each group of bones that defines the semi-hierarchical organization of the human skull, reflecting fundamental differences in the ontogenetic patterns of growth and the structural constraints that generate each module. Our study also demonstrates the adequacy of network analysis as an innovative tool to understand the morphological complexity of anatomical systems.

Introduction

The morphological integration and modularity of the adult human skull is the result of a mosaic evolution of embryonary parts with diverse developmental mechanisms (Cheverud, 1982; Bastir and Rosas, 2005; Bastir et al., 2008; Klingenberg, 2008; Bastir and Rosas, 2009; Lieberman, 2011; Martínez-Abadías et al., 2012). Studies of the morphological integration and modularity of the human skull start by establishing a developmental or

functional hypothesis; this is then tested by means of patterns of covariation and correlation using different morphometric tools (Chernoff and Magwene, 1999; Bastir, 2008; Mitteroecker and Bookstein, 2008). Even though this approach has proven very successful, it uses morphological information only as datasets to test a priori biological hypotheses. In contrast, few efforts have been devoted to articulate theoretical and mechanistic models to quantify integration and describe modules at a morphological level without functional or developmental assumptions (but see Eble, 2005; Rasskin-Gutman and Buscalioni, 2001; Rasskin-Gutman, 2005). Such an approach can be carried out in the skull using network models of bone connectivity patterns (Rasskin-Gutman, 2003, 2005; Esteve-Altava et al., 2011). Within this framework, modules are recognized based exclusively on morphological organization without a priori assumptions. However, the number and pattern of connections for each bone can be seen also as developmental and functional dependencies, providing a quantitative estimate of Riedl's burden rank (Riedl, 1978; Schoch, 2010, see also 5.2.2) and allowing, in turn, an a posteriori direct measure of integration and modularity.

We build these network models formalizing each bone and suture of the skull as nodes and links in an adjacency matrix. This type of analysis provides a new modeling framework to understand evolutionary patterns, developmental constraints, and morphospace occupation (Rasskin-Gutman, 2005; Dera et al., 2008). Following this approach, we have previously studied Williston's Law in a broad sample of tetrapod skulls, including all major phylogenetic groups (see Chapter 9). Our results suggested that the loss of poorly connected bones constitutes a mechanism that underlies a general trend toward an increase in morphological complexity and variation in the degree of integration. In addition, the human skull network showed the highest degree of morphological complexity in terms of structural organization, integration, and biomechanical or functional efficiency. This prompted us to further investigate the network structure of the human skull as a null model to provide new insights on its integration and modularity in an evo-devo context.

Here we show that the human skull is a small-world network with two differently organized connectivity modules, cranial and facial. The facial module has a hierarchical sub-modular structure in blocks, which we have named frontonasal, left maxillary, right maxillary, and ethmoidal blocks. The cranial module lacks this kind of internal organization; rather, its structure resembles that of a regular network. The significance of these results is discussed together with the morphogenetic processes involved in skull development and evolution within a general trend of bone loss and fusion in the evolution of tetrapod skulls. In the following sections, we extend the conceptual framework introduced

in Chapter 5 to analyze morphological networks, providing the necessary background to put our results in context.

Integration and Biological Burden

Morphological integration is generally defined as the covariation among morphological structures due to common developmental and functional causes (Olson and Miller, 1958). Given the role of craniofacial sutures in bone growth (Opperman, 2000; Rice, 2008), intracranial movements of bones (Jaslow, 1990), and strain sinks (Rafferty et al., 2003; Moazen et al., 2009), it is reasonable to expect that bones with more suture connections have central structural and functional roles affecting the morphology of the entire skull; in other words, the higher the number of connections, the stronger the functional and developmental dependencies (structural constraints). This association between the number of connections and the intensity of constraints, due to acquired developmental and evolutionary compromises, immediately resonates with 'biological burden' (Riedl, 1978; Wimsatt, 1986; Schoch, 2010). The concept of burden neatly links development and evolution (Wagner and Laubichler, 2004) and underlies the evolutionary pattern of skull bone reduction in Williston's Law.

'Small-Worldness' in Morphological Networks

Network structures can be assessed in different ways. While the number of connections for each bone defines its burden rank, there are other network parameters that quantify morphological integration for the entire skull, such as the clustering coefficient and characteristic path length (see 5.2.2). These parameters capture information about the degree of integration of the entire skull, the former by quantifying short-range feedback loops, and the latter by quantifying effective proximity. Together, by comparing them with random networks, they can be used to detect the presence of a special kind of network configuration that is known as small-world (Watts and Strogatz, 1998, see also 5.2.4). Small-world networks are more clustered than random ones (sometimes even more than regular networks), and yet the effective proximity between elements is as small as it is in random networks. One consequence of this order in small-world networks is the emergence of modularity because of the heterogeneous pattern of connections (Pereira-Leal et al., 2006; Gallos et al., 2012). Correcting for network size, small networks (as in a skull) can also be tested for 'small-worldness' (see Methods). In addition, this type of organization in a skull would indicate that bones connect to each other following a certain order, one that

lies between regularity and randomness. Riedl already recognized that morphological systems have this dual organization and defined this as *"a region of unspecified probability, a no-man's-land between accident and necessity."*

Skull Modularity

Morphological integration and modularity are strongly linked concepts; modularity emerges as a consequence of the presence of heterogeneous patterns of integration. Indeed, we are able to perceive parts in a system only because these parts are integrated differently within the system (Klingenberg, 2008)–that is why regular systems lack sub-divisions. To identify the parts of the system (modules) and the strengths of their interaction (integration) we need a precise and operative definition of module and modularity as it relates to integration (for general reviews of the modularity concept see Schlosser and Wagner, 2004; Callebaut and Rasskin-Gutman, 2005). In the context of network analysis, quantifying connectivity patterns readily accomplishes this. In a skull network, a connectivity module is a highly connected group of bones (see5.2.4) allowing a precise detection of modules by using general network analysis tools. It is important to note that datasets to infer connectivity modules are totally different from the ones used to infer other morphological modules, such as variational ones (e.g., Mitteroecker and Bookstein, 2007; Wagner et al., 2007; Klingenberg, 2010). In connectivity modules raw data is taken from connections between morphological units, whereas in variational modules it is taken from the shapes of these units.

Skull Bone Hierarchy

Various studies reported different shape and growth rates for different skull regions, suggesting that the human skull is organized hierarchically (reviewed in Bastir, 2008). In networks, there is a hierarchical organization when nodes within modules tend to group in highly clustered sub-modules or blocks (Ravasz et al., 2002). In many biological networks, this type of analysis suggested that some network elements specialize in different roles related to the maintenance of the network architecture and function (Guimerà and Nunes-Amaral, 2005). For instance, in metabolic networks, nodes with few connections tend to cluster into blocks, while highly connected nodes integrate those blocks into modules (Jeong et al., 2000); this is the case also in brain networks (Meunier et al., 2010). Finding a hierarchical organization in the network model would suggest that along with

shape and growth, connectivity patterns are also involved in the hierarchy of the human skull.

Skull Bone Connectivity Role

In modular structures that exhibit a hierarchical organization, each component has a connectivity role, based on which level it occupies in the hierarchy. Network analysis tools allow a quantitative definition of these roles (see 5.2.2 and 5.2.2). The relationship of individual bone connectivity pattern within and between modules gives each bone a specific structural role. Bones that are above in the hierarchy are those that contribute greatly to integration between blocks or modules. Some bones are keystones that hold together all the bones in a module by having a high number of connections within the module (*local hubs*); some bones are also highly connected but their connections are shared between modules (*connector hubs*); and some are scarcely connected within or between modules (*local* and *connector non-hubs*). As we will show, each role has different theoretical relevance for integration and modularity in the development and evolution of the human skull.

Material and Methods

Network Analysis

The materials and methods used to build and analyze the adult human skull network have been described in Chapter 4.

Morphometric Analysis of Network Modules

We tested the correspondence between connectivity and variational modules, using a geometric morphometric analysis. We used growth allometries to characterize different developmental units; with this method, a module is taken as a developmental unit if it shows a specific allometric growth pattern with the expectation that the best modularity hypothesis is the one that, summing the variance of both modules, explains most of the overall skull variance (Rosas and Bastir, 2004). We used a total of 51 landmarks and semilandmarks digitized on lateral radiographs from a full ontogenetic sample (n=225) of 28 individuals of the Denver Growth Study (see Bastir et al., 2006, for a detailed description of the sample, technical information, and landmarks location). These landmarks capture information from external and internal structures of the human skull projected on the

sagittal plane. Although a full 3D dataset could bring more information, major portions in human craniofacial growth occur antero-vertically (i.e., sagittally) in the skull (Enlow, 1990; Enlow and Hans, 1996); this has been demonstrated in both 2D and 3D growth studies (Bastir and Rosas, 2004; Bastir et al., 2006, 2007). Hence, given the nature of our sample, we are capturing most of the relevant variation needed to test the modularity hypothesis.

We performed multivariate regressions of shape on size. We tested for overall skull centroid size and partition-specific centroid size. Each shape consisted of combinations of landmarks that represented different modules according to different modularity models: one based on network modules (Model A) and three alternative ones (Models B, C, and D) to further test the results of the connectivity hypothesis. We based the composition of these four models on the results of the connectivity analysis, which yielded two distinct modules, facial and cranial. Since two bones–the frontal and the zygomatics–were shown to act as connectors between both modules, we further tested alternative modularity hypotheses to explore the validity of the connectivity hypothesis. Thus, Model A represents the result of the network analysis; Model B considers the zygomatics as part of the face; in Model C the frontal is in the cranial module; and in Model D the zygomatics are in the facial and the frontal in the cranial module. We performed these multivariate regression analyses in MorphoJ (Klingenberg, 2011).

Results

Network Parameters

We modeled the human skull as a network (Fig. 12.1A) and analyzed its structure. The clustering coefficient is 0.634 and the characteristic path length is 1.741. These values exceed by more than two times the SD of those observed in the random equivalent networks simulated ($\overline{C}_{rand} = 0.444$, SD = 0.036; $\overline{L}_{rand} = 1.678$, SD = 0.019). Accordingly, $[(\overline{C}/\overline{C}_{rand})/(\overline{L}/\overline{L}_{rand})] = 1.3762$, which is also higher than that expected for a random network of the same size as the human skull (0.35). This indicates with confidence that the human skull network is small-world. In addition, both $P(k)$ and $C(k)$ distributions fit a power-law function (Fig. 12.1B-C), which indicates a hierarchical organization of connections. The ethmoid, the frontal, and the sphenoid bones show the highest burden-rank estimated by their significant above-average number of connections (13, 12, and 12). Table 12.1 summarizes the values of all calculated parameters for the human skull

network and each single bone.

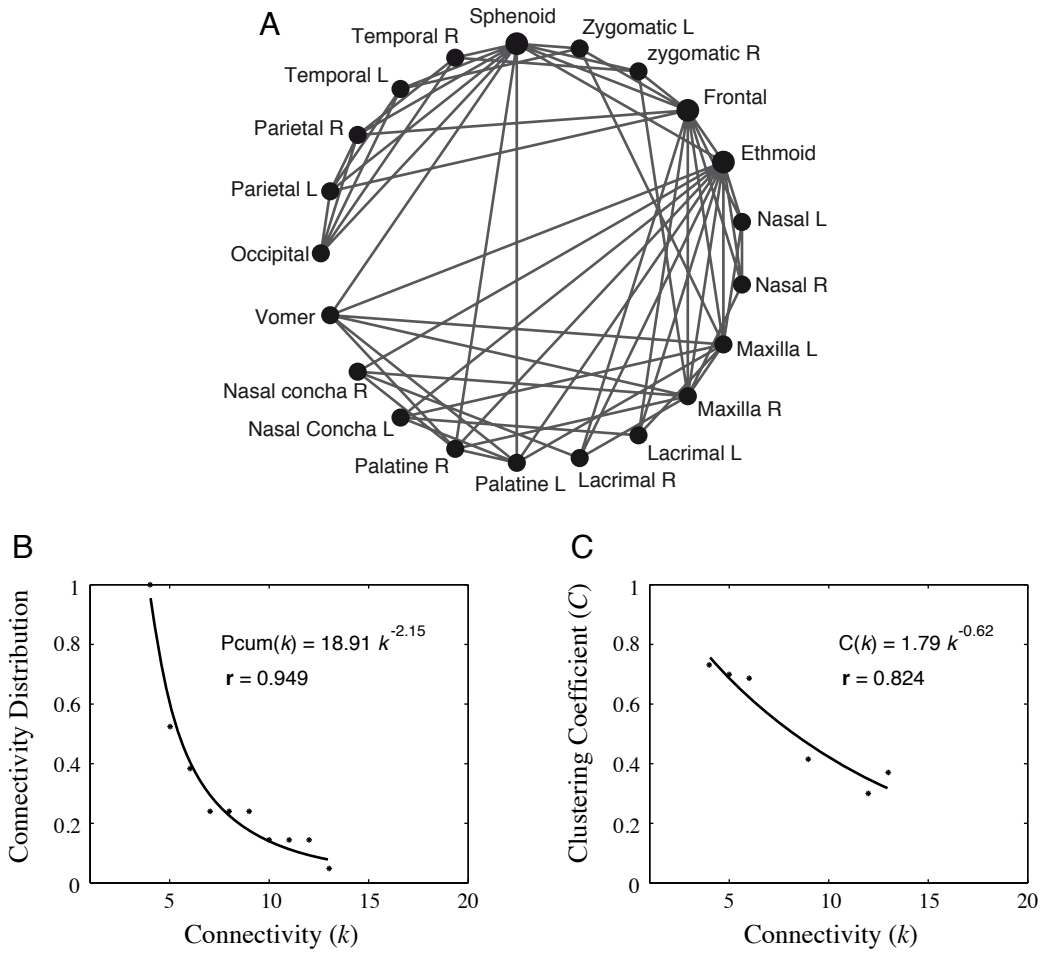

Figure 12.1: Connectivity pattern of the human skull network model. (A) Circular graph. (B) The cumulative connectivity distribution shows that the frequency of bones decays with the number of connections as a power-law. (C) The clustering coefficient distribution also follows a power-law function, showing an inverse relationship between the number of connections and the clustering coefficient. The fit of both distributions to a power-law function indicates a hierarchical organization of connections in the human skull network (see 4.1.4).

Table 12.1: Human skull whole network and single bone parameter values

	k_i	C_i	L_i	P_i	Z_i
Human Skull	–	0.63	1.74	–	–
Ethmoid	13	0.37	1.35	0.14	2.6
Frontal	12	0.30	1.40	0.49	0.54
Inf. Nasal Concha	4	0.83	2.1	0	-0.70
Lacrimal	4	0.83	1.95	0	-0.70
Maxilla	9	0.42	1.65	0.20	0.95
Nasal	4	0.83	1.95	0	-0.70
Occipital	5	0.7	2.15	0	0.62
Palatine	6	0.67	1.7	0.28	-0.28
Parietal	5	0.7	1.85	0.32	0
Sphenoid	12	0.30	1.4	0.49	1.87
Temporal	4	0.67	2.15	0	0
Vomer	6	0.73	1.7	0.28	-0.28
Zygomatic	4	0.5	1.85	0.5	-1.25

Modularity and Bone-Role

The analysis of modularity yields two modules (Fig. 12.2). The first module (facial) groups together the frontal, ethmoid, inferior nasal conchas, vomer, maxillas, lacrimals, nasals, and palatines. The second module (cranial) groups together the sphenoid, occipital, parietals, temporals, and zygomatics. The hierarchy test shown in the previous section indicates that the human skull has a hierarchical structure. However, looking at each module separately, we observe that only the facial module shows a clear hierarchical structure further sub-divided into four blocks. In contrast, the cranial module shows no hierarchical structure, as a consequence of a more regular pattern of connections. We name each block in the facial module after the most connected bone present in it. Accordingly, the four blocks are: (1) frontal, composed of frontal and nasal bones; (2) left and (3) right maxillary, composed of the respective left and right maxilla, lacrimal, and nasal concha bones; and (4) ethmoidal, composed of ethmoid, vomer, and palatine bones. The length of the dendrogram branches for each block indicates that they are highly consistent (see Jain and Dubes, 1988).

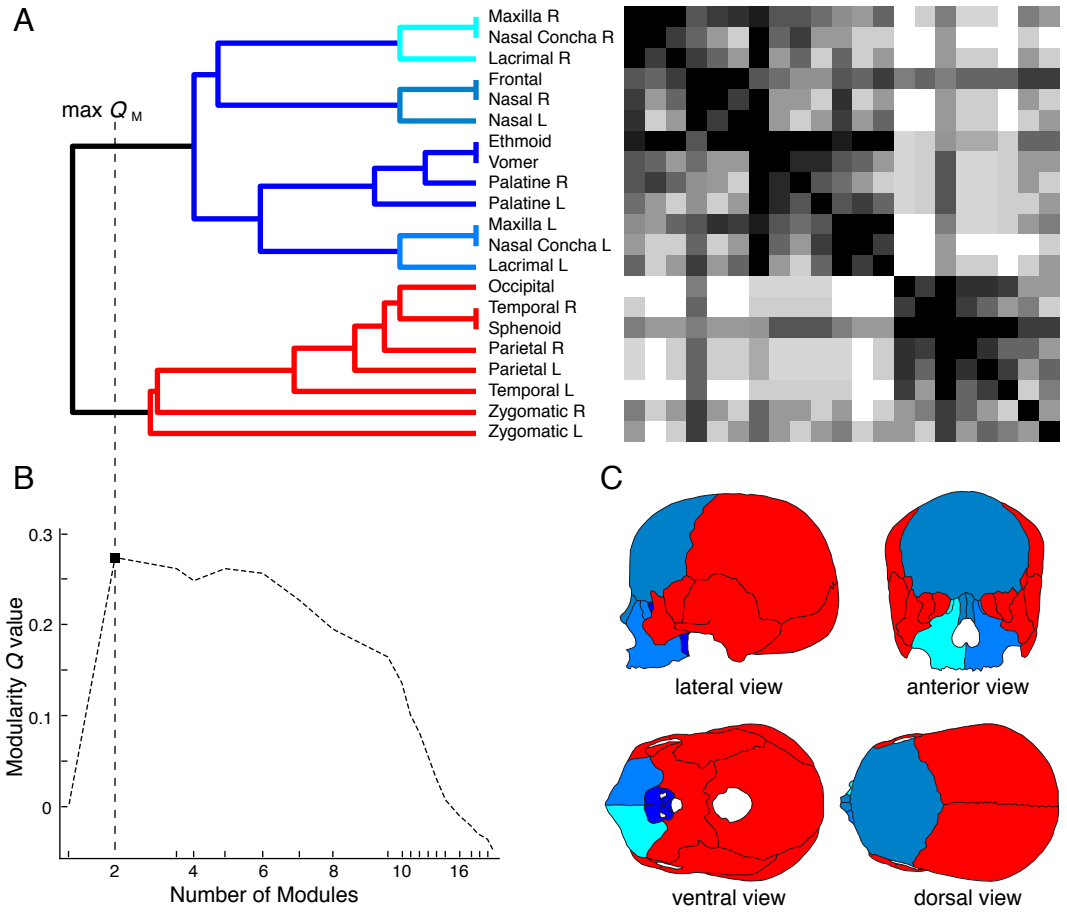

Figure 12.2: Analysis of modularity in the human skull network. According to the topological overlap matrix of similarity (A *right*), the cluster analysis shows two modules (A *left*) based on the highest Q value (B). The dendrogram also shows that only the facial module has a hierarchical internal sub-organization in four blocks of spatially related bones. (C) Each module and block is shown in different views: the cranial module is colored in red and the four blocks that compose the facial module are colored in different shades of blue.

The values of parameters Z_i and P_i within this modular organization classify each bone into one specific structural role[1] (Fig. 12.3): the ethmoid has its connections within the facial module (local hub); the sphenoid spreads its many connections between the facial and cranial modules (connector hub); the frontal and zygomatics are more involved in connecting the facial and cranial modules than in participating in their internal integration (connector non-hubs); and the vomer, the occipital, maxillas, temporals, parietals, lacrimals, nasals, nasal conchas, and palatines just contribute their few connections to their own module (local non-hubs).

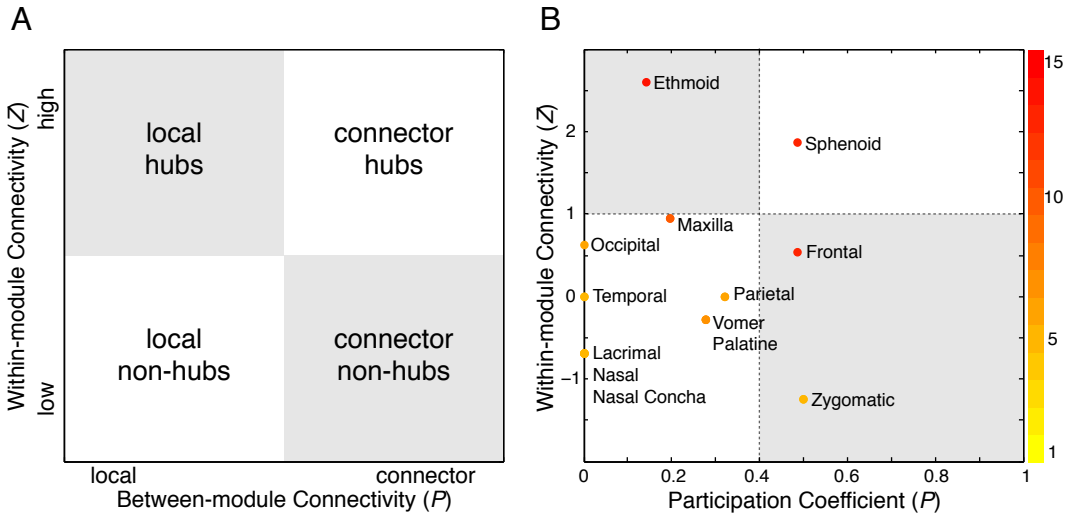

Figure 12.3: The role of each bone in the modular organization of the human skull is given by its position in the ZP space. (A) According to the number of connections within and between modules, four categories of bones can be defined: local hubs, connector hubs, local non-hubs, and connector non-hubs. (B) For the human skull the P_i value that discriminates between local and connector role is 0.4, while the Z_i value that discriminates between hubs and non-hubs is 1. Notice that burden-rank alone, indicated by the colored bar, cannot discriminate between hubs (ethmoid and sphenoid) and non-hubs (all other bones) as classified in the ZP space.

[1]For this article the Z_i threshold to discriminate between hubs and non-hubs was 1 insted of 2, which was used for the broader comparative analysis in Chapter 10.

Network Modules and Morphometrics

All regressions were highly statistically significant at $p < 0.001$ assessed from 1,000 randomizations. The amount of explained variance varied slightly according to whether we used the same overall skull size for both partitions or each partition-specific centroid size. Figure 12.4 shows the sum of total variance explained by both modules (cranial in red and facial in blue) for four alternative models. Model A explains most of the total variance, and performs slightly better than Model B; both of them perform better than Model C and Model D, thus supporting the result of the modularity hypothesis based on the network analysis.

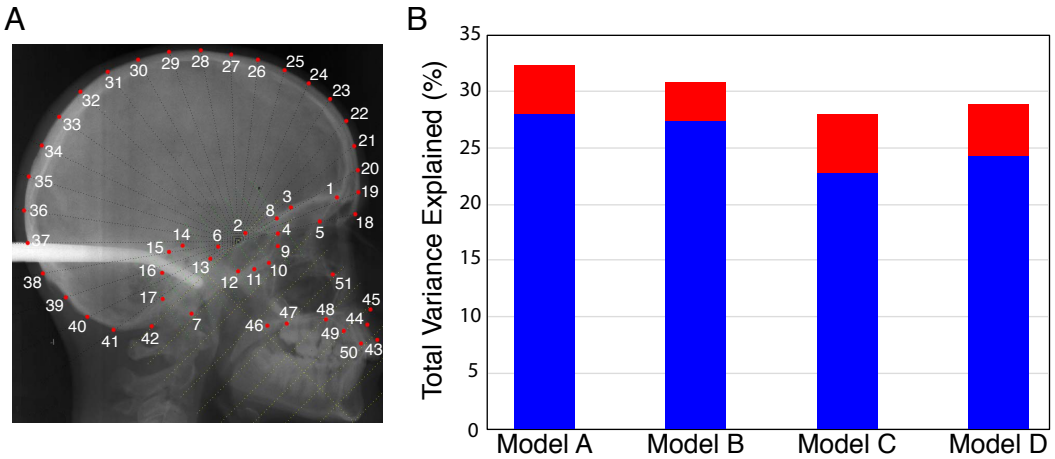

Figure 12.4: Maximum allometric growth variation test of connectivity modules using multivariate regression of shape on size. (A) Landmarks used in the analysis; mandibular landmarks have been excluded (landmarks 43, 44, 45, 46, 47, 48, 49, 50, and 51 in the figure correspond to landmarks 58, 59, 60, 61, 62, 63, 64, 65, and 66 in Bastir et al., 2006). (B) Results indicating the sum of total variance explained for the four alternative models of two partitions (blue, facial module; red, cranial module) for partition-specific centroid-size adjustment. Model A represents modularity as defined by the network analysis. Facial module: frontal, ethmoid, inferior nasal conchas, vomer, maxillas, lacrimals, nasals, and palatines; cranial module: sphenoid, occipital, parietals, temporals, and zygomatics. In Model B, the zygomatics have been shifted to the facial module. In Model C, the frontal has been shifted to the cranial module. In Model D, the zygomatics have been shifted to the facial module whereas the frontal has been shifted to the cranial module. Note that Model A explains the maximum amount of total variance; hence it supports the network modularity hypothesis.

Discussion

We have shown that the pattern of connections between bones in the human skull is neither regular nor random. Instead, it follows a small-world organization that promotes the formation of highly integrated connectivity modules: (1) an anterior facial module, related to face and palate; and (2) a posterior cranial module, related to the cranial vault and base. The internal structure of each module is different: the facial module shows a hierarchical pattern sub-divided in blocks (frontonasal, left maxillary, right maxillary, and ethmoidal), whereas the cranial module exhibits a non-hierarchical, regular structure. Within these modules each bone has a distinctive connectivity pattern that allowed us to identify their structural role within the skull. In particular, three bones turn out to have key roles: the ethmoid, the sphenoid, and the frontal. The ethmoid bridges the blocks of the facial module; the sphenoid gives more cohesion to the regular structure of the cranial module and, along with the frontal, connects both modules together (a task shared with the zygomatics). It is worth noting that the connectivity modules resemble the classical, intuitive division of the human skull in an anterior face and a posterior cranial vault. However, our results support the adscription of the frontal and ethmoid bones to the facial module (Hofer, 1965; Bastir et al., 2006). Furthermore, the ethmoidal block resembles the nasal capsule, an embryological, morphological, and evolutionary unit with a distinctive pattern of integration within the face (Bastir and Rosas, 2011). As noted, the zygomatics also play a key structural role in the skull by connecting both modules together, although their connectivity pattern make them part of the cranial module. However, this integrative role influences both cranial vault and facial growth and shape (e.g., orbits and zygomatic arch; reviewed in Lieberman, 2011), functionally redistributing tensile and compressive forces between skull regions (Witzel et al., 2004). Along with the other connector bones (frontal and sphenoid), the zygomatics provide inter-module integration, which could partly explain why it is so difficult to identify variational modules in the human skull (Martínez-Abadías et al., 2012).

Growth Correlates of Connectivity Modules

Traditionally, the human skull is divided in three modules–an anterior face, and posterior neurocranium and basicranium–a division which has long been accepted based on genetic, developmental, and phenotypic shape variation criteria (reviewed in Bastir, 2008). However, a recent work by Martínez-Abadías et al. (2012) has challenged this general modularity hypothesis showing that morphometric modules cannot be clearly delimited

(i.e., they show a stronger co-variation within modules than between them), highlighting the weakness of these criteria to delimit *"true modules"* in the human skull. In other words, any a priori assumptions depend on genetically and environmentally determined factors that overlap in such an intricate way as to make it impossible to discern modules with certainty. These difficulties have been extensively reviewed under the concept of the palimpsest model of covariation structure, which precisely argues that covariation factors influence each other over time, making the reverse analysis of trying to decipher those factors from phenotypic data a daunting task (Hallgrímsson et al., 2009).

Our approach tackles the problem from a completely different perspective, using the information encapsulated in connectivity patterns from which the modules are obtained. This allowed us to make a morphological a priori hypothesis of modularity and then to test it with morphometric tools based on independent landmark data. This test is based on maximum allometric growth variation; thus, the results suggest that there are growth patterns at play that determine connectivity patterns in the skull. Furthermore, the different internal structure of each connectivity module–hierarchical for the facial and regular for the cranial–also points in the same direction. As a consequence, our connectivity modules resemble, to a great extent but not completely, the ethmomaxillary and neurobasicranial complexes proposed as developmental units with different maturation timing (Enlow, 1990; Enlow and Hans, 1996; Bastir et al., 2006). Why this should be the case is neither trivial nor expected, since there is no need for one-to-one correlation between modular network organization and modular allometric variation (Eble, 2005; Hallgrímsson et al., 2009). We think this correlation occurs in the human skull because the allometric mechanisms of growth determine connectivity patterns, which, in turn, influence the individual shape of each skull bone. If this is true, skull networks could be interpreted as shape correlation maps (for a related approach, see Chernoff and Magwene, 1999; Magwene, 2001, 2008).

Bones within the same connectivity module share the same allometric growth pattern. Therefore, the best modularity hypothesis has to be the one that explains most of the total variance of the skull shape during ontogeny. We used the morphometric analysis to compare Model A (based on our connectivity hypothesis of modularity) to three alternative models, which were constructed by shifting connector bones (zygomatics and frontal) to a different module. Results indicated that Models A and B explain better the allometric patterns than Models C and D. Furthermore, Model A explains better the total variance than Model B, in which zygomatic bones are part of the face. This result supports the placement of the frontal bone as a facial element and of the zygomatic bones as cranial elements, as the analysis of connectivity patterns revealed.

Bone's Burden-Rank

The integration of modules and blocks in the human skull relies on three main bones: the ethmoid, the sphenoid, and the frontal; by themselves, they account for more than half of all connections in the skull network. The three bones have developmental and evolutionary origins that fit nicely within the concept of evolutionary burden: their formation during development is the result of many fusions of different ossification centers (Opperman, 2000; Rice and Rice, 2008); and the evolution of each can be traced back at least to the origin of early mammals as the fusion of several distinct bones (Sidor, 2001; Depew et al., 2008). Both the sphenoid and the ethmoid bones are the evolutionary result of the fusion of an original unpaired bone with several neighboring paired (e.g., pterygoids, orbitosphenoids, and cribriform plates) and unpaired (e.g., basisphenoid, parasphenoid, and presphenoid) bones (Goodrich, 1958; Romer and Parsons, 1977). The link between development and evolution is paradigmatic for the frontal bone. The frontal bone develops as two paired bones early in the ontogeny of the human skull; these paired frontals will fuse totally during the first years of life, giving rise to the unpaired condition of the adult frontal (Weinzweig et al., 2003). Evolutionarily, frontal paired bones are a primitive condition in primates; the closure of the metopic suture (interfrontal) occurred several times independently within this group and before the origin of anthropoids (Rosenberger and Pagano, 2008). The morphogenetic process underlying this pattern relates to different timing in the closure of skull bone sutures at an evolutionary scale (Morriss-Kay, 2001; Richtsmeier et al., 2006), which can sometimes cause severe pathologies in the human skull, known as craniosynostosis (Heuzé et al., 2011; Percival and Richtsmeier, 2011).

As a consequence of multiple fusions, these evolutionarily new unpaired bones have a higher number of connections, increasing their functional and developmental dependencies with other bones. A high number of dependencies (i.e., connections) and being above in the hierarchy of the structure are two of the characteristics that identify anatomical elements with high burden-rank (Riedl, 1978; Schoch, 2010). Given the multiple tasks of sutures–sites of skull growth, intracranial movements, and strain sinks (Jaslow, 1990; Opperman, 2000; Rafferty et al., 2003; Rice, 2008; Moazen et al., 2009)–it is reasonable to expect that bones that participate in many sutures have central developmental and functional roles as well, possibly affecting the entire skull morphology. This observation carries with it a general evolutionary implication: some bones (those with higher burden-rank: sphenoid, ethmoid, and frontal in the case of the human skull) will be more difficult to be lost than those that are less connected (see Chapter 9). Indeed, it is known that

bones that have few connections, such as the jugal, postfrontal, postorbital, prefrontal, and supratemporal, have been repeatedly lost in many tetrapod lineages (see Table 1.1). This has been additionally confirmed by computer simulations, within a thorough phylogenetic analysis for all major groups in tetrapods, including mammals, and has been suggested as the basis for the reduction in skull bone number as seen in Williston's Law (Esteve-Altava et al., 2013b,c).

How bones are connected to each other will directly affect their possibility for shape change, as they form ontogenetic growth units during development; conversely, changes in shape bone proportions will directly affect the overall skull connectivity pattern (Rasskin-Gutman, 2003). To further explore this claim, a strong effort has to be made to study pair-wise bone shape-covariation that can be related to skull connectivity patterns of organization. To our knowledge, there is a lack of modern studies systematically analyzing the relationship between shape and connectivity in the entire skull, which is the type of information needed to test our claim that connection dependencies impose structural constraints on shape bone proportions. However, Pearson and Woo (1935) carried out a pioneering study analyzing craniometrical measures on single bones in human skulls, concluding that adjacency (i.e., connectivity) was the second most important factor of shape correlation after symmetry.

All in all, connectivity relations can be directly interpreted as correlations of changes in size and shape due to their developmental role as sites of bone growth. In sum, connections are a fundamental source of morphological integration and modularity in the human skull. This cannot be otherwise, since the interplay between development and evolution has determined the co-dependencies among the skull bones, burdening those with more sutural connections while freeing the remaining ones to undergo independent variation. And that is more grist in Rupert Riedl's mill!

12.2 Complexity and Integration in Skull Network Models of Craniosynostosis

Abstract – Craniosynostosis is a pathological condition in which some sutures of a juvenile skull close too early in development. The premature closure of skull bone sutures affect primates, including humans, as well as other tetrapods. Because they can be in many instances phenotypically viable for the individual, their phenomenology can be used as a model for macro-evolutionary skull bone reduction in mammals. Network analysis was used to model and compare changes in connectivity properties of bones in skulls with craniosynostosis: metopic, sagittal, coronal, unilateral lambdoidal, and bilateral lambdoidal. In particular, how changes in connectivity patterns due to craniosynostosis affect the morphological integration and modular organization of the human skull network. Results indicated that the relationship among bones in the human skull is strongly dependent on connectivity distance. This opens new ways to study the correlation of size and shape changes in skull bones as a function of how bones are connected to each other, the presence of hub bones, and the formation of bone clusters.

Introduction

The reduction in number of skull bones is a macro-evolutionary trend in all tetrapod lineages (Esteve-Altava et al., 2013c). This reduction occurs mainly due to two developmental processes: the loss and the fusion of bones (see Chapter 9). The skull of primitive tetrapods is composed of approximately 60 bones, while derived forms have around 30 and even less. Reduction in the number of bones also occurs during ontogeny; for example the adult human skull has typically 21 bones, while the newborn skull has 25 bones (Fig. 12.5). In the mammalian skull, losses are common for pre- and post-frontal, postorbital, and quadratojugal bones (Hildebrand, 1988; Benton, 1990; Kardong, 2005, see also 1.2.1); while fusions of bones generally involve the formation of unpaired bones in the sagittal plane, such as the occipital, the sphenoid, and the frontal bones. In an evolutionary context, bone fusion is a source of variation and novelty in the connectivity pattern of the skull related to bone number reduction and skull shape changes (Richtsmeier et al., 2006; Esteve-Altava et al., 2013c, see also 12.1). Moreover, a premature fusion of bone is also an example of heterochrony (i.e., a change in timing of developmental events), which

is common during skull evolution.

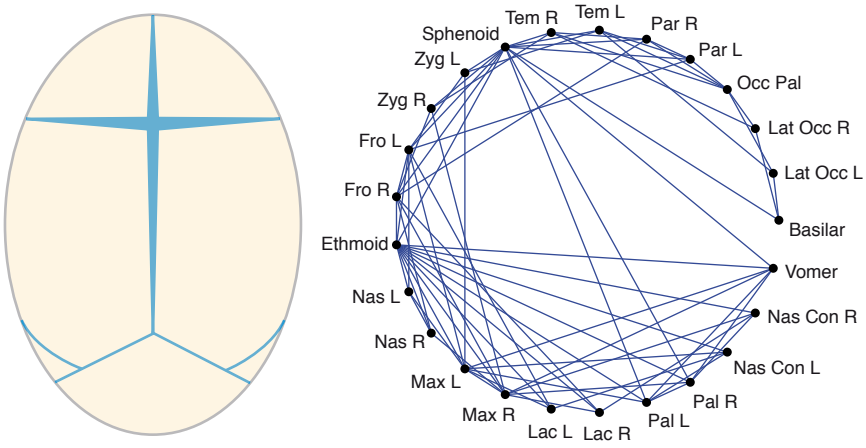

Figure 12.5: Newborn skull network with a schematic dorsal view. *Labels: Con, concha; Fro, frontal; Lac, lacrimal; Lat, lateral; Max, maxilla; Nas, nasal; Occ, occipital; Pal, palatal; Par, parietal; Tem, temporal; Zyg, zygomatic; L, left; R, right.*

From a medical point of view, the premature fusion of bones is a pathological condition in human newborns known as craniosynostosis (Fig. 12.6). This condition is often related to congenital dysmorphologies of the skull because it prevents further bone growth in the obliterated suture, which is compensated with growth in other parts of the skull, such as the cranial vault, orbits, and face (Hukki et al., 2008; Heuzé et al., 2011). Severity of skull malformations (shape modifications) depends on which sutures are affected, the extension of the obliteration, and the number of sutures fused at the same time; thus, effects range from totally asymptomatic forms to great abnormalities (including death). Craniosynostosis can occur isolated or as part of a more severe syndrome, and as a consequence of genetic, mechanical, or environmental factors (Percival and Richtsmeier, 2011). For instance, some genetic disorders, such as the Apert and Crouzon syndromes, are associated with craniosynostosis in one or several sutures leading to severe malformations (Rice, 2008); however, in most newborns, craniosynostosis do not generate severe malformations (Hukki et al., 2008). Usually, non-syndromic craniosynostosis involve non-inherited premature fusion of only one suture.

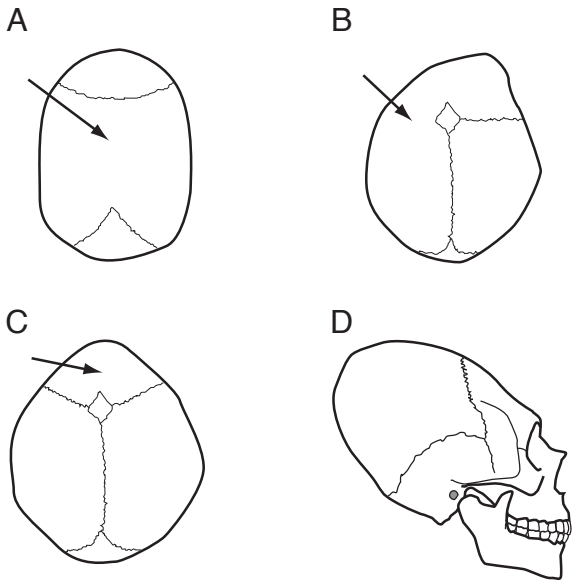

Figure 12.6: Example of skull shape changes caused by the premature fusion of cranial skull bones in humans. A) Scaphocephaly by premature fusion of the sagittal suture. B) Plagiocephaly by premature fusion of the coronal suture. C) Trigonocephaly by premature fusion of the metopic suture. D) Turricephaly by premature fusion of the coronal and the lambdoid sutures. From Lieberman (2011).

Here, we approach craniosynostosis as a developmental model of the evolution of the organization of suture connections among bones in the skull. By means of a unified mathematical framework, network theory, we explore if an isolated premature fusion can cause shifts in connectivity patterns like those observed in large-scale evolution (Esteve-Altava et al., 2013c). In addition, we quantify the effects of craniosynostosis in connectivity properties of the remaining bones that might affect shape changes. To do so, we built and analyze network models of juvenile human skulls, with and without craniosynostosis, and quantify changes in connectivity patterns of skulls and bones.

Material & Methods

Network Models of Craniosynostosis

The skull network of a normal child at birth, with paired frontals and occipital bones not fused, was compared to network models for each of the following craniosynostosis

conditions (Fig. 12.7): (1) metopic, paired frontals fused at the metopic suture forming an unpaired frontal bone; (2) sagittal, parietals fused at the sagittal suture forming an unpaired parietal bone; (3) left hemicoronal, left parietal and left frontal fused at the coronal suture forming a frontoparietal bone (*Fp*); (4) bicoronal, parietals and frontals fused at the coronal suture forming two frontoparietal bones; (5) lambdoidal, occipital plate and left parietal fused at the lambdoidal suture forming an unpaired occipitoparietal bone (*Op*); and (6) 'true' lambdoidal, occipital plate, left parietal, and left temporal fused at the lambdoidal and occipitomastoid sutures forming an unpaired occipitoparietotemporal bone (*Opt*).

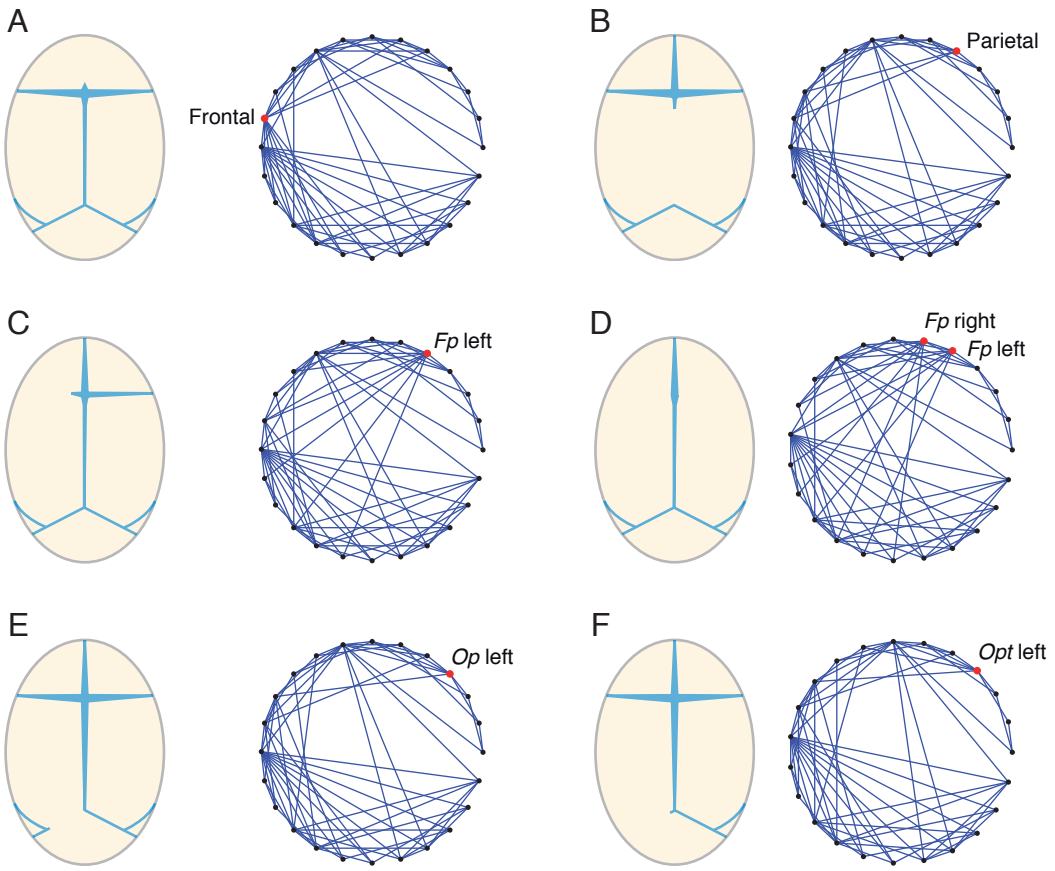

Figure 12.7: Skull networks with craniosynostosis in A) the metopic suture, B) the sagittal suture, C) the left hemicoronal suture, D) the bicoronal suture, E) the lambdoidal suture, and F) the lambdoidal plus occipitomastoid suture. Red dots indicate the new bone formed by the fusion event.

To estimate the complexity and structural organization of each network we measure the following network parameters: density of connections, mean clustering coefficient ($\overline{C}$), mean shortest path length($\overline{L}$), heterogeneity(H), and unpaired bone ratio (UBR); see Chapter 4 for description of each parameter. For individual bones, an additional parameter has been quantified in order to detect more subtle changes between related networks: the node betweenness centrality (Eq. 12.1), which is a variation of the shorest path length that measures the central position of a node in the network:

$$BC_i = \sum_{p \neq q} \frac{SP(p,i,q)}{SP(p,q)}, \tag{12.1}$$

were *SP(p,i,q)* is the sum of all shortest paths from node p to node q that passes through node i; *SP(p,q)* is the sum of all shortest paths from p to q. For each bone, the BC_i has been evaluated, before and after craniosynostosis, to test whether effective proximity (i.e., $\overline{L}$) of other bones to fused bones affects their connectivity.

Results & Discussion

System Descriptors in Newborns and Craniosynostosis

Newborn skull networks with and without craniosynostosis show slight differences in complexity and integration parameters. Table 12.2 summarizes the network analysis on each skull network.

Table 12.2: Analysis of skull networks with craniosynostosis.

Suture Fusion	*Density*	$\overline{C}$	$\overline{L}$	H	UBR
None (Newborn)	0.2433	0.5067	1.9936	0.4960	0.2
Metopic	0.2536	0.5341	1.9653	0.5072	0.25
Sagittal	0.2536	0.5125	1.9792	0.4892	0.25
Coronal	0.2572	0.5233	1.9236	0.5147	0.2083
Bicoronal	0.2688	0.532	1.879	0.4915	0.2174
Lambdoidal	0.2536	0.5228	1.934	0.5147	0.2083
True Lambdoidal	0.2648	0.5194	1.913	0.5140	0.2174

When comparing the values of the newborn skull with those of the abnormal ones, we observe a slight increase in skull complexity (i.e., increase in De and $\overline{C}$, decrease in $\overline{L}$); this pattern of change is similar to that observed in the evolution of tetrapods in general, and synapsids in particular (Esteve-Altava et al., 2013c, see also Chapter 9). In the same manner, anisomerism is not observed in the variation of H), but in the increase of the UBR (otherwise normal, according to the phenomena studied). Thus, although there is a net reduction of the number of bones in the skull networks after craniosynostosis, only one connection is lost (by obliteration). This causes an increase of connections in bones involved in the fusion and their neighbors, increasing the density, but also the clustering coefficient; consequently, the shortest path lengths between bones decreases.

Effect of Effective Proximity in the Centrality of Bones

The BC_i measures the importance of a node in the network, in terms of the number of paths that crosses it. The more paths crossing a node, the more important this node is for the network structure (Goh et al., 2001). Figure 12.8 shows the variation of BC_i of bones in skulls after craniosynostosis depending on their distance to the fusion.

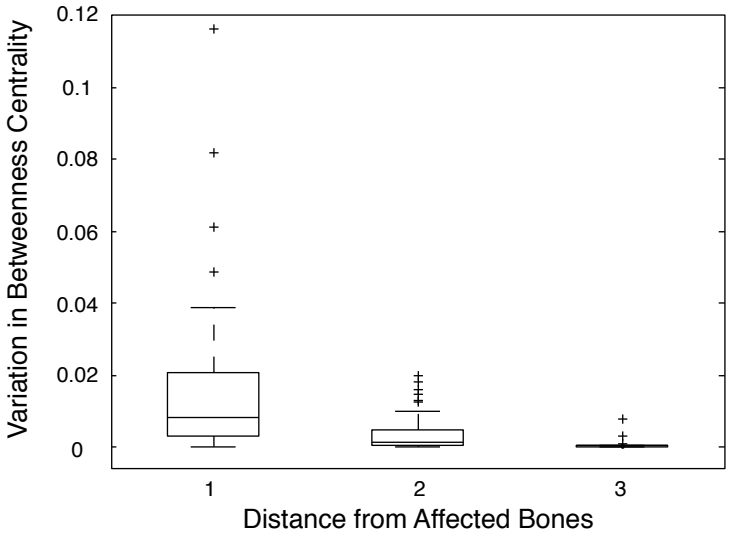

Figure 12.8: Betweenness centrality variation depending on the distance of each bone to fused bones. The farther the distance to the fusion, the minor the changes in connectivity of bones.

After a fusion event, connectivity relations among bones change; these connectivity changes not only affect those bones directly involved in the fusion, but also others. The effects of changes in connectivity are transmitted to other parts of the skull network, with more or less intensity, depending on the effective proximity between bones. Other node parameters (k_i, C_i, and $\ell_{i,n}$) show no sign of variation after only one fusion event, so they are not informative of the effect of the effective proximity in the skulls analyzed.

The influence of effective proximity in the spread of changes in connectivity suggests how information is transmitted in the skull after craniosynostosis: according to connectivity distances between bones, rather than geometric distances. The key role of the sutures as primary sites of bone growth are likely to be the main cause why this effect occurs. Indeed, after a premature fusion, bone growth occurs in other directions to compensate this blockade, especially in parallel with the lost suture (Sperber, 2001), but also at other sutures without any known preference (Jane and Persing, 2001). In this respect, a network approach sets the preference of transmission of such morphological changes towards the bones closer in connectivity distance.

Concluding Remarks

The human skull exhibits a high level of plasticity: variation is the rule, not the exception. Pathological variations, such as craniosynostosis, should always be put in a broader, evolutionary context, which brings a new perspective to understand. Thus, craniosynostosis reproduces at an ontogenetic scale the evolutionary patterns found in Williston's Law (see Chapter 9): an increase in morphological complexity but not in heterogeneity. This result further reinforces the relation between bone fusion and the evolutionary increase of morphological complexity in the skull (see Chapter 9), by offering a developmental basis to this evolutionary pattern.

12.3 Connectivity Modules in Skull Network Models of Craniosynostosis

Abstract – Premature fusion of bones changes the connectivity patterns that determine the modular organization of the skull. Modularity analysis were performed for each of the above described craniosynostosis conditions. Three theoretical factors affecting skull modularity were evaluated: the formation of unpaired bones during development, the importance of asymmetry in connectivity patterns, and the importance of the number of bones fused in forming different modular organizations. Results suggest two general rules related to bone fusion and the formation of connectivity modules: (1) not all bones fused along the midline generate bilateral modules, only those with a specific connectivity pattern that makes possible a left-right integration; and (2) fusion of paired bones in contralateral sides do not generate, *per se*, significative changes in connectivity patterns.

Introduction

The fusion of bones is a developmental process that can have important evolutionary consequences, for example, in the morphological complexity of the skull (see Chapter 9); however, when fusions occur prematurely, they cause different pathological disorders, as has been shown in the previous section. Fusions also affect the formation of connectivity modules, specially, when they produce new unpaired bones (see 10.2). Here, I analyze the effect of craniosynostosis in the modular organization of the human skull by comparing the modular organization of skull networks with craniosynostosis with the normal newborn skull. The analysis has been separated in three complementary comparisons: first, the effect of premature fusions along the midline, to further test the importance of unpaired bones; second, the difference between a symmetric fusion (left and right frontal and parietal along the coronal suture vs. an asymmetric fusion, only the left side); and third, the effect of the fusion of more than two bones along the lambdoidal suture.

Material & Methods

Modularity has been analyzed in the normal newborn skull and each of the following craniosynostosis conditions: (1) metopic, (2) sagittal, (3) left hemicoronal, (4) bicoronal,

(5) lambdoidal, and (6) left lambdoidal plus occipitomastoid (see Fig. 12.7 and *Methods* in the previous section).

The grouping method used to analyze modularity has been described in Chapter 4. This method is based on a definition of connectivity module as a group of bones more connected to bones within the group than to other bones outside the group. To identify such groups, an agglomerative hierarchical cluster analysis was carried out using the topological overlap between bones as the measure of similarity between their connectivity patterns (i.e., number and correspondence of neighbors).

Results & Discussion

The analysis of modularity in the skull network of the newborn humans shows three modules: one for the posterior bones of the vault and two for the anterior bones of the face (Fig. 12.9). The two facial modules are specular asymmetric, although, three out of four blocks present in the adult skull are already present in the newborn: the ethmoidal (vomer, ethmoid, and palatines), the left maxillary (maxilla, nasal concha, and lacrimal), and the right maxillary (see Fig. 12.2). These modules will appear in all skulls with craniosynostosis since none of these bones are directly involved in fusions; their indirect involvement does not cause any change in their connectivity pattern regarding their participation in blocks. Bones of the cranial module are the same that will make the cranial module in the adult skull with two exceptions: the basilar bone, a central part of the occipital, that has been left unassigned; and the zygomatics, already formed as in the adult skull, that have changed their assignment from the cranial to the facial module. It is worth noting that this shift is in tune with the structural role of zygomatics as connector non-hubs, which makes them to have influence on both modules (see Model B in Fig. 12.4). If one considers a two-module partition of the hierarchical cluster analysis, the basilar part of the occipital falls within the posterior cranial module and both facial modules are merged into only one module, like in the adult skull network. Furthermore, an ethmoidal block comprising the ethmoid, vomer, and palatines is already present in the newborn skull–and is conserved in all human skull networks as an invariant aggrupation of bones. This block resembles the nasal capsule, an embryological, morphological, and evolutionary unit with a distinctive pattern of integration within the face (Bastir and Rosas, 2011).

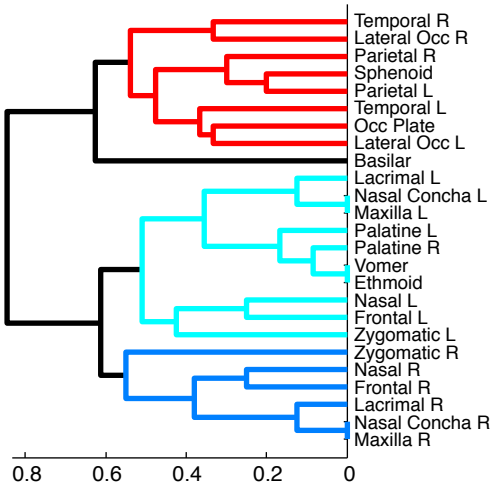

Figure 12.9: Modularity analysis of the human newborn skull: in red, posterior cranial module; in light and dark blue, facial modules.

Craniosynostosis along the Midline

The skull network with craniosynostosis in the metopic suture (between frontal bones) shows two bilateral modules that group the same bones in the adult skull (Fig. 12.10A). The same four blocks appear in the facial module: the three already present in the newborn skull plus the frontonasal block, which group the newly formed frontal bone and the nasals. The cranial module is divided in two blocks: one anterodorsal with zygomatics, parietals and sphenoid; and one posteroventral, with occipital bones and temporals. The skull network with craniosynostosis in the sagittal suture (between parietal bones) shows also two specular asymmetric modules: the left zygomatic groups with the facial module, while the right zygomatic groups with the cranial module (Fig. 12.10B). Only three of the four blocks of the face are present, the same than in the newborn. The premature fusions of the metopic and sagittal sutures have different consequences in the modular organization of the skull, although both occur in the midline between two paired bones. While the fusion of the frontals generates two bilateral modules, like in the adult (Fig. 12.2), the fusion of the parietals generates asymmetric specular modules. Facial blocks are kept except for the frontonasal that is dependent on the fusion of the frontals either prematurely or in the adult. This result suggests that the formation of bilateral modules is specific of the connectivity pattern of the bones fused, which must be capable of integrating both sides. Thus, the unpaired frontal bone, perhaps due to its structural role

as a connector hub (see Fig. 12.3), can integrate both sides, while the unpaired parietal fails to do so.

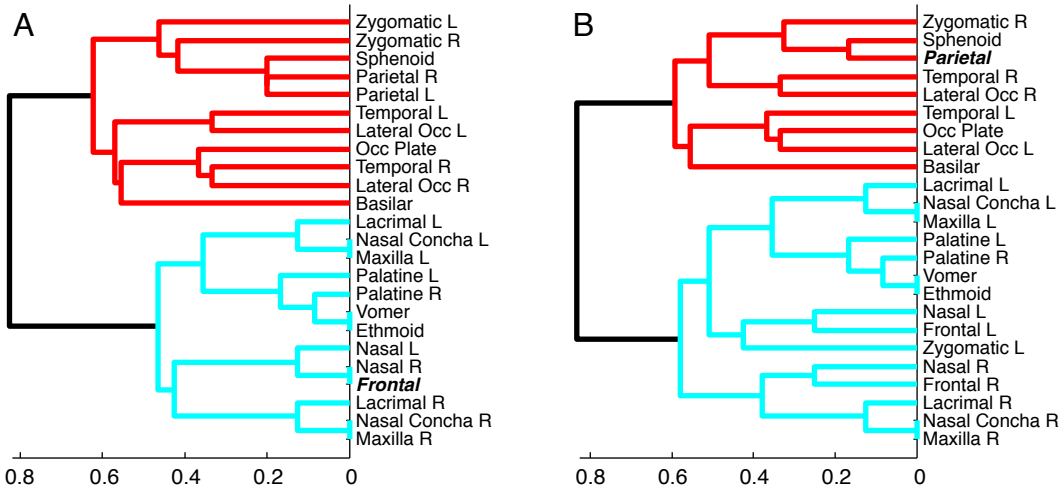

Figure 12.10: Modularity analysis of craniosynostosis along the midline. A) Craniosynostosis of the metopic suture between the frontal bones. B) Craniosynostosis of the metopic suture between the parietal bones.

Asymmetric and Symmetric Craniosynostosis

The skull network with craniosynostosis in the left hemicoronal suture (between the frontal and the parietal bones) shows two specular asymmetric modules (Fig. 12.11A): one cranial including the left frontoparietal, and one facial including the right frontal bone. The skull network with bicoronal craniosynostosis (between both parietal and frontal) shows two bilateral modules: one facial and one cranial that includes both fused bones (Fig. 12.11B). These results suggest that differences between an asymmetric and a symmetric craniosynostosis in humans is quite trivial since the bone that causes the asymmetry is the bone that results from the fusion between one facial and one cranial bone.

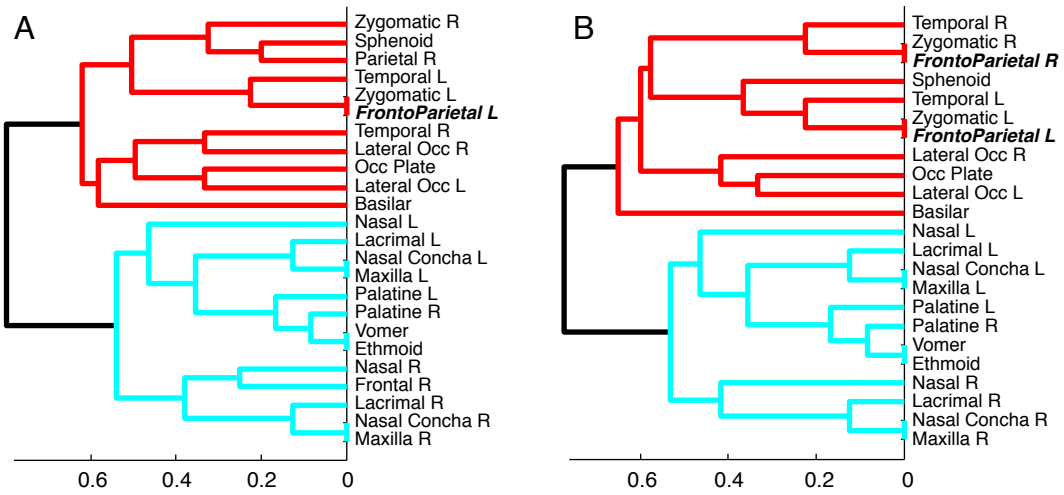

Figure 12.11: Modularity analysis of asymmetric and symmetric craniosynostosis. A) Craniosynostosis of the left hemicoronal suture between the frontal and the parietal bones. B) Craniosynostosis of the bicoronal suture.

Multiple Craniosynostosis

The skull network with craniosynostosis in the lambdoidal suture between the left parietal and the left lateral occipital bones shows a triple asymmetry of modules (Fig. 12.12A). The cranial module, which also includes the right zygomatic, resembles that of the normal newborn skull, while there are also two specular facial modules. The skull network with craniosynostosis in the lambdoidal and occipitomastoid sutures between the left parietal, the left lateral occipital, and the left temporal shows one cranial bilateral module and two facial specular asymmetric modules (Fig. 12.12B). Paradoxically, a skull network with a more severe craniosynostosis (involving three bones) show a modular organization with more symmetry; the reason is that the new bone generated after the fusion makes two connections of the zygomatic bones to the cranial vault redundant, facilitating the grouping of both zygomatic bones to the facial modules.

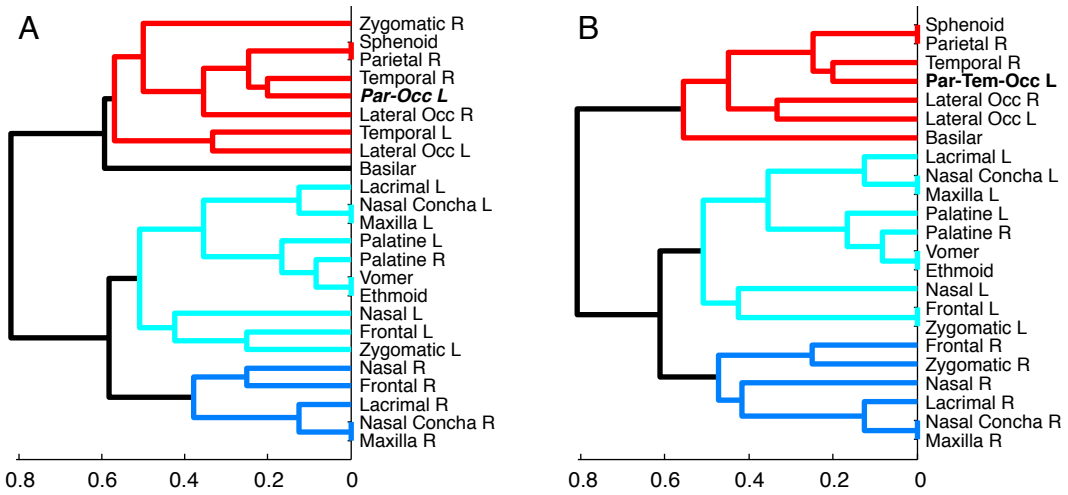

Figure 12.12: Modularity analysis of multiple craniosynostosis. A) Craniosynostosis of the left lambdoidal suture between the parietal and the lateral occipital. B) Craniosynostosis of the left lambdoidal plus occipitomastoid suture between the parietal, the lateral occipital, and the temporal.

Concluding Remarks

The comparison of modular organizations of skulls with craniosynostosis highlighted two generalizations in the formation of connectivity modules in skulls. The first generalization is related to the formation of bilateral modules and the presence of unpaired bones (as it has been shown already in 10.2). However, observation of natural fusions during abnormal development revealed that just the fusion of paired bones along the midline is not enough to form a bilateral module: the new unpaired bone must have the adequate connectivity pattern capable to integrate the left and right sides, for example, by being a connector hub as the frontal bone.

The second generalization is related to the fusion of paired bones in one or both sides at the same time, a phenomenon also reported in the evolution of the tetrapod skull. When bones of different modules fuse at the boundary of two modules, the symmetry or not of the craniosynostosis events has no effects on the symmetry of resulting modules, besides the inclusion of fused unpaired bones to one module or the other.

Conclusions

Conclusions

These are the main conclusions reached in this thesis:

Evolutionary Trends in Morphological Complexity

1. The reduction in bone number during the evolution of the tetrapod skull due to bone loss and fusion is accompanied by a trend toward a more complex organization, rather than toward simplification.

2. Losses and fusions of bones affect skull morphological complexity differently whether they target bones at random or selectively depending on the number of bone connections. This implies that bone connections impose structural constraints on bone loss and fusion. Since connections between bones are related to functional and developmental co-dependences (bone burden), the higher the number of connections, the higher the burden.

3. A mixed evolutionary scenario explains the increase in morphological complexity due to bone number reduction: the random loss of poorly connected bones and the selective fusion of the most connected ones.

4. Complementing this evolutionary scenario, several structural constraints have been identified: (1) the absence of any bias due to body axis size in the formation of connections in the ancestral skull, (2) the presence of a few unpaired bones in the ancestral skull, and (3) a higher frequency of loss than fusion events during skull evolution.

Morphological Integration and Modularity

5. The tetrapod skull shows a small-world organization of connectivity patterns, a type of organization between randomness and regularity that promotes the formation of connectivity modules.

6. Connectivity modules in the skull are of three types: (1) bilateral modules, grouping bones from the left and right side together; (2) specular modules, grouping bones from only one side; and (3) asymmetric specular modules, grouping bones from only one side, but including also one or more unpaired bones, which make these modules asymmetric in relation to their contralateral specular modules.

7. In general, the formation of bilateral modules depends on the presence of unpaired bones, which act integrating both sides of the skull in a single module; when this integration fails, asymmetric specular modules are formed; and when unpaired bones are absent, specular modules are formed.

8. Connectivity modules tend to follow a hierarchical order of formation, by which bones are grouped together according to their position in the three body axes: dorsoventral, left-right, and anteroposterior. This process is highly influenced by the presence of unpaired bones.

Theoretical Morphology

9. The analysis of theoretical morphospaces indicates that the generative morphospace that better captures the disparity of skull structures is the one built using a growth rule based on geometric proximity (Gabriel rule), in which bones are positioned with bilateral symmetry, and unpaired bones are present (i.e., the Symmetric Proximal morphospace).

10. This Symmetric Proximal morphospace is asymmetric with respect to number of connections: it is wider (higher disparity in the number of connections) for bigger networks and narrower for smaller networks.

11. Early tetrapod skulls occupy the wider region of the morphospace during the Devonian and Carboniferous Periods. As the wider area begins to empty out during the Mesozoic, more derived skulls occupy the narrower area of the morphospace in the Cenozoic.

12. This directional occupation of the morphospace is concomitant with Williston's Law, which suggests that the tetrapod skull has evolved toward more constrained morphological organizations while it increased its morphological complexity due to bone number reduction.

The Human Skull

13. The detailed analysis of the morphological integration and modularity of the human skull showed that it is composed of two well-delimited connectivity modules: one facial organized around the ethmoid bone, and one cranial organized around the sphenoid bone.

14. The facial module shows a hierarchy of clustered blocks of bones and the cranial modules shows a regular pattern of connections. It is the morphological integration of each group of bones that defines the semi-hierarchical organization of the human skull, reflecting fundamental differences in the ontogenetic patterns of growth and the structural constraints that generate each module.

15. Since connectivity modules resemble units of allometric growth, connectivity relations can be directly interpreted as correlation of changes in size and shape due to their developmental role as sites of bone growth. Thus, connections are a fundamental source of morphological integration and modularity.

16. Newborn human skulls with premature fusion of bones (i.e., craniosynostosis) reproduce ontogenetically the evolutionary patterns found in Williston's Law due to bone fusion: an increase of morphological complexity because of the reduction in the number of bones, which stresses the relationship between craniosynostosis and macro-evolutionary patterns.

17. Craniosynostosis affects also connectivity patterns that determine the modular organization of the human skull. Fusions along the midline (e.g., metopic and sagittal suture) produce an adult-like modular organization, while fusions in only one side (e.g., hemicoronal and lambdoidal) produce asymmetric connectivity modules that deviate from the adult form.

New Lines of Research in Morphological Networks

18. Future network analyses have to be focused in the study of smaller groups in order to study small changes in connectivity patterns. For instance, turtles and mammals, due to their well-conserved connectivity patterns, are better suited to study small variations, such as the formation of an unpaired vomer; while archosaurs, lepidosaurs

and amphibians show a high intra-group variation and can be used to study evolutionary transitions, such as the aquatic-terrestrial transition or the origin of the avian skull.

19. More sophisticated methods are required to solve particular morphological problems, such as ontogenetic sequences analysis or connectivity-shape correlations.

20. Network tools developed in this thesis can be applyied to other skeletal structures, non-skeletal organs, or even structures of plants.

Bibliography

Adams, D. C., Rohlf, F. J., and Slice, D. E. (2004). Geometric morphometrics: ten years of progress following the revolution. *Ital. J. Zool.*, 71:5–16.

Alberch, P. (1980). Ontogenesis and morphological diversification. *Amer. Zool.*, 20:653–667.

Alberch, P. and Gale, E. A. (1985). A developmental analysis of an evolutionary trend: digital reduction in amphibians. *Evolution*, 39:8–23.

Albert, R. and Barabási, A.-L. (2002). Statistical mechanics of complex networks. *Rev. Mod. Phys.*, 74:47–97.

Albert, R., Jeong, H., and Barabási, A.-L. (2000). Error and attack tolerance of complex networks. *Nature*, 406:378–381.

Aldridge, K., Marsh, J. L., Govier, D., and Richtsmeier, J. T. (2002). Central nervous system phenotypes in craniosynostosis. *J. Anat.*, 201:31–39.

Alroy, J. (1998). Cope's rule and the dynamics of body mass evolution in North American fossil mammals. *Science*, 280:731–734.

Appel, T. A. (1987). *The Cuvier-Geoffroy Debate. French Biology in the Decades Before Darwin*. Oxford University Press, Oxford.

Barabasi, A.-L. and Bonabeau, E. (2003). Scale-free networks. *Scientific American*, 288:50–59.

Barabási, A.-L. and Albert, R. (1990). Emergence of scaling in random networks. *Science*, 286:509–512.

Barabási, A.-L. and Oltvai, Z. N. (2002). Network biology: understanding the cell's functional organization. *Nat. Rev. Genet.*, 5:101–113.

Bastir, B., Rosas, A., and Sheets, H. D. (2005). The morphological integration of the hominoid skull: a partial least squares and PC analysis with implications for European middle pleistocene mandibular variation. In Slice, D. E., editor, *Modern Morphometrics in Physical Anthropology*, pages 265–284. Kluwer Academy.

Bastir, M. (2008). A systems-model for the morphological analysis of integration and modularity in the human craniofacial evolution. *J. Anthropol. Sci.*, 86:37–58.

Bastir, M., O'Higgins, P., and Rosas, A. (2007). Facial ontogeny in neanderthals and modern humans. *Proc. R. Soc. B.*, 274:1125–1132.

Bastir, M. and Rosas, A. (2004). Comparative ontogeny in humans and chimpanzees: similarities, differences and paradoxes in postnatal growth and development of the skull. *Ann. Anat.*, 186:503–509.

Bastir, M. and Rosas, A. (2005). The hierarchical nature of morphological integration and modularity in the human posterior face. *Am. J. Phys. Anthropol.*, 128:26–34.

Bastir, M. and Rosas, A. (2009). Mosaic evolution of the basicranium in *Homo* and its relation to modular development. *Evol. Biol.*, 36:57–70.

Bastir, M. and Rosas, A. (2011). Nasal form and function in Midpleistocene human facial evolution. A first approach. *Am. J. Phys. Anthropol.*, 144(S52):83.

Bastir, M., Rosas, A., Lieberman, D. E., and O'Higgins, P. (2008). Middle cranial fossa anatomy and the origins of modern humans. *Anat. Rec.*, 291:130–140.

Bastir, M., Rosas, A., and O'Higgins, P. (2006). Craniofacial levels and the morphological maturation of the human skull. *J. Anat.*, 209:637–654.

Benton, M. J. (1990). Reptiles. In McNamara, K. J., editor, *Evolutionary Trends*, pages 279–300. University of Arizona Press.

Benton, M. J. (2005). *Vertebrate Paleontology*. Blackwell Publishing, Oxford.

Berry, A. C. and Berry, R. J. (1967). Epigenetic variation in the human cranium. *J. Anat.*, 10:361–379.

Bhullar, B.-A. S., Marugán-Lobón, J., Racimo, F., Bever, G. S., Rowe, T. B., Norell, M. A., and Abzhanov, A. (2012). Birds have paedomorphic dinosaur skulls. *Nature*, 487:223–226.

Bolker, J. (2000). Modularity in development and why it matters to evo-devo. *Amer. Zool.*, 40:770–776.

Bonner, J. T. (1988). *The Evolution of Complexity by Means of Natural Selection*. Princeton University Press, Princeton.

Bookstein, F. L., Gunz, P., Mitteroecker, P., Prossinger, H., Schaefer, K., and Seidler, H. (2006). Cranial integration in *Homo*: singular warps analysis of the midsagittal plane in ontogeny and evolution. *J. Hum. Evol.*, 44:167–187.

Boonstra, L. D. (1936). The cranial morpholgy of some titanosuchid deinocephalians. *B. Am. Mus. Nat. Hist.*, 72:99–116.

Breiger, R., Boorman, S., and Arabie, P. (1975). An algorithm for clustering relational data with applications to social network analysis and comparison with multidimensional scaling. *J. Math. Psychol.*, 12:328–383.

Butts, C. T. (2009). Revisiting the foundations of network analysis. *Science*, 325:414–416.

Callebaut, W. (2005). The ubiquity of modularity. In Callebaut, W. and Rasskin-Gutman, D., editors, *Modularity: Understanding the Develpment and Evolution of Natural Complex Systems*, pages 3–28. MIT Press.

Callebaut, W. and Rasskin-Gutman, D. (2005). *Modularity. Understanding the Development and Evolution of Natural Complex Systems*. MIT Press, Cambridge.

Cannatella, D. (2008). *Living Amphibians. Frogs and toads, salamanders, newts, and caecilians. Version 28 November 2008*. Tree of Life Web Project, Available at http://tolweb.org/LivingAmphibians/14997/2008.11.28.

Carroll, R. L. (1988). *Vertebrate Paleontology and Evolution*. W. H. Freeman and Company, New York.

Carroll, R. L. and Lindsay, W. (1985). Cranial anatomy of the primitive reptile *Procolophon*. *Can. J. Earth Sci.*, 22:1571–1587.

Case, E. C. (1904). The osteology of the skull of the pelycosaurian genus, *Dimetrodon*. *J. Geol.*, 12:304–311.

Chase, K., Carrier, D. R., Jarvik, F. R. A. T., Ostrander, E. A., Lorentzen, T. D., and Lark, K. G. (2002). Genetic basis for systems of skeletal quantitative traits: principal component analysis of the canid skeleton. *Proc. Natl. Acad. Sci. USA*, 104:15224–15229.

Chernoff, B. and Magwene, P. M. (1999). Afterword. In Olson, E. C. and Miller, P. L., editors, *Morphological Integration*, pages 319–353. University of Chicago Press.

Cheverud, J. M. (1982). Phenotypic, genetic, and environmental morphological integration in the cranium. *Evolution*, 36:499–516.

Cheverud, J. M., Rutledge, J. J., and Atchley, W. R. (1983). Quantitative genetics of development: genetic correlations among age-specific trait values and the evolution of ontogeny. *Evolution*, 37:895–905.

Claeson, K. M., Bemis, W., and Hagadorn, J. W. (2007). New interpretations of the skull of a primitive bony fish *Erpetoichthys calabaricus* (Actinopterygii: Cladistia). *J. Morphol.*, 268:1021–1039.

Couly, G. F., Coltey, P. M., and Douarin, N. M. L. (1993). The triple origin of skull in higher vertebrates: a study in quail-chick chimeras. *Development*, 117:409–429.

Couly, G. F., Coltey, P. M., and Douarin, N. M. L. (2007). Modularity and sequence heterochrony in the mammalian skull. *Evol. Dev.*, 9:291–299.

De Renzi, M. (1997). La forma: sus reglas y evolución, y los datos del registro fósil. In Aguirre, E., Morales, J., and Soria, D., editors, *Registros Fósiles e Historia de la Tierra*, pages 57–77. Editorial Complutense.

De Renzi, M. (2009a). Cuestiones de forma: desde el pensamiento de darwin hasta la actualidad. In Palmqvist, P. and Pérez-Claros, J. A., editors, *XXV Jornadas de la Sociedad Española de Paleontología*, pages 26–50. Empress Málaga.

De Renzi, M. (2009b). Evolución y registro fósil: hacia una perspectiva más amplia. *Ludus Vitalis*, 27:231–246.

De Renzi, M., Pardo, M. V., Belinchón, M., Peñalver, E., Montoya, P., and Márquez-Aliaga, A. (2002). *Current Topics on Taphonomy and Fossilization*. Editorial Ilmo. Ayuntamiento de Valencia, Valencia.

Depew, M. J., Compagnucci, C., and Griffin, J. (2008). Suture neontology and paleontology: the bases for where, when and how boundaries between bones have been established and have evolved. In Rice, D. P., editor, *Craniofacial Sutures, Development, Disease and Treatment. Frontiers of Oral Biology Vol. 12*, pages 57–78. Karger.

Dera, G., Eble, G. J., Neige, P., and David, B. (2008). The flourishing diversity of models in theoretical morphology: from current practices to future macroevolutionary and bioenvironmental challenges. *Paleobiology*, 34:301–317.

Dorogovtsev, S. N. and Mendes, J. F. F. (2003). *Evolution of Networks: From Biological Networks to the Internet and WWW*. Oxford University Press, Oxford, UK.

Dunne, J. A., Williams, R. J., and Martínez, N. D. (2008a). Food-web structure and network theory: the role of connectance and size. *Proc. Natl. Acad. Sci. USA*, 99:12917–12922.

Dunne, J. A., Williams, R. J., Martínez, N. D., Wood, R. A., and Erwin, D. H. (2008b). Compilation and network analyses of Cambrian food webs. *PLoS Biol.*, 6:e102.

Eaton, J. W. (2002). *GNU Octave Manual*. Network theory Ltd., Bristol, UK.

Eble, G. J. (2005). Morphological modularity and macroevolution: conceptual and empirical aspects. In Callebaut, W. and Rasskin-Gutman, D., editors, *Modularity: Understanding the Development and Evolution of Natural Complex Systems*, pages 221–238. MIT Press.

Enlow, D. H. (1990). *Facial Growth*. WB Saunders Company, Philadelphia.

Enlow, D. H. and Bang, S. (1956). Growth and remodelling of the human maxilla. *Amer. J. Orthodontics*, 51:446–464.

Enlow, D. H. and Hans, M. G. (1996). *Essentials of Facial Growth*. WB Saunders Company, Philadelphia.

Erdös, P. and Rényi, A. (1959). On random graphs. *Publ. Math. Debrecen.*, 6:290–297.

Estes, R. (1961). Cranial anatomy of the cynodont reptile *Thrinaxodon liorhinus*. *B. Mus. Com. Zool.*, 125:165–180.

Estes, R., Queiroz, K., and Gauthier, J. (1988). Phylogenetic relationships within Squamata. In Lucas, G., Cassinis, G., and Schneider, J. W., editors, *Phylogenetic Relationships of the Lizard Families: Essays Commemorating Charles L. Camp*, pages 119–281. Stanford University Press.

Esteve-Altava, B., Marugán-Lobón, J., Bastir, M., Botella, H., and Rasskin-Gutman, D. (2013a). Grist for riedl's mill: a network model perspective on the integration and modularity of the human skull. *J. Exp. Zool. (Mol. Dev. Evol.)*, doi 10.1002/jez.b.22524.

Esteve-Altava, B., Marugán-Lobón, J., Botella, H., and Rasskin-Gutman, D. (2011). Network models in anatomical systems. *J. Anthropol. Sci.*, 89:175–184.

Esteve-Altava, B., Marugán-Lobón, J., Botella, H., and Rasskin-Gutman, D. (2013b). Random loss and selective fusion of bones originate morphological complexity trends in tetrapod skull networks. *Evol. Biol.*, doi 10.1007/s11692-013-9245-4.

Esteve-Altava, B., Marugán-Lobón, J., Botella, H., and Rasskin-Gutman, D. (2013c). Structural constraints in the evolution of the tetrapod skull complexity: Williston's law revisited using network models. *Evol. Biol.*, 40:209–219.

Esteve-Altava, B. and Rasskin-Gutman, D. (2009). Tamaño y complejidad: generalizaciones evolutivas del cambio morfológico. In Dopazo, H. and Navarro, A., editors, *Adaptación y Evolución: 150 Años Después del Origen*, pages 229–237. Obrapropia Editorial.

Esteve-Altava, B. and Rasskin-Gutman, D. (2013). Theoretical morphology of tetrapod skull networks. *C. R. Palevol.*, Accepted.

Felsenstein, J. (1985). Phylogenies and the comparative method. *Am. Nat.*, 375:1–15.

Finarelli, J. and Goswami, A. (2009). The evolution of orbit orientation and encephalization in the carnivora (Mammalia). *J. Anat.*, 214:671–678.

Fox-Keller, E. (2005). Revisiting scale-free networks. *BioEssays*, 27:1060–1068.

Franz-Odendaal, T. (2011). Epigenetics in bone and cartilage development. In Hallgrímsson, B. and Hall, B. K., editors, *Epigenetics: Linking Genotype and Phenotype in Development and Evolution*, pages 195–220. University of California Press.

Gabriel, K. R. and Sokal, R. R. (1969). A new statistical approach to geographic variation analysis. *Syst. Zool.*, 18:259–270.

Gabriel, K. R. and Sokal, R. R. (1980). Properties of gabriel graph relevant to geographic variation research and the clustering of points in the plane. *Georg. Anal.*, 12:205–222.

Gaffney, E. S. (1979). Comparative cranial morphology of recent and fossil turtles. *B. Am. Mus. Nat. Hist.*, 164:65–376.

Gaffney, E. S. (1990). The comparative osteology of the triassic turtle *Proganochelys*. *B. Am. Mus. Nat. Hist.*, 194:2–263.

Galatius, A., Berta, A., Frandsen, M. S., and Goodall, R. N. P. (2010). Interspecific variation of ontogeny and skull shape among porpoises (Phocoenidae). *J. Morphol.*, 272:136–142.

Gallos, L. K., Makse, H. A., and Sigman, M. (2012). A small world of weak ties provides optimal global integration of self-similar modules in functional brain networks. *Proc. Natl. Acad. Sci. USA*, 109:2825–2830.

Gardner, N. M., Holliday, C. M., and O'Keefe, F. R. (2010). The Braincase of *Youngina capensis* (Reptilia: Diapsida): new insights from high-resolution CT scanning of the Holotype. *Palaeontol. Electron.*, 13:19A.

Geoffroy Saint-Hilaire, E. (1818). *Philosphie Anatomique*. J. B. Baillière, Paris.

Giannini, N. P., Wible, J. R., and Simmons, N. B. (2006). On the cranial osteology of Chiroptera. 1, *Pteropus* (Megachiroptera: Pteropodidae). *B. Am. Mus. Nat. Hist.*, 295:1–134.

Gibbard, L. P., Head, M. J., and Walker, M. J. C. (2010). Formal ratification of the Quaternary System/Period and the Pleistocene Series/Epoch with a base at 2.58 Ma. *J. Quaternary. Sci.*, 25:96–102.

Gilbert, S. F. (2006). *Developmental Biology*. Sinauer, Sunderland.

Gilmore, C. W. (1914). Osteology of the armored dinosauria in the United States National Museum, with special reference to the genus *Stegosaurus*. *B. Am. Mus. Nat. Hist.*, 89:2–159.

Girgis, F. G. and Pritchard, J. J. (1958). Effects of skull damage on the development of sutural patterns in the rat. *J. Anat.*, 92:39–61.

Godsil, C. and Royle, G. (2004). *Algebraic Graph Theory*. Springer-Verlag, New York.

Goh, K. I., Kahng, B., and Kim, D. (2001). Universal behavior of load distribution in scale-free networks. *Phys. Rev. Lett.*, 87:278701.

González, P. N., Pérez, S. I., and Bernal, V. (2010). Ontogeny of robusticity of craniofacial traits in modern humans: a study of South American populations. *Am. J. Phys. Anthropol.*, 142:367–379.

González-José, R., Escapa, I., Neves, W. A., Cúneo, R., and Pucciarelli, H. (2008). Cladistic analysis of continuous modularized traits provides phylogenetic signals in *Homo* evolution. *Nature*, 453:775–778.

Goodrich, E. S. (1958). *Studies on the Structure and Development of Vertebrates*. Dover Publications, New York.

Goswami, A. (2006). Morphological integration in the carnivoran skull. *Evolution*, 60:169–183.

Goswami, A. and Polly, P. D. (2010). The influence of modularity on cranial morphological disparity in carnivora and primates (Mammalia). *PLoS One*, 5:e9517.

Goswami, A., Weisbecker, V., and Sánchez-Villagra, M. R. (2009). Developmental modularity and the marsupial-placental dichotomy. *J. Exp. Zool. (Mol. Dev. Evol.)*, 312:186–195.

Gould, S. J. (1988). Trends as changes in variance: a new slant on progress and directionality in evolution. *J. Paleontol.*, 62:319–329.

Gould, S. J. (1990). Speciation and sorting as the source of evolutionary trends, or 'things are seldom what they seem'. In McNamara, K. J., editor, *Evolutionary Trends*, pages 3–27. University of Arizona Press.

Gould, S. J. (2002). *The Structure of Evolutionary Theory*. Belknap Press, Harvard.

Gould, S. J. and Eldredge, N. (1977). Punctuated equilibria: the tempo and mode of evolution reconsidered. *Paleobiology*, 3:115–151.

Gradstein, F. M., Agterberg, F. P., Ogg, J. G., Hardenbol, J., Van Veen, P., and Thierry, J. (1995). A Triassic, Jurassic, and Cretaceous time scale. *SEPM*, 54.

Gray, H. (1918). *Anatomy of the Human Body.* Lea and Febiger, Philadelphia.

Gregory, W. K. (1927). The palaeomorphology of the human head: ten structural stage from fish to man. the skull in *norma lateralis*. *Q. Rev. Biol.*, 2:267–279.

Gregory, W. K. (1929). The palaeomorphology of the human head: ten structural stage from fish to man. the skull in *norma basalis*. *Q. Rev. Biol.*, 4:233–247.

Gregory, W. K. (1933). Fish skulls: a study of the evolution of natural mechanisms. *Trans. Am. Philos. Soc.*, 23:75–481.

Gregory, W. K. (1934). Polysomerism and anisomerism in cranial and dental evolution among vertebrates. *Proc. Natl. Acad. Sci. USA*, 20:1–9.

Gregory, W. K. (1935). Williston's law relating to the evolution of skull bones in the vertebrates. *Am. J. Phys. Anthropol.*, 20:123–152.

Guimerà, R. and Nunes-Amaral, L. A. (2005). Functional cartography of complex metabolic networks. *Nature*, 433:895–900.

Guimerà, R., Sales-Pardo, M., and Amaral, A. N. (2007). Classes of complex networks defined by role-to-role connectivity profiles. *Nat. Phys.*, 3:63–69.

Haberland, M., Mokalled, M. H., and Montgomery, R. L. (2009). Epigenetic control of skull morphogenesis by histone deacetylase 8. *Gene. Dev.*, 23:1625–1630.

Hall, B. K. (2005). *Bones and Cartilage. Developmental and Evolutionary Skeletal Biology.* Elsevier, San Diego.

Hall, B. K. and Miyake, T. (2000). All for one and one for all: condensations and the initiation of skeletal development. *BioEssays*, 22:138–147.

Hallgrimsson, B. and Hall, B. K. (2011). *Epigenetics. Linking Genotype and Phenotype in Development and Evolution.* University of California Press, Berkeley.

Hallgrímsson, B. (1998). Fluctuating asymmetry in the mammalian skeleton: evolutionary and ontogenetic implications. *Evol. Biol.*, 30:187–251.

Hallgrímsson, B., Jamniczky, H., Young, N. M., Rolian, C., Parsons, T. E., Boughner, J. C., and Marcucio, R. S. (2009). Deciphering the palimpsest: studying the relationship between morphological integration and phenotypic covariation. *Evol. Biol.*, 36:355–376.

Hallgrímsson, B. and Lieberman, D. E. (2008). Mouse models and the evolutionary developmental biology of the skull. *Int. Comp. Biol.*, 48:373–384.

Harvati, K. (2003). Quantitative analysis of neanderthal temporal bone morphology using three dimensional geometric morphometrics. *Am. J. Phys. Anthropol.*, 120:823–838.

Heuzé, Y., Martínez-Abadías, N., Stella, J. M., Senders, C. W., Boyadjiev, S. A., Lo, L.-J., and Richtsmeier, J. T. (2011). Unilateral and bilateral expression of a quantitative trait: asymmetry and symmetry in coronal craniosynostosis. *J. Exp. Zool. (Mol. Dev. Evol.)*, 318:109–122.

Hildebrand, M. (1988). *Analysis of Vertebrate Structure*. John Wiley and Sons, New York.

Hinegardner, R. and Engelberg, J. (1983). Biological complexity. *J. Theo. Biol.*, 104:7–20.

Hofer, H. (1965). Die morphologische analyse des schädels des menschen. In Heberer, G., editor, *Menschliche Abstammungslehre, Fortschritte der Anthropogenie*, pages 145–226. Gustav Fischer Verlag.

Horvath, S. and Dong, J. (2008). Geometric interpretation of gene coexpression network analysis. *PLoS Comput. Biol.*, 4:e1000117.

Hugall, A. F., Foster, R., and Lee, M. S. (2007). Calibration choice, rate smoothing, and the pattern of tetrapod diversification according to the long nuclear gene RAG-1. *Syst. Biol.*, 56:543–563.

Hukki, J., Saarinen, P., and Kangasniemi, M. (2008). Single suture craniosynostosis: diagnosis and imaging. In Rice, D. P., editor, *Craniofacial Sutures, Development, Disease and Treatment. Frontiers of Oral Biology Vol. 12*, pages 79–90. Karger.

Hull, D. L. (1988). *Science as a Process: An Evolutionary Account of the Social and Conceptual Development of Science*. University of Chicago Press, Chicago.

Humphries, M. D. and Gurney, K. (2008). Network 'small-world-ness': a quantitative method for determining canonical network equivalence. *PLoS One*, 3:e0002051.

Huxley, J. S. (1932). *Problems of Relative Growth.* Methuen and Company, Lodon, UK.

Ibañes, M. and Izpisúa-Belmonte, J. C. (2009). Left–right axis determination. *WIREs Syst. Biol. Med.*, 1:210–219.

Jain, A. and Dubes, R. (1988). *Algorithms for Clustering Data.* Prentice-Hall, New Jersey.

Jamniczky, H. A. and Russell, A. P. (2007). *Emys orbicularis (Digital Morphology).* Available at, www.digimorph.org.

Jane, J. and Persing, J. (2001). Neurosurgical treatment of craniosynostosis. In Cohen, M. J. and Maclean, R., editors, *Craniosynostosis: Diagnosis, Evaluation, and Management*, page Chap. 18. Oxford University Press.

Jaslow, C. R. (1990). Mechanical properties of cranial sutures. *J. Biomech*, 23:313–321.

Jeong, H., Tombor, B., Albert, R., Oltvai, Z. N., and Barabási, A.-L. (2000). The large-scale organization of metabolic networks. *Nature*, 407:651–654.

Josse, S., Moreau, T., and Laurin, M. (2011). *Stratigraphic Tools for Mesquite.* Open source, Available at http://mesquiteproject.org/packages/stratigraphicTools/.

Kardong, K. V. (2005). *Vertebrates. Comparative Anatomy, Function, Evolution.* Mcgraw Hill, New York.

Klingenberg, C. P. (2008). Morphological integration and developmental modularity. *Annu. Rev. Ecol. Evol. S.*, 39:115–132.

Klingenberg, C. P. (2009). Morphometric integration and modularity in configurations of landmarks: tools for evaluating a priori hypotheses. *Evol. Dev.*, 11:405–421.

Klingenberg, C. P. (2010). Evolution and development of shape: integrating quantitative approaches. *Nat. Rev. Genet.*, 11:623–635.

Klingenberg, C. P. (2011). Morphoj: an integrated software package for geometric morphometrics. *Mol. Ecol. Resour.*, 11:353–357.

Klingenberg, C. P. and Marugán-Lobón, J. (2013). Evolutionary covariation in geometric morphometrics data: analyzing integration, modularity and allometry in a phylogenetic context. *Syst. Biol.*, 62:591–610.

Knight, C. G. and Pinney, J. W. (2009). Making the right connections: biological networks in the light of evolution. *BioEssays*, 31:1080–1090.

Koyabu, D., Endo, H., Mitgutsch, C., Suwa, G., Catania, K. C., Zollikofer, C. P. E., Oda, S., Koyasu, K., Ando, M., and Sánchez-Villagra, M. R. (2011). Heterochrony and developmental modularity of cranial osteogenesis in lipotyphlan mammals. *EvoDevo*, 2:1–18.

Koyabu, D., Maier, W., and Sanchez-Villagra, M. R. (2012). Paleontological and developmental evidence resolve the homology and dual embryonic origin of a mammalian skull bone, the interparietal. *Proc. Natl. Acad. Sci. USA*, 109:14075–14080.

Kuratani, S. (2005). Craniofacial development and the evolution of the vertebrates: the old problems on a new background. *J. Anat.*, 22:1–19.

Laffont, R., Firmat, C., Alibert, P., David, B., Montuire, S., and Saucède, T. (2011). Biodiversity and evolution in the light of morphometrics: from patterns to processes. *C. R. Palevol.*, 10:133–142.

Laurin, M. (1996). A redescription of the cranial anatomy of *Seymouria baylorensis*, the best known seymouriamorph (Vertebrata: Seymouriamorpha). *PaleoBios*, 17:1–16.

Laurin, M. (2004). The evolution of body size, Cope's rule, and the origin of amniotes. *Syst. Biol.*, 54:594–622.

Laurin, M. (2011). *Terrestrial vertebrates. Stegocephalians: Tetrapods and other digit-bearing vertebrates. Version 21 April 2011.* Tree of Life Web Project, Available at http://tolweb.org/TerrestrialVertebrates/14952/2011.04.21.

Laurin, M., Canoville, A., and Quilhac, A. (2009). Use of paleontological and molecular data in supertrees for comparative studies: the example of lissamphibian femoral microanatomy. *J. Anat.*, 215:110–123.

Laurin, M. and Gauthier, J. A. (2012). *Amniota. Mammals, reptiles (turtles, lizards, Sphenodon, crocodiles, birds) and their extinct relatives. Version 30 January 2012.* http://tolweb.org/Amniota/14990/2012.01.30 in The Tree of Life Web Project, http://tolweb.org/.

Laurin, M. and Reisz, R. R. (2011). *Synapsida. Mammals and their extinct relatives. Version 14 August 2011.* Tree of Life Web Project, Available at http://tolweb.org/Synapsida/14845/2011.08.14.

Le Guyader, H. (2003). *Geoffroy Saint-Hilaire: A Visionary Naturalist.* University of Chicago Press, Chicago.

Lewin, R. (1992). *Complexity. Life at the Edge of Chaos.* University of Chicago Press, Chicago.

Lieberman, D. E. (1998). Sphenoid shortening and the evolution of modern human cranial shape. *Nature*, 393:158–162.

Lieberman, D. E. (2011). *The Evolution of the Human Head.* Harvard University Press, Cambridge.

Lieberman, D. E., Carlo, J., de Leon, M. P., and Zollikofer, C. P. E. (2007). A geometric morphometric analysis of heterochrony in the cranium of chimpanzees and bonobos. *J. Hum. Evol.*, 52:647–662.

Lieberman, D. E., Hallgrímsson, B., Liu, W., Parsons, T. E., and Jamnizcky, H. A. (2008). Spatial packing, cranial base angulation and craniofacial shape variation in the mammalian skull: testing a new model using mice. *J. Anat.*, 212:720–735.

Lockwood, C. A., Lynch, J. M., and Kimbel, W. H. (2002). Quantifying temporal bone morphology of great apes and humans: an approach using geometric morphometrics. *J. Anat.*, 201:447–464.

Louys, J., Aplin, K., Beck, R. M. D., and Archer, M. (2009). Cranial anatomy of Oligo-Miocene koalas (Diprotodontia: Phascolarctidae): stages in the evolution of an extreme leaf-eating specialization. *J. Vertebr. Paleontol.*, 29:981–992.

Luczak, T. (1990). Component behaviour near the critical point of the random graph process. *Random Struct. Algor.*, 1:287–310.

Mabbutt, L. W. and Kokich, V. G. (1979). Calvarial and sutural re-development following craniectomy in the neonatal rabbit. *J. Anat.*, 129:413–422.

Maddin, H. C., Sidor, C. A., and Reisz, R. R. (2008). Cranial anatomy of *Ennatosaurus tecton* (Synapsida: Caseidae) from the Middle Permian of Russia and the evolutionary relationships of Caseidae. *J. Vertebr. Paleontol.*, 28:160–180.

Maddison, W. P. (1991). Squared-change parsimony reconstructions of ancestral states for continuous-valued characters on a phylogenetic tree. *Syst. Zool.*, 40:304–314.

Maddison, W. P. and Maddison, D. R. (2011). *Mesquite: A Modular System for Evolutionary Analysis. Version 2.75.* Open source, Available at http://mesquiteproject.org.

Magwene, P. M. (2001). New tools for studying integration and modularity. *Evolution*, 55:1734–1745.

Magwene, P. M. (2008). Using correlation proximity graphs to study phenotypic integration. *Evol. Biol.*, 35:191–198.

Maisano, J. A., Kearney, M., and Rowe, T. (2006). Cranial anatomy of the spade-headed amphisbaenian *Diplometopon zarudnyi* (Squamata: Amphisbaenia) based on high-resolution X-ray computed tomography. *J. Morphol.*, 267:70–102.

Marjanovic, D. and Laurin, M. (2008). A reevaluation of the evidence supporting an unorthodox hypothesis on the origin of extant amphibians. *Contrib. Zool.*, 77:149–199.

Martínez-Abadías, N. (2007). *Evolutionary Patterns of the Human Skull. A Quantitative Genetic Analysis of Craniofacial Phenotypic Variation (PhD Thesis).* Universiyt of Barcelona, Barcelona.

Martínez-Abadías, N., Esparza, M., Sjøvold, T., González-José, R., Santos, M., Hernández, M., and Klingenberg, C. P. (2012). Pervasive genetic integration directs the evolution of human skull shape. *Evolution*, 66:1010–1023.

Martínez-Abadías, N., Paschetta, C., Azevedo, S., Esparza, M., and González-José, R. (2009). Developmental and genetic constraints on neurocranial globularity: insights from analyses of deformed skulls and quantitative genetics. *Evol. Biol.*, 36:37–56.

Marugán-Lobón, J. and Buscalioni, A. D. (2003). Disparity and geometry of the skull in Archosauria (Reptilia: Diapsida). *Biol. J. Linn. Soc.*, 80:67–88.

Marugán-Lobón, J. and Buscalioni, A. D. (2009). New insight on the anatomy and architecture of the avian neurocranium. *Anat. Rec.*, 292:364–370.

Mason, O. and Verwoerd, M. (2007). Graph theory and networks in biology. *IET Syst. Biol.*, 1:89–119.

MATLAB (2010). *Version 7.10.0 (R2010a)*. The MathWorks Inc., Natick, Massachusetts.

Mayr, E. (1982). *The Growth of Biological Thought*. Harvard University Press, Cambridge.

McGhee, G. R. (1998). *Theoretical Morphology: The Concept and its Applications*. Columbia University Press, New York.

McGhee, G. R. (2007). *The Geometry of Evolution: Adaptive Landscapes and Theoretical Morphospaces*. Cambridge University Press, Cambridge.

McKinney, M. K. (1990). Trends in body-size evolution. In McNamara, K. J., editor, *Evolutionary trends*, pages 75–118. University of Arizona Press.

MCPA2 (2005). *Mammalian crania photographic archive*. Available at, www.macro.dokkyomed.ac.jp.

McShea, D. W. (1991). Complexity and evolution: what everybody knows. *Biol. Philos.*, 6:303–324.

McShea, D. W. (1993). Evolutionary change in the morphological complexity of the mammalian vertebral column. *Evolution*, 47:730–740.

McShea, D. W. (1994). Mechanisms of large-scale evolutionary trends. *Evolution*, 48:1747–1763.

McShea, D. W. (1996). Metazoan complexity and evolution: is there a trend? *Evolution*, 50:477–492.

McShea, D. W. (1998). Possible largest-scale trends in organismal evolution: eight 'live hypotheses'. *Annu. Rev. Ecol. Syst.*, 29:293–318.

McShea, D. W. and Brandon, R. N. (2010). *Biology's First Faw. The Tendency for Diversity and Complexity to Increase in Evolutionary Systems*. University of Chicago Press, Chicago.

McShea, D. W. and Hordijk, W. (2013). Complexity by subtraction. *Evol. Biol.*, doi 10.1007/s11692-013-9227-6.

Mead, J. G. and Fordyce, R. E. (2009). The therian skull: a lexicon with emphasis on the odontocetes. *Smithsonian Contr. Zool.*, 627:1–248.

Meunier, D., Lambiotte, R., and Bullmore, E. T. (2010). Modular and hierarchically modular organization of brain networks. *Front. Neurosci.*, 4:200.

Meylan, P. (2001). *Testudines. Turtles, tortoises and terrapins. Version 31 May 2001.* Tree of Life Web Project, Available at http://tolweb.org/Testudines/14861/2001.05.31.

Midford, P., Garland, T. J., and Maddison, W. P. (2003). *PDAP Package for Mesquite.* Open source, Available at http://mesquiteproject.org/pdapmesquite/index.html.

Mitteroecker, P. (2009). The developmental basis of variational modularity: insights from quantitative genetics, morphometrics, and developmental biology. *Evol. Biol.*, 36:377–385.

Mitteroecker, P. and Bookstein, F. (2007). The conceptual statistical relationship between modularity and morphological integration. *Syst. Biol.*, 56:818–836.

Mitteroecker, P. and Bookstein, F. (2008). The evolutionary role of modularity and integration in the hominoid cranium. *Evolution*, 62:943–958.

Mitteroecker, P. and Bookstein, F. (2009). The ontogenetic trajectory of the phenotypic covariance matrix, with examples from craniofacial shape in rats and humans. *Evolution*, 63:727–737.

Mitteroecker, P., Gunz, P., Neubauer, S., and Müller, G. (2012). How to explore morphological integration in human evolution and development? *Evol. Biol.*, 39:536–553.

Mitteroecker, P. and Huttegger, S. M. (2009). The concept of morphospaces in evolutionary and developmental biology: mathematics and metaphors. *Biol. Theo.*, 4:54–67.

Moazen, M., Curtis, N., O'Higgins, P., Jones, M. E. H., Evans, S. E., and Fagan, M. J. (2009). Assessment of the role of sutures in a lizard skull: a computer modelling study. *Proc. R. Soc. B.*, 276:39–46.

Moisy, F. (2010). *EzyFit Toolbox for Matlab.* Lab. FAST, University Paris-Sud, Paris, France.

Morriss-Kay, G. M. (2001). Derivation of the mammalian skull vault. *J. Anat.*, 199:143–151.

Moss, M. L. (1962). The functional matrix. In Kraus, B. and Reidel, R., editors, *Vistas in Orthodontics*, pages 85–98. Lea and Febiger.

Moss, M. L. and Young, R. W. (1960). A functional approach to craniology. *Am. J. Phys. Anthropol.*, 48:1747–1763.

Müller, G. B. and Newman, S. A. (2003). *Origination of Organismal Form.* MIT Press, Cambridge.

Newman, M. E. J. (2003). The structure and function of complex networks. *SIAM Review*, 45:167–256.

Newman, M. E. J., Barabási, A.-L., and Watts, D. J. (2006). *The Structure and Dynamics of Networks.* Princeton University Press, Princeton.

Newman, M. E. J. and Girvan, M. (2004). Finding and evaluating community structure in networks. *Phys. Rev. E.*, 69:026113.

Newman, S. A. and Forgacs, G. (2005). Complexity and self-organization in biological development and evolution. In Bonchev, D. and Rouvray, D. H., editors, *Complexity in Chemistry, Biology, and Ecology*, pages 49–190. Springer Science.

Nicholson, D. J. and Gawne, R. (2013). Rethinking Woodger's legacy in the philosophy of biology. *J. Hist. Biol.*, doi 10.1007/s10739-013-9364-x.

Nitecki, M. H. and Hoffman, A. (1987). *Neutral Models in Biology.* Oxford University Press, New York.

Nussbaum, R. A. (1977). Rhinatrematidae: a new family of caecilians (Amphibia: Gymnophiona). *Occ. P. Mus. Zool. Univ. Michigan*, 628:1–30.

Nuño de la Rosa, L. (2012). *El Concepto de Forma en la Biología Contemporanea. Examen Filosófico (PhD Thesis).* Universidad Complutense de Madrid and Université Paris 1 Panthéon-Sorbone, Madrid and Paris.

Ochoa, C. and Barahona, A. (2009). El debate entre Cuvier y Geoffroy, y el origen de la homología y la analogía. *Ludus Vitalis*, 17:37–54.

Okajima, Y. and Kumazawa, Y. (2010). Mitochondrial genomes of acrodont lizards: timing of gene rearrangements and phylogenetic and biogeographic implications. *BMC Evol. Biol.*, 10:141e.

Olson, E. C. and Miller, R. L. (1958). *Morphological Integration.* University of Chicago Press, Chicago.

Opperman, L. A. (2000). Cranial sutures as intramembranous bone growth sites. *Dev. Dynam.*, 219:472–485.

Ostrom, J. H. (1961). Cranial morphology of the hadrosaurian dinosaurs of North America. *B. Am. Mus. Nat. Hist.*, 122:33–195.

Ozekhan, H. (1971). Planning and human action. In Weiss, P. A., editor, *Hierarchically Organized Systems in Theory and Practice*, page 123–230. Hafner Publishing Company.

Pace, J. K., Gilbert, C., Clark, M. S., and Feschotte, C. (2008). Repeated horizontal transfer of a DNA transposon in mammals and other tetrapods. *Proc. Natl. Acad. Sci. USA*, 105:17023–17028.

Padian, K. (1984). Pterosaur remains from the Kayenta Formation (?Early Jurassic) of Arizona. *Paleobiology*, 27:407–413.

Payne, S. L., Holliday, C. M., and Vickaryous, M. K. (2011). An osteological and histological investigation of cranial joints in geckos. *Anat. Rec.*, 294:399–405.

Pearson, K. and Woo, T. L. (1935). Further investigation of the morphometric characters of the individual bones of the human skull. *Biometrika*, 27:424–465.

Percival, C. J. and Richtsmeier, J. T. (2011). The epigenetics of dysmorphology. In Hallgrímson, B. and Hall, B. K., editors, *Epigenetics. Linking Genotype and Phenotype in Development and Evolution*, pages 377–397. University of California Press.

Pereira-Leal, J. B., Levy, E. D., and Teichmann, S. A. (2006). The origins and evolution of functional modules: lessons from protein complexes. *Phil. Trans. R. Soc. B*, 361:507–517.

Phillips, M. J., Bennett, T., and Lee, M. S. Y. (2009). Molecules and morphology suggest a recent, amphibious ancestry for echidnas. *Proc. Natl. Acad. Sci. USA*, 106:17089–17094.

Piagliucci, M. and Preston, K. (2004). *Phenotypic Integration. Studing the Ecology and Evolution of Complex Phenotypes*. Oxford University Press, Oxford.

Pierce, S. E., Angielczyk, K. D., and Rayfield, E. J. (2008). Patterns of morphospace occupation and mechanical performance in extant crocodilian skulls: a combined geometric morphometric and finite element modeling approach. *J. Morphol.*, 268:840–864.

Porter, M. A., Onella, J.-P., and Mucha, P. J. (2009). Communities in networks. *Not. Am. Math. Soc.*, 56:1082–1097.

Porto, A., Shirai, F. B. O. L. T., De Conto, V., and Marroig, G. (2009). The evolution of modularity in the mammalian skull: morphological integration patterns and magnitudes. *Evol. Biol.*, 36:118–135.

Proulx, S. R., Promislow, D. E., and Phillips, P. C. (2005). Network thinking in ecology and evolution. *Trends Ecol. Evol.*, 20:345–353.

Raff, R. A. (1996). *The Shape of Life. Gene, Development, and the Evolution of Animal Form*. University of Chicago Press, Chicago and Lodon.

Rafferty, K. L., Herring, S. W., and Marshall, C. D. (2003). Biomechanics of the rostrum and the facial sutures. *J. Morphol.*, 257:33–44.

Rashevsky, N. (1954). Topology and life. *B. Math. Biophys.*, 16:317–348.

Rashevsky, N. (1960). Contributions to relational biology. *B. Math. Biophys.*, 22:73–83.

Rasskin-Gutman, D. (1995). *Modelos Geométricos y Topológicos en Morfología: Exploración de los Límites del Morfoespacio Afin. Aplicaciones en Paleobiología*. Tesis Doctoral, Universidad Autónoma de Madrid.

Rasskin-Gutman, D. (2003). Boundary constraints for the emergence of form. In Müller, G. and Newman, S., editors, *Origination of Organismal Form*, pages 305–322. MIT Press.

Rasskin-Gutman, D. (2005). Modularity: jumping forms within morphospace. In Callebaut, W. and Rasskin-Gutman, D., editors, *Modularity: Understanding the Development and Evolution of Natural Complex Systems*, pages 207–219. MIT Press.

Rasskin-Gutman, D. and Buscalioni, A. D. (2001). Theoretical morphology of the archosaur (Reptilia: Diapsida) pelvic girdle. *Paleobiology*, 27:59–78.

Rasskin-Gutman, D. and De Renzi, M. (2007). *Pere Alberch. The Creative Trajectory of an Evo-Devo Biologist*. Publicaciones de la Universidad de Valencia, Valencia.

Rasskin-Gutman, D. and Esteve-Altava, B. (2008). The multiple directions of evolutionary change. *BioEssays*, 30:521–525.

Rasskin-Gutman, D. and Esteve-Altava, B. (2009). Modeling evo-devo: broken hierarchies and multiple scales of organization and complexity. In Sinclair, R. M. and Stiefel, K. M., editors, *Phenomena in Biology: Proceedings of the 2nd Okinawa Conference on Mathematics and Biology*, pages 43–56. American Institute of Physics.

Rasskin-Gutman, D. and Izpisua-Belmonte, J. C. (2004). Theoretical morphology of left-right asymmetries. *BioEssays*, 26:405–412.

Raup, D. M. (1961). The geometry of coiling in gastropods. *Proc. Natl. Acad. Sci. USA*, 47:602–609.

Raup, D. M. (1962). Computer as aid in describing form in gastropod shells. *Science*, 138:150–152.

Raup, D. M. (1966). Geometric analysis of shell coiling: general problems. *J. Paleontol.*, 40:1178–1190.

Raup, D. M. (1967). Geometric analysis of shell coiling: coiling in ammonoids. *J. Paleontol.*, 41:43–65.

Raup, D. M. (1968). Theoretical morphology of echinoid growth. *J. Paleontol.*, 42:50–63.

Ravasz, E., Somera, A. L., Mongru, D. A., Oltvai, Z. N., and Barabási, A.-L. (2002). Hierarchical organization of modularity in metabolic networks. *Science*, 297:1551–1555.

Reisz, R. (1981). A diapsid reptile from the Pennsylvanian of Kansas. *Univ. Kansas Mus. Nat. H. Spec. P.*, 7:1–74.

Rice, D. P. (2008). *Craniofacial Sutures, Development, Disease and Treatment. Frontiers of Oral Biology Vol. 12*. Karger, Basel, Switzerland.

Rice, D. P. and Rice, R. (2008). Locate, condense, differentiate, grow and confront: developmental mechanisms controlling intramembranous bone and suture formation and function. In Rice, D. P., editor, *Craniofacial Sutures, Development, Disease and Treatment. Frontiers of Oral Biology Vol. 12*, pages 22–40. Karger.

Richtsmeier, J. T., Aldridge, K., DeLeon, V. B., Panchal, J., Kane, A. A., Marsh, J. L., Yan, P., and Cole, T. M. (2006). Phenotypic integration of neurocranium and brain. *J. Exp. Zool. (Mol. Dev. Evol.)*, 306:360–378.

Riedl, R. (1975). *Die Ordnung des Lebendigen.* Parey, Berlin.

Riedl, R. (1978). *Order in Living Organisms: A Systems Analysis of Evolution.* Wiley, New York.

Rieppel, O. (1984). Miniaturization of the lizard skull: its functional and evolutionary implications. In Ferguson, M. W. J., editor, *The structure, development, and evolution of reptiles*, pages 503–520. London Academic Press.

Rieppel, O. (1993). Patterns of diversity in the reptilian skull. In Hanken, J. and Hall, B. K., editors, *The Skull. Vol. 2*, pages 344–390. University of Chicago Press.

Rieppel, O. (1995). Studies on skeleton formation in reptiles: implications for turtle relationships. *Zool. Anal. Complex. Sy.*, 298-308:98.

Rieppel, O. (2006). Type in morphology and phylogeny. *J. Morphol.*, 267:528–535.

Rohlf, F. J. (2002). Geometric morphometrics in phylogeny. In Forey, P. and Macleod, N., editors, *Morphology, Shape, and Phylogenetics*, pages 175–193. Francis and Taylor.

Romer, A. S. (1969). The cranial anatomy of the Permian amphibian *Pantylus*. *Breviora*, 314:29–38.

Romer, A. S. and Parsons, T. S. (1977). *The Vertebrate Body.* Holt-Saunders International, Philadelphia.

Rosas, A. and Bastir, M. (2004). Geometric morphometric analysis of allometric variation in the mandibular morphology of the hominids of Atapuerca, Sima de los Huesos site. *Anat. Rec.*, 278:551–560.

Roscher, M. and Schneider, J. W. (2006). Permo-Carboniferous climate: Early Pennsylvanian to Late Permian climate development of central Europe in a regional and global context. In Lucas, G., Cassinis, G., and Schneider, J. W., editors, *Non-marine Permian Biostratigraphy and Biochronology*, pages 95–136. Geological Society of London.

Rosen, E. S. (1916). *Form and Function. A Contribution to the History of Animal Morphology.* John Murray, London.

Rosen, R. (1991). *Life Itself: A Comprehensive Inquiry into the Nature, Origin, and Fabrication of Life.* Columbia University Press, New York.

Rosen, R. (2000). *Essays of Life Itself.* Columbia University Press, New York.

Rosenberger, A. L. and Pagano, A. S. (2008). Frontal fusion: collapse of another anthropoid synapomorphy. *Anat. Rec.*, 291:308–317.

Roth, V. L. and Mercer, J. M. (2000). Morphometrics in development and evolution. *Amer. Zool.*, 40:801–810.

Rowe, T. (2002). *Digital Morphology.* Available at, www.digimorph.org.

Rubinov, M. and Sporns, O. (2010). Complex network measures of brain connectivity: uses and interpretations. *Neuroimage*, 52:1059–1069.

Saheb, H. S., Mavishetter, G. F., Thomas, S. T., Prasanna, L. C., and Muralidhar, P. (2011). A study of sutural morphology of the pterion and asterion among human adult Indian skulls. *Biomed. Res-India*, 22:73–75.

Sales-Pardo, M., Guimerà, R., Moreira, A. A., and Nunes-Amaral, L. A. (2007). Extracting the hierarchical organization of complex systems. *Proc. Natl. Acad. Sci. USA*, 104:15224–15229.

Sanger, T. J., Mahler, D. L., Abzhanov, A., and Losos, J. B. (2011). Roles for modularity and constraint in the evolution of cranial diversity among anolis lizards. *Evolution*, 66:1525–1542.

Santagati, F. and Rijli, F. M. (2003). Cranial neural crest and the building of the vertebrate head. *Nat. Rev. Neurosci.*, 4:806–818.

Sardi, M. L., Ventrice, F., and Ramírez-Rozzi, F. (2007). Allometries throughout the late prenatal and early postnatal human craniofacial ontogeny. *Anat. Rec.*, 290:1112–1120.

Schlosser, G. and Wagner, G. P. (2004). *Modularity in Development and Evolution.* University of Chicago Press, Chicago.

Schoch, R. R. (2006). Skull ontogeny: dsevelopmental patterns of fishes conserved across major tetrapod clades. *Evol. Dev.*, 8:524–536.

Schoch, R. R. (2010). Riedl's burden and the body plan: selection, constraints, and deep time. *J. Exp. Zool. (Mol. Dev. Evol.)*, 314:1–10.

Seilacher, A. (1991). Self-organizing mechanisms in morphogenesis and evolution. In Palmqvist, P. and Pérez-Claros, J. A., editors, *Constructional Morphology and Evolution*, pages 251–271. Springer-Verlag.

Sereno, P. C. (1997). The origin and evolution of dinosaur. *Annu. Rev. Earth Pl. Sc.*, 25:435–489.

Sidor, C. A. (2001). Simplification as a trend in synapsid cranial evolution. *Evolution*, 55:1419–1442.

Simon, H. A. (1962). The architecture of complexity. *Proc. Amer. Phil. Soc.*, 106:467–482.

Simpson, G. G. (1961). *Principles of Animal Taxonomy.* Columbia University Press, New York.

Solé, R. V. and Goodwin, B. C. (2000). *Signs of Life. How Complexity Pervades Biology.* Basic Books, New York.

Solé, R. V., Valverde, S., and Rodriguez-Caso, C. (2007). Modularity in biological networks. In Képès, F., editor, *Biological Networks. Complex Systems and Interdisciplinary Science Vol. 3*, pages 21–40. World Scientific.

Spencer, H. (1889). *First Principle.* D. Appleton and Company, New York.

Sperber, G. H. (2001). *Craniofacial Development.* BC Decker Inc, Ontario.

Sporns, O. (2002). Network analysis, complexity, and brain function. *Complexity*, 8:56–60.

Springer, M. S., Murphy, W. J., Eizirik, E., and O'Brien, J. (2003). Placental mammal diversification and the Cretaceous-Tertiary boundary. *Proc. Natl. Acad. Sci. USA*, 100:1056–1061.

Sterli, J. and Joyce, W. G. (2007). The cranial anatomy of the Early Jurassic turtle *Kayentachelys aprix*. *Acta Paleontol. Pol.*, 52:675–694.

Taylor, P. J. (2005). *Unruly Complexity.* University of Chicago Press, Chicago.

Terentjev, P. V. (1931). Biometrische Untersuchungen über die morphologischen Merkmale von *Rana ridibunda* Pall. (Amphibia: Salientia). *Biometrika*, 23:23–51.

Thompson, D. W. (1992). *On Growth and Form. Dover Reprint of 1942 2nd Ed. (1st ed., 1917).* Dover Publications, New York.

Torres-Carvajal, O. (2003). Cranial osteology of the andean lizard *Stenocercus guentheri* (Squamata: Tropiduridae) and its postembryonic development. *J. Morphol.*, 255:94–113.

Trueb, L. (1993). Patterns of cranial diversity among the lissamphibia. In Hanken, J. and Hall, B. K., editors, *The Skull. Vol. 2*, pages 255–343. University of Chicago Press.

Trueb, L. and Alberch, P. (1985). Miniaturization in the anuran skull: a case study of heterochrony. In Duncker, H. R. and Fleischer, G., editors, *Vertebrate Morphology*, pages 503–520. Gustav Fisher Verlag.

Valen, L. V. (1962). A study of fluctuating asymmetry. *Evolution*, 16:125–142.

Valentine, J. W. (2003). The architectures of biological complexity. *Integr. Comp. Biol.*, 43:99–103.

Valentine, J. W., Collins, A. G., and Meyer, C. P. (1994). Morphological complexity increase in metazoans. *Paleobiology*, 20:131–142.

Waddington, C. H. (1956). *Princeples of Embryology.* Allen and Unwin, Wales.

Wagner, G. P. and Laubichler, M. D. (2004). Rupert Riedl and the re-synthesis of evolutionary and developmental biology. *J. Exp. Zool. (Mol. Dev. Evol.)*, 302:92–102.

Wagner, G. P., Pavlicev, M., and Cheverud, J. M. (2007). The road to modularity. *Nat. Rev.*, 8:921–931.

Waldrop, M. M. (1992). *Complexity. The Emerging Science at the Edge of Order and Chaos.* Penguin, London.

Wang, Q., Opperman, L. A., Havill, L. M., Carlson, D. S., and Dechow, P. C. (2006). Inheritance of sutural pattern at the pterion in *Rhesus monkey* skulls. *Anat. Rec. A. Discov. Mol. Cell. Evol. Biol.*, 288:1042–1049.

Watts, D. J. and Strogatz, S. H. (1998). Collective dynamics of small-world networks. *Nature*, 393:440–442.

Weinzweig, J., Kirschner, R. E., Farley, A., Reiss, P., Hunter, J., Whitaker, L. A., and Bartett, S. P. (2003). Metopic synostosis: defining the temporal sequence of normal suture fusion and differentiating it from synostosis on the basis of computed tomography images. *Plast. Reconstr. Surg.*, 112:1211–1218.

Weishampel, D. B. (1995). Fossils, function, and phylogeny. In Thomason, J., editor, *Functional Morphology in Vertebrate Paleontology*, pages 34–54. Cambridge University Press.

Weishampel, D. B., Dodson, P., and Osmólska, H. (1993). *The Dinosauria*. California University Press, Los Angeles.

Weiss, P. (1939). *Principles of Development*. Henry Holt and Company, New York.

Weiss, P. A. (1971). The basic concept of hierarchic systems. In Weiss, P. A., editor, *Hierarchically Organized Systems in Theory and Practice*, page 1–44. Hafner Publishing Company.

Werneburg, I. and Sánchez-Villagra, M. R. (2009). Timing of organogenesis support basal position of turtles in the amniote tree of life. *BMC Evol. Biol.*, 9:e82.

West, G. B., Brown, J. H., and Enquist, B. J. (1997). A general model for the origin of allometric scaling laws in biology. *Science*, 276:122–126.

White, T. E. (1939). Osteology of *Seymouria baylorensis* Broili. *B. Mus. Com. Zool.*, 85:325–409.

Wicken, J. S. (1979). The generation of complexity in evolution: a thermodynamic and information-theoretical discussion. *J. Theo. Biol*, 77:349–365.

Williams, G. C. (1966). *Adaptation and Natural Selection*. Princeton University Press, Princeton.

Williston, S. W. (1914). *Water Reptiles of the Past and Present*. University of Chicago Press, Chicago.

Willmore, K. E., Klingenberg, C. P., and Hallgrímsson, B. (2005). Congruence of fluctuating asymmetry and environmental variance in *Rhesus macaque* skulls. *Evolution*, 59:898–909.

Willmore, K. E., Leamy, L., and Hallgrímson, B. (2006). Effects of developmental and functional interactions on mouse cranial variability through late ontogeny. *Evol. Dev.*, 8:550–567.

Willmore, K. E., Young, N. M., and Richtsmeier, J. T. (2007). Phenotypic variability: its components, measurement and underlying developmental processes. *Evol. Biol.*, 34:99–120.

Wilson, L. A. B., Schradin, C., Mitgutsch, C., Galliari, F. C., Mess, A., and Sánchez-Villagra, M. R. (2010). Skeletogenesis and sequence heterochrony in rodent evolution, with particular emphasis on the African striped mouse, *Rhabdomys pumilio* (Mammalia). *Org. Divers. Evol.*, 10:243–258.

Wilson, L. A. B. and Sánchez-Villagra, M. R. (2009). Heterochrony and patterns of cranial suture closure in hystricognath rodents. *J. Anat.*, 214:339–335.

Wimsatt, W. C. (1986). Developmental constraints, generative entrenchment, and the innate-acquired distinction. In Bechtel, W., editor, *Integrating Scientific Disciplines*, pages 185–208. Martinus Nijhoff Publishers.

Witzel, U., Preuschoft, H., and Sick, H. (2004). The role of the zygomatic arch in the statics of the skull and its adaptive shape. *Folia Primatol.*, 75:202–218.

Wolpert, L. (1977). *The Development of Pattern and Form in Animals.* Carolina Biological, Burlington.

Woo, T. L. (1931). On the asymmetry of the human skull. *Biometrika*, 22:324–352.

Woodger, J. H. (1945). On biological transformations. In Gross, W. E. L. and Medawar, P. B., editors, *Essays on Growth and Form Presented to D'A. W. Thompson*, pages 95–120. Oxford University Press.

Wutchy, S., Ravasz, E., and Barabási, A.-L. (2006). The architecture of biological networks. In Deisboeck, T. S. and Kresh, J. T., editors, *Complex Systems Science in Biomedicine*, pages 165–181. Sringer.

Xu, K., Bezakova, I., Bunimovich, L., and Yi, S. V. (2011). Path lengths in protein-protein interaction networks and biological complexity. *Proteomics*, 11:1857–1867.

Zar, J. H. (1999). *Biostatistical Analysis.* Prentice Hall, Upper Saddle River.

Appendices

Appendix A: AnNA Toolbox

```
% AnNA Protocol

% Network and Node Parameters
[network_basics, node_basics, correlation, sw]=anne_basics(Graph);

% Distributions Fit
k_distribution(Graph);
c_distribution(Graph);

% Modularity Analysis
GTOM=computeGTOM(Graph,1);
[Z,H,T,PERM, distVector]=hcluster(Graph,GTOM);

% Robustness Test
robustness(Graph,Del);

% Circular Representation
plot_circular(Graph);
```

Own Functions in AnNA Toolbox

Node and Network Parameters

```
function [n_basic,N_basic,PC,Sig] = anne_basics(Graph)
% Returns the basic parameters from a Graph
% 1. n_basic: degree, clustering, path length, and betweenness
% 2. N_basic: density, clustering, path length, and
    heterogeneity.
% 3. Pearson's correlation coefficient between node parameters.
% 4. Presence of the small-workd effect by sigma calculation.
% Include functions from Brain Connectivity Toolbox.
% by Borja Esteve-Altava 2012

N=size(Graph,1); K=nnz(triu(Graph)); D=distance_bin(Graph);
[cluster_network,cluster_node]=clustercoeff_bu(Graph);
degrees=degrees_und(Graph);
path_node=sum(D,2)./(N-1);
BC = betweenness_bin(Graph);
n_basic=[degrees' cluster_node path_node BC];

density=K/((N^2-N)/2);
lambda=charpath(distance_bin(Graph));
hetero=std(degrees_und(Graph))/mean(degrees_und(Graph));
N_basic=[density cluster_network lambda hetero];

PC=corr(node_basics);

alpha=sum(sum(Graph(Graph~=Inf)))/length(nonzeros(Graph~=Inf));
R=randomizer_bin_und(Graph,alpha);
clusterR=clustercoeff_bu(R);
Dr=distance_bin(R); lambdaR=charpath(Dr);
Sig=(cluster/clusterR)/(lambda/lambdaR);
return
```

Degree Distribution Fit

```
function [Frequency Cumulative] = k_distribution(Graph)
% Cumulative degree distribution goodness-of-fit to:
% 1) power-law, 2) exponential, 3) linear, and 4) binomial
% Include functions from EzyFit Toolbox.
% by Borja Esteve-Altava 2012

Graph=double(Graph~=0); deg=sum(Graph)';
K=[min(deg):1:max(deg)]'; K(:,2)=zeros;
for i=1:length(deg)
    for j=1:length(K)
        if deg(i)==K(j,1)
            K(j,2)=K(j,2)+1;
        end
    end
end

Frequency=[K(:,1),K(:,2)/length(deg)];
Cumulative=[K(:,1),K(:,2).*0];
for h=1:length(Cumulative)
    Cumulative(h,2)=sum(Frequency(h:length(K),2));
end

POWER=ezfit(Cumulative(:,1),Cumulative(:,2),'power; lin');
EXP=ezfit(Cumulative(:,1),Cumulative(:,2),'exp; lin');
UNIFORM=ezfit(Cumulative(:,1),Cumulative(:,2),'affine; lin');
BINOMIAL=ezfit(Cumulative(:,1),Cumulative(:,2),'poly2; lin');

cP=struct2cell(POWER); cPFit=cell2mat(cP(6));
cE=struct2cell(EXP); cEFit=cell2mat(cE(6));
cU=struct2cell(UNIFORM); cUFit=cell2mat(cU(6));
cB=struct2cell(BINOMIAL); cBFit=cell2mat(cB(6));

bestfit=[cPFit cEFit cUFit cBFit];
```

```
34
35 if bestfit(1)==max(bestfit); rutina='power'; end;
36 if bestfit(2)==max(bestfit); rutina='exp'; end;
37 if bestfit(3)==max(bestfit); rutina='uniform'; end;
38 if bestfit(4)==max(bestfit); rutina='binomial'; end;
39
40 clf
41 plot(Cumulative(:,1),Cumulative(:,2),'*k'); hold on;
42 axis([1 20 0 1])
43 set(gca,'XTick',0:5:20)
44 set(gca,'YTick',0:0.2:1)
45 xlabel 'Degree (number of connections)';
46 ylabel 'Cumulative Degree Distribution';
47
48 switch lower(rutina)
49     case 'power'
50         showfit(POWER,'fitcolor','blue','fitlinewidth',1.5);
51     case 'exp'
52         showfit(EXP,'fitcolor','blue','fitlinewidth',1.5);
53     case 'uniform'
54         showfit(UNIFORM,'fitcolor','blue','fitlinewidth',1.5);
55     case 'binomial'
56         showfit(BINOMIAL,'fitcolor','blue','fitlinewith',1.5);
57     otherwise
58         disp('An error has occurred in distribution fit');
59 end
60
61 'Fits: POWER | EXP | LINE | BINOMIAL'
62 bestfit
63 return;
```

Clustering Coefficient Distribution Fit

```
function [Cdist] = c_distribution(Graph)
% Clustering coefficient distribution goodness-of-fit to:
% 1) power-law, 2) exponential, 3) linear, and 4) binomial
% Include functions from EzyFit Toolbox.
% by Borja Esteve-Altava 2012

C=clustering_coef_bu(Graph); deg=sum(Graph)';
K=count_unique(deg);
for i=1:length(K)
    Cm(i)=mean(C(find(deg==K(i))));
end
Cdist=[K Cm'];

POWER=ezfit(Cdist(:,1),Cdist(:,2),'power; lin');
EXP=ezfit(Cdist(:,1),Cdist(:,2),'exp; lin');
UNIFORM=ezfit(Cdist(:,1),Cdist(:,2),'affine; lin');
BINOMIAL=ezfit(Cdist(:,1),Cdist(:,2),'poly2; lin');

cP=struct2cell(POWER); cPFit=cell2mat(cP(6));
cE=struct2cell(EXP); cEFit=cell2mat(cE(6));
cU=struct2cell(UNIFORM); cUFit=cell2mat(cU(6));
cB=struct2cell(BINOMIAL); cBFit=cell2mat(cB(6));

bestfit=[cPFit cEFit cUFit cBFit];

if bestfit(1)==max(bestfit); rutina='power'; end;
if bestfit(2)==max(bestfit); rutina='exp'; end;
if bestfit(3)==max(bestfit); rutina='uniform'; end;
if bestfit(4)==max(bestfit); rutina='binomial'; end;

clf
plot(Cdist(:,1),Cdist(:,2),'*k'); hold on;
axis([1 20 0 1])
```

```
34 set(gca,'XTick',0:5:20)
35 set(gca,'YTick',0:0.2:1)
36 xlabel 'Connectivity (ki)';
37 ylabel 'Clustering Coefficient (Ci)';
38
39 switch lower(rutina)
40     case 'power'
41         showfit(POWER,'fitcolor','blue','fitlinewidth',1.5);
42     case 'exp'
43         showfit(EXP,'fitcolor','blue','fitlinewidth',1.5);
44     case 'uniform'
45         showfit(UNIFORM,'fitcolor','blue','fitlinewidth',1.5);
46     case 'binomial'
47         showfit(BINOMIAL,'fitcolor','blue','fitlinewith',1.5);
48     otherwise
49         disp('An error has occurred in distribution fit');
50 end
51
52 'Fits: POWER | EXP | LINE | BINOMIAL'
53 bestfit
54 return;
```

Robustness Test

```
function robustness(Graph,Del)
% Perform a robustness test for deletion of nodes.
% Preference of deletion: 1) most connected, 2) random, 3) less
    connected.
% Inputs: Graph, undirected binary matrix; Del, number of
    deletions.
% Output: graphic and network parameters.
% Include functions from Brain Connectivity Toolbox.
% by Borja Esteve-Graphltava 2012

% Initial Settings
if (nargin < 2); Del=[]; end;
if (isempty(Del)); Del=floor(0.2*length(Graph)); end;
Initial_Density=density_und(Graph);
Initial_Cluster=clustercoeff_bu(Graph);
Initial_Path=charpath(distance_bin(Graph));

% Deletion of Most Connected Nodes
for it=1:100
    Graphdel=Graph;
    for step=2:Del+1
        % find most connected
        Degree=degrees_und(Graphdel); t=1;
        for i=1:length(Degree)
            if Degree(i)==max(Degree)
                todelete(t)=i; t=t+1;
            end
        end
        % random selection among most connected
        hub=randi([1,length(todelete)]);
        vdel=todelete(hub);
        % deletion
        Graphdel(vdel,:)=[]; Graphdel(:,vdel)=[];
```

```
32          % save parameters
33          hub_N(it,step)= length(find(sum(Graphdel)==0));
34          hub_Density(it,step)=density_und(Graphdel);
35          hub_Cluster(it,step)=clustercoeff_bu(Graphdel);
36          hub_Path(it,step)=charpath(distance_bin(Graphdel));
37      end
38  end
39
40  % Deletion of Random Nodes
41  for it=1:10000
42      Graphdel=Graph;
43      for step=2:Del+1
44          % choose at random
45          R=randi([1,length(Graphdel)]);
46          % deletion
47          Graphdel(R,:)=[]; Graphdel(:,R)=[];
48          % save parameters
49          rand_N(it,step)=length(find(sum(Graphdel)==0));
50          rand_Density(it,step)=density_und(Graphdel);
51          rand_Cluster(it,step)=clustercoeff_bu(Graphdel);
52          rand_Path(it,step)=charpath(distance_bin(Graphdel));
53      end
54  end
55
56  % Deletion of Less Connected Nodes
57  for it=1:100
58      Graphdel=Graph;
59      for step=2:Del+1
60          % find less connected
61          Degree=degrees_und(Graphdel); t=1;
62          for i=1:length(Degree)
63              if Degree(i)==min(Degree)
64                  todelete(t)=i; t=t+1;
65              end
66          end
```

```
67          % random selection among less connected
68          hub=randi([1,length(todelete)]);
69          vdel=todelete(hub);
70          % deletion
71          Graphdel(vdel,:)=[]; Graphdel(:,vdel)=[];
72          % save parameters
73          anti_hub_N(it,step)=length(find(sum(Graphdel)==0));
74          anti_hub_Density(it,step)=density_und(Graphdel);
75          anti_hub_Cluster(it,step)=clustercoeff_bu(Graphdel);
76          anti_hub_Path(it,step)=charpath(distance_bin(Graphdel));
77      end
78  end
79
80  % Robustness Test Plots
81  figure(1)
82  set(1,'Position',[0 0 600 1200])
83
84  subplot(4,1,1),errorbar(mean(hub_N),std(hub_N),'or'); hold on;
85  errorbar(mean(rand_N),std(rand_N),'sb'); hold on;
86  errorbar(mean(anti_hub_N),std(anti_hub_N),'og');
87  ylabel 'Disconnected Nodes (#N)';
88  set(gca,'YTick',0:0.5:max(hub_N(:))+1)
89  set(gca,'XTick',1:1:Del+1)
90  set(gca,'XTickLabel',[0:1:Del+1])
91  axis([0 Del+2 0 max(hub_N(:))+1])
92  grid on
93
94  subplot(4,1,2),errorbar(mean(hub_Density),std(hub_Density),'or')
        ; hold on;
95  errorbar(mean(rand_Density),std(rand_Density),'sb'); hold on;
96  errorbar(mean(anti_hub_Density),std(anti_hub_Density),'og');
97  ylabel 'Density of Connections';
98  set(gca,'YTick',0:0.2:1)
99  set(gca,'XTick',1:1:Del+1)
100 set(gca,'XTickLabel',[0:1:Del+1])
```

```
101 axis([0 Del+2 0 1])
102 grid on
103
104 subplot(4,1,3),errorbar(mean(hub_Cluster),std(hub_Cluster),'or')
      ; hold on;
105 errorbar(mean(rand_Cluster),std(rand_Cluster),'sb'); hold on;
106 errorbar(mean(anti_hub_Cluster),std(anti_hub_Cluster),'og');
107 ylabel 'Clustering Coefficient';
108 set(gca,'YTick',0:0.2:1)
109 set(gca,'XTick',1:1:Del+1)
110 set(gca,'XTickLabel',[0:1:Del+1])
111 axis([0 Del+2 0 1])
112 grid on
113
114 subplot(4,1,4),errorbar(mean(hub_Path),std(hub_Path),'or'); hold
      on;
115 errorbar(mean(rand_Path),std(rand_Path),'sb'); hold on;
116 errorbar(mean(anti_hub_Path),std(anti_hub_Path),'og');
117 xlabel 'Nodes Removed(#N)';ylabel 'Characteristic Path Length';
118 set(gca,'YTick',1:0.5:max(hub_Path(:)))
119 set(gca,'XTick',1:1:Del+1)
120 set(gca,'XTickLabel',[0:1:Del+1])
121 axis([0 Del+2 1 max(hub_Path(:))])
122 grid on
123 return;
```

Circular Network Plot

```
function plot_circular(Graph)
% Plots the network in a circle.
% by Borja Esteve-Altava 2012

nodes=length(Graph)+1;
theta=linspace(0,2*pi,nodes);theta=theta(1:end-1);
[x,y]=pol2cart(theta,1);
links=Graph;
for i=1:length(links)
    for j=1:length(links)
        if i>j
            links(i,j)=0;
        end
    end
end
[ind1,ind2]=ind2sub(size(links),find(links(:)));

h=figure(1);clf(h);
plot(x,y,'.k','markersize',20);hold on
arrayfun(@(p,q)line([x(p),x(q)],[y(p),y(q)]),ind1,ind2);
axis equal off
return
```

Borrowed functions in the AnNE Toolbox

Borrowed functions in the AnNA Toolbox

Source	Author	Year	Function
Brain Connectivity Toolbox	Power	2010	randomizer_bin_und
	Rubinov	2010	betweenness_bin
			clustering_coef_bu
			distance_bin
			module_degree_zscore
			participation_coef
			charpath
	Sporns	2008	degrees_und
			density_und
EzyFit Toolbox	Moisy	2010	ezyfit
MatLab Repository	Helmick	2007	varycolor
	Goñi, Martincorena	2007	computeGTOM
			hcluster

Appendix B: Computational Model

```
% Computational Model of Skull Evolution
% Inputs:
        % Number of Iterations
        % Minimal Network Size (stop)
        % Value of the Selection Processes (Loss_Selection,
            Fuse_Selection)
        % Value of the Loss:Fusion (LFR)
        % Initial Number of Bones (U_bones, P_bones)
        % Spatial Boundaries(x, y, anz z factors)
% Outcome:
        % Number of Matches of the model (counts)
        % Density of Connections, Clustering Coefficient,
            Shortest Path Length, and Heterogeneity vectors
% by Borja Esteve-Altava 2013

% Settings
Stop=15;
it=100;

% Initial Model Conditions

    % Selection Process
    Loss_Selection='1'; % 1) least, 2) most, and 3) random
    Fuse_Selection='2'; % 1) least, 2) most, and 3) random

    % Loss:Fusion Ratio
    LFR=0.5; % 1=only Fusion; 0=only Loss

    % Number of Bones
    U_bones=1;
    P_bones=30;
    Bones=U_bones+2*P_bones;
```

```
31
32      % Spatial Boundary
33      x_factor=1;
34      y_factor=1;
35      z_factor=1;
36      midline=x_factor/2;
37
38 % Recording Vectors
39 density=zeros(it,Bones);
40 cluster=zeros(it,Bones);
41 path=zeros(it,Bones);
42 heter=zeros(it,Bones);
43
44 % Start Simulation
45 for iteration=1:it
46
47      % Creation of the Position Vector
48      Position=zeros(Bones,6);
49      for i=1:2:P_bones*2
50          Position(i,:)=[rand*midline rand*y_factor rand*z_factor
                i 0 0];
51          Position(i+1,:)=[(x_factor-Position(i,1)) Position(i,2)
                Position(i,3) i 0 0];
52      end
53      for i=1+P_bones*2:Bones
54          Position(i,:)=[midline rand*y_factor rand*z_factor i 0
                1];
55      end
56
57      % Creation of the Ancestral Skull
58      Graph=Gabriel(Position(:,[1:3]));
59
60      % Sequential Reduction of the Number of Bones
61      while length(Graph)>Stop
62
```

```
63          % Measure Parameters
64          density(iteration,length(Graph))=density_und(Graph);
65          cluster(iteration,length(Graph))=clustercoeff_watts(
                Graph);
66          path(iteration,length(Graph))=charpath(distance_bin(
                Graph));
67          heter(iteration,length(Graph))=(std(degrees_und(Graph)))
                /(mean(degrees_und(Graph)));
68
69          % Decide between Fusion or Loss
70          if rand>LFR
71              % Select a Bone for Loss (here we obtain its ID)
72              switch (Loss_Selection)
73                  case '1' % least connected
74                      % List all least connected and chose one
75                      deg=degrees_und(Graph);
76                      mindeg=find(deg==min(deg));
77                      IDtoLOSS=Position(mindeg(randi([1,length(
                            mindeg)]))),4);
78                  case '2' % most connected
79                      % List all most connected and chose one
80                      deg=degrees_und(Graph);
81                      maxdeg=find(deg==max(deg));
82                      IDtoLOSS=Position(maxdeg(randi([1,length(
                            maxdeg)]))),4);
83                  case '3' % random
84                      % choose one at random
85                      IDtoLOSS=Position(randi([1,length(Position)
                            ]),4);
86                  otherwise
87                      disp('error selecting for LOSS')
88              end
89              % Assign Routines for loss
90              if Position(find(Position(:,4)==IDtoLOSS,1),1)==
                    midline
```

```
91                routine='loss_unpair';
92            else
93                routine='loss_pair';
94            end
95        else
96            % Select a Bone for Fusion (here we obtain its ID)
97            switch (Fuse_Selection)
98                case '1' % least connected
99                    % List all least connected and chose one
100                   deg=degrees_und(Graph);
101                       deg(deg==0)=200; % avoid disconnected to
                              be fused
102                   mindeg=find(deg==min(deg));
103                   IDtoFUSE=Position(mindeg(randi([1,length(
                          mindeg)])),4);
104                   % Chose one of its neighbors for fusion at
                          random
105                   neighbors=find(Graph(find(Position(:,4)==
                          IDtoFUSE,1),:)==1);
106                   IDtoFUSEwith=Position(neighbors(randi([1,
                          length(neighbors)])),4);
107               case '2' % most connected
108                   % List all most connected and chose one
109                   deg=degrees_und(Graph);
110                   maxdeg=find(deg==max(deg));
111                   IDtoFUSE=Position(maxdeg(randi([1,length(
                          maxdeg)])),4);
112                   % Chose one of its neighbors for fusion at
                          random
113                   neighbors=find(Graph(find(Position(:,4)==
                          IDtoFUSE,1),:)==1);
114                   IDtoFUSEwith=Position(neighbors(randi([1,
                          length(neighbors)])),4);
115               case '3' % random
116                   % Choose one at random avoiding disconnected
```

```
117                     check_disc=0;
118                     while check_disc==0
119                         IDtoFUSE=Position(randi([1,length(
                                Position)]),4);
120                         if sum(Graph(find(Position(:,4)==
                                IDtoFUSE,1),:))==0
121
122                         else
123                             neighbors=find(Graph(find(Position
                                    (:,4)==IDtoFUSE,1),:)==1);
124                             IDtoFUSEwith=Position(neighbors(
                                    randi([1,length(neighbors)])),4);
125                             check_disc=1;
126                         end
127                     end
128                 otherwise
129                     disp('error selecting for FUSION')
130             end
131             % Assign Routines for fusion
132             if Position(find(Position(:,4)==IDtoFUSE,1),4)~=
                    Position(find(Position(:,4)==IDtoFUSEwith,1),4) %
                     bones have different ID
133                 if (Position(find(Position(:,4)==IDtoFUSE,1),6)
                        ==0)&&(Position(find(Position(:,4)==
                        IDtoFUSEwith,1),6)==0) % both bones are pair
134                     routine='fusion_parpar';
135                 elseif (Position(find(Position(:,4)==IDtoFUSE,1)
                        ,6)==1)&&(Position(find(Position(:,4)==
                        IDtoFUSEwith,1),6)==1) % both bones are
                        unpaired
136                     routine='fusion_unparunpar';
137                 else % only one is unpaired
138                     routine='fusion_parunpar';
139                 end
140             else % bones have same ID (contralateral bones)
```

```
141             routine='fusion_medial';
142         end
143     end % end Selection of ID and Routines
144
145     % Apply routine
146     switch (routine)
147         case 'loss_pair'
148             % Locate all neighbors
149             neighbors1=find(Graph(find(Position(:,4)==
                    IDtoLOSS,1),:)==1);
150             neighbors2=find(Graph(find(Position(:,4)==
                    IDtoLOSS,1)+1,:)==1);
151             % Decide if they add new connections
152             if length(neighbors1)>2
153                 subGraph=Gabriel(Position(neighbors1,[1:3]))
                        ;
154                 for i=1:length(subGraph)
155                     for j=1:length(subGraph)
156                         if subGraph(i,j)==1
157                             Graph(neighbors1(i),neighbors1(j
                                    ))=1;
158                         end
159                     end
160                 end
161             elseif length(neighbors1)==2
162                 Graph(neighbors1(1),neighbors1(2))=1;
163                 Graph(neighbors1(2),neighbors1(1))=1;
164             end
165             if length(neighbors2)>2
166                 subGraph=Gabriel(Position(neighbors2,[1:3]))
                        ;
167                 for i=1:length(subGraph)
168                     for j=1:length(subGraph)
169                         if subGraph(i,j)==1
```

```
170                                 Graph(neighbors2(i),neighbors2(j
                                        ))=1;
171                             end
172                         end
173                     end
174                 elseif length(neighbors2)==2
175                     Graph(neighbors2(1),neighbors2(2))=1;
176                     Graph(neighbors2(2),neighbors2(1))=1;
177                 end
178                 % Clear Graph
179                 Graph(find(Position(:,4)==IDtoLOSS,1)+1,:)=[];
180                 Graph(:,find(Position(:,4)==IDtoLOSS,1)+1)=[];
181                 Graph(find(Position(:,4)==IDtoLOSS,1),:)=[];
182                 Graph(:,find(Position(:,4)==IDtoLOSS,1))=[];
183                 % Clear Position Vector
184                 Position(Position(:,4)==IDtoLOSS,:)=[];
185             case 'loss_unpair'
186                 % Locate all neighbors
187                 neighbors1=find(Graph(find(Position(:,4)==
                        IDtoLOSS,1),:)==1);
188                 % Decide if they add new connections
189                 if length(neighbors1)>2
190                     subGraph=Gabriel(Position(neighbors1,[1:3]))
                            ;
191                     for i=1:length(subGraph)
192                         for j=1:length(subGraph)
193                             if subGraph(i,j)==1
194                                 Graph(neighbors1(i),neighbors1(j
                                        ))=1;
195                             end
196                         end
197                     end
198                 elseif length(neighbors1)==2
199                     Graph(neighbors1(1),neighbors1(2))=1;
200                     Graph(neighbors1(2),neighbors1(1))=1;
```

```
201             end
202             % Clear Graph
203             Graph(find(Position(:,4)==IDtoLOSS,1),:)=[];
204             Graph(:,find(Position(:,4)==IDtoLOSS,1))=[];
205             % Clear Position Vector
206             Position(Position(:,4)==IDtoLOSS,:)=[];
207         case 'fusion_parpar'
208             % Add connections to IDtoFUSE in both sides
209             Graph(find(Position(:,4)==IDtoFUSE,1),:)=Graph(
                    find(Position(:,4)==IDtoFUSE,1),:)|Graph(find
                    (Position(:,4)==IDtoFUSEwith,1),:);
210             Graph(:,find(Position(:,4)==IDtoFUSE,1))=Graph
                    (:,find(Position(:,4)==IDtoFUSE,1))|Graph(:,
                    find(Position(:,4)==IDtoFUSEwith,1));
211             Graph(find(Position(:,4)==IDtoFUSE,1)+1,:)=Graph
                    (find(Position(:,4)==IDtoFUSE,1)+1,:)|Graph(
                    find(Position(:,4)==IDtoFUSEwith,1)+1,:);
212             Graph(:,find(Position(:,4)==IDtoFUSE,1)+1)=Graph
                    (:,find(Position(:,4)==IDtoFUSE,1)+1)|Graph
                    (:,find(Position(:,4)==IDtoFUSEwith,1)+1);
213             Graph(1:length(Graph)+1:length(Graph)*length(
                    Graph))=0; % set diagonal to 0
214             % Set new Position and Fuse state (1)
215             Position(Position(:,4)==IDtoFUSE,1:3)=(Position(
                    Position(:,4)==IDtoFUSE,1:3)+Position(
                    Position(:,4)==IDtoFUSEwith,1:3))./2;
216             Position(Position(:,4)==IDtoFUSE,5)=1;
217             % Delete IDtoFUSEwith+1 and IDtoFUSEwith
218             Graph(find(Position(:,4)==IDtoFUSEwith,1)+1,:)
                    =[];
219             Graph(:,find(Position(:,4)==IDtoFUSEwith,1)+1)
                    =[];
220             Graph(find(Position(:,4)==IDtoFUSEwith,1),:)=[];
221             Graph(:,find(Position(:,4)==IDtoFUSEwith,1))=[];
```

```
222             Position(Position(:,4)==IDtoFUSEwith,:)=[]; %
                    delete all rows with ID
223         case 'fusion_unparunpar'
224             % Add connections to IDtoFUSE
225             Graph(find(Position(:,4)==IDtoFUSE,1),:)=Graph(
                    find(Position(:,4)==IDtoFUSE,1),:)|Graph(find
                    (Position(:,4)==IDtoFUSEwith,1),:);
226             Graph(:,find(Position(:,4)==IDtoFUSE,1))=Graph
                    (:,find(Position(:,4)==IDtoFUSE,1))|Graph(:,
                    find(Position(:,4)==IDtoFUSEwith,1));
227             Graph(1:length(Graph)+1:length(Graph)*length(
                    Graph))=0; % set diagonal to 0
228             % Set new Position and Fused state (1)
229             Position(Position(:,4)==IDtoFUSE,1:3)=(Position(
                    Position(:,4)==IDtoFUSE,1:3)+Position(
                    Position(:,4)==IDtoFUSEwith,1:3))./2;
230             Position(Position(:,4)==IDtoFUSE,5)=1;
231             % Delete IDtoFUSEwith
232             Graph(find(Position(:,4)==IDtoFUSEwith,1),:)=[];
233             Graph(:,find(Position(:,4)==IDtoFUSEwith,1))=[];
234             Position(Position(:,4)==IDtoFUSEwith,:)=[]; %
                    delete all rows with ID
235         case 'fusion_parunpar'
236             if Position(find(Position(:,4)==IDtoFUSE,1),6)
                    ==1 % if IDtoFUSE is the unpaired bone
237                 % Add connections to IDtoFUSE
238                  Graph(find(Position(:,4)==IDtoFUSE,1),:)=
                         Graph(find(Position(:,4)==IDtoFUSE,1),:)|
                         Graph(find(Position(:,4)==IDtoFUSEwith,1)
                         ,:)|Graph((find(Position(:,4)==
                         IDtoFUSEwith,1)+1),:);
239                  Graph(:,find(Position(:,4)==IDtoFUSE,1))=
                         Graph(:,find(Position(:,4)==IDtoFUSE,1))|
                         Graph(:,find(Position(:,4)==IDtoFUSEwith
```

```
                ,1))|Graph(:,(find(Position(:,4)==
                IDtoFUSEwith,1))+1);
240             Graph(1:length(Graph)+1:length(Graph)*length
                (Graph))=0; % set diagonal to 0
241             % Set new Position and Fuse state(1)
242             Position(Position(:,4)==IDtoFUSE,1:3)=(
                Position(Position(:,4)==IDtoFUSE,1:3) +
                Position(find(Position(:,4)==IDtoFUSEwith
                ,1),1:3) + Position((find(Position(:,4)==
                IDtoFUSEwith,1))+1,1:3))./3;
243             Position(Position(:,4)==IDtoFUSE,5)=1;
244             % DeleteIDtoFUSEwith
245             Graph(find(Position(:,4)==IDtoFUSEwith,1)
                +1,:)=[];
246             Graph(:,find(Position(:,4)==IDtoFUSEwith,1)
                +1)=[];
247             Graph(find(Position(:,4)==IDtoFUSEwith,1),:)
                =[];
248             Graph(:,find(Position(:,4)==IDtoFUSEwith,1))
                =[];
249             Position(Position(:,4)==IDtoFUSEwith,:)=[];
                % delete all rows with ID
250         else % if IDtoFUSEwith is the unpaired bone
251             % Add connections to IDtoFUSE
252             Graph(find(Position(:,4)==IDtoFUSEwith,1),:)
                =Graph(find(Position(:,4)==IDtoFUSEwith
                ,1),:)|Graph(find(Position(:,4)==IDtoFUSE
                ,1),:)|Graph(find(Position(:,4)==IDtoFUSE
                ,1)+1,:);
253             Graph(:,find(Position(:,4)==IDtoFUSEwith,1))
                =Graph(:,find(Position(:,4)==IDtoFUSEwith
                ,1))|Graph(:,find(Position(:,4)==IDtoFUSE
                ,1))|Graph(:,find(Position(:,4)==IDtoFUSE
                ,1)+1);
```

```
254                 Graph(1:length(Graph)+1:length(Graph)*length
                        (Graph))=0; % set diagonal to 0
255                 % Set new Position and Fuse state(1)
256                 Position(Position(:,4)==IDtoFUSEwith,1:3)=(
                        Position(Position(:,4)==IDtoFUSEwith,1:3)
                         + Position(find(Position(:,4)==IDtoFUSE
                        ,1),1:3) + Position((find(Position(:,4)==
                        IDtoFUSE,1))+1,1:3))./3;
257                 Position(Position(:,4)==IDtoFUSEwith,5)=1;
258                 % DeleteIDtoFUSEwith
259                 Graph(find(Position(:,4)==IDtoFUSE,1)+1,:)
                        =[];
260                 Graph(:,find(Position(:,4)==IDtoFUSE,1)+1)
                        =[];
261                 Graph(find(Position(:,4)==IDtoFUSE,1),:)=[];
262                 Graph(:,find(Position(:,4)==IDtoFUSE,1))=[];
263                 Position(Position(:,4)==IDtoFUSE,:)=[]; %
                        delete all rows with ID
264             end
265         case 'fusion_medial'
266             % Add connections to IDtoFUSE
267             Graph(find(Position(:,4)==IDtoFUSE,1),:)=Graph(
                    find(Position(:,4)==IDtoFUSE,1),:)|Graph((
                    find(Position(:,4)==IDtoFUSEwith,1))+1,:);
268             Graph(:,find(Position(:,4)==IDtoFUSE,1))=Graph
                    (:,find(Position(:,4)==IDtoFUSE,1))|Graph(:,(
                    find(Position(:,4)==IDtoFUSEwith,1))+1);
269             Graph(1:length(Graph)+1:length(Graph)*length(
                    Graph))=0; % set diagonal to 0
270             % Set new Position, Fused state (1), and
                    Unpaired state(1)
271             Position(Position(:,4)==IDtoFUSE,1)=midline;
272             Position(Position(:,4)==IDtoFUSE,5)=1; %fuse
273             Position(Position(:,4)==IDtoFUSE,6)=1; %unpaired
274             % Delete IDtoFUSEwith+1
```

```
275                     Graph((find(Position(:,4)==IDtoFUSEwith,1))+1,:)
                            =[];
276                     Graph(:,(find(Position(:,4)==IDtoFUSEwith,1))+1)
                            =[];
277                     Position(find(Position(:,4)==IDtoFUSEwith,1)
                            +1,:)=[]; % delete all rows with ID
278                 otherwise
279                     disp('error applying ROUTINE')
280             end
281         end % end Reduction
282 end % end Simulation
283
284 % Find Number of Matches
285 density(density==0)=NaN;
286 cluster(cluster==0)=NaN;
287 path(path==0)=NaN;
288 heter(heter==0)=NaN;
289 DcM=nanmean(density)';
290 DcV=nanstd(density)';
291 CcM=nanmean(cluster)';
292 CcV=nanstd(cluster)';
293 LcM=nanmean(path)';
294 LcV=nanstd(path)';
295 HcM=nanmean(heter)';
296 HcV=nanstd(heter)';
297 load SkullsDCL % Matrix of empirical skull networks data
298 count=0;
299 for x=1:44
300     if SkullsDCL(x,2)>=(DcM(SkullsDCL(x,1))-2*DcV(SkullsDCL(x,1))
          )&&SkullsDCL(x,2)<=(DcM(SkullsDCL(x,1))+2*DcV(SkullsDCL(x
          ,1)))
301         if SkullsDCL(x,3)>=(CcM(SkullsDCL(x,1))-2*CcV(SkullsDCL(x
              ,1)))&&SkullsDCL(x,3)<=(CcM(SkullsDCL(x,1))+2*CcV(
              SkullsDCL(x,1)))
```

```
302                 if SkullsDCL(x,4)>=(LcM(SkullsDCL(x,1))-2*LcV(
                        SkullsDCL(x,1)))&&SkullsDCL(x,4)<=(LcM(SkullsDCL(x
                        ,1))+2*LcV(SkullsDCL(x,1)))
303                     if SkullsDCL(x,5)>=(HcM(SkullsDCL(x,1))-2*HcV(
                            SkullsDCL(x,1)))&&SkullsDCL(x,5)<=(HcM(
                            SkullsDCL(x,1))+2*HcV(SkullsDCL(x,1)))
304                         count=count+1;
305                     end
306                 end
307             end
308         end
309 end
310
311 count % number of matches of the simulation
```

Appendix C: Generative Morphospaces

The Random Morphospace

```
% Generative Morphospace of the Erdos and Renyi Model
% Input: p = linkage probability (p = 2*K/N^2)
% Outcome: Random Generative Morphospace
% by Borja Esteve-Altava 2012

% Initial Settings
p=0.1; a=0;

% Generation
for bones=15:60 % range of bones
a=a+1;
    for ite=1:10000 % iteration
        % network generation
        ProbNet=zeros(bones,bones);
        for i=1:length(ProbNet)
            for j=1:length(ProbNet)
                if j<i
                    ProbNet(i,j)=rand;
                    ProbNet(j,i)=ProbNet(i,j);
                end
            end
        end
        ProbNet(ProbNet>p)=0;
        ProbNet(ProbNet~=0)=1;
        % save tratis
        nodes(ite,a)=bones;
        links(ite,a)=sum(sum(ProbNet))/2;
    end
end
```

The Preferential Morphospace

```
% Generative Morphospace of the Barabasi and Albert Model
% Input: m = number of connections introduced by new bones
% Outcome: Random Generative Morphospace
% by Borja Esteve-Altava 2012

% Initial Settings
m=1; % number of new connection

% Generation
for ite=1:10000
    % start with a fix number of bones randomly connected
    Ni=5;
    Graph=zeros(Ni,Ni);
    a=1;
    p=0.2;
    for i=1:Ni
        for j=1:Ni
            if j<i
                Graph(i,j)=rand;
                Graph(j,i)=Graph(i,j);
            end
        end
    end
    Graph(Graph<1-p)=0;
    Graph(Graph>=1-p)=1;
    % start network growth by preferential attachment
    for n=6:60
        a=a+1;
        % set preferential attachment
        deg=degrees_und(Graph)';
        PA=deg./(sum(deg)-deg);
        % add bone
        Graph(n,:)=zeros; Graph(:,n)=zeros;
```

```
34          % Add connections
35          new_m=0;
36          while new_m<m
37              for i=1:length(PA)
38                  if PA(i)>rand
39                      Graph(n,i)=1; Graph(i,n)=1;
40                      new_m=new_m+1;
41                      if new_m==m
42                          PA(:)=0;
43                      end
44                  end
45              end
46          end
47          %save traits
48          nodes(ite,a)=n;
49          links(ite,a)=sum(sum(Graph))/2;
50      end
51  end
```

The Proximal Morphospace

```
% Generative Morphospace of the Gabriel Model
% Input: a set of bones randomly located
% Outcome: Proximate Generative Morphospace
% by Borja Esteve-Altava 2012

% Initial Settings
a=0;

% Generation
for bones=10:60 % range of bones
    a=a+1;
    for ite=1:10000 % iteration
        % bones location
        x=rand(bones,1)*2;
        y=rand(bones,1)*1;
        z=rand(bones,1)*4;
        coord=[x y z];
        % generation of a Gabriel network
        Graph=Gabriel(coord);
        % save traits
        nodes(ite,a)=bones;
        links(ite,a)=sum(sum(Graph))/2;
    end
end
```

The Symmetric Proximal Morphospace

```
% Generative Morphospace of the Symmetric Gabriel Model
% Input: bones located symmetrically and unpaired bones
% Outcome: Symmetric Proximate Generative Morphospace
% by Borja Esteve-Altava 2012

% Initial Settings
impar=1; a=0;

% Generation
for par=2:30 % growing number of paired bones
    a=a+1;
    bones=impar+(par*2); % range of bones
    for ite=1:10000 % iteration
        % bones location
        coord=zeros(bones,3);
        for i=1:2:par*2
            coord(i,:)=[rand*1 rand*1 rand*4];
            coord(i+1,:)=[1+(1-coord(i,1)) coord(i,2) coord(i,3)
                ];
        end
        for j=i+1:bones
            coord(j,:)=[1 rand*1 rand*4];
        end
        % Create Gabriel Graph
        Graph=Gabriel(coord);
        % Parameters
        nodes(ite,a)=bones;
        links(ite,a)=sum(sum(Graph))/2;
    end
end
```